UV-Advanced Oxidation Process without additives in liquid phase - Process characterization and validation

Von der Fakultät Energie-, Verfahrens- und Biotechnik der Universität Stuttgart

zur Erlangung der Würde eines

Doktors der-Ingenieurwissenschaften (Dr.-Ing.)

genehmigte Abhandlung

Vorgelegt von

Jorge Mario Toro Santamaria M.Sc.

aus Pereira

Hauptberichter: Prof. Dr. Thomas Hirth

Mitberichter: Dr. Montserrat Perez-Moya

Mitberichter: Prof. Dr. Gunter Tovar

Tag der mündlichen Prüfung: 13.10.2020

Institut für Grenzflächenverfahrenstechnik und Plasmatechnologie

IGVP Universität Stuttgart

2020

Eidesstattliche Erklärung

Ich erkläre hiermit an Eides statt, dass ich die vorliegende Doktorarbeit selbständig verfasst und nur die angegebenen Literaturquellen und Literaturverzeichnis verwendet habe.

_____

Jorge Mario Toro Santamaria, Stuttgart 2020

Affirmation of Independent Work

I hereby certify that this thesis represents my own work completed without extraneous help apart from resources and technical works, which are quoted appropriately as references.

_____

Jorge Mario Toro Santamaria, Stuttgart 2020

Acknowledgement

Completing my PhD is a blessing, during this time I have gained not only technical knowledge but also have reinforced the ability of handling complex topics and most important of long term dedication and perseverance. The achievement of this would have never been possible without the support and contribution of many people, to whom I am endless grateful.

First of all, I would like to express my appreciation to Prof. Dr. Thomas Hirth for the support and advice during my PhD research. My sincere thanks to Dipl.-Ing. Siegfried Egner to give me the opportunity and the resources to conduct my thesis as part of the Physical Process Technology department at Fraunhofer IGB.

Many thanks to Dr. Perez-Moya for agreeing on co-supervise my thesis and facilitating me the access to the European PhD School on Advanced Oxidation Processes and hosting me in UPC Barcelona during the final experimental campaign.

I would like to thank Prof. Dr. Gunter Tovar for agreeing on co-supervise my thesis as part of the Stuttgart University.

This work would have not been possible without the support of Dr. Ursula Schliessmann, Dr. Thomas Scherer and Dr. Gerd Sulz. I really appreciate your advices and words of encouragement.

My special thanks to my colleagues from IGB. Especially to Ben Elkin, Christiane Chaumette and Eckart Binder for the support that helped me to develop this work.

I want to express my gratitude to all student assistants who support me during the experimental work of my thesis: Linda Bamberg, Alexander Offner, René Schiebel, Carol Sofia Barrera Sandoval and Julia Giebel.

My endless gratitude to my family for their unconditional support during this learning time. Your words and prayers gave me always the strength to continue and achieve my dreams.

Content

List of Figures

List of Tables

Abbreviations

ABB	ABB Corporate Research Center in Switzerland
AHTN	Acetyl hexamethyl tetralin
AlGaN	Aluminium Gallium Nitrogen Detector
AOPs	Advanced Oxidation Processes
ATR	Attenuated Total Reflection
BPA	Bisphenol A BPA is employed to make certain plastics and epoxy resins
CAF	Caffeine It is a central nervous system (CNS) stimulant of the methylxanthine class
CBZ	Carbamazepine medication used in the treatment of epilepsy and neuropathic pain
CFD	Computational Fluid Dynamics
DBD	Dielectric Barrier Discharge
DEET	N,N-Diethyl-meta-toluamide active ingredient in insect repellents
DMEM	Dulbecco's Modified Eagle Medium
DOC	Dissolved Organic Carbon
EC	European Commission
EDTA	Ethylenediaminetetraacetic acid, complexing agent
EG	Ethylene Glycol
EQS	European Quality Standards
FID	Flame Ionization Detector
FUV (VUV)	Far Ultra Violet Electromagnetic Radiation 10-200 nm
FWHM	Full width at Half Maximum also called Half-Width
GC	Gas Chromatography
HHCB	Galaxolide synthetic fragrance
HPLC	High Performance Liquid Chromatography
IAF	Fraunhofer-Institut für Angewandte Festkörperphysik
IC	Inorganic Carbon
IFAM	Fraunhofer-Institut Fertigungstechnik und angewandte Materialforschung
IOSB	Fraunhofer-Institut für Optronik, Systemtechnik und Bildauswertung
IPM	Fraunhofer-Institut für Physikalische Messtechnik
IR	Infra-Red Electromagnetic Radiation 800 nm to 1 mm
IRE	Internal Reflection Element
ISIT	Fraunhofer-Institut für Siliziumtechnologie
ISWA	Institut für Siedlungswasserbau, Wassergüte- und Abfallwirtscaft in Stuttgart
IUPAC	International Union of Pure and Applied Chemistry
LD50	lethal dose, 50%
LP	Low Pressure
MB	Methylene Blue
MCPA	2-methyl-4-chlorophenoxyacetic acid, phenoxy herbicide
MeOH	Methanol
MP	Medium Pressure
MS	Mass Spectrometry
MTT	Dye 3-(4,5-dimethylthiazol-2-yl)-2,5-diphenyltetrazolium bromide
NDIR	Non-dispersive infrared detector
NIR	Near Infra-Red Electromagnetic Radiation 800 nm to 2000 nm
NP	Nonylphenol
NTA	Nitrilotriacetic acid, complexing agent
OH	Hydroxyl Radical
OP	Octylphenol
PAH	Polycyclic aromatic hydrocarbons
PBDE	Polybrominated diphenyl ethers
PCB	Polychlorinated biphenyl

PHS	Priority Hazardous Substances
PS	Priority Substances
SHM	Staggered Herringbone Mixer
SQX	Sulfaquinoxaline veterinary medicine to treat coccidiosis
TC	Total Carbon
TOC	Total Organic Carbon Content
US	Ultra Sound
UV	Ultra Violet Electromagnetic Radiation 200-400 nm
UV-A	Ultra Violet Electromagnetic Radiation 320-400 nm
UV-B	Ultra Violet Electromagnetic Radiation 280-320 nm
UV-C	Ultra Violet Electromagnetic Radiation 200-280 nm
VIS	Visible Spectrum 400-800 nm (visible to the human eye)
VUV	Vacuum Ultra Violet Electromagnetic Radiation 10-200 nm
WFD	Water Framework Directive
WWTP	Wastewater Treatment Plants

Chemical Formulas

Ar	Argon
$ArCl^{\bullet}$	Argon chloride
Br	Bromine
CH_2O	Formaldehyde
$CH_3^{\bullet}$	Methyl radical
$CH_3O^{\bullet}$	Methoxyl radical
CH_3OH	Methanol
$(CH_2OH)_2$	Ethylene glycol
Cl	Chorine
$^{\bullet}COO^{-}$	Deprotonated formyl radical
CO_2	Carbon dioxide
e^-_{aq}	Solvated electron, free electron in solution, smallest possible anion
F	Fluorine
Fe^{2+}	Ferrous ion
$H^{\bullet}$	Hydrogen radical
H^+	Positively charged Hydrogen ion, Proton
H_2	Molecular hydrogen
H_2O	Water
H_2O_2	Hydrogen peroxide
H_2SO_4	Sulfuric acid
HBr	Hydrobromic acid
HCl	Hydrogen chloride
$HCOO^{\bullet}$	Protonate formyl radical
$HCOO^{-}$	Formate ion
$HCOOH$	Formate
He	Helium
Hg	Mercury
HNO_2	Nitrous acid
HNO_3	Nitric acid
$HOCH_2^{\bullet}$	Hydroxymethyl radical
I	Iodine
Kr	Krypton
$KrCl^{\bullet}$	Krypton chloride

M	Molecule
M^+	Molecule +1 oxidation state
M^n	Molecule n oxidation state
M^{n+1}	Molecule n+1 oxidation state
$M^\bullet$	Molecule with an unpaired valence electron, Free radical
N_2O	Nitrous oxide
Ne	Neon
O_2	Molecular oxygen
O_3	Ozone
$^\bullet OH$	Hydroxyl radical
$^\bullet OOCH_2OH$	Peroxyl methyl radical
R-H	Organic functional group attached to hydrogen
$R^\bullet$	Organic functional group as a free radical
TiO_2	Titanium oxide
X^-	Halogen ion
$X^{\bullet -}$	Halogen free radical with negative charge
Xe	Xenon
$Xe_2^\bullet$	Excited dimer of Xenon
$XeCl^\bullet$	Xenon chloride

Nomenclature

A	Transfer area [m^2]
A_{10}	Absorbance (logarithm to the base 10)
A_d	Active are of detection [cm^2]
A_i	Absorbance of substrate i
C_i	Concentration of substrate i [mol L^{-1}] and [mg L^{-1}]
C_{MB}	Methylene blue concentration [mg L^{-1}]
D	Diffusion coefficient [m^2 L^{-1}]
E	Spectral radiant power [W]
$E_{e,\lambda}$	Spectral radiant power which produces a signal in a radiometer [W]
E_P	Photon flow [mol s^{-1}]
E^{Lamp}	Spectral radiant power of a Lamp [W]
E_λ^0	Spectral radiant power of incident monochromatic radiation [W]
$E_{\lambda A}^0$	Irradiance (flux density) [W/m^2]
E_p^{abs}	Spectral radiant power absorbed [W]
E_λ^{trans}	Spectral radiant Power of transmitted monochromatic radiation [W]
$G_{e,\lambda}$	General radiometric concept
$G_{p,\lambda}$	General photometric concept
I	Irradiance [W/m^2]
I_r	Radiant intensity [W/sr]
M_p	Photon flux [photon s^{-1} m^{-2}] or [Einstein s^{-1} m^{-2}]
N_λ	Number of photons [photons]
$N(\lambda)$	Refractive index
$P(x)$	Pressure of the fluid as a function of the distance from the inlet [Pa]
Q	Volumetric flow [m^3 s^{-1}]
Q_e	Radiant energy [J]
R	Reflectance R_p p-polarized, R_s s-polarized
Re	Reynolds number
T	Temperature [°C]
T	Transmittance

V	Volume of the solution [m^3] and [L]
W_λ	Energy of photon [J]
a	Decadic absorption coefficient [m^{-1}]
b	Fraction b of light absorbed by a material
c	Light velocity [m s^{-1}]
f	Fraction f of light reflected of a beam passing from a material 1 to material 2
f_i	Fraction of photons absorbed by a substrate i
h	Plank's constant
i	Electrical signal [A]
k	Extinction coefficient imaginary part of the complex refractive index
l	Thickness of the material traversed by the UV radiation, optical path length
n_i	Refraction index of material i
$n(M)$	Number of moles of a substrate M [mol]
r_i	Initial reaction rate [mg $L^{-1}s^{-1}$]
s_λ	Response of a radiometer [A W^{-1}]
y	Molar fraction
α	Naperian absorption coefficient [m^{-1}]
ε_λ	Molar decadic absorption coefficient [L mol^{-1} cm^{-1}]
ϕ_λ	Quantum yield at a specific wave length [mol M mol $photons^{-1}$]
λ	Wavelength [nm]
θ	Angle [°]
ρ	Density [Kg L^{-1}]
σ_λ	Attenuation cross section [M^{-1} cm^{-1}]
$v_x(y)$	Velocity of the fluid as a function of the distance from the wall [m s^{-1}]
ν_λ	Frequency of a photon at the specific wavelength

Abstract

Human activities are gradually generating a strong impact on the environment and the quality of natural water resources. Traces of hazardous substances are detected not only in wastewater but also already in natural water bodies (surface and ground water) around the globe. The source of these trace substances is broad, starting with chemicals from industrial production like polycyclic aromatic hydrocarbons, pesticides, food ingredients, pharmaceuticals, to components of personal care, just to mention examples. Because of their constantly growing presence in water resources, and the fact that some of those are seriously affecting natural biological processes, there is an increasing need for finding ways to impede those substances to reach water bodies.

The European community has adopted the water pollution problematic as one of their main concerns. As a result, on the 23 October 2000, the Directive 2000/60/EC of the European Commission was adopted. The main purpose of the directive is the protection of European natural water resources by enhancing the status of the water bodies as well as preventing further contamination. In particular, the requirement of complying with European environmental quality standards (EQS) for priority substances (PD) became compulsory. In order to meet these requirements and directives, industry and the scientific community working in the fields of water treatment, do approach new treatment processes with the purpose of upgrading current treatment plants to destruct or reduce trace substances. One alternative are the so called Advanced Oxidation Processes (AOPs), which are able to treat persistent and hardly biodegradable pollutants by oxidation processes. Between the varieties of potential AOPs the photo-induced advanced oxidation, centred on photolysis of water by radiation below 200 nm has received special attention. The key feature of the photo induced AOP is the facts of the efficient production of hydroxyl radicals as the highest possible oxidant and the singularity of no need for auxiliary oxidants like hydrogen peroxide, ozone, peroxydisulfate or peroxymonosulfate, needed in other AOPs.

One of the most important steps to bring the photo induced AOP to be used in the real field, is to prove that the process can be operated under efficient conditions, controlling the generation of hydroxyl radicals and utilizing them efficiently for the goal of treatment. An important action to push the technology to the path of product development is therefore, the integration of efficient UV sources to a photo reactor, taking into account the peculiarities of the process.

Overall, the research presented in this thesis focuses on the characterization of the photoreaction zone, the light penetration and absorption process as well as the hydroxyl radical generation and

provides the understanding and database to enable different approaches for the engineering of photo induced AOP.

Concretely, this thesis is structured in five parts. Part I includes the literature search and its analysis; different calculations and simulations were performed with the aim of describing the heterogeneity of the reaction zone, the theoretical penetration of radiation in water and understanding the theoretical spatial generation of hydroxyl radicals.

Part II includes the reactor characterization. The photo induced AOP was first tested following the degradation of Methylene Blue (MB). Subsequently it was studied the impact of the channel dimensions in the oxidation process under different operational parameters and the characterization of the photo reactor in terms of radiation intensity using three different methods. It was found that channel thicknesses larger than 500 µm develop a boundary layer along the lamp, which is larger than the photoreaction zone leading to reaction limited by diffusion. Mixing enhancement prevent stable boundary layer formation extending the option to use larger channel up to 1000 µm. Additionally, a system for UV characterization at wavelengths lower than 200 nm by means of an AlGaN-detector in an inert environment was built and established. The detector is blind for radiation above 360 nm and does not show degradation, it was possible to perform a calibration, permitting an accurate and interference free intensity measurement. The values of irradiance measured in this thesis using this method was 1,43 mW/cm^2 for the photo-reactor system. All lamps were analysed with this method.

Part III includes the process characterization where the investigations were focused on the penetration of radiation into water and the generation of hydroxyl radicals by means of two methodologies: the transmission measurements in thin water films and the degradation of methanol as reference substance. It was found that the absorption coefficient of water at 172 nm is 180 000 m^{-1}. Therefore, the total penetration of radiation at this wavelength happens in a layer of 11 µm for 99 % absorption of radiation. Additionally, the quantum yield for the generation of Hydroxyl radicals obtained in this study was ϕ_W = 1.82 ± 0.02 molOH/mol Photons. This singularity is possible only under special conditions like series of chain reactions and/or formation of intermediate products, which act as a catalyst. This implies that the chemical system model may be more complex than expected.

Part IV includes the tailor made reactor validation. In this part, the focus was directed to verify the numeric models and gain data enabling the design, construction and validation of a reactor system using flat lamps. Validation of the photo induced AOP was performed by means of degradation of the pharmaceuticals Sulfaquinoxaline (SQX) and Carbamazepin (CBZ), as well as the degradation of an organic substance coming from the chemical industry Bisphenol A (BPA) and a food ingredient

Caffeine (CAF). During the validation phase the concentration of the substances, the Total Organic Carbon (TOC) and the cytotoxicity using VERO and COS cell lines for each experiments were followed.

Oxidation of the trace substances was confirmed, and 100% elimination of the target components was achieved in less than 20 minutes of irradiation, with UV Dose below 1000 mJ/cm^2. 80 % of Total organic carbon was mineralized in 120 minutes. Furthermore, cytotoxicity assays revealed the feasibility of the UV photo induced AOP treatment for removal of the model compounds, as well as the possibility to stop this process at any convenient time as no increase of toxicity was detected.

Part V summarizes the results. In general, it was found that the process shows attractive potential and advantages in comparison with other oxidation technologies. For example: the steady and local production of hydroxyl radical without the addition of supplementary oxidation agents; the not strong selectivity and the capacity of mineralization of the process; the pH independency of the oxidation process; the fact that cytotoxicity of the byproducts does not overpass the initial toxicity of the tested substances and the Dose requirements for oxidation is comparable with existing process without using any additive.

After all, the different experimental setups developed for this thesis and the gained results in knowledge enabled as an outcome the filing of 2 patents, the participation in publications and research projects, as well as generation of basis for the design of a demo-plant based on a flat-lamp-reactor-system for the further studies of UV photo-induced oxidation of contaminants in water.

Kurzfassung

Menschliches Handeln hat einen starken Einfluss auf die Umwelt und insbesondere auf die Qualität der natürlichen Wasserressourcen. Spuren gefährlicher Stoffe werden nicht nur im Abwasser, sondern auch bereits in natürlichen Gewässern (Oberflächen- und Grundwasser) rund um den Globus nachgewiesen. Die Quelle dieser Chemikalien ist breit gefächert, angefangen bei Chemikalien aus der industriellen Produktion wie polyzyklische aromatische Kohlenwasserstoffe, Pestizide, Pharmazeutika bis hin zu Komponenten der Körperpflege, um nur einige Beispiele zu nennen. Aufgrund ihrer ständig zunehmenden Präsenz in den Wasserressourcen und der Tatsache, dass einige von ihnen natürliche biologische Prozesse durch ihre hormonähnlichen Strukturen beeinflussen, hat dies verschiedene nachteilige Auswirkungen auf die Gesundheit von Mensch und Tier.

Eine solche Wasserverschmutzung in Kombination mit Wasserknappheit ist eine der größten globalen Herausforderungen, eines der Hauptanliegen der Europäischen Gemeinschaft. Infolgedessen wurde am 23. Oktober 2000 die Richtlinie 2000/60 / EG der Europäischen Kommission verabschiedet. Seitdem wurden mehrere Änderungen vorgenommen, um gesetzliche Vorgaben der Gemeinschaft im Bereich der Wasserwirtschaft zu etablieren. Hauptzweck der Richtlinie ist der Schutz der natürlichen Wasserressourcen in Europa, indem ein Rahmen geschaffen wird, der es ermöglicht, den Zustand der Gewässer zu verbessern und eine weitere Kontamination zu verhindern. Insbesondere wird der Wasserqualitätsstatus durch die Einhaltung der europäischen Umweltqualitätsnormen (EQS) für prioritäre Stoffe (PD) definiert. Die Erfordernisse der Einhaltung von EQS führte zur Notwendigkeit, Behandlungsverfahren zu finden, die in der Lage sind, mit diesen Substanzen effizient umzugehen.

Eine dieser Optionen sind die sogenannten erweiterten Oxidationsprozesse oder Advanced Oxidation Processes (AOP), die diese schädlichen Verbindungen durch Oxidation mineralisieren. Im Bereich der existierenden AOP-Verfahren hat die photoinduzierte Oxidation - Photolyse mit Strahlung unter 200 nm - aufgrund der Tatsache, dass Hydroxylradikale als höchstmögliches Oxidationsmittel effizient erzeugt werden und keine zusätzlichen Oxidationsmittel wie Wasserstoffperoxid, Ozon, Peroxydisulfat oder Peroxymonosulfat erforderlich sind, breite Aufmerksamkeit erlangt.

Eine Analyse des Standes der Technik ergab, dass eine weitere Verbesserung der photoinduzierten AOP ein besseres Verständnis der Reaktionszone erfordert, insbesondere der Hydrodynamik an der Oberfläche des Lampenkörpers für einen verbesserten Stoffübergang in die Photoreaktionszone, sowie ein verbessertes Verständnis der Reaktionskinetik zur Optimierung des Lampenreaktorsystems oder zur Neugestaltung der Strahlergeometrie.

Die in dieser Arbeit vorgestellten Forschungsergebnisse umfassen die Charakterisierung der Photoreaktionszone, des Lichtpenetrations- und Absorptionsprozesses sowie der Erzeugung von Hydroxylradikalen und liefern die Grundlagen und die Datenbasis, um Ansätze für das Engineering von photoinduziertem AOP zu ermöglichen. Konkret gliedert sich diese Arbeit in fünf Teile. Teil I umfasst die Literaturrecherche und ihre Analyse, die Definition und Parametrisierung numerischer Modelle sowie die Ableitung von Schlussfolgerungen, die den Entwurf und den Betrieb einer flachen Mikrokanalreaktorkammer in Verbindung mit dem neuesten kommerziellen Xenon-Excimerlampensystem ermöglichen. Der Reaktoraufbau wurde daher so konzipiert, dass Experimente mit unterschiedlichen Kanaldicken und damit verschiedenen hydrodynamischen Profilen während der Durchführung der photolytischen Oxidation möglich sind.

Teil II beinhaltet die Charakterisierung des Reaktors. Verschiedene Berechnungen und Simulationen wurden durchgeführt, um die Heterogenität der Reaktionszone, das Eindringen von Strahlung in Wasser und die lokale Erzeugung von Hydroxylradikalen theoretisch zu beschreiben. Der photoinduzierte AOP-Prozess wurde zuerst anhand des Abbaus von Methylenblau-MB getestet. Anschließend wurden der Einfluss der Kanaldimensionen auf den Oxidationsprozess unter verschiedenen Betriebsparametern und die Charakterisierung des VUV-Reaktors hinsichtlich der Strahlungsintensität mit drei verschiedenen Methoden untersucht. Es wurde festgestellt, dass Kanaldicken von mehr als 500 µm zu einer Grenzschicht entlang der Lampe führen, die größer ist als die Photoreaktionszone, was zu einer durch Diffusion begrenzten Reaktion führt. Die Mischungsverbesserung verhindert eine stabile Grenzschichtbildung und erweitert die Möglichkeit, einen größeren Kanal bis zu 1000 µm zu verwenden. Zusätzlich wurde ein System zur UV-Charakterisierung bei Wellenlängen von weniger als 200 nm mittels eines AlGaN-Detektors in einer inerten Umgebung aufgebaut und etabliert. Da der Detektor für Strahlung oberhalb von 360 nm blind ist und keine Degradation zeigt, konnte eine Kalibrierung durchgeführt werden, die eine genaue und störungsfreie Intensitätsmessung erlaubt. Alle Lampen wurden mit dieser Methode analysiert.

Teil III umfasst die Prozesscharakterisierung, bei der das Eindringen von Strahlung in Wasser und die Erzeugung von Hydroxylradikalen anhand zweier Methoden untersucht wurden - Transmissionsmessungen in dünnen Wasserfilmen und Abbau von Methanol als Referenzsubstanz. Es wurde festgestellt, dass der Absorptionskoeffizient von Wasser bei 172 nm 180 000 m^{-1} beträgt. Die gesamte Durchdringung der Strahlung bei dieser Wellenlänge geschieht also in einer Schicht von 11 µm bei 99 % Absorption der Strahlung. Zusätzlich wurde in dieser Studie eine Quantenausbeute für die Erzeugung von Hydroxylradikalen erzielt ϕ_W= 1,82 ± 0,02 molOH/mol Photonen. Diese Singularität ist nur unter besonderen Bedingungen wie dem Auftreten von Kettenreaktionen und/oder der Bildung

von Zwischenprodukten, die als Katalysator wirken, möglich. Dies impliziert, dass das chemische Modell möglicherweise komplexer ist als erwartet.

Teil IV enthält die maßgeschneiderte Validierung des Reaktors. In diesem Teil wurde der Fokus daraufgelegt, die numerischen Modelle zu verifizieren und Daten zu gewinnen, die den Entwurf, die Konstruktion und die Validierung eines Reaktorsystems unter Verwendung von Flachlampen ermöglichen. Die Validierung des photoinduzierten AOP erfolgte durch Abbau der Pharmazeutika Sulfaquinoxalin (SQX) und Carbamazepin (CBZ) sowie durch Abbau einer organischen Substanz aus der chemischen Industrie Bisphenol A (BPA) und eines Lebensmittelinhaltsstoffs Coffein (CAF). Während der Validierungsphase wurden die Konzentration der Substanzen, der gesamte organische Kohlenstoff-(TOC) und die Zytotoxizität unter Verwendung von VERO- und COS-Zellen für jedes Experiment verfolgt. Die Oxidation von Spurensubstanzen wurde untersucht, und die 100%ige Eliminierung der Zielkomponenten wurde in weniger als 20 Minuten Bestrahlung erreicht, wobei die UV-Dosis unter 1000 mJ/cm^2 lag. 80 % des gesamten organischen Kohlenstoffs wurden in 120 Minuten mineralisiert. Darüber hinaus zeigten Zytotoxizitätstests die Wirksamkeit der UV-Photo-induzierten AOP-Behandlung zum Abbau der Modellverbindungen sowie die Möglichkeit, diesen Prozess jederzeit zu stoppen, da keine Zunahme der Toxizität festgestellt wurde.

Teil V fasst die Ergebnisse zusammen. Im Allgemeinen wurde festgestellt, dass das Verfahren im Vergleich zu anderen Oxidationstechnologien ein attraktives Potenzial und Vorteile aufweist, wie beispielsweise die gleichmässige und lokale Bildung von Hydroxylradikalen ohne den Zusatz von zusätzlichen Oxidationsmitteln; der hohe Mineralisierungsgrad des Verfahrens; die pH-Unabhängigkeit des Oxidationsprozesses; die Tatsache, dass die Zytotoxizität der Nebenprodukte nicht höher ist als die Toxizität der getesteten Substanzen und die UV-Dosisanforderungen für die Oxidation mit ändere Verfahren vergleichbar ist.

Die verschiedenen Versuchsanordnungen, die für diese Arbeit entwickelt wurden, wie die Photoreaktoren oder die Messanordnungen für die Bestrahlungsstärke und Absorption von Strahlung in dünnen Flüssigkeitsfilmen sowie die gewonnenen Erkenntnisse ermöglichten als Resultat die Einreichung von zwei Patenten und eine Demonstrationsdemo-Anlage basierend auf einem Flachlampen-Reaktorsystem zur weiteren Untersuchung der VUV-Photo-induzierten Oxidation von Schadstoffen in Wasser.

1. Introduction

1.1. Motivation

Human activities are gradually generating a strong impact on the environment and the quality of natural water resources in particular [1-6]. One of the causes are the efforts of the industry to produce more stable and complexes chemicals with specific features for a wide range of applications in markets of private consumption. Unfortunately, some of these features result in toxicity against biological organism and persistency against degradability in nature; therefore having a negative impact to the environment [5, 7-12]. Around the globe traces of such hazardous substances are detected not only in wastewater but also already in natural water bodies such as surface and ground water. Their presence covers a large spectrum of concentrations from nano to milligram per litre [5]. The source of these chemicals is broad, starting with chemicals from industrial production like poly cyclic aromatic hydrocarbons, pesticides, food ingredients, pharmaceuticals, to components of personal care, just to mention examples.

According to the application and the environmental behavior of the organic chemical substances, they can be transported in the environment via different paths. For example, into the municipal wastewater, organic trace substances are discharged via industrial and commercial wastewater releases, domestic wastewater as well as precipitation water discharges from sealed areas. The discharge of organic trace substances of the municipal waste water into the environment can take place via sewage treatment plant effluents, precipitation and mixed water discharges as well as through the agricultural sewage sludge utilization.

Estimations in literature [6, 13] show that organic trace substances from centralized sewage treatment plants play a primary role in the pollution of the aquatic environments in Europe. Therefore and in order to perform a selective treatment and prevent discharges of organic traces in the environment alternatives to central wastewater disposal as separate collection and treatment of heavily polluted wastewater streams has been in several publications openly suggested [13].

Many organic pollutant extend via domestic wastewater into municipal sewer systems. The separation associated with other highly contaminated household wastewater streams such urine is not meaningful in industrialized countries with existing wastewater infrastructure. Therefore, the use of technical measures to reduce the discharge of organic trace substances focuses primarily on the central sewage and sludge treatment. Of particular importance is the development of technical solutions for

the upgrading or expansion of conventional wastewater treatment, in this regard Advanced Oxidation Processes [1, 2, 14, 15].

No targeted elimination of hazardous organic substances has been implemented in the planning and operation of municipal centralized wastewater treatment plants to this point. However and due to the requirements of the European Commission Water Framework Directive (EC WFD) (Directive 2000/60/EC) on the state of European surface waters, this could change in the near future. The EC WFD marked the beginning of a new era for European water management based on a holistic approach focusing on understanding and integrating all the different aspects related to the water environment to be effective and sustainable [16].

Several amendments have been introduced to the EC WFD. As a first step the Directive 2455/2001/EC, established a list of priority substances (PS), including the priority hazardous substances (PHS) that became the Annex X of WFD. Especially priority hazardous substances PHS are the PS that "are persistent, toxic and liable to bio accumulate, or that give rise to an equivalent level of concern".

This Directive 2455/2001/EC amends Directive 2000/60/EC that specifies that specific measures must be adopted to reduce or even, in the case of for priority hazardous substances, to cease the discharges, emissions and losses into the aquatic environment, within 20 years after their adoption at Community level. The final purpose is achieving concentrations approaching background values for naturally occurring substances and close to zero for man-made synthetic substances. As a result, additional measures would be necessary in many cases in the wastewater sector to reduce the discharge of organic hazardous trace substances. The ideal way to minimize the discharge of such substances would be a production ban of such substances, as this is not possible in many cases, there is a need to study and investigate the technological options for the elimination of hazardous substances from water and wastewater [17].

The most relevant alternatives for the elimination of hazardous substances from water and wastewater are the so called Advanced Oxidation Processes AOPs. They are based on the generation of hydroxyl radical. These radicals, due to their high oxidation potential, are able to oxidize every component to its maximum oxidation state. This oxidation effect is usually described as a chain reaction and can reach complete mineralization. There is one AOP, the photo induced oxidation using radiation below 200 nm, which has received special attention due to the fact of the constant production of hydroxyl radicals, the minimum interference of the trace organic substance in the generation of radicals and the no need for auxiliary oxidants like hydrogen peroxide, ozone, peroxydisulfate or peroxymonosulfate for the oxidation process.

Laurent and Braun were the first to use xenon excimer lamps (emitting radiation below 200 nm) for oxidation purposes in the early 90's [18, 19]. Although Oppenländer, Heit and other authors attempted to characterize the phenomena in the following years, and due to the limited radiation sources and reactors, they all agreed that to reach the maximum efficacy of the Xe excimer lamp for photo induced advanced oxidation, further engineering optimization of photo-reactor concepts was necessary [19-24].

One of the most important steps to bring the photo induced AOP to be used in the real field, is to prove that the process can be operated under efficient conditions controlling the generation of hydroxyl radicals and utilizing them efficiently for the goal of treatment. The integration of efficient UV sources to a photo reactor, which take into account the peculiarities of the process, are therefore important measures to push the technology to the path of product development.

The research presented in this thesis focuses on the characterization of the photo reaction zone, the light penetration and absorption process as well as the hydroxyl radical generation and provides the understanding and database to enable different approaches for the engineering of photo induced AOP. To perform the laboratory test trials for verification and data collection, a photoreaction chambers was designed based on the theoretical models and latest available xenon excimer lamps, enabling to explore different reactor channel thicknesses and to research the relations between hydrodynamics in flat micro-channels and the reaction performance resp. the kinetic in particular.

In this case, an effective photo-reactor design requires a deep understanding of the physical and chemical phenomena, the optics, the fluid dynamics, and reaction mechanisms involved and their interrelated influences.

1.2. Thesis scope

A key aspect of this research is to understand the individual different phenomena present in the photo induced oxidation and characterize their effects, exploring an alternative to the coaxial reactor used in literature to overcome limitations of mixing and channel thickness influences; Understanding of the dependency on space-time of the oxidation process and the need to ensure efficient mixing are, though, prerequisites for the further development of this technology in the field of water treatment. These results bring us one step closer to reach the maximum efficacy of the Xe excimer lamp for photo induced Advanced Oxidation. Once the phenomena are understood the validation of the oxi-

dation process by means of degradation of the pharmaceuticals Sulfaquinoxaline (SQX) and Carbamazepin (CBZ), the organic substance coming from the chemical industry Bisphenol A (BPA) and a food ingredient Caffeine (CAF), is performed.

This research is not aiming to investigate the fate of the trace substances in the concentration range which is reported in literature being several orders of magnitude smaller than those concentrations tested here. It is also not intended to investigate the fate of the trace substances in natural waters and its complex matrices under photo induced AOP.

This thesis aims to evaluate the efficiency and limitations of different characterization approaches of the photo-induced Advanced Oxidation Process using Xenon excimer lamps in order to achieve enough understanding of the impact of channel dimensions, hydrodynamic and operational parameters for the effective elimination of contaminants in water solutions.

This thesis provides a deep understanding to the heterogeneity of the photo-reaction, the dependency on space-time of the oxidation process, the penetration of radiation in water, the irradiance characterization of radiation sources, and a validation of the oxidation process against relevant pollutants, so based on these achievements in understanding of the individual different phenomena and characterize their effects, new designs of photo-reactors and photo-AOP-systems can be developed.

1.3. Objectives

Overall, the work presented here aims to provide understanding and database to enable different approaches for the engineering of photo induced AOP for the treatment of recalcitrant, persistent and hardly biodegradable pollutants via water photolysis products by ultraviolet radiation due to the efficient production of hydroxyl radicals as the highest possible oxidant and no need for auxiliary oxidants, enabling to explore different reactor channel thicknesses and to research the relations between hydrodynamics in flat micro-channels and the reaction performance with an assessment of the different conditions of flow and mixing in order to run the oxidation process in reaction controlled regime.

In particular, this thesis

- Qualitative and quantitative characterise the photolysis of water at 172 nm for AOPs, direct attention to the phenomena: absorption, transmittance, and radical formation, degradation rate of pollutants, molecular diffusion and flow characteristics to identify optimal operational conditions and channel geometries to increase performance.

- Establish two channel thickness variable photo-reactors types in a laboratory scale batch operation set ups to experimentally assess the different operational conditions to increase performance.
- Qualitatively and quantitatively characterise the effects of channel size, flow and mixing performance in the degradation of a reference substance identifying maximum performance.
- Radiation intensity measurements using actinometry and photometry establishing a measurement set up for radiation source characterisation using cis-, trans- cyclooctene as actinometer and Si and Ga detectors.
- Absorption coefficient measurements using thin film transmission method and spectrophotometry in VUV establishing a measurement set up for absorption coefficient measurements for short-penetrating UV wavelengths.
- Measurement of the production of hydroxyl radicals by means of methanol degradation by photo-induced hydroxyl radical formation.
- Qualitatively and quantitatively characterises the oxidation of recalcitrant organic matter in irradiated solutions as a function of irradiation time. (case study trace substances Sulfaquinoxaline SQX, Carbamazepine CBZ, Bisphenol A BPA and Caffeine CAF)

To achieve the objectives, the work performed in this thesis followed the subsequent structure.

1.4. Thesis structure

This thesis is divided into five parts (Figure 1.1). Part I includes the literature search and its analysis, the definition and parametrization of numeric models and the derivation of conclusions enabling the design, and operation of a flat micro-channel reactor chamber coupled with the latest commercial Xenon excimer lamp system. The reactor set-up was therefore designed to allow experiments using different channel thicknesses to perform various hydro-dynamic profiles while running the photolytic oxidation.

Part II includes the reactor characterization. Different calculations and simulations were performed with the aim of describing the heterogeneity of the reaction zone, the theoretical penetration of radiation in water and understanding the theoretical spatial generation of hydroxyl radicals. The photo induced AOP was first tested following the degradation of Methylene Blue MB. Subsequently it was studied the impact of the channel dimensions in the oxidation process under different operational parameters and the characterization of the VUV reactor in terms of radiation intensity using three different methods.

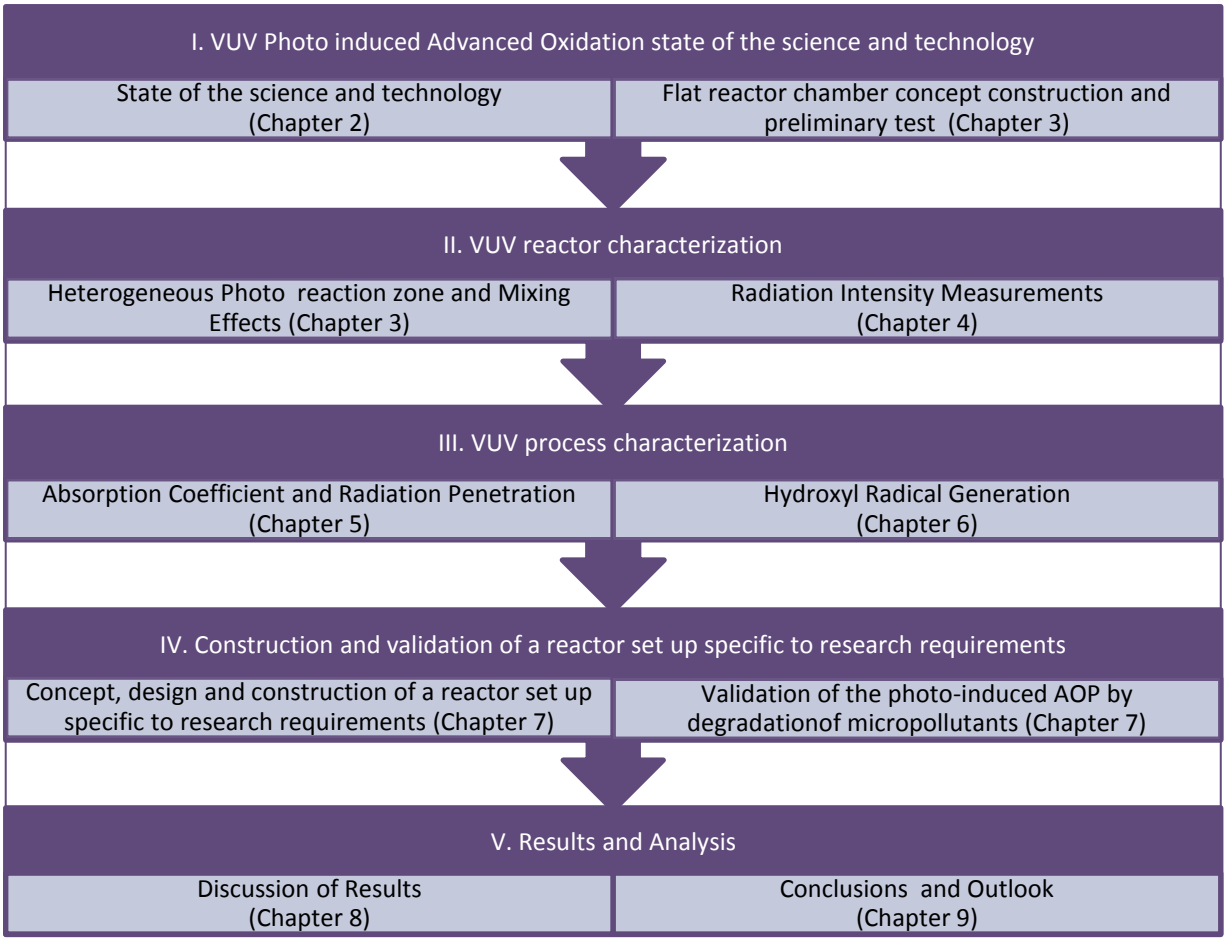

Figure 1.1 Thesis Structure

Part III includes the process characterization where the investigations were focused on the penetration of radiation into water and the generation of hydroxyl radicals by means of two methodologies: the transmission measurements in thin water films and the degradation of methanol as reference substance.

Part IV includes the validation of a reactor set up specific for the research requirements. In this part the focus was directed to verify the numeric models and gain data enabling the design, construction and validation of a reactor system using flat lamps. Validation of the photo induced AOP was performed by means of degradation of the pharmaceuticals Sulfaquinoxaline SQX and Carbamazepine CBZ, as well as the degradation of an organic substance coming from the chemical industry Bisphenol A BPA and a food ingredient Caffeine CAF. During the validation phase the concentration of the substances, the Total Organic Carbon TOC and the cytotoxicity using VERO and COS cells for each experiments were followed. In Part V the united results and conclusions are presented.

2. Photo Induced advanced oxidation - State of the science and technology

2.1. Advanced oxidation processes

Advanced oxidation processes (AOPs) are defined as those which involve the generation of hydroxyl radicals ($^{\bullet}OH$) [25] in sufficient quantity to enable oxidation of pollutants in order to attain water and air quality standards which fulfil government regulations according to emission ordinances [26]. The different production methods can be classified as homogeneous or heterogeneous processes and further subdivided into processes which use energy and processes which not. A detailed classification of AOPs is described in Figure 2.1. there is a wide range of AOPs being currently studied for the possible use in water treatment.

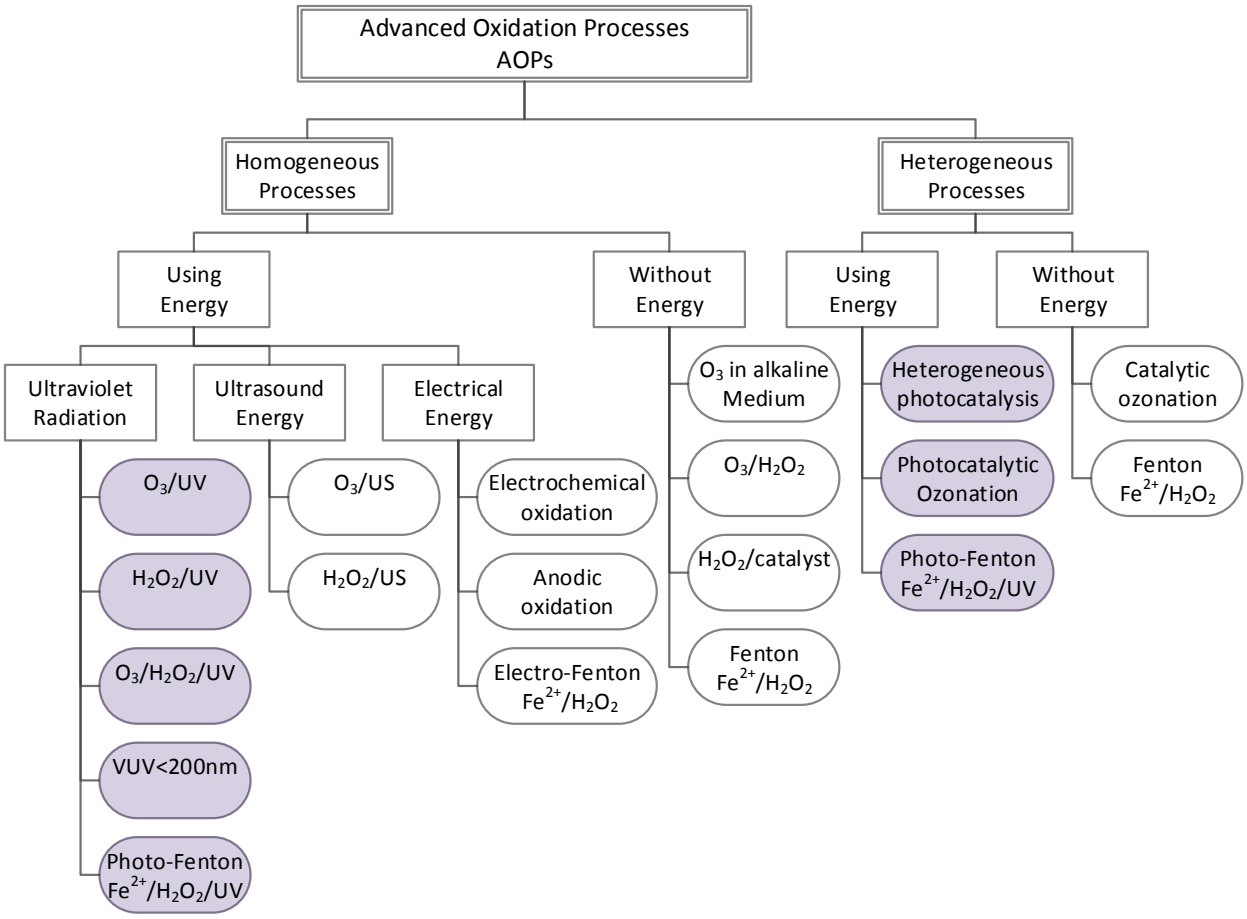

Figure 2.1 AOPs classification homogeneous/heterogeneous processes (redrew from [25])

The relevant AOPs using Electromagnetic radiation as a precursor for the generation of hydroxyl radicals are highlighted in Lila.

The hydroxyl radical produced in AOPs is one of the most powerful oxidizing agents known (E° = +2.7 V in acid solution) and reacts with most organic compounds by abstraction of hydrogen atoms, addition to unsaturated molecules breaking triple and double bonds. The hydroxyl radical can oxidize organic and inorganic substrates. AOPs are an attractive alternative to non-destructive physical water and air treatment processes, where the main process characteristic is the separation of the contaminant (forced transport) to produce a purified or diluted stream and a contaminated or concentrated one.

Although AOPs use different reagent systems, they all produce and use hydroxyl radicals as reagent responsible for oxidation; The production of radicals differs in the physico-chemical way of formation, for example, Fenton process produce hydroxyl radicals by the reaction of Iron ions and hydrogen peroxide, this reaction takes place everywhere in the fluid and is a function of the concentration of reagents (Iron and hydrogen peroxide), in the other hand, in the UV-hydrogen peroxide process the generation of hydroxyl radicals is dependent on the absorption of UV by the hydrogen peroxide, therefore the production does not take place homogeneously in the whole volume [25]. Consequently efficiency of production and concentration density of radicals in the reaction zone is completely method dependent.

In general AOPs in water represent the transformation of general organic molecules $C_nH_mX_z$ (named the pollutant) into the following:

- organic carbon atoms to carbon dioxide or carbonate species,
- hydrogen atoms to water, and
- hetero-atoms X into the corresponding mineral acids HCl, HBr, HNO_3, HNO_2, H_2SO_4, etc.

the above mentioned transformation occurs just if complete mineralization is achieved [20].

As AOPs are used when the polluted water components have a high chemical stability and/or low biodegradability. These processes can be lead to produce complete mineralization of pollutants as described before. If mineralization is not achieved, the partial oxidation of the non-biodegradable organic pollutants can lead to simple biodegradable molecules [25].

However there are cases of AOPs reported in literature when the total mineralization was not reached and toxic substances were produced. Therefore toxicity measurements in AOPs are recommended.

2.2. Photo-induced advanced oxidation processes

Photo-induced AOPs are those processes which use ultraviolet radiation (UV) for the production of the hydroxyl radicals; photoexcitation process and the release of hydroxyl radicals occurs in the presence of oxidative auxiliaries or photo catalyst when UV is low energy radiation above 200 nm (<6 eV); when UV below 200 nm is used (high energy radiation > 6 eV) the photoexcitation process occurs in the water molecule releasing the needed hydroxyl radicals. Photo-induced AOPs can be therefore classified as homogeneous and heterogeneous.

UV radiation is an electromagnetic wave with a wavelength shorter than that of visible light (400-800 nm), but longer than X-rays (0,01-10 nm), in the range of 100 to 400 nm, and energies from 3eV to 124 eV. The Figure 2.2 shows the classification of electromagnetic radiation below 1200 nm. UV radiation is found in sunlight and is also emitted by electric arcs and specialized lights such as black lights. It can cause chemical reactions and makes some substances glow or fluoresce. UV radiation between 200 and 400 nm is classified as non-ionizing radiation and it is the most studied, it is subdivided into three ranges UV-C, UV-B and UV-A, the last one having the lowest energy per photon. The higher energies of the ultraviolet spectrum from 100 to 200 nm (vacuum ultraviolet or VUV) are ionizing. Ultraviolet light leads to the formation of sensitized molecules and can thereby induce photoreactions [20, 27].

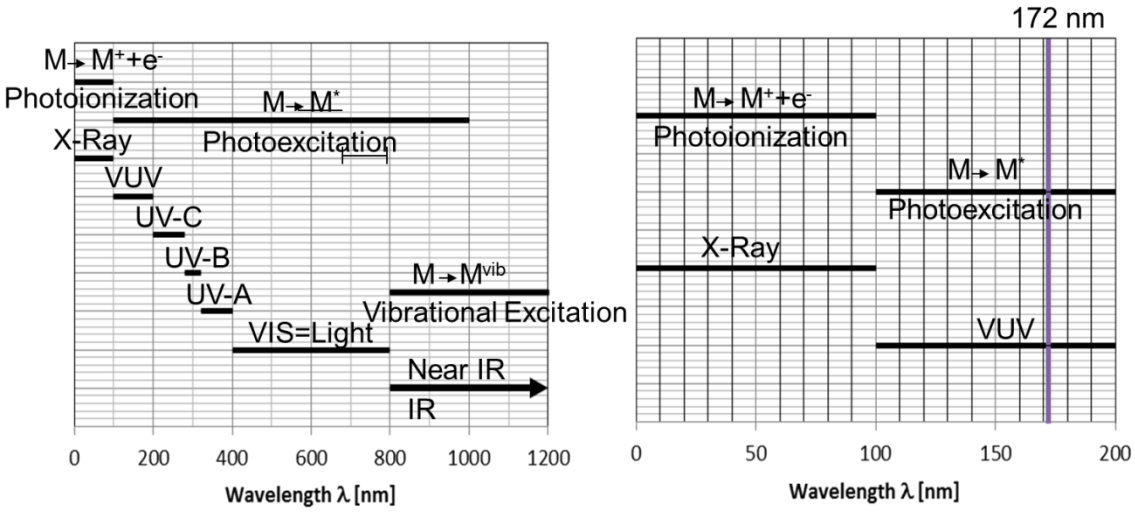

Figure 2.2 Classification of electromagnetic radiation in the wavelength range below 1200 nm with specific names and the interaction with molecules (redrew from [20])

The interaction of UV radiation with matter (atoms, molecules) takes places within the electron shell by promoting one electron from its ground to an electronically excited state. This "reaction" is the primary step in a photochemical or photo-physical event and it is called absorption. Photon absorption

is the fastest process observed in nature. It occurs within a time scale of femto seconds. The electronically excited molecule can get rid of this energy either by photo-physical deactivation process (heat release or photon emission), by photo-chemical process (chemical reaction) or by photo-biological pathways [20, 28].

Photo induced AOPs are therefore, those which use UV/VIS absorbed energy as a precursor for a photo-chemical process leading to the generation of hydroxyl radicals, mostly in presence of oxidative auxiliaries and/or photo-catalyst. The general principle of photochemical AOP's is based in the absorption of the UV/VIS energy by a molecule which directly photolyses to produce hydroxyl radicals. Usually the molecules absorbing refer to oxidative auxiliaries like hydrogen peroxide and ozone. Water can, as well, be efficiently photolysed to produce Hydroxyl radicals when interacts whit high energy VUV or a catalyst and UV/VIS [20, 28].

UV radiation is absorbed in different degrees by individual chemicals, UV-C radiation is absorbed by some substances in particular for AOPs the auxiliary oxidizers hydrogen peroxide and ozone. VUV radiation is absorbed by almost all substances including water, carbon dioxide and oxygen. Therefore, it can only be transmitted under vacuum or at least under non-absorbing gas conditions [29] e.g. Nitrogen atmosphere. The importance of VUV radiation to AOPs is related to the fact that it is efficiently absorbed by water in a liquid or gaseous phase. The up-taken energy causes the photolysis of water molecules with the formation of hydrogen atoms and hydroxyl radicals [30-34].

It is important to mention that, there are two further photochemical effects not related with production of hydroxyl radical, but well known and stablished processes, the disinfection process and the photo-degradation of pollutants. Both are based on the absorption of low energy UV above 200 nm wavelength and energies below the 6 eV.

In Disinfection the UV radiation is absorbed by the bacteria internal structure, this absorption modify the DNA of the bacteria which cannot reproduce therefore cannot spread [35].

In photo-degradation of pollutants the absorbed UV radiation leads to breakdown but not to mineralization. Not all molecules are susceptible to photo-degradation.

These processes are not classified as Photochemical AOPs and attention was not pay to them during the present thesis [36].

The general reaction schemes for photo induced AOPs are summarized in the Table 2.1.The state of the knowledge of photochemical AOPs, concerning the complex and interrelated photochemical,

photo physical and radical mechanism, as well as, lamp technologies in many cases still underdeveloped [37].

Despite the interrogations, the field of photochemical AOPs has shown an undoubtedly growth and development. This indicates their large-scale feasibility, surely with some restrictions concerning energy cost, lamp development and reliability [38].

Table 2.1 Summary of reaction schemes Photochemical AOPs (according to [20, 25, 38])

Photochemical AOP	Reaction scheme	
O_3/UV And O_3/H_2O_2/UV	$O_3+UV\rightarrow O_2+O(_1D)$ $O(_1D)+H_2O\rightarrow[^{\bullet}OH\cdots{}^{\bullet}OH]\rightarrow H_2O_2$ $H_2O_2+UV\rightarrow 2^{\bullet}OH$	**(2.1)** **(2.2)** **(2.3)**
H_2O_2/UV	$H_2O_2+UV\rightarrow 2^{\bullet}OH$	
VUV<190nm	$H_2O+UV\rightarrow {}^{\bullet}OH+H^{\bullet}+e^-_{aq}$	**(2.4)**
Photo-Fenton Fe^{2+}/H_2O_2/UV	$Fe^{3+}+H_2O+UV\rightarrow Fe^{2+}+{}^{\bullet}OH+H^+$ $Fe^{2+}+H_2O_2\rightarrow Fe^{3+}+{}^{\bullet}OH+OH^-$ $Fe^{3+}+H_2O_2\rightarrow Fe^{2+}+{}^{\bullet}OOH+H^+$ $H_2O_2+UV\rightarrow 2^{\bullet}OH$	**(2.5)** **(2.6)** **(2.7)**
Heterogeneous Photo-catalysis	$TiO_2+UV\rightarrow h^+_{TiO_2}+e^-_{TiO_2}$ $h^+_{TiO_2}+H_2O\rightarrow {}^{\bullet}OH_{TiO_2}+H^+$ $e^-_{TiO_2}+O_2\rightarrow {}^{\bullet}O^-_{2TiO_2}$	**(2.8)** **(2.9)** **(2.10)**

Oppenländer [20], classified the photochemical AOPs into VUV and UV oxidation, which are ran in homogeneous phase, and photo-catalysis, which can be ran in homogeneous and heterogeneous phases.

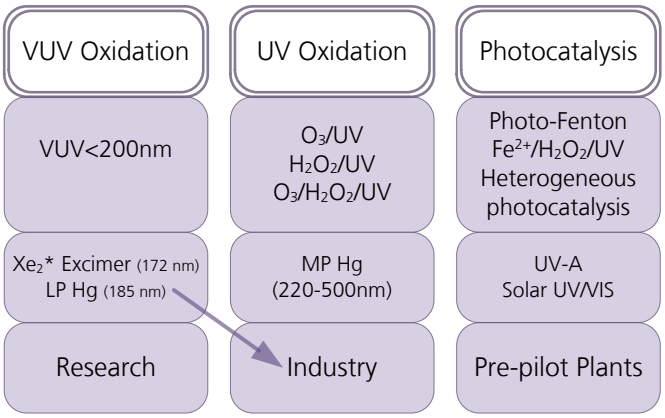

Figure 2.3 State of the Art of Photochemical AOPs (redrew from)[20]

Hydroxyl radicals are the base of AOPs. The hydroxyl radical (•OH) is one of the most powerful oxidizing agents known (E° = +2.7 V in acid solution) and reacts with most organic compounds at diffusion controlled rates. The hydroxyl radical can oxidize organic and inorganic substrates (M, R-H…) by different types of reactions:

- Abstraction of a hydrogen atom: usually with aliphatic hydrocarbon groups

$$^{\bullet}OH + R\text{-}H \rightarrow R^{\bullet} + H_2O \quad \textbf{(2.11)}$$

- Electrophilic addition: usually with unsaturated or aromatic hydrocarbon groups

$$^{\bullet}OH + R_2C{=}CR_2 \rightarrow {}^{\bullet}CR_2\text{-}C(OH)R_2 \quad \textbf{(2.12)}$$

- Electron transfer: usually with inorganic compounds

$$^{\bullet}OH + M^n \rightarrow M^{n+1} + OH^-_{aq} \quad \textbf{(2.13)}$$

Simple electron transfer reactions seem to be unlikely because of the large solvent reorganization energy involved in the formation of the hydrated hydroxide ion. Instead, in the case of halide ions $\mathbf{X^-}$, the formation of intermediate adducts with hydroxyl radicals is observed:

$$^{\bullet}OH + X^- \rightarrow HOX^{\bullet -} \quad \textbf{(2.14)}$$

The scavenging reactions of •OH radicals are usually referred to as electron transfer reactions.

- Radical-radical reactions, for example:

$$HO^{\bullet}_2 + {}^{\bullet}OH \rightarrow H_2O + O_2 \quad \textbf{(2.15)}$$

The ·OH radical is rapidly consumed and its reactivity is thus limited to the region where it is generated continuously. The ·OH radical absorbs UV weakly, only a small fraction of UV is actually absorbed, since the steady-state concentration of ·OH radicals is usually below 10^{-9} M.

2.3. Radiation sources

UV radiation in general can be produced by activating electrons to higher orbital state of an element; the return of that activated species to lower energy states is accompanied by the emission of electromagnetic radiation. The most commonly used method of generating and sustaining a low-temperature plasma for technological and technical applications is by applying an electric field to a neutral gas or mixture of gases [39, 40]. The main radiation sources used are the metal vapour mercury lamps and excimer lamps.

2.3.1. Mercury lamps

Activation of mercury atoms by electrons is currently by far the most widely used technology in generating UV radiation. Mercury is the most volatile metal element for which activation in the gas phase can be acquired at temperatures compatible with the structure and materials of the lamps. Additionally, it has an ionization energy low enough to enable an "avalanche effect," a chain reaction underlying the electrical discharge [20, 28, 40, 41].

The most common filler gas is argon, as well as, inert gases. These gases have completed outer electron shells and high ionization energies. The ionization energy of argon is 15,8 eV, but the lowest activated metastable state is at 11,6 eV. The energy of this metastable state can be lost by collision with a mercury atom, ionization of the latter can take place and this can be followed by emission of radiation. When the energy of the metastable state is higher than the ionization energy of mercury, the whole constitutes a Penning mixture. Penning mixtures are possible with mercury, argon, neon, helium, but not with krypton and xenon. The role of the filling gas is not only to facilitate the starting of the discharge but also to promote the starting activation-ionization of the mercury [20, 28, 40, 41].

2.3.1.1. Low pressure mercury lamp technologies

The low pressure mercury lamp (LP Hg) for the generation of UV radiation is normally operated at a total gas pressure in the range of 10^2 to 10^3 Pa, the carrier gas is in excess in a proportion from 10 to 100. In practice, the low pressure mercury lamps are supplied by alternative current sources, with a cathode and anode side constantly alternating. The effect of fluctuations in voltage of the electrical energy supply is a direct increase of efficiency on the UV output yield of this lamps.

Temperature outside of the lamp has a minimal effect, however in order not to affect the equilibrium vapour pressure of the mercury along the inner wall of the lamp is recommended an optimum temperature of around 40°C [40].

In water treatment practice the lamps should be mounted within a quartz tube preferably with open ends through which air is circulating freely to moderate the effect of cooling by water. The spectrum of low pressure mercury lamps is concentrated at a limited number of well-defined lines and the source is called monochromatic. The resonance lines at 253,7 and 185 nm are by far the most important, the normalized emission spectrum of a low pressure mercury lamp is presented in Figure 2.4.

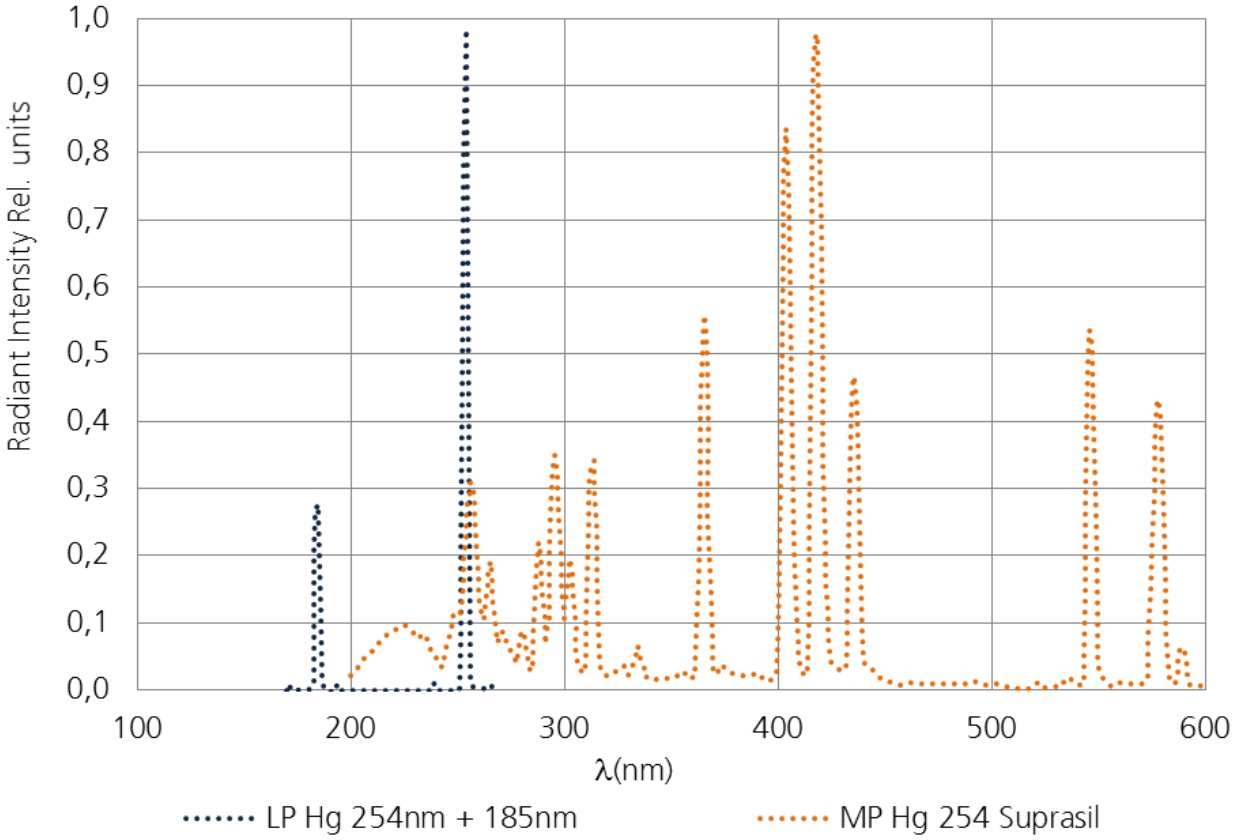

Figure 2.4 Emission spectrum of low-pressure and medium pressure Hg Lamps (redrew from) [42]

The 253,7 nm line represents around 85 % of the total UV intensity emitted and is directly useful for disinfection. The 185 nm line represents the remaining 15 % of the UV intensity and is responsible for the formation of Ozone if in contact with air. Radiation at 185 nm in contact with water lead to the generation of hydroxyl radicals. There are in the market lamps which eliminated the 185 nm light by using appropriate lamp materials such as optical glass or quartz doped with titanium dioxide [40].

2.3.1.2. Medium pressure mercury lamp technologies

The medium pressure mercury lamp (MP Hg) operates at a total gas pressure range of 10^4 to 10^6 Pa and at temperatures of 6000 K. All the mercury within the lamp enclosure is gaseous. In stable operation the temperature in the main body of the lamp is in the range of 600 to 800°C. These operating temperatures make the use of an open (possibly vented) quartz enclosure of the lamp absolutely necessary to avoid direct contact of the surface of the lamp with water.

The emission of medium pressure mercury lamps is polychromatic and results from a series of emissions in the UV region and in the visible and IR range as well. 30% of the emitting light is in the UV-

C range useful for photo induced AOP or disinfection, the remaining 60 % is UV-B, UV-A and IR. The normalize emission spectrum at 200 to 600 nm can be observed in the Figure 2.4. In the medium pressure technologies, the continuum around 220 nm probably is due to barracking effects by collisions of atoms and electrons. If the goal is disinfection and not photochemical oxidation, the entire range under 220 nm can be cut off by the material of the lamp enclosure.

2.3.2. Excimer DBD lamps

An excimer (originally short for excited dimer) is a short-lived dimeric or heterodimeric molecule formed from two species, at least one of which has completely filled valence shell by electrons (for example, rare gases). In this case, formation of the dimer molecule is possible only if such atom is in an electronic excited state. Hetero-nuclear molecules and molecules that have more than two species are also called exciplex molecules (originally short for excited complex). Excimers are often diatomic and are composed of two atoms or molecules that would not bond if both were in the ground state. The lifetime of an excimer is very short, on the order of nanoseconds [43].

The first excimer lamps mentioned in the literature were small VUV sources used for spectroscopic purposes [44]. The reasonably wide second excimer continua of the rare gases were used as background radiation for absorption measurements in the VUV range between 70 and 180 nm. Lately powerful efficient VUV excimer lamps were developed that have found new important industrial applications. Excimer formation is directly dependent on collision, therefore high excimer formation is favoured by high collision rates, which only can be obtained by high pressure and efficient excitation or ionisation of precursor species, meaning non-equilibrium discharge.

Dielectric barrier discharge (DBD) is characterized by the presence of at least one insulating layer in contact with the discharge between two planar or cylindrical electrodes connected to a power supply [45, 46]. A summary of the principal excimer DBD lamp configuration, electrode and shape arrangements is shown in the Figure 2.5.

In Figure 2.5 A the different possible configurations of the electrodes and Dielectric Material (synthetic Quartz) in excimer discharge are shown. In Figure 2.5 B the co-planar lamp configuration is presented. Here the electrodes are placed in parallel planes and not in contact with the excimer gas. In Figure 2.5 C the co-planar lamp configuration with alternating electrodes placed in one plane is presented, this configuration is common used as backlight for computer screen monitors where the radiation generated in the discharge gap is absorbed by a phosphor coating which emits visible light. In Figure 2.5 D the simple linear tubular DBD configuration is presented. In Figure 2.5 E and F the actual lamp

outer vessel carries a centrally aligned second dielectric tube containing a centre electrode. Both electrodes and tubes are oriented coaxially gibing the name to this lamps.

The main characteristics of excimer DBD lamps are listed below:

- The generation of the excimer is almost independent on the gas temperature, therefore excimer DBD lamps do not require a warm up time and can be reignite anytime.
- The excimer DBD lamp output is available instantly (on-off operation).

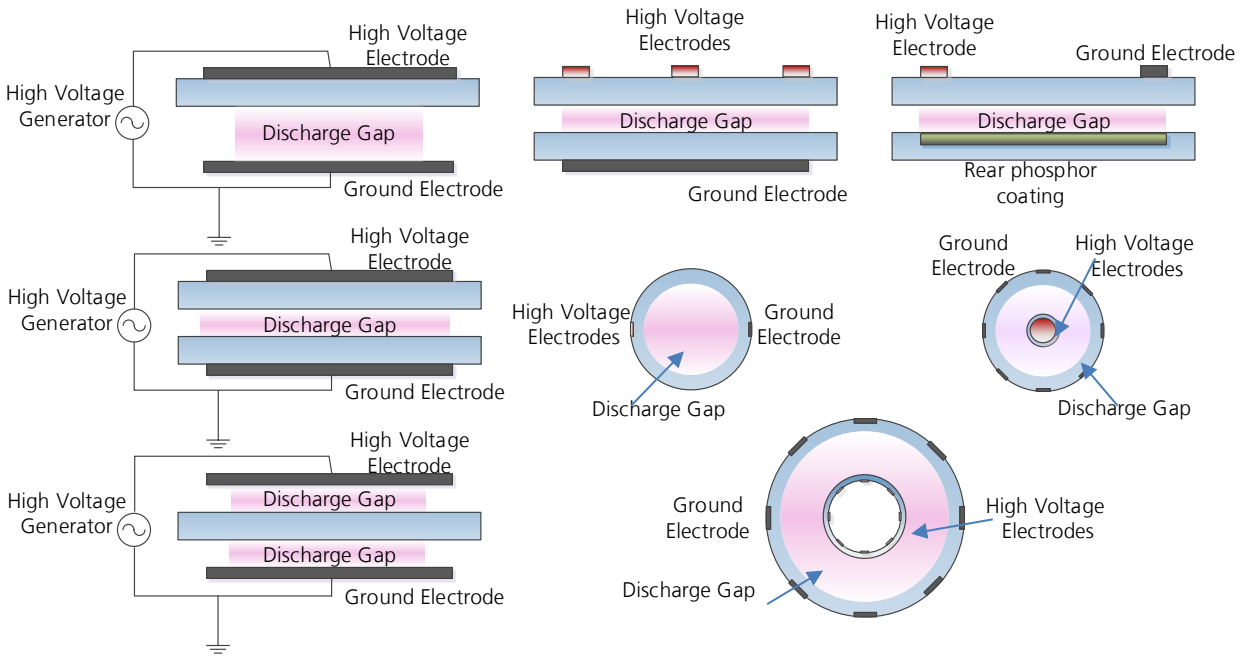

Figure 2.5 Excimer DBD Lamp configuration, electrode and shape arrangements (redrew from) [46, 47]

- Electrodes are not galvanically connected with the gas discharge, which offers a theoretically long lifetime up to 80.000 hours [48].
- The most efficient excimer DBD lamps operate with noble-gas or noble-gas halogen fillings. They are mercury-free which makes them especially environmentally friendly.
- Depending on the gas or gas mixture used the VUV/ UV output to electrical input efficiency of Xe excimer DBD lamps can theoretically be as high as 78 %). Efficiencies of up to 58 % and 60 % were already experimentally verified [46, 49].
- The optical output spectral distribution of excimer DBD lamps is mostly very narrow which is beneficial to wavelength-selective processes.

- The spectral output can be tailored by selecting from a variety of excimer gases and gas mixtures or by transferring the radiation spectrum to longer wavelengths by a coating.
- Excimer DBD lamps may be constructed in a broad variety of possible geometries. Linear, coaxial and plane configurations are already available as commercial products or are in research state.

Dielectric-barrier discharges in high density rare gases operated at about 0.1 MPa, they can efficiently convert electron kinetic energy in electronic excitation energy. The Table 2.2 shows the excimer emission which can be obtained from the excitation of rare gases or a mixture halogen-rare gases in DBDs. It is reported in literature that best results are obtained with high voltage, short-pulse excitation. There are several studies [46, 47], related to the development of an optimized power supply for excimer lamps which delivers the high voltage in short-pulses in the exact combination to have the highest efficiency.

Table 2.2 Halogen dimers and rare gas halide excimers which can be obtained from halogens and rare gases and their corresponding emission [50]

Rare Gas		He	Ne	Ar	Kr	Xe
Halogen						
		74nm	83nm	126nm	146nm	**172nm**
F	157nm		108nm	193nm	248nm	354nm
Cl	259nm			175nm	222nm	308nm
Br	289nm			165nm	207nm	282nm
I	341nm				190nm	253nm

The most studied rare gas excimers are those of Argon, Krypton, Xenon and their halide excimer with chlorine. Their emission lines in the range from 100 to 400 nm is represented in the Figure 2.6.

Many investigations [46, 49, 51, 52] show Xe_2* as the most effective excimer system. Conversion efficiencies were reported to be approximately 60% with pulsed high voltage operation.

Although excimer DBD lamps are usually described as under development [28] a wide variety of excimer-based UV and VUV lamps are commercially available. The 20 W to 100 W tubular Xeradex® manufactured by Osram generates a 172 nm irradiance of 40 and up to 80 mW/cm² (just possible under active cooling and reduced lifetime) at a lifetime of 2500 hours. Heraeus Noblelight offers similar lamps with irradiance of 50 mW/cm² at 172 nm. Ushio offers the same irradiance with its comparable tubular compact excimer UV lamps and for industrial applications an array of lamps for a large irradiation unit with an irradiance of 40 mW/cm² across an operation width of 220 cm.

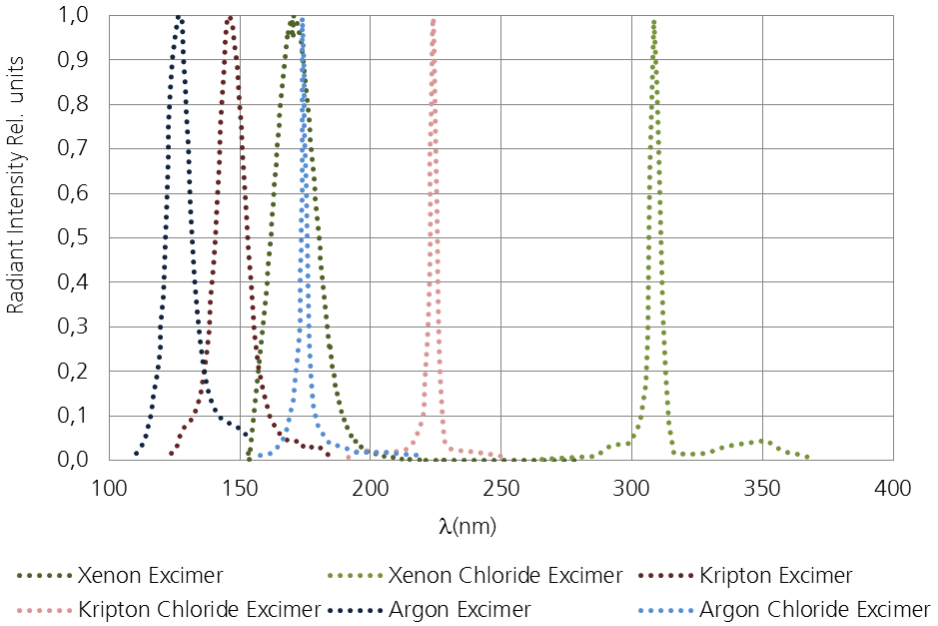

Figure 2.6 Emission spectra of various excimer lamps (redrew from) [50, 53-55]

The CiMAX lamp from Ushio generates up to 100 mW/cm² irradiance at a lifetime of 1000 hours. The QEX1600 lamp from quark-tec generates VUV irradiance of 70 mW/cm² at a lifetime of 2500 hours. The tubular UVS 172-01® system of UV Solutions Inc. is a corona discharge tube offering an outstanding radiation power of 700 mW/cm (length).

The German Company IOT GmbH provides the Excirad radiation system having active widths of 10 to 250 cm and a radiation power of 30 mW per cm unit length [46]. The Table 2.3 summarises the commercially available Xe excimer-based DBD lamps emitting VUV at 172 nm.

Table 2.3 Summary of excimer-based DBD VUV lamps commercially available. [46]

Manufacturer	Name	Power [W]	Life time [hours]	Intensity [mW/cm²]
OSRAM	Xeradex®	20-100	2500	40-80
Heraeus	Noblelight	20-100	2500	50
Ushio	CiMAX	40	1000	40-100
quark-tec	QEX1600	20	2500	70
UV Solutions Inc	UVS 172-01®	20	1000	70
IOT GmbH	Excirad	20-50	1000	30

2.3.2.1. Xenon DBD excimers in AOPs

The xenon excimer emission shows a broad band in the VUV region ranging from wavelengths of 160 nm to 200 nm. The xenon excimer emission shows a pick at a wavelength of 172 nm with a full width at half maximum (FWHM, half-width) of 14nm. Nearly no other emission is present (0,07%UV, 0,22%VIS and 0,78%NIR) [56].

The radiation emitted by the Xenon DBD excimer interacts with water during the absorption process. This absorption process refers to a reduction of the intensity of the radiated energy as a result of an energy conversion in the medium. When a molecule or atom absorbs UV radiation its electronic state changes. This excited singlet state can result in one of three effects described below.

- Return to the ground state either by emission of a photon (fluorescence) or by converting the excess energy to heat (internal conversion).
- Transform to a 'metastable' long-lived triplet excited state (conversion, called intersystem crossing), which can then emit a photon (phosphorescence) or convert the excess energy to heat.
- Undergo chemical reaction (i.e., photochemistry) with quantum yields (ϕ_λ) from the excited state (either from the initially formed state or from the lowest triplet state). Photochemistry involves breaking or rearrangement of chemical bonds in the molecule.

At the radiation emitted by the Xenon DBD excimer 172 nm, water absorbs strongly. The decadic absorption coefficient value most use in the Literature for pure water at 172 nm is 550 cm^{-1} [57]. Assuming 99% of absorption and using the Beer-Lambert equation and the decadic absorption coefficient the theoretical penetration of radiation can be calculated as 36 µm.

The photolysis of water molecules by VUV irradiation, starts with the absorption of the photon, this energy is used to undergo a chemical reaction, which products are hydrogen and hydroxyl radicals as major primary species, in addition a small amount of hydrated electrons and hydrogen ion following the equation [23, 32]. The whole generation takes place in the theoretical layer of 36 µm.

$$H_2O + UV \rightarrow {}^{\bullet}OH + H^{\bullet} + e^-_{aq} \qquad \textbf{(2.4)}$$

the quantum yield of the reaction in liquid phase at a wavelength of 172 nm is 0,42 mol of $^{\bullet}OH$ per mol of photons absorbed [23, 58]. The water photolysis in liquid phase starts at wavelengths below 190 nm and its quantum yield sharply increases with decreasing wavelengths reaching the unity around 123 nm [32, 59].

$$H_2O_{(g)} + UV \rightarrow {}^{\bullet}OH + H^{\bullet} \qquad \textbf{(2.16)}$$

The irradiation of water vapour leads to photolysis producing hydrogen and hydroxyl radicals; the quantum yield of this reaction is reported to be unity for wavelengths below 190 nm [60].

The photolysis of water process is of great interest for practical applications, in this study we focus on the formation of the highly reactive •OH which is one of the most efficient oxidants and the base of the advanced oxidation processes as described before.

Xenon excimer emission has been used in different studies for water photolysis in water treatment; the typical experimental configuration is characterized by the presence of at least one dielectric (VUV transparent quartz Suprasil or similar in quality) and a discharge gap between two electrodes. In this configurations the medium to be treated is in direct contact with the VUV transparent dielectric (Lamp body) and can be in direct contact with one of the electrodes.

Theoretically, the coupling of the excimer radiation and the photochemical oxidation process in one unit can be distributed in two main arrangements; Flow channel - transparent electrode - discharge gap – electrode or electrode – flow channel – discharge gap – electrode. Two main tubular radiation geometries can be found in the literature, the outward directed radiation or the inward directed radiation systems, these geometries are presented in the Figure 2.7.

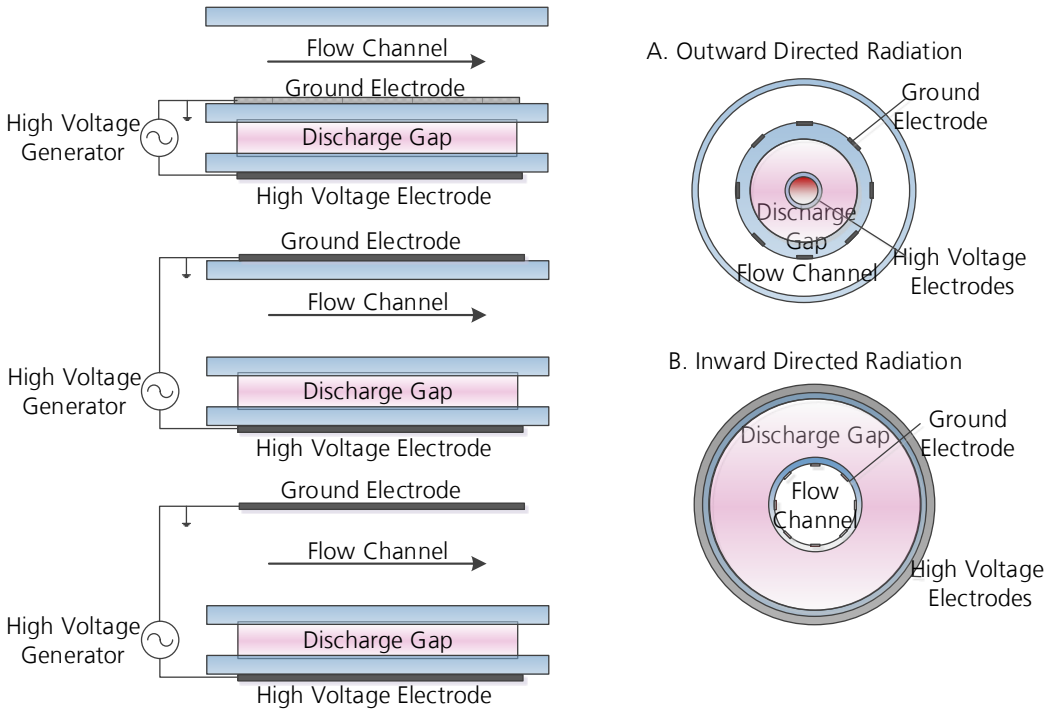

Figure 2.7 Various excimer DBD Lamp/reactor configurations in AOPs (redrew from) [20, 21]

Although there is an existent flexibility for constructing different geometries using DBD excimer lamps, there is no evidence that other geometries have been used to investigate the oxidation of pollutants with xenon excimer technologies [20, 21, 23].

The manufacture of the electrode must be adjusted to the desired radiation direction of the Lamp/reactor system, by use of UV-reflecting aluminium as an outer electrode for inward directed radiation and a net like inner electrode, or by use of a net-like as an outer electrode for outward radiating lamp. These single lamp-reactor configurations (inward and outward directed radiation) can be found in the most relevant studies in literature [20, 22, 23, 61, 62]. The annular discharge gap used by Oppenländer and Baum [20, 61] represented in the Figure 2.8 (B. Inward Directed Radiation) consist of a cylindrical inner tube of Suprasil quartz that is surrounded by an outer tube with a slightly greater diameter. Thus, the hermetically sealed discharge gap is produced that contains the excimer gas, the inner electrode usually consist of a metal wire or optionally of metallic static mixer.

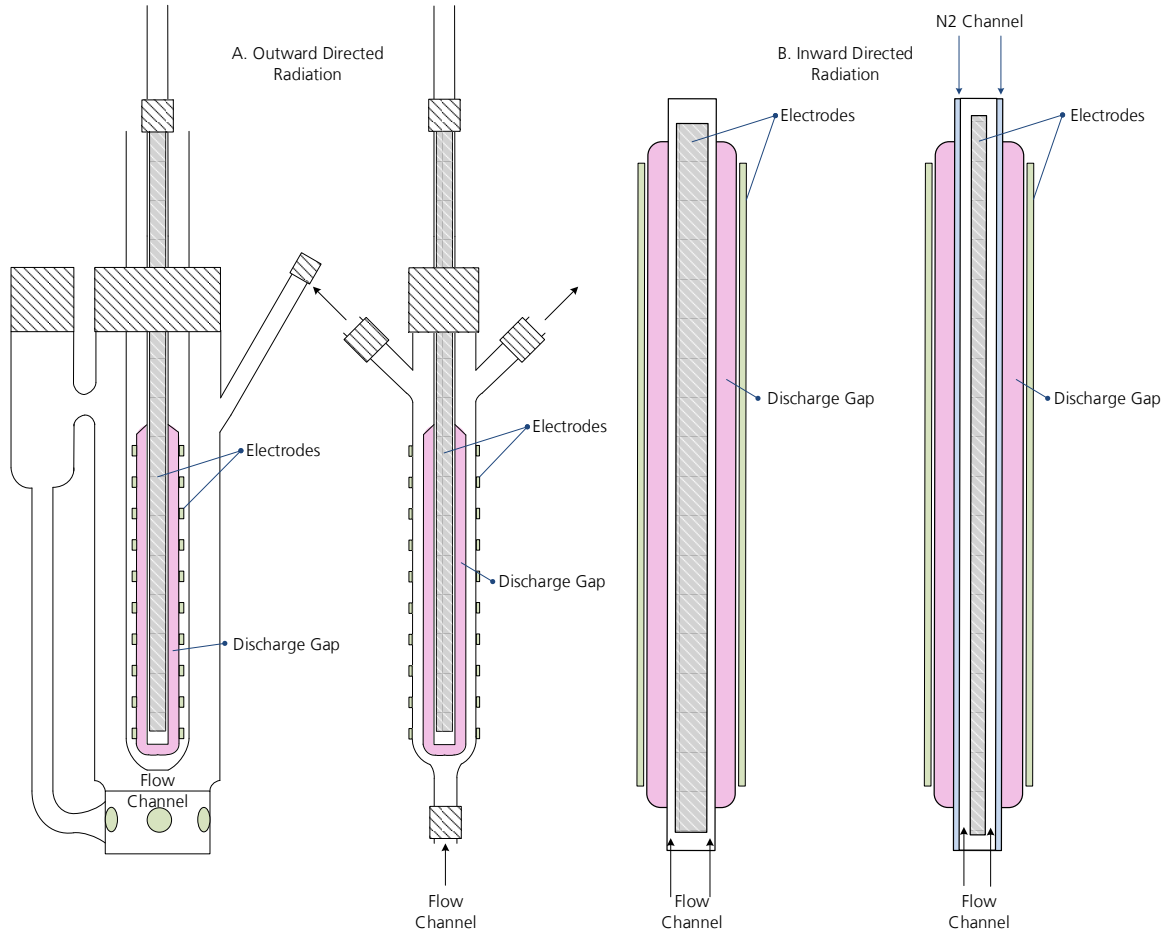

Figure 2.8 Schematic representation of an annular (coaxial) incoherent excimer VUV source with inward and outward directed radiation (redrew from [20, 23, 58, 63])

Gonzalez and Braun [62] used a cylindrical Xe excimer lamp of 25 cm length and 3 cm external diameter developed by ABB (Baden, Switzerland) emitting 172 nm as the irradiation source (A. Outward Directed Radiation). The photochemical reactor was of annular geometry with volume 220 mL. Further studies presented in the Literature review are based or were performed using the described setup from Oppenländer and Braun.

Due to the short life time of the primary radicals generated in the illuminated zone, the ideal mixing assumption required during collimated beam studies cannot be used. Certainly, lack of sufficient mixing would result in a deviation from the preferred kinetically-controlled reaction regime; lack of sufficient mixing has as a consequence a mass transfer controlled process (Diffusion controlled). Devices used to produce the current literature in the field were not taking into account the relation of channel thickness (in mm) and photo reaction zone (in μm); the formation of a boundary layer even under turbulent regime of flow larger than the photoreaction zone is highly probable where the ratio channel thickness photo-reaction zone is large. Without analyzing this situation and overcoming a possible lack of mixing, the current literature in the photo-induced AOP may not be representative of reaction kinetics [24].

The mismatch between reactor gaps and light penetration of the above mentioned VUV photo reactors with an annular fluid gap in millimeters and a photoreaction zone in micrometers, has a result that they may be working under the maximum potential for oxidation efficiency, the generation of a boundary layer larger to the active photoreaction zone, producing a zone were highly active radicals are being formed but not reaching the target pollutant which reach the photoreaction zone just by diffusion. This thesis has as objective the characterization of the channel thickness influence as well as other important aspects of the VUV process by developing new more flexible reactor geometries and configurations.

3. Quantifying the heterogeneity of reaction zone, relation of channel thickness in the oxidation process and mixing enhancement

3.1. Introduction

In this section, the spatial behavior of the photo-induced photolysis phenomena was studied. An alternative flat design to the standard annular flow apparatus (Figure 3.5) is developed and investigated in this section of the thesis to enable the study of the different phenomena in the water photolysis under 172 nm radiation and the VUV photo induced AOP.

A special feature which differentiate the flat design from the standard annular flow reactor is the option to have different channel thicknesses in the range of 25 to 1500 µm. Different operational flows can be as well studied. The UV light is delivered by a commercial excimer OXRAM system containing two lamps in aluminum housing with special UV reflectors for homogeneous radiation. The flat reaction chamber is attached to the commercial system and radiation reach the flat reaction chamber through a synthetic quartz glass window. This new apparatus allows the study of the interaction of channel thickness and flow as well as the effects of mixing in the performance of oxidation processes by water photolysis. Degradation of Methylene Blue as a model pollutant in deionized water was investigated.

First, the primary concepts, equations and optical constants are described. Then, a mathematical model is defined and used to study the penetration of radiation and the spatial generation of hydroxyl radicals. Afterwards, experiments were conducted following a combination of full factorial design with a response surface methodology for the analysis of the trials. Two factors with a different number of levels were established.

The experiments were performed in order to macroscopically characterize the system and study the correlation between different operational parameters.

Finally, a brief description of the interaction of the main products of the photolysis with the media and organic and inorganic substrates is presented. The importance of the mixing conditions for the advanced oxidation of pollutants application is explained and quantified.

Different methods of mixing enhancement were studied and modeled and an experimental validation of the concepts used was performed and analyzed.

3.2. Fundamental principles of photo chemistry

In order to characterize the VUV process in aqueous systems using radiation emitted by a Xenon DBD excimer, it is important to define first some basic concepts. Fundamental principles of photo-chemistry and photo-physics related with the interaction of UV radiation with matter will be briefly discussed.

Physical and chemical phenomena like reflection, refraction and scattering as well as, absorption are defined as:

- Reflection: it is the change in direction of an electromagnetic wave at an interface between two different media so that the electromagnetic wave returns into the medium from which it originated. Whenever light passes through an interface between two media of different refractive index, a certain fraction of the light is reflected at the angle $\Theta_r = \Theta_1$ (see Figure 3.1 below); the rest passes through the interface into the second medium and undergoes refraction [28]
- Refraction: it is the change in direction of an electromagnetic wave due to a change in its speed. This is most commonly observed when an electromagnetic wave passes from one medium to another at any angle other than 90° or 0° [28]

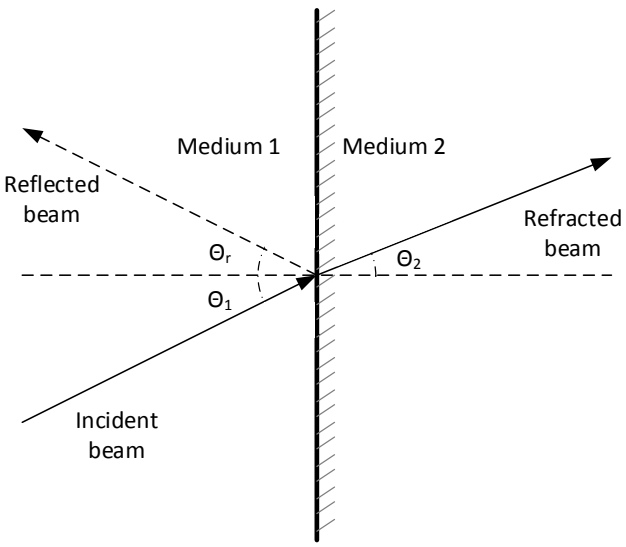

Figure 3.1 Reflection and refraction as a light beam passes from one medium to another [28]

- Absorption: it refers to a reduction of the intensity of any form of radiated energy as a result of energy conversion in a medium. When light is absorbed in a medium it causes changes in the electronic state of components in the medium (electronically exited state of the components) [28]

3. Quantifying the heterogeneity of reaction zone, relation of channel thickness in the oxidation process and mixing enhancement

---

- Absorbance A_{10} : it is a measure of the capacity of a substance to absorb light of a specified wavelength. The logarithm to the base 10 of the ratio of the spectral radiant power of incident essentially monochromatic radiation E_{λ}^{0}, to the radiant power transmitted radiation $\mathrm{E}_{\lambda}^{\mathrm{trans}}$ [28]

$$A_{10} = \log \frac{\mathrm{E}_{\lambda}^{0}}{\mathrm{E}_{\lambda}^{\mathrm{trans}}} \quad \textbf{(3.1)}$$

- Transmittance: Internal transmittance refers to energy loss by absorption [64]. The ratio of the transmitted spectral radiant power $\mathrm{E}_{\lambda}^{\mathrm{trans}}$ to the incident on the sample E_{λ}^{0} [28]

$$\mathrm{T} = \frac{\mathrm{E}_{\lambda}^{\mathrm{trans}}}{\mathrm{E}_{\lambda}^{0}} \quad \textbf{(3.2)}$$

- Spectral Radiant Power E : it is by definition the quantity of energy crossing a surface bounded by a closed curve per unit time for a specific wavelength:

$$\mathrm{E} = \frac{\mathrm{dQ}}{\mathrm{dt}} \quad [\mathrm{W}] \quad \textbf{(3.3)}$$

  For any source, this quantity E is the total power emitted in all directions by the radiant source. It is equal to the total power crossing a spherical surface enclosing the source [28, 65].

- Irradiance I : Irradiance is related to the power received per unit area of a receiving surface:

$$\mathrm{I} = \frac{\mathrm{dE}}{\mathrm{dA}} \quad [\mathrm{W/m^2}] \quad \textbf{(3.4)}$$

  The surface is not the surface of the radiation source, it is the surface of the receiving body (detector, photo-reactor, etc.). Irradiance express the power density received by a surface [28, 65].

- Dose: Irradiation dose or exposure is defined as the radiation absorbed by an irradiated object, it is expressed in J/m^2 and measures the quantity of energy received per unit surface perpendicular to the direction of propagation. This quantity is also the product of the irradiance expressed in W/m^2 and the duration of the irradiation in seconds, for uniform irradiation [28]
- Photon: it is defined as an elementary excitation of a single mode representing a quantum of light or other electromagnetic radiation. A photon carries energy proportional to the radiation frequency but has zero rest mass. The energy carried by a photon is equal to $\mathrm{h}\nu_{\lambda}$ where h is the Plank's constant and is the frequency of the photon at the specific wavelength.
- Photon flow: The photon flow of a radiation source can be described by:

$$\mathrm{E_P} = 8{,}3593 \left[\frac{\mathrm{mol}}{\mathrm{Wms}}\right] \times \mathrm{E}^{\mathrm{Lamp}}[\mathrm{W}] \times \lambda[\mathrm{m}] \quad [\text{mol per second, mol s}^{-1}] \quad \textbf{(3.5)}$$

For modeling of the process it is necessary to follow the Intensity of the radiation spatially; the intensities of the incident and the transmitted beam are correlated by the Beer-Lambert law, which quantitatively describes the attenuation of radiation by transmitting into an absorbing medium [20, 28].

$$A_{10} = \log \frac{E_{\lambda}^{0}}{E_{\lambda}^{trans}} = \log \frac{1}{T} = -\log T = \varepsilon_{\lambda} cl \qquad (3.6)$$

Where,

A_{10} is the decadic absorbance of a beam of collimated monochromatic radiation in a homogeneous isotropic medium;

E_{λ}^{0} is the incident spectral radiant power;

E_{λ}^{trans} is the transmitted spectral radiant power;

T is the transmittance, which is defined as the ratio of the transmitted spectral radiant power to that incident on the sample;

ε_{λ} is the molar decadic absorption coefficient in $Lmol^{-1}cm^{-1}$;

c is the concentration of the substrate in mol L^{-1};

l is the thickness of the solution traversed by the UV radiation;

- Molar decadic absorption coefficient ε_{λ}: it is defined as the absorbance divided by the absorption path-length, l , and the amount of concentration, c :

$$\varepsilon_{\lambda} = \frac{A_{10}}{cl} \quad [M^{-1}\ cm^{-1}] \qquad (3.7)$$

- Decadic absorption coefficient a: it is defined as the absorbance divided by the optical path-length. Since absorbance is a dimensionless quantity, the coherent SI unit for a is m^{-1}; the common unit is cm^{-1}.

$$a = \varepsilon_{\lambda} c = \frac{A_{10}}{l} \quad [cm^{-1}] \qquad (3.8)$$

Optical properties of water have been studied since the beginning of the spectrometry, the most relevant literature in terms of decadic absorption coefficient of water is presented in the following Figure 3.2. Four different methods have been reported in literature; each method is suitable for a specific range of wavelength, depending on the behaviour of the absorption process, the complete analysis of the decadic absorption coefficient will be discussed in chapter 5.

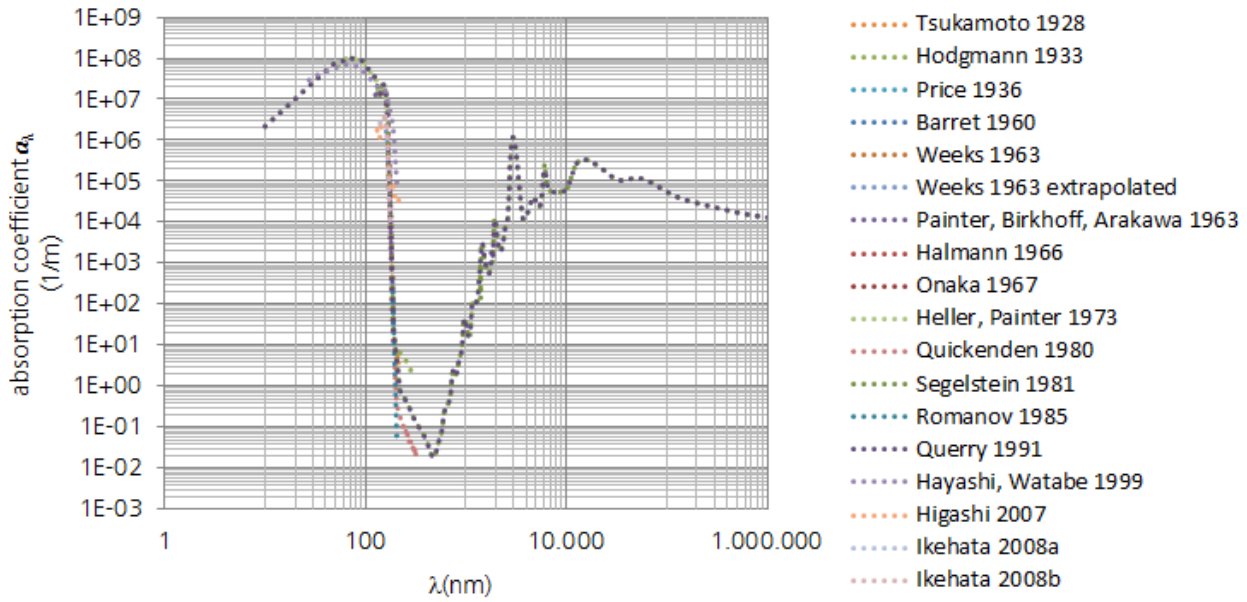

Figure 3.2 Decadic absorption coefficient of liquid water. Redraw different authors [33, 57, 66-74]

In order to model the penetration of light the decadic absorption coefficient of water in the range of work is needed. The following Figure 3.3 shows the authors who published optical properties of water in the range of study.

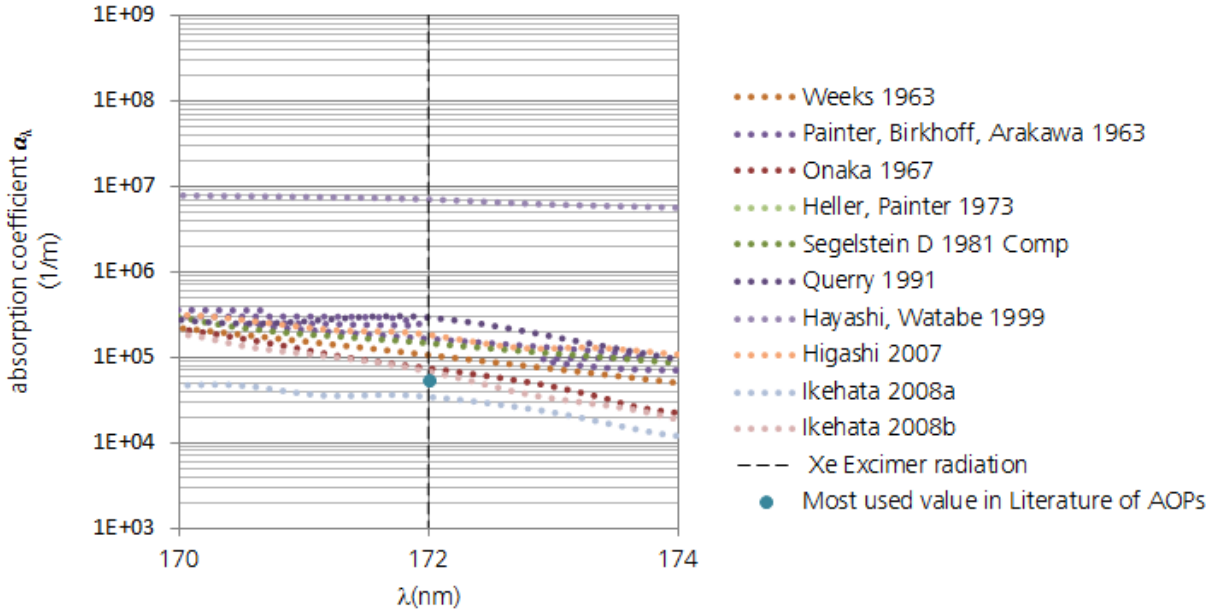

Figure 3.3 Decadic absorption coefficient of liquid water at 172 nm "monochromatic" Xe excimer radiation. Redraw different authors [33, 57, 66-74]

The most used value of absorption coefficient of water at 172 nm is 550 cm^{-1}. Using the Beer-Lambert law and assuming 99% absorption of VUV radiation at 172nm, it is possible to calculate the theoretical penetration of radiation.

$$A_{10} = \log\frac{E_\lambda^0}{E_\lambda^{trans}} = \log\frac{100\%}{1\%} = 2; \quad l = \frac{A_{10}}{a} = \frac{2}{550\ cm^{-1}} = 0{,}00364\ cm$$

The value of 36,4 µm represents the theoretical photo-reaction zone of the VUV oxidation process [20]. The Figure 3.4 is a graphical representation of the photoreaction zone.

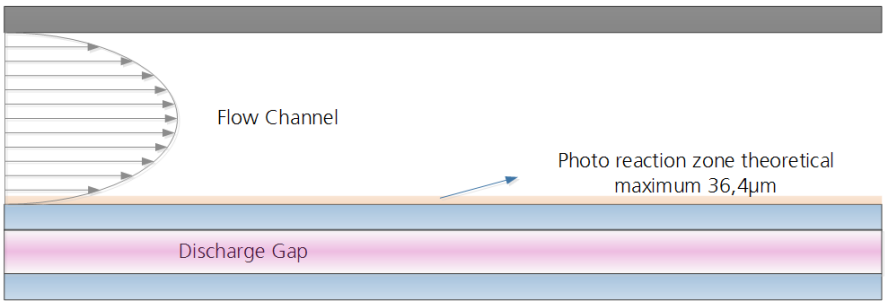

Figure 3.4 Theoretical photo reaction zone in the VUV oxidation process

This phenomena was indirectly verified by Heit and Braun (1997) measuring the spatial resolution of dissolved molecular oxygen concentrations during VUV photolysis of aqueous systems using a miniaturized oxygen optode [75]. The result of this study confirmed the existence of a thin film where the oxygen is depleted due to the reaction with the hydroxyl radical generated in the photoreaction zone. In that study it was measured an oxygen depletion zone of about 500 µm from the lamp surface, the authors clarified this phenomenon as a result of the reaction of the long-lived carbon centered radicals produced by the reaction of hydroxyl radicals with organic molecules which after leaving the photoreaction zone react with the oxygen [20, 75]. This strong heterogeneity (photo reaction zone-Bulk dark zone) can lead to a lack of substrate to be oxidized in the photoreaction zone after some centimeters from the inlet. Intensive mixing between the bulk zone and the photoreaction zone must be achieved.

- Quantum Yield ϕ_λ : it is defined as a quantitative measure of the overall efficiency of a photophysical or photo-chemical process [65]. It is a unit-less constant which usually ranges from zero to one; several authors denote it as mol $Einstein^{-1}$ (Einstein = mol photons). Quantum yields greater than one indicate photo-induced chain reactions, which may involve radical species or photo-generation of a catalyst. The quantum yield can be expressed in terms of the reactant or the product. It is usually dependent on the wavelength of the absorbed UV radiation, however

many photo-chemical systems exist that have a constant quantum yield over a defined range [20]. if a system or reaction has a constant and well known quantum yield, this one can be used for the measurement of the absorbed photon flow E_p^{abs} ; this systems are called actinometers, and they are used to measure the absorbed photon flow in photo-reactors of specific geometry and for a well-defined spectral range [20]

$$\phi_\lambda = \frac{dn(M)/dt}{E_p^{abs}} \quad \textbf{(3.9)}$$

The quantum yield for the photolysis of water under VUV at 172 nm was quantitatively measured by Heit and Braun. In their study, the quantum yield or overall efficiency of the photo induced AOP for the generation of hydroxyl radicals was measure to be 0,42 [23].

3.3. Materials and methods

3.3.1. Flat micro channel reactor apparatus

The flat micro channel reactor apparatus used in this study is schematically represented in

Figure 3.5. It consist of two Xe excimer UV lamps contained in a metallic housing with UV reflectors (Xeradex System) emitting homogeneous 172 nm radiation and a custom made flat micro channel reactor with variable channel thickness. The complete system was built to be gas tight to create an oxygen free atmosphere for the efficient use of the VUV radiation.

The channel thickness in the flat micro channel reactor can be modified between 25 and 1500 µm, the radiation reach the reaction channel through a synthetic quartz window 255 cm^2 (170 mm x 150 mm). The flow is uniform along the channel over the synthetic quartz window.

The flat micro channel reactor is connected to a 1L jacketed reactor glassware as reservoir with, a cooling glass column and a gear pump VerderGear VGS096 (Verder, Germany) which controls the flow from 100 to 2400 mL/min range. All tubing and periphery are made of materials with highly crack and stress resistance, low permeability, no moisture absorption and low level of chemicals extractable to assure a wide range of experimental fluids and pollutants.

Concentration of reactants was followed by absorbance measurements, conducted at the wavelength of interest (example 664 nm to quantify methylene blue concentration), using a Thermo Scientific UV-10 UV-Vis spectrophotometer and the software VISIONlite® auto sampler system.

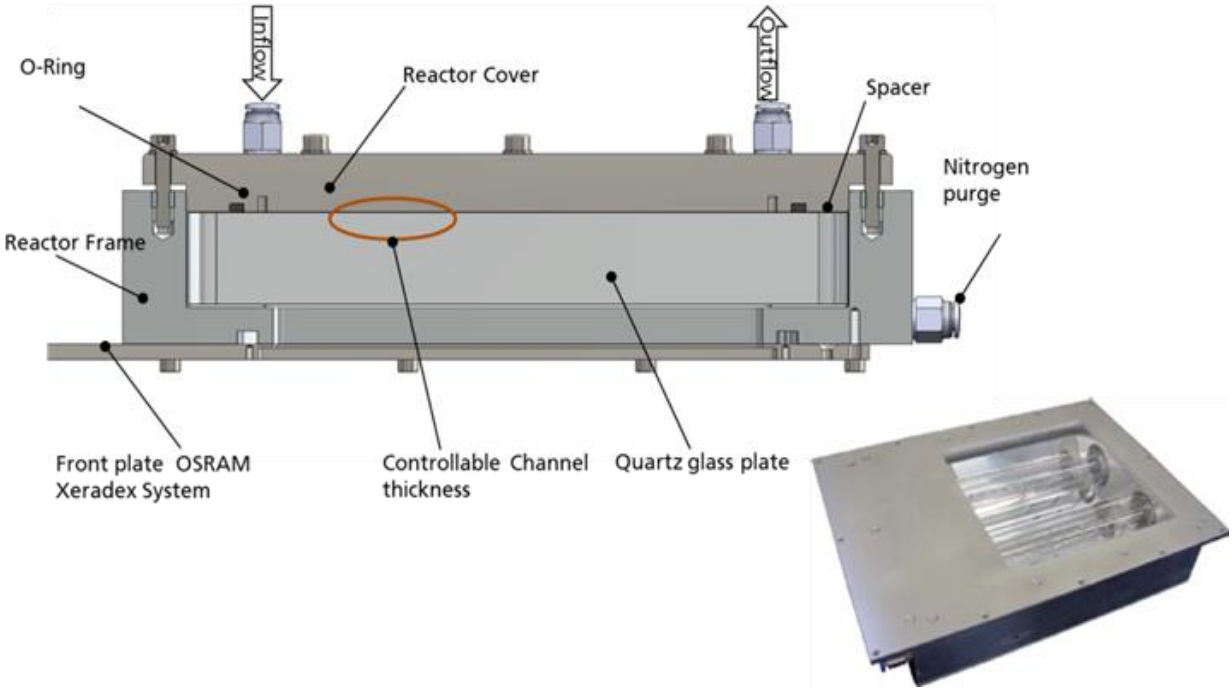

Figure 3.5 VUV AOP Laboratory scale reactor system in this study

The complete set-up and flow loop is represented in the Figure 3.6, the set-up follows the design of a batch photo-reactor system.

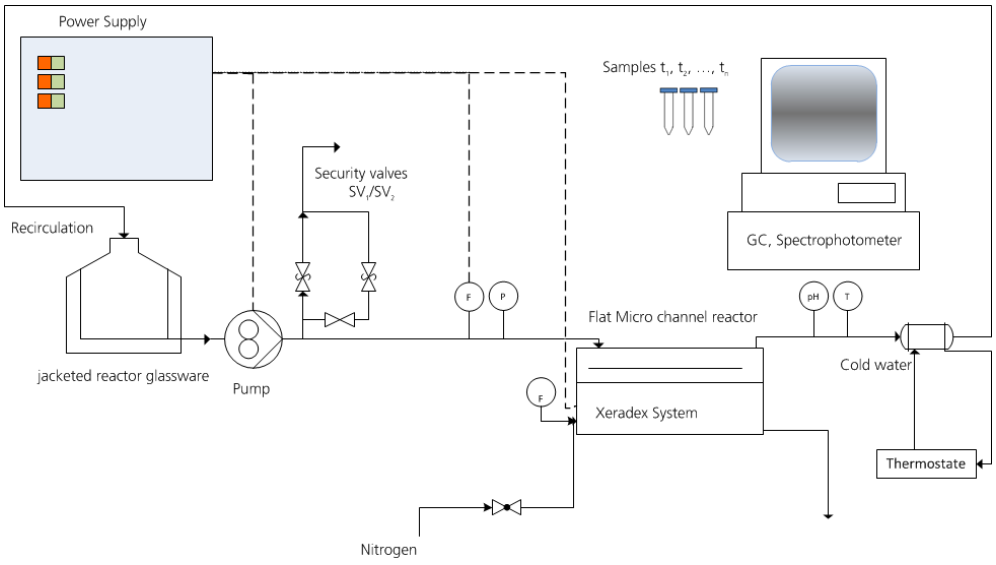

Figure 3.6 Schematic representation of the flow loop used for the study

Here, the solution goes from the jacketed reactor glassware of 1000 ml to the pump passing through the photo-reactor and back to the jacketed reactor, this loop is maintained regulating the recirculation flow velocity.

The whole system can be kept a stabile temperature using the jacket of the reactor glassware as well as the cooling system. The volumetric flow was recorded. The batch configuration has been widely used for the mineralization of pollutants in water in a lab scale.

The Figure 3.7 gives the front view of the set-up and its subunits installed in the laboratory. Special care was taken to prevent the generation of Ozone (no radiation is in contact with oxygen from air) and the efficient use of the radiation emitted by the xeradex system.

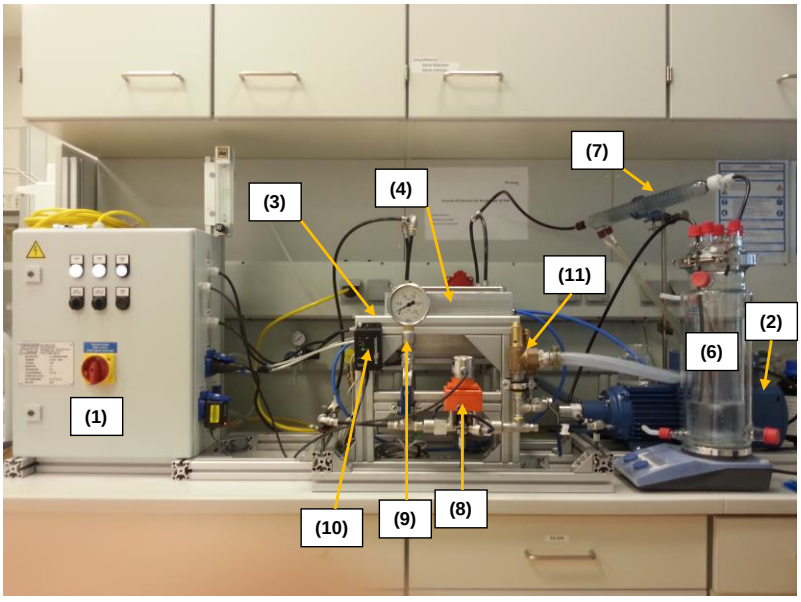

1. Main power supply cabinet
2. Pump (gear pump)
3. Xeradex double lamp system
4. Reactor body
5. Thermostat
6. Jacketed reactor glassware
7. Cooling system
8. Flow sensor
9. Manometer
10. Ozone sensor
11. Security valves

Figure 3.7 Front view VUV AOP laboratory scale reactor system used for the study

3.3.2. Chemicals, experimental procedure and analytics

Methylene Blue (MB) ($C_{16}H_{18}N_3SCl$) is a dark green water soluble and chemical stable powder. Once these crystals are dissolved in water the solution becomes dark blue. MB is harmful and a highly water contaminating chemical (Color). Its main application is the dying of fabrics and paper. Other applications of MB include redox indicator and specific areas of medicine and analytics.

In AOPs, MB has been used as a photosensitizer for a singlet molecular oxygen production [20] and, in this context by means of the degradation behavior as an indicator of the oxidation process

and indirectly to the intensity of the UV radiation. A summary of general information of MB is presented in Table 3.1.

Table 3.1 Reference substance selected for this study

Properties	
Methylene Blue	
Structure	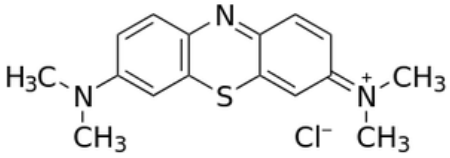
CAS No.	61-73-4
Molecular weight	319,86 g/mol
Water solubility	40 g/L
Uses	It is a dye used primarily fabrics and paper
Initial concentration	25,0 mg/L
Initial TOC theoretical	15,0 mg/L

One liter of MB (Sigma-Aldrich 99% purity) solution was prepared with concentrations of 2 g/L in deionized (DI) water as a stock solution. This was used to prepare the subsequent 1 liter solutions for each experiment 25 mg/L MB concentration. The solution was added into the reactor glassware and recirculated in the system for 2 minutes before starting the UV irradiation.

3.3.2.1. Experiments smooth chamber

The objective of this section was to characterize the operation range of the equipment and evaluate the effect of flow velocity and channel thickness in the degradation of a model component.

During this experimental campaign it was used a smooth chamber with ultra-polished surfaces including quartz glass.

In order to analyze and evaluate the interaction between the channel thickness and volumetric flow in the oxidation process, a combination of full factorial design with a response surface methodology for the analysis of the experiments was used. Two factors with a different number of levels were established Table 3.2.

Three replicates of each experiment were performed and a surface response analysis was done with for the two factors (channel thickness and recirculation flow) at different levels, the experimental points are represented in Figure 3.8.

Table 3.2 Factors, levels and range definition for experimental design

Factors	Levels	Ranges
Volumetric Flow	**5**	**100, 500, 1000, 1400, 2400 mL/min**
Channel thickness	**6**	**75,150, 250, 500, 750 and 1000 μm**

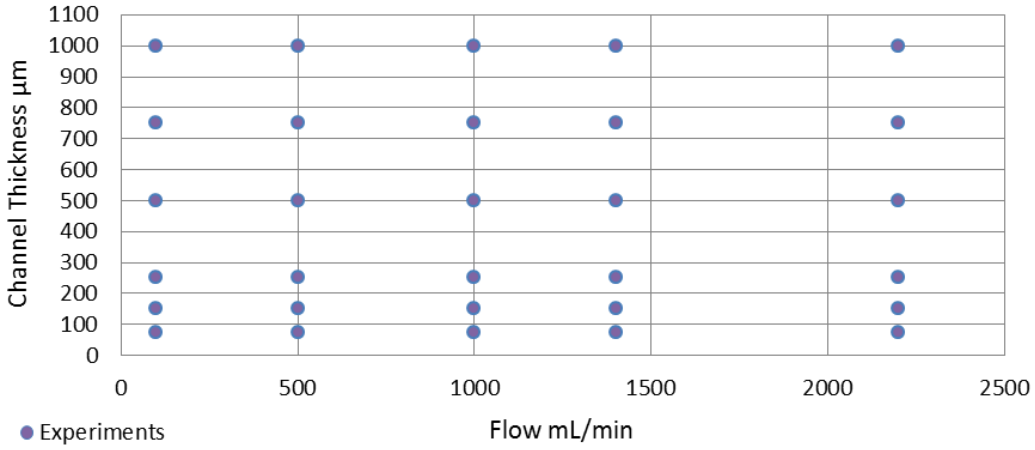

Figure 3.8 Experimental planning

As a response from each experiment was used the initial reaction rate of MB degradation, defined as follow: Δt was defined as 5 minutes of experiment.

$$R_i = \frac{\delta c_{MB}}{\delta t} \cong \frac{\Delta c_{MB}}{\Delta t} \quad \textbf{(3.10)}$$

Using the initial reaction rate as a response, a model can be built to represent the interaction between the two factors. This method is used to identify the optimum response (output variable) which is influenced by several independent variables (input variables).

3.3.2.2. Experiments with mixing enhancement

As it was described, the performance of the VUV AOP process depends on the avoidance of depletion of the substrate concentration phenomena occurring due to the thin photoreaction zone and the limited mixing between the bulk of the fluid and the fluid elements adjacent to the interface quartz water. Therefore two mixing methodologies in flat channels were experimentally studied.

Due to the small characteristic dimension H of the ducts in micro and mili fluidic systems, flows are characterized by low Reynolds number,

$$\mathrm{Re} = \frac{\mathrm{UH}}{\nu} < 100 \qquad \textbf{(3.11)}$$

Independently of the annular shape or flat channel reactor, the characteristic dimension for the calculation of Reynolds is the distance between the quartz glass water interface and the opposite surface (micro and mili range), in this regime and working with small characteristic dimension numbers, flows are laminar, inertial effects are weak, and turbulence does not occur. One consequence of the laminar flow is that two or more streams flowing in contact with each other will not mix except by diffusion.

Concentration of the substrate to be oxidized decrease rapidly in the photo-reaction zone (a few micrometers from the quartz glass interface) and lack of substrate is to be expected after few centimeters from the inlet. After depletion zone is developed the oxidation process is limited to diffusion of the substrate to the photo-reaction zone.

Due to the typical length scale of microfluidic devices, the time for this diffusive mixing often exceeds typical microfluidic processing times which are supposed to be faster for other steps, e.g. transport and analysis. For instance, small solutes with diffusion coefficients on the order of $D = 10^{-9}$ m^2/s, mixing by diffusion across a 500 µm wide channel would result in a mixing time of several minutes.

The introduction of secondary flows that stir the fluid leads a way of decreasing the thickness of the boundary layer and may prevent the formation of a zone of depleted reactive solute or substrate, relative to the above described, uniaxial case in rectangular micro channel Figure 3.4. Secondary flows can be generated in different ways, two main scenarios are analyzed.

3.3.2.2.1. Spacer filled channels

Mass transfer in flat channel modules is usually enhanced by the presence of net-like turbulence promoters; they are mostly used in membrane technology and are called spacers due to the function of keeping adjacent membrane leaves apart to form a feed channel, they also promote the mixing between the bulk of the fluid and the fluid element adjacent to the membrane surface to keep membrane surface relatively clean, this second role is the important effect which is desired in the VUV AOP process. An efficient membrane module performance depends on the efficacy of the spacers to increase mass transport away from the membrane surface to reduce concentration polarization by increasing the shear rate at the membrane surface [76].

The last explained concept can be rewrite as: an efficient VUV-AOP process performance depends on the efficacy of the measures taken to increase mass transport away from the interface quartz-water to reduce concentration depletion in the photoreaction zone by increasing shear rate at the quartz surface.

The woven metal mesh used as net-type mixing promoters are shown in the Figure 3.9, they consist of symmetric wires woven and interlocked; six different net-type mixing promoters for different channel thicknesses were investigated.

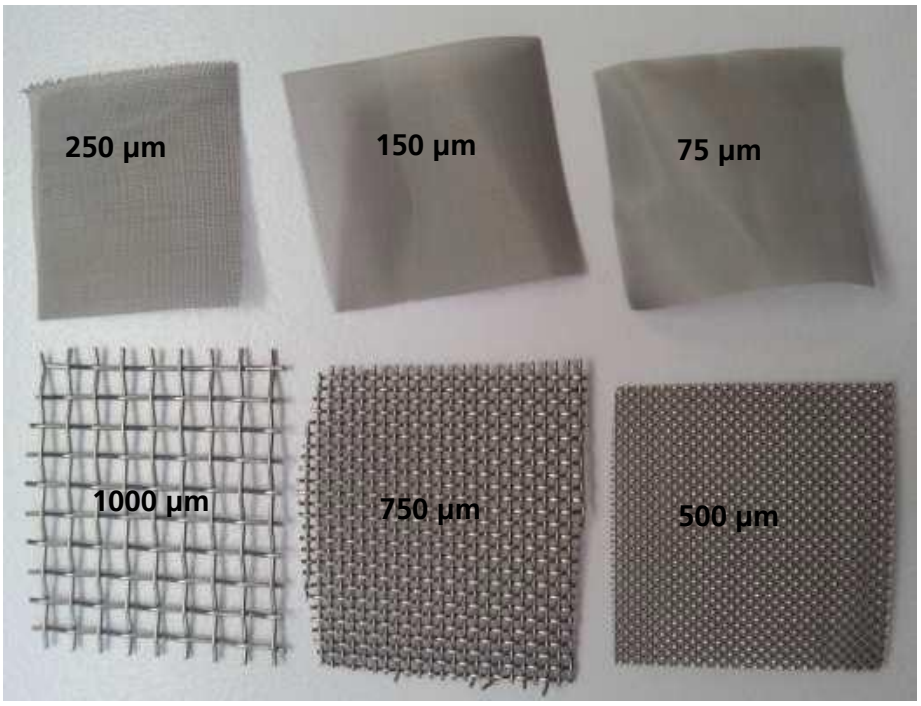

Figure 3.9 Sample of Net-Like mixing promoters used in the experimental setup for each channel thickness

3.3.2.2.2. Grooved channel wall

Mass transfer in flat channel modules can be enhanced by the presence of grooves on one wall of a rectangular channel. This grooved channel wall present an anisotropic resistance (directionally dependent) to viscous flows (low Reynolds numbers); there is less resistance to flow in the direction parallel to the peaks and valleys (direction of the grooves) than in the orthogonal direction. As a result of this anisotropy, an axial pressure gradient along the direction of the grooves generates a mean transverse component in the flow [77].

In other words the grooves in the bottom or top of a channel generate secondary flows in the cross-section. When the pattern of the grooves is constant along the channel, the resulting flow is three dimensional and follows a helical pattern non-chaotic mixing (Figure 3.10 (i)). When the patterns varies, the resulting flow is three dimensional and follows chaotic mixing [78].

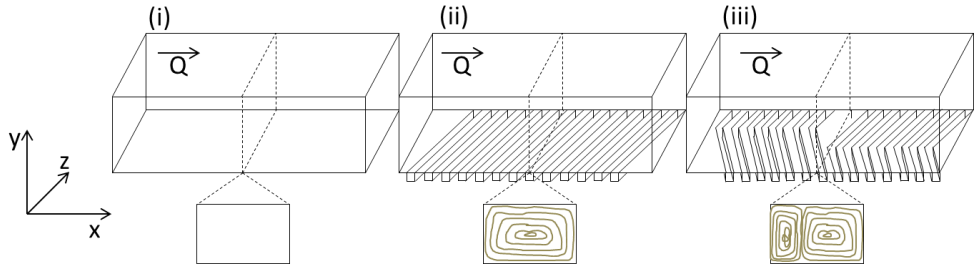

Figure 3.10 Uniaxial, non-chaotic and chaotic representation [79]. (i)) mixing is prohibitively slow, and the length of a channel required for diffusive mixing is on the order of meters. (ii) and (iii)) grooves reduce the time necessary for the mixing process by redistributing the fluids, decreasing the necessary length for diffusion and increasing the probability for solute transport between fluids [80].

Chaotic mixing promoted by Staggered Herringbone grooves on one wall of a channel, also called staggered herringbone mixer SHM has been investigated recently due to its simplicity. The SHM works as follow: in laminar flow regime, where viscous forces dominate (length scales of the flow are very small 10^{1}-10^{3} micrometers), these grooves cause transverse flow in the channel, resulting in two counter rotating vortices along the channel length (Figure 3.10 (iii)).

The vertices of the grooves are offset to approximately one third of the way across the channel width, and each set of herringbones alternates with a complementary set, mirrored across the centerline of the channel, to create a full mixing cycle. This alteration reorients the flow periodically, disturbing the relatively untouched elliptic points in each of the vortices to dramatically improve mixing. The effects of individual half cycle approximate lid-driven duct flow, a non-chaotic process (Figure 3.10 (ii)), however the reorientation of the circulating flow produces chaotic mixing [80, 81].

For the study of the mixing effects in the performance of the VUV oxidation process the following SHM structures grooved in the reactor plates were studied. The structures were grooved in the reactor plates using fine boring tools. The structures are represented in Figure 3.11.

3. Quantifying the heterogeneity of reaction zone, relation of channel thickness in the oxidation process and mixing enhancement

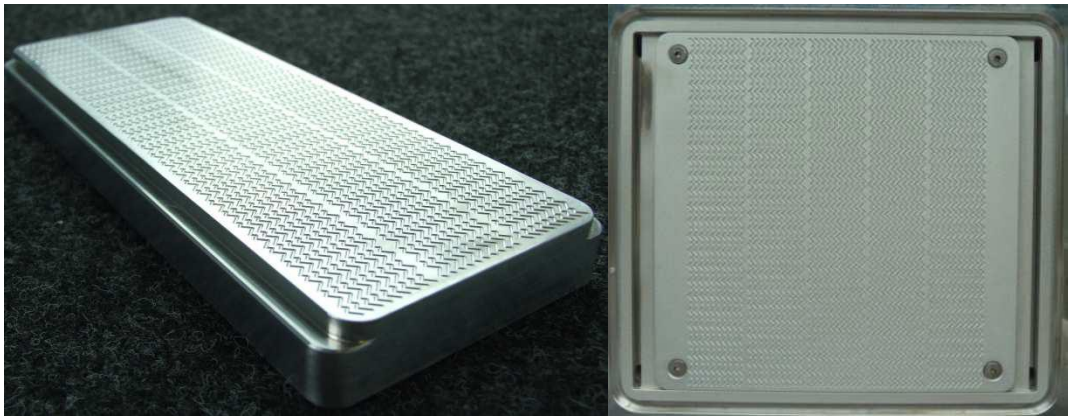

Figure 3.11 Samples of SHM promoters used in the experimental setup

The SHM mixing devices are suitable mixing alternative for continuous flow operation, due to the continuous redistribution of the flow over the entire channel cross section, reducing Taylor dispersion (dispersion phenomena where the solute spreads faster in the direction of the bulk flow), and resulting in a nearly uniform residence time distribution [78].

3.3.2.3. Analytics

25 mg/L solutions of MB (Sigma-Aldrich) were prepared in deionized water for each experiment. Before and during the degradation of the solution samples were taken and analyzed. MB concentrations were analyzed by measuring the absorbance in a 1 cm quartz cuvette at 664 nm wavelength using a Thermo scientific UV-10 UV-Vis spectrophotometer and the software VISIONlite® auto sampler system. Chemical oxygen demand COD of the samples was measured using the MERCK CELL TEST (Photometric test kits); by means of reagent, the component of a sample to be analysed is converted into a coloured compound in a specific reaction. The intensity of the colour solution, measured as the absorbance, is proportional to the concentration of the respective substance in the specific range.

3.3.3. CFD governing equations

Two dimensional CFD simulations were carried out to solve the flow established in the flat micro channel reactor. Comsol Multiphysics 4.3a was used in order to numerically solve the governing equations in Cartesian coordinate system.

The phenomena can be modelled using the Poiseuille flow concept between parallel plates. The Figure 3.12 shows the flow between plates, which is characterized as a pressure driven flow where the

pressure in the inlet is higher than the pressure at the outlet, the velocity profile is independent on time and just depend on the distance to the walls.

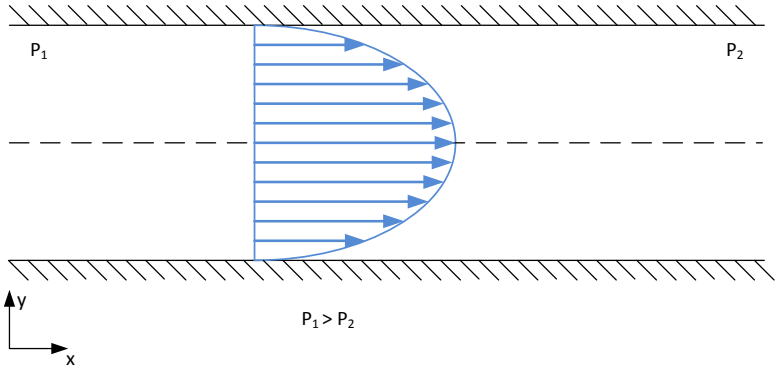

Figure 3.12 Schematic representation of Poiseuille Flow between Parallel Plate

The flow between plates is characterized as a Pressure driven Flow where the Pressure in the inlet is higher than the pressure at the outlet, the Velocity profile is independent on time and just depend on the distance to the walls.

Continuity equation

The continuity equation for an incompressible, constant-density fluid is given by:

$$\frac{\delta(\rho v_x)}{\delta x} = 0 \qquad \textbf{(3.12)}$$

Where, $v_y = v_z = 0$ and $v_x = f(y)$

Navier-Stokes equations

The Navier-Stokes equations for an incompressible, constant-density fluid is given by:

$$-\frac{\delta P}{\delta x} + \mu\frac{\delta^2(v_x)}{\delta y^2} = 0 \qquad \textbf{(3.12)}$$

Where, $\frac{\delta P}{\delta y} = \frac{\delta P}{\delta z} = 0$; $P = f(x)$ and $v_x = f(y)$

In order to model the fluid dynamics with the generation of hydroxyl radicals, it was necessary to couple the fluid flow solution with the absorption of radiation process and the quantum yield. A combination of the equations 3.5 to 3.9 are used in the model. The resulting radiative transfer equation used in the model is as follows:

$$\frac{\delta E_\lambda^{trans}}{\delta y} = -E_\lambda^0 \times a \times 2{,}302 \times e^{-ay} \qquad \textbf{(3.13)}$$

3. Quantifying the heterogeneity of reaction zone, relation of channel thickness in the oxidation process and mixing enhancement

---

3.4. Results and discussion

3.4.1. Theoretical penetration of radiation and theoretical spatial generation of hydroxyl radicals

The theoretical penetration of radiation and the spatial generation of hydroxyl radicals were calculated using the flow transport equation and radiative transfer equation. Two dimensional CFD simulations were carried out to solve the flow and the radiation phenomena. The Figure 3.13 shows the decrease in radiation intensity due to absorption by water of a 172 nm beam.

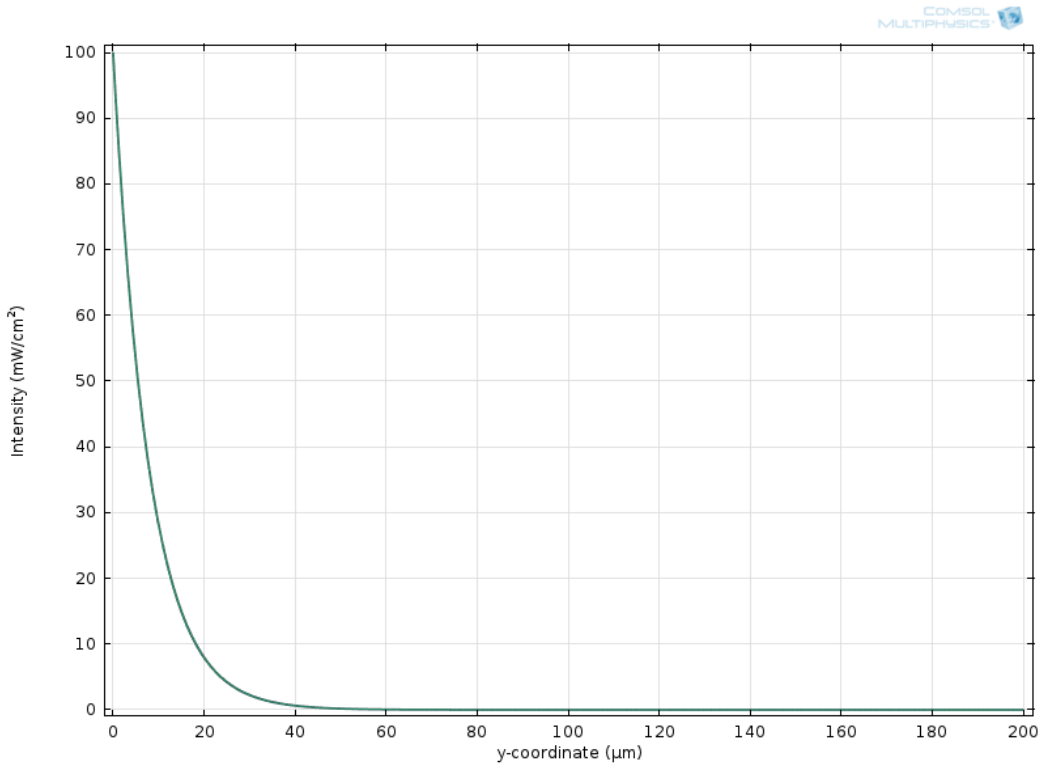

Figure 3.13 Decrease of radiation intensity of 172 nm beam in water

The penetration of radiation and the spatial generation of hydroxyl radicals are not dependent or affected by the channel thickness, therefore for this calculation a frame of 200 µm in height (y-coordinate) for 200 µm in length (x-coordinate) was taken as a calculation area. The Initial Intensity for the calculation model was set at 100 mW/cm^2.

The radiation intensity in water changes as function of the distance from the quartz-water interface (0 y-coordinate). Theoretically, radiation at 172 nm is completely absorbed within the first 40 µm of water from the radiation source.

The spatial representation of the intensity decrease of 172 nm radiation in water is presented using the 200 µm in height and 200 µm in length calculation frame. As it is shown as well in the Figure 3.14, the maximum theoretical penetration of the radiation at 172 nm in water is 40 µm.

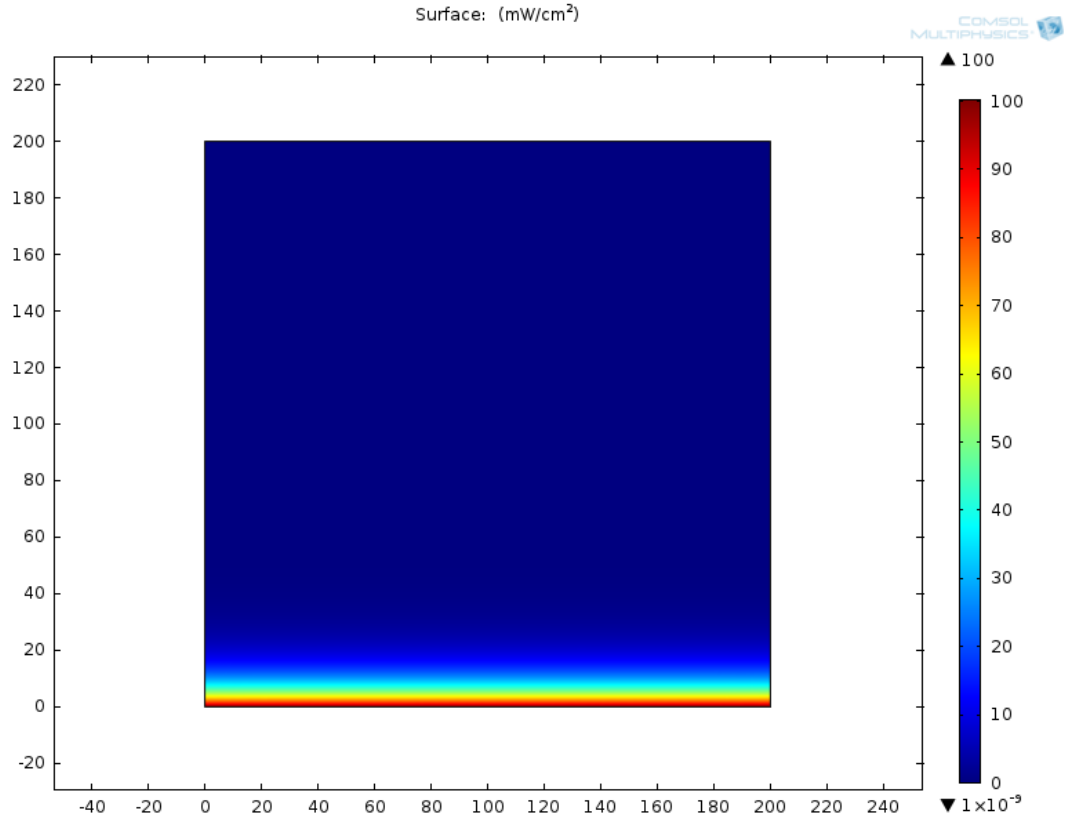

Figure 3.14 Spatial representation of 172 nm radiation penetration in water

The maximum theoretical penetration is a function of the value of decadic absorption coefficient used in the calculation. The decadic absorption coefficient values found in literature for the VUV range of wavelengths differs from author to author, therefore a direct measurement of the transmission of radiation may lead to an accurate decadic absorption coefficient, and a precise radiation penetration assessment.

As the radiation is being absorbed, the photolysis of water takes places, the generation of hydroxyl radicals occurs immediately and in the same place where the photons are being absorbed. Relating the theoretic absorption coefficient of radiation in water and the theoretical quantum yield of hydroxyl radical generation at 172 nm is it possible to calculate the instantaneous generation rate of the radicals. The Figure 3.15 exemplifies the spatial representation of hydroxyl radical generation in the calculation frame.

3. Quantifying the heterogeneity of reaction zone, relation of channel thickness in the oxidation process and mixing enhancement

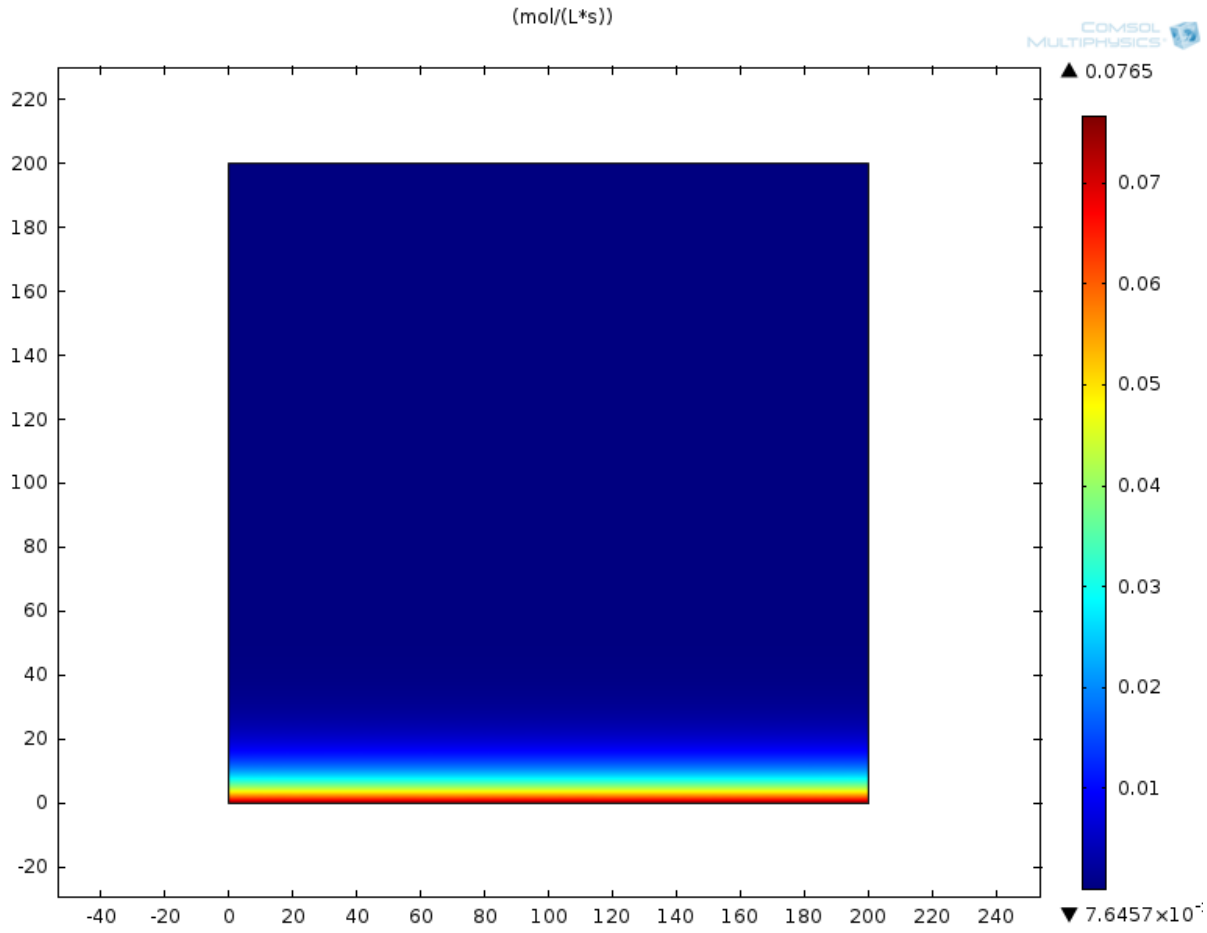

Figure 3.15 Spatial representation of the hydroxyl radical generation

The generated hydroxyl radical are extremely reactive and their average life time is in the order of 10 µs [82]. The high reactivity and their short lifetime lead to an extremely low steady-state concentration. Therefore, the spatial distribution of the instantaneous generation of hydroxyl radicals in mol/Ls was calculated. For the calculation a radiation intensity immediately after the interface quartz-water of 100 mW/cm^2 was used.

3.4.2. The effects of flow velocity and channel thickness for the advanced oxidation of pollutants application

In this section, the initial reaction rate of the degradation of MB, the total % in reduction of COD and the time for reduction of concentration of MB in one order of magnitude under different operational parameters (combination of flow and channel thickness of the reactor) were experimentally determined and compared. Table 3.3 reports the results of the different experiments.

Table 3.3 Results MB degradation experiments,

Thickness (μm)	Flow (mL/min)	Ri (mg/Lmin)	Time MB to be reduced 90% (min)	Time COD to be reduced 50%(min)	% COD reduction per experiment
75	100	0,33±0,04	83,5±0,1	44,0±3,5	93,2±2,8
75	500	1,68±0,09	21,4±0,2	25,3±3,5	82,9±2,8
75	1000	2,14±0,14	18,5±0,2	29,4±3,5	85,8±2,8
75	1400	2,53±0,06	13,7±0,1	25,5±3,5	87,3±2,8
150	100	0,42±0,01	57,9±0,0	43,8±3,5	92,2±2,8
150	500	1,68±0,06	24,4±0,1	43,7±3,5	89,4±2,8
150	1000	2,22±0,09	17,5±0,2	27,8±3,5	89,0±2,8
150	1400	2,34±0,06	16,1±0,1	25,0±3,5	89,8±2,8
150	2200	2,70±0,13	14,1±0,2	26,8±3,5	92,5±2,8
250	100	0,47±0,02	56,1±0,0	42,6±3,5	91,3±2,8
250	500	1,46±0,12	27,9±0,2	34,4±3,5	91,8±2,8
250	1000	2,08±0,08	19,5±0,1	27,6±3,5	91,6±2,8
250	1400	2,30±0,12	16,7±0,2	24,3±3,5	93,5±2,8
250	2200	2,52±0,08	12,9±0,1	22,7±3,5	90,4±2,8
500	100	0,36±0,04	53,1±0,1	71,8±3,5	84,4±2,8
500	500	1,28±0,06	27,2±0,1	31,9±3,5	83,0±2,8
500	1000	1,19±0,29	35,5±0,5	157,0±3,5	85,8±2,8
500	1400	1,18±0,44	41,1±0,8	34,7±3,5	87,7±2,8
500	2200	1,40±0,49	28,1±0,8	137,0±3,5	77,2±2,8
750	100	0,37±0,06	40,3±0,1	38,3±3,5	86,8±2,8
750	500	1,33±0,04	27,2±0,1	39,2±3,5	93,8±2,8
750	1000	1,60±0,03	27,3±0,1	51,3±3,5	89,3±2,8
750	1400	1,85±0,06	19,1±0,1	21,2±3,5	96,5±2,8
750	2200	1,74±0,06	24,2±0,1	34,6±3,5	89,3±2,8
1000	100	0,50±0,06	54,3±0,1	72,7±3,5	84,5±2,8
1000	500	1,15±0,02	35,7±0,0	83,4±3,5	99,0±2,8
1000	1000	1,37±0,09	31,1±0,2	67,7±3,5	90,2±2,8
1000	1400	1,64±0,07	23,2±0,1	28,2±3,5	93,3±2,8
1000	2200	1,49±0,11	25,9±0,2	40,2±3,5	90,5±2,8

Table 3.3 reports the initial reaction rate, the time for MB to be reduced 90% (one order of magnitude), the time for COD to be reduced 50% (half-life) and the percentage of COD reduction after 2 hours of irradiation. Comparison was performed with the purpose of identify the region where it is obtained the maximum responses, which can be attributed to an optimal operational parameter combination for this specific system.

For every channel thickness the initial reaction rate has a direct positive influence with the increment of flow until a plateau.

This phenomenon can be explained using the analogy of catalytic surface reaction model, which explains that during a catalytic reaction in a surface with a moving flow in the surrounding the reaction rate is diffusion limited if the flow is too small to prevent exchange of substrate. If the flow is large enough to permit continue exchange of substrate the reaction rate is not more diffusion limited but reaction limited. The Figure 3.16 is a representation of the 2 regions where the catalytic surface reaction is diffusion limited and reaction limited as the flow varies.

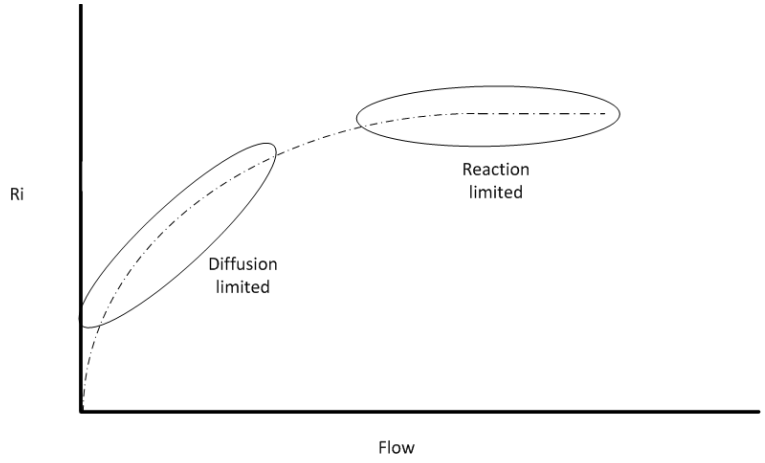

Figure 3.16 Catalytic surface theory, diffusion limited and reaction limited reaction rate

When drawn together, the results of initial reaction rate in the operational parameter space chosen for experimentation the above mentioned phenomenon is confirmed. The Figure 3.17 represents the generated surface response of the reaction rate, as function of channel thickness and flow for the experimental region.

It can be appreciated that experiments with operational flows below 1000 mL/min in every channel thickness showed initial reaction rate values in the area where the reaction is diffusion limited oxidation, operations under diffusion limited oxidation has a higher probability of the existence of a depletion zone were hydroxyl radicals are being produced and not being used optimally. Another interesting result is the strong influence of the channel thickness in this experimental setup. Experiments with channels above 500 μm independently of the operational flow in the range of the setup, showed a plateau in the initial reaction rate clearly lower than the one measured using small channel thicknesses. An increase in channel thickness increases the probability of a thicker boundary layer (stagnation of the fluid) which simultaneously decreases the probability of substrate reaching the photoreaction zone and increment the probability of developing depletion zones where hydroxyl radical cannot be efficiently used.

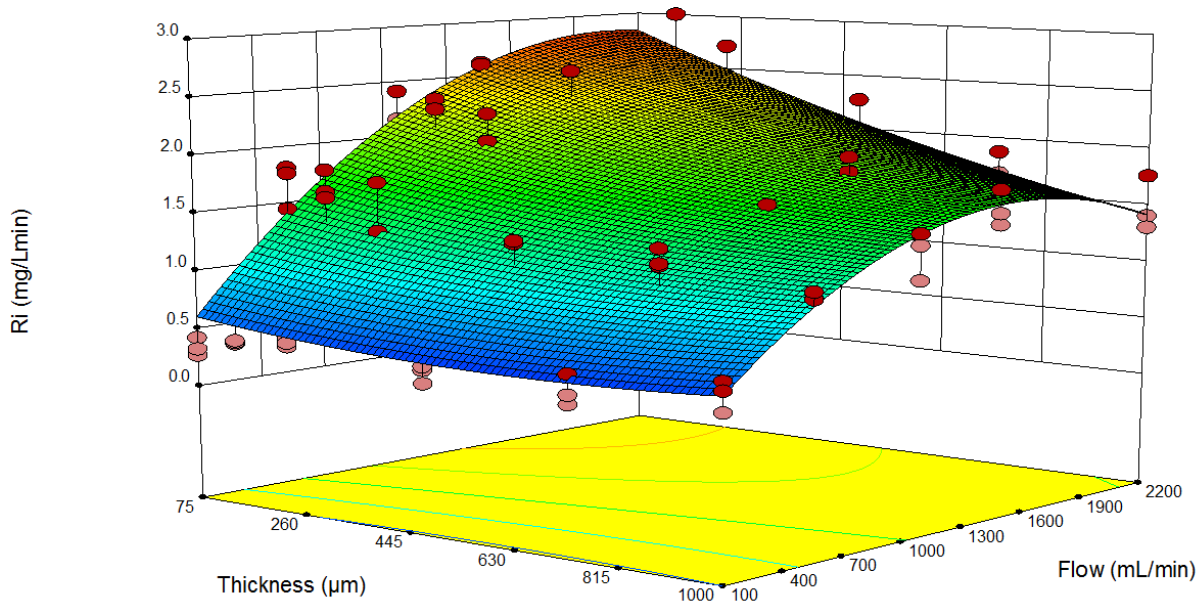

Figure 3.17 Smooth channel thickness - Generated surface of the relation Initial reaction rate, channel thickness and flow

The Figure 3.18 shows the calculated boundary layer thicknesses at different Reynolds numbers and at different distances of the inlet.

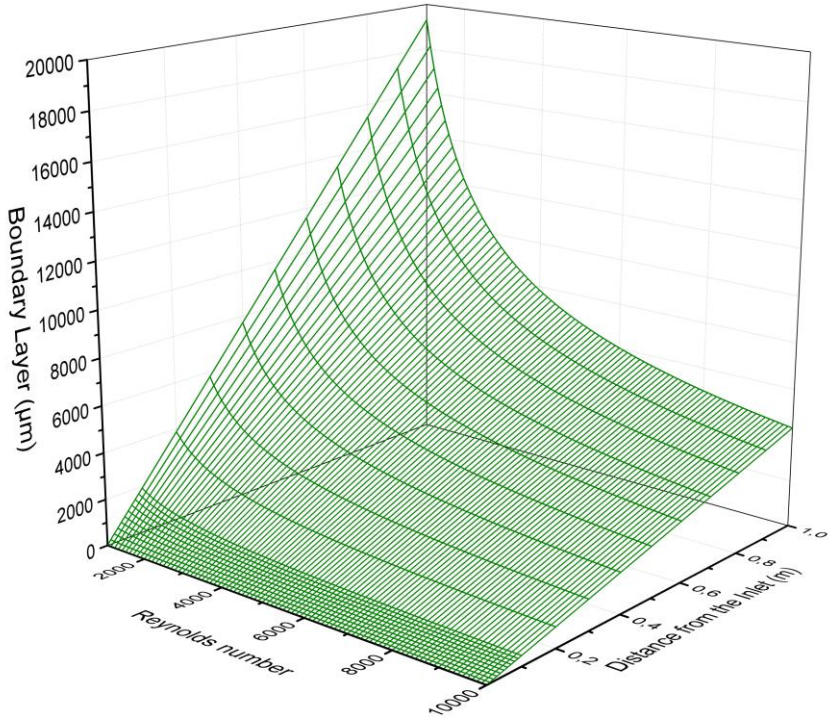

Figure 3.18 Boundary layer thickness as a function of Reynold number and distance from the inlet (independent of geometry of the channel) [83]

The thickness of a boundary layer in water flowing on a smooth flat quartz surface can reach in the first centimetres from the inlet greater values than the theoretical photoreaction zone. [83] The existence of boundary layers thicker than the photoreaction zone after 2 centimetres of the inlet for Reynold numbers from 10 to 10000, and the experimental results for the smooth flat reactor system are strong evidence than active induced mixing is required and cannot be reached by increases on the flow velocity. The existence of boundary layer larger than the photo reaction zone implies that within the photo reaction zone just laminar flow is dominating independently of the regime in the bulk flow.

The flow of the boundary layer becomes unstable only when the local Reynolds number exceeds a value of 600. Therefore laminar flow will occur everywhere in the boundary layer on a flat plate when the overall Reynolds is less than $1{,}2x10^5$ [83].

In our system, however a plateau of maximum initial reaction was measured and was reached using channel thickness smaller than 500 µm with volume flow higher than 1000 mL/min. under this combination of parameters it can be concluded the velocity of feed substrate to the reactor and the entry of substrate to the photoreaction zone are in balance (photo reaction volume is proportional to reactor volume). In other cases of larger channel thickness, an increase of volume flow does not have an immediate effect due to formation of boundary layers larger than the photoreaction zone and bulk fresh substrate is not reaching photoreaction zone.

The comparison of the times that the concentration of MB needed to be reduced one order of magnitude, shows that at smaller channel thicknesses and larger volume flows the reaction of MB with the hydroxyl radicals generated in the photo-induced AOP takes place more effectively, the time needed for MB concentration to be reduced one order of magnitude is smaller in the region where the initial reaction rate is larger. These results agree with the analysis of the initial reaction rate and indicate as well the optimal operational range of the setup (channel thicknesses lower than 500 µm and flows larger than 100 mL/min). The Figure 3.19 represents the generated surface response of the time needed to reduce the MB concentration one order of magnitude, as function of channel thickness and flow for the experimental region.

The comparison of the times that the concentration of COD needed to be reduced to half of the initial concentration, shows that at smaller channel thicknesses and larger volume flows the reaction of oxidable molecules with the hydroxyl radicals generated in the photo-induced AOP takes place more effectively, the time needed for MB concentration to be reduced one order of magnitude is smaller in the region where the Initial reaction rate is larger.

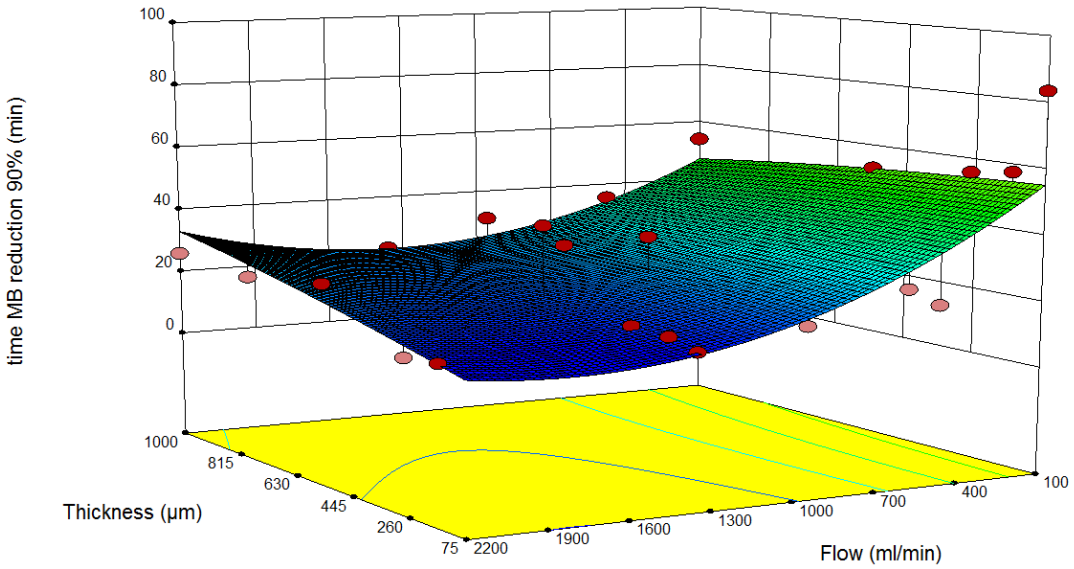

Figure 3.19 Time for the reduction of concentration of MB 90% of initial concentration (one order of magnitude)

The Figure 3.20 shows these results, which agree with the analysis of the initial reaction rate and indicate as well the optimal operational range of the setup (channel thicknesses lower than 500 µm and Flows larger than 100 mL/min).

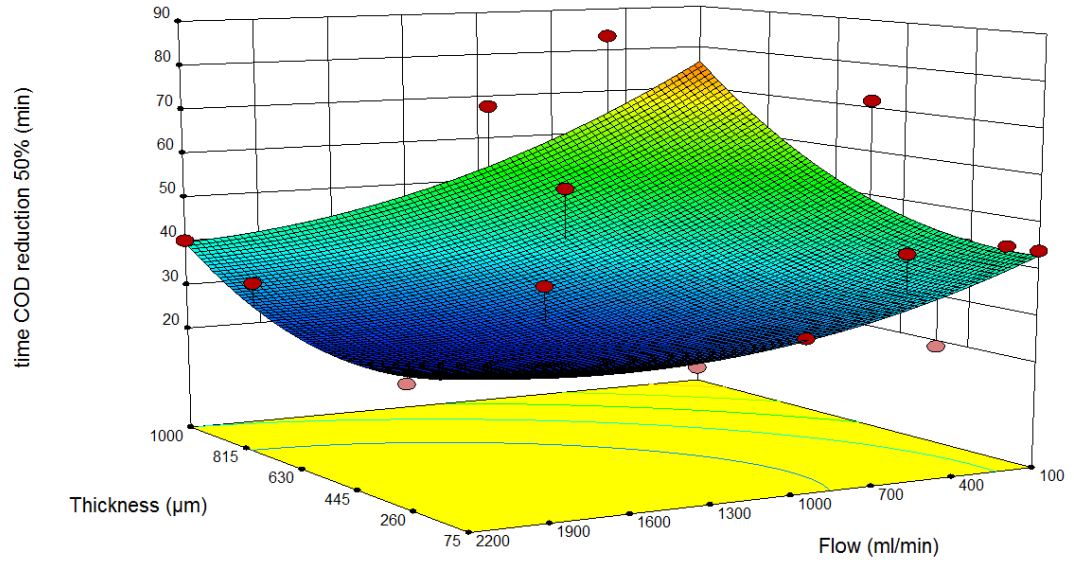

Figure 3.20 Time for the reduction of concentration of COD 50% of initial concentration

The Figure 3.21 show the reduction of COD in percentage after 2 hour of irradiation. In all cases the reduction of COD is higher than 80%. This results demonstrate the strong oxidation power of the photo-induced oxidation, total mineralization of organic molecules is possible with this technology.

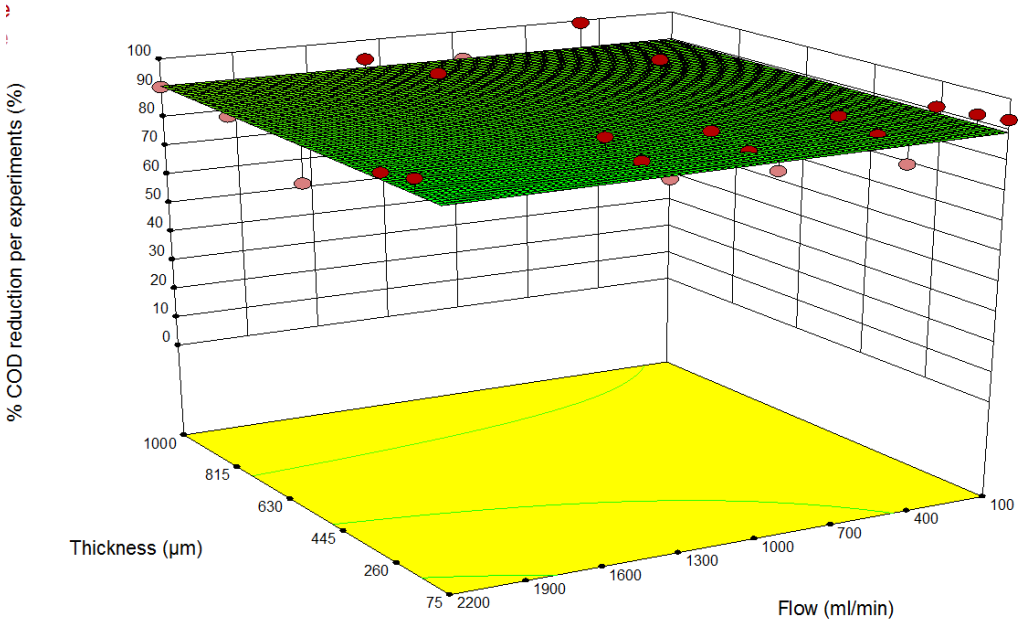

Figure 3.21 Percentage of COD reduction per experiment after two hours of irradiation

3.4.3. The importance of the mixing conditions for the advanced oxidation of pollutants application

As discussed in the last section, the importance of having proportional volume relation between the reactor total volume and the photo reaction zone is crucial for the efficiency of the oxidation process. Due to the difficult of building reactors with volume proportional to the volume of the photoreaction zone for photo induced AOPs, different alternatives to increase the exchange of substrate of the bulk flow and the photo reaction zone within the boundary layer were investigated.

Mixing enhancement in laminar flows was investigated. Two methods of mixing enhancement were proposed and tested; the results show a clear positive influence in the initial reaction rate of the VUV photo-oxidation process, each method in a different combination of operational parameters.

The Figure 3.22 shows the results of the photo-induced oxidation process using the first method of mixing enhancement the SHM. This method the grooved structure has a marked enhancement of the process specially in experiments with a small channel thickness and small recirculation flow, in this region the grooved top plate successfully generate secondary flows in the cross-section, generating a rotation of the fluid and a periodical mixing of the laminar layers overcoming the diffusion controlled substrate exchange, bringing substrate to the photo-reaction zone and showing a comparable effect in the initial reaction rate.

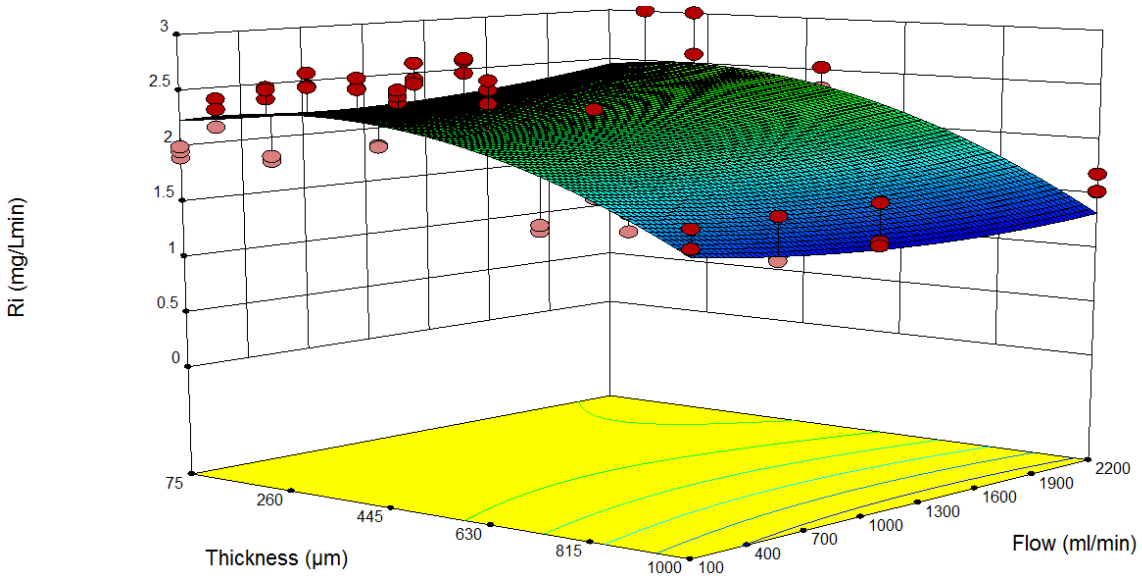

Figure 3.22 Generated surface of the relation initial reaction rate, channel thickness and flow during mixing enhancement grooved channel

The plateau of initial reaction rate is observable along the whole range of flows for channel thicknesses lower than 500 µm. Unfortunately this mixing effect cannot be seen in experiments with a larger channel thickness. This can be explained taking in to account that the flow resistance in the larger channels is smaller in the direction of the flow than in the direction of the grooves. In this case the laminar flow follows the path with less resistance and there is just stagnation of fluid in the groove channels. The change of direction of the fluid intended by the grooves does not work for channel thicknesses larger than 500 µm.

The grooved surface as a medium for generating mixing does have a mixing effect when the channel thickness generates a resistance of the flow in the direction of the channel greater than the resistance of the flow to follow the grooves.

The Figure 3.23 shows the results of the photo-induced oxidation process using the second method of mixing enhancement, the net-like mixing promoter. This second method has a marked enhancement of the process, especially in experiments with larger channel thickness and higher flow, in this region the Net like mixing promoter successfully generate secondary flows in the cross-section, producing mixing of the laminar layers therefore overcoming the diffusion controlled substrate exchange, bringing substrate to the photo-reaction zone and showing a comparable effect in the initial reaction rate.

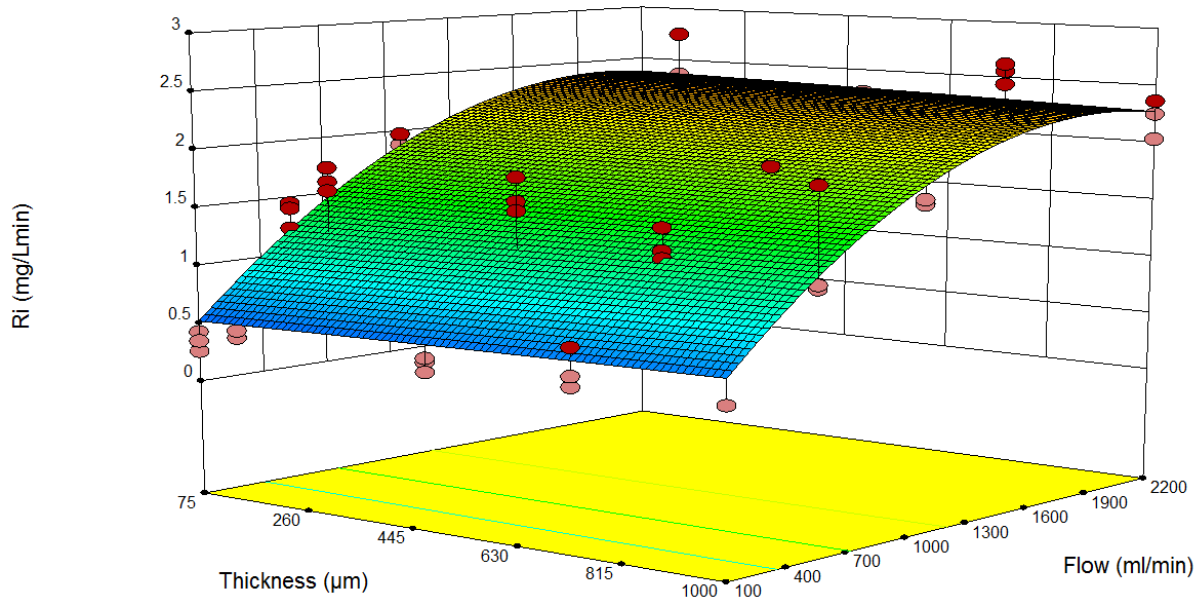

Figure 3.23 Generated surface of the relation initial reaction rate, channel thickness and flow during mixing enhancement channel with net like

The plateau of initial reaction rate is observable along the whole range of channel thicknesses with flows larger than 1000 mL/min. Unfortunately, this mixing effect cannot be seen in experiments with flows smaller than 1000 mL/min. This can be explained taking in to account that a minimum velocity of the fluid is needed in order to have an effective collision of the fluid and the net-like mixing promoter, just by effective collisions the direction of the fluid can be effectively affected producing mixing of laminar layers.

The change of direction of the fluid intended by the net does not have a strong influence for flows smaller than 1000 mL/min. The small changes of direction and velocity of the laminar fluid packages deform these packages but not generate effective transport to the photo reaction zone.

The presence of the net-like mixing promoter help to increase mixing conditions and mass transport to the photoreaction zone, especially in the relative larger channel thicknesses above , however the pressure drop in the system increase when compared with smooth wall channel of the same dimensions.

For the study of the mixing effects in the performance of the oxidation process a net-like mixing promoters were used for each different channel thicknesses. The Table 3.4 present a summary of the parameters studied in this chapter their effects in the overall process as well as the recommendations to keep in mind for further applications.

Table 3.4 Summary Parameters studied Effects and recommendations

Parameter	Effects	Recommendations
Channel thickness	Increase of the channel thickness has a negative influence in the initial degradation rate of Methylene blue as well in the overall oxidation process The occurrence of a laminar boundary layer larger than the photo reaction zone in channel thicknesses larger than 500 µm, prevent for efficient mixing and decrease the oxidation velocity.	Channel thicknesses without mixing enhancement below 500 µm show a maximum initial reaction rate for MB oxidation Channel thicknesses larger than 500µm required mixing enhancement
Flow	Increase of the flow has a positive effect in the initial reaction rate, however by channel thicknesses above 500 µm, the effects on the initial degradation rate are reduced In order to destabilize the laminar behavior of boundary layers larger than the photo reaction zone, the Reynolds number in the bulk fluid must reach values of 10^5 [83].	For processes without mixing enhancement maximum flow of the system is recommended. For processes with mixing enhancement net like turbulence promoters a flow larger than 1000 mL/min are necessary to have a mixing effect
Mixing by Grooved plate	Grooved plates have a positive effect on the increase of the Initial reaction rate by mixing in low velocity flow, for long reactors and continues processes it can be a good solution	More experiments are recommended to investigate the real effect of the mixing in larger photo reactor modules
Mixing by Net-like turbulence promoter	Below 500 µm, the net like turbulence promoter does not bring any significant positive effect in the increase of initial degradation rate, however above this value the net shows the same effect results for MB degradation as those of channel thickness proportional to the photoreaction zone.	If 1000 µm channels are used the use of a net-like turbulence promoter is recommended

3.5. Conclusions

The main goal of the work in this chapter was to study the spatial behavior of the photo-induced photolysis to find the circumstances for which the mass transfer (photo-reaction zone and bulk flow) in narrow channels is most efficient by means of measuring the efficiency of the oxidation process.

To achieve the goal of this study, a flat reactor chamber concept was conceived, built and tested. Channel thickness and Flow recirculation were adjusted for each experiment depending of the required operational conditions. The system was designed to be flexible, the test of six different levels of channel thickness and five different recirculation flows were possible.

The channel thickness and volumetric flow have a strong influence in the exchange of substrate from the bulk to the photoreaction zone; this is reflected and was followed using the initial reaction rate for the destruction of MB measured in experiments.

The photo-induced AOP has as a main characteristic the existence of 2 marked zones, the bulk or dark zone and the photo reaction zone where the oxidation is taking place. The photo reaction zone is limited by the radiation absorption process and is theoretically less than 40 µm thick. Under these process circumstances a boundary layers thicker than the photo reaction zone have a larger probability to be present, a thicker boundary layer (dominated by laminar flow) than a photo reaction zone, has the impact of limiting the overall oxidation of substrate. The reaction is therefore limited to diffusion controlled transport of substrate from the bulk flow to the photo reaction zone.

The theoretical thickness of boundary layers were calculated for different scenarios. Systems using large channel thickness (mm range) have a high probability of generating boundary layers larger than the theoretical photo reaction zone of the process. The flow of the boundary layer becomes unstable only when the local Reynolds number exceeds a value of 600. Therefore Laminar flow will occur everywhere in the boundary Layer on a flat plate when the overall Reynolds is less than $1{,}2 \times 10^5$ [83].

One measure to prevent larger boundary layers than the photo-reaction zone in photo-induced AOP is using channel thickness smaller than 500µm.

Other measure to prevent larger boundary layers and increase the exchange of material between the photoreaction zone within the boundary layer and the bulk fluid is the enhancement by means of mixing in the surroundings of the lamp. Two methods of mixing enhancement were tested, the passive negative profile in form of herringbone structures and the active net like mixing promoters acting like a static mixer. Both methods induce local secondary flows at different angles, disturbing the bulk flow direction and the generation of stable laminar flow within the boundary layer.

Herringbone structures are useful for mixing in continues processes, when high flow velocity is not desired (pressure restrictions). It is important to keep in mind that channel thickness plays an important role in the effect of the mixing with herringbone structures. Chanel thicknesses larger than 500 µm may not bring the desired mixing. Only in channel thicknesses lower than 500 µm the resistance to flow in the direction of the peaks and valleys of the grooves is less than the resistance on the orthogonal direction, generating the transverse component in the flow. At the moment the limiting factor for the use of this concept is the price of manufacture of herringbone structures in large surfaces.

Net like mixing promoters are a good alternative to overcome the negative effects of the formation of larger boundary layer than the photoreaction zone. It was found that effects of mixing expand the channel thickness range of usage in this technology. It was found in experiments that systems for photo-induce oxidation with channel thicknesses of 1 mm using net-like mixing promoter could reach

oxidation efficiencies in the same order of magnitude as those found for the optimal channel thickness. For further understanding and identifying the limits of this mixing measure, it is necessary to check in future studies the influence or the impact of net-like mixing promoter in systems with larger channel thicknesses.

Large velocities (in smooth channels), therefore large Reynolds numbers do not necessary mean higher reaction efficiencies in surface reaction systems. In the literature it is explained that Reynolds larger than 10^4 are required to destabilized the laminar flow in the boundary layer [83].

The selection of channel thickness and the use of active mixing plays an important role in the overall efficiency of a surface reaction process. The operational parameters to obtain the maximum oxidation efficiency for the setup in study were found. Channel thicknesses between 500 µm and 1000 µm as well as the use of the respective net-like turbulence promoter as static mixer with flows larger than 2000 mL/min are the operational parameter which give the highest initial reaction rate for MB destruction. Outside this range of channel thicknesses oxidation efficiency decreases. Under the above mentioned operational conditions more than 80% mineralization was achieved in all experiments after 2 hours of irradiation.

4. Radiation Intensity measurements

4.1. Introduction

Among the first possible technical applications, VUV photolysis of aqueous systems must be considered as a potential alternative to established "advanced oxidation procedures" (AOP). For the design and dimensioning of corresponding reactors, incident photon rates must be determined. Therefore, radiation intensity measurements were performed using two approaches: the relative method chemical actinometry using a reaction of reference whose quantum yield is known (cis-trans photo-isomerization of cyclooctene) and the absolute method photometry, measuring the energetic radiation received by the system using a calibrated detector (Si photo-diode and AlGaN sensor).

In the IUPAC chemical actinometry technical report 2004, one method has been listed under the section liquid-phase chemical actinometers, to be the standards for measuring the radiation intensity of VUV sources emitting at 172 nm: The cis-cyclooctene cis-trans photo-isomerization. Experiments to follow the cis-trans photo-isomerization reactions were performed using the designed reactor from chapter 3.

The increasing number of commercial, scientific and technical applications involving ultraviolet UV radiation has pushed the manufacturers of UV measuring devices to produce simple optically filtered sensor systems to accomplish the varied measurement needs. In the range of VUV Si photodiodes and AlGaN sensors are the last innovation. For the specific case of intensity at 172 nm emitted by excimer Xe lamps there is not an official standard. For the measurement of radiation intensity a novel measurement set up was build and the two above sensor types were used.

4.2. Chemical actinometry and photometry

In order to characterize the photo-reactor by measuring the radiation intensity the following relevant concepts described in chapter 3 are going to be use: reflection, refraction, absorption, absorbance, transmission, radiant power, irradiance, dose, photon, photon flow and absorbed photon.

Additionally the following concepts are necessary for the study and analysis of the radiation intensity by means of chemical actinometry.

- Quantum Yield ϕ_λ : it is defined as a quantitative measure of the overall efficiency of a photo-physical or photo-chemical process [65]. It is a unit-less constant which usually ranges from zero to one; it is denoted it as mol Einstein-1 (Einstein = mol photons). Quantum yields greater than

one indicate photo-induced chain reactions, which may involve radical species or photo-generation of a catalyst. The quantum yield can be expressed in terms of the reactant or the product. It is usually dependent on the wavelength of the absorbed UV radiation, however many photochemical systems exist that have a constant quantum yield over a defined range [20]. If a system or reaction has a constant and well known quantum yield, this one can be used for the measurement of the absorbed photon flow $\mathrm{E_p^{abs}}$; this systems are called actinometers, and they are used to measure the absorbed photon flow in photo-reactors of specific geometry and for a well-defined spectral range [20]

$$\phi_\lambda = \frac{\mathrm{dn(M)/dt}}{\mathrm{E_p^{abs}}} \qquad \textbf{(4.1)}$$

- Chemical actinometer: it is a chemical system (fluid, gas, solid in a space determined environment or chemical reactor) that undergoes a light-induced reaction (at a certain wavelength,λ) for which the quantum yieldϕ_λ, is accurately known. Measuring the reaction rate allows the calculation of the absorbed photon flux. It is important to perform the measurement in a way that the assumption of total absorption is accomplished. Determination of conversion to the products affords the total number of photons absorbed by the liquid or gas volume or solid surface, which may have any form or geometry.

Additionally to actinometry for measuring radiation intensity by means of radiometry and photometry the following supplementary concepts are described.

- Spectral Radiant Power E : it is by definition the quantity of energy crossing a surface bounded by a closed curve per unit time for a specific wavelength:

$$\mathrm{E} = \frac{\mathrm{dQ_e}}{\mathrm{dt}} \qquad [\mathrm{W}] \qquad \textbf{(4.2)}$$

  For any source, this quantity E is the total power emitted in all directions by the radiant source. It is equal to the total power crossing a spherical surface enclosing the source. [28, 65]

- Radiant Energy: it is the energy of the electromagnetic wave emitted by a radiation source to the surroundings [65]:

$$\mathrm{Q_e} = \int_{t_1}^{t_2} \mathrm{E\,dt} \qquad [\mathrm{J}] \qquad \textbf{(4.3)}$$

- Radiant intensity: this concept only applies to point sources. It is related to the light flux emitted per unit solid angle, in a given direction:

$$I_r = \frac{dE}{d\Omega} \qquad [W/sr] \qquad \textbf{(4.4)}$$

In reality, point sources do not exist. However the approximation can be applied if the source-receiver distance is at least 20 times greater than the source dimension [65].

- Irradiance (flux density): Radiant power received by a surface per unit area. This is sometimes also confusingly called "intensity":

$$E^0_{\lambda A} = \frac{E^0_\lambda}{A} \qquad [W/m^2] \qquad \textbf{(4.5)}$$

- Energy of photon: The energy of photons of a wavelength λ is given by Planck's relation [65]:

$$W_\lambda = \frac{hc}{\lambda} \qquad [J],\ \lambda\ [m] \qquad \textbf{(4.6)}$$

- Number of photons: The number of photons emitted by a monochromatic source at a wavelength λ and of radiant energy is given by the equation:

$$N_\lambda = \frac{Q_\lambda}{W_\lambda} = Q_\lambda \frac{\lambda}{hc} \qquad \textbf{(4.7)}$$

For a polychromatic source, the number of photons is given by the integral of the photon spectral distribution curve over the wavelength range of the source:

$$N = \int_{\lambda_1}^{\lambda_2} N_\lambda \, d\lambda = \frac{1}{hc} \int_{\lambda_1}^{\lambda_2} Q_\lambda \lambda d\lambda \qquad \textbf{(4.8)}$$

This expression provides the correspondence between the photonic and radiometric quantities [65].

- Photon flow: The photon flow of a radiation source can be described by:

$$E_P = 8{,}3593 \left[\frac{mol}{Wms}\right] \times E^{Lamp}[W] \times \lambda[m] \qquad [mol\ s^{-1}] \qquad \textbf{(4.9)}$$

- Photon flux: The photon flux, emitted or received, is defined in a manner analogous to the exitance (emitted photons) or to the irradiance (photons received),

$$M_p = \frac{dE_p}{dA} = \frac{d^2N}{dtdA} \qquad [Photon\ s^{-1}\ m^{-2}] \qquad \textbf{(4.10)}$$

Photon flux (photon irradiance) is often found in the literature in units of einstein/s*m^2 [65].

The relation between radiometric and photometric concepts: By definition, for a given wavelength, the photon and radiometric spectral quantities are related by the expression:

$$G_{p,\lambda} = \frac{\lambda}{hc} G_{e,\lambda} \qquad \textbf{(4.11)}$$

Experimentally, the measured quantities from monochromatic sources are often radiometric quantities. For a polychromatic source, photon quantities are not simply calculated from the radiometric quantities. Since the calculation of the photon quantity G_p, where

$$G_p = \int_{\lambda_1}^{\lambda_2} G_p(\lambda)d\lambda \quad \textbf{(4.12)}$$

$$G_p = \frac{1}{hc}\int_{\lambda_1}^{\lambda_2} G_e(\lambda)\lambda d\lambda \quad \textbf{(4.13)}$$

Requires the knowledge of the corresponding spectral distribution of the radiometric quantity known, that is, the relative spectral distribution of the radiant source or of the light utilized.

4.2.1. Photometers

Photometers are detectors of radiation which convert the radiant energy to an electrical signal, the strength of which is a function of the magnitude of the incident radiation.

The response of a photometer at a given wavelength is defined as the ratio of the electrical signal, for example current, to the radiant power that causes this signal:

$$s_\lambda = \frac{I}{E_{e,\lambda}} \text{ [A/W]} \quad \textbf{(4.14)}$$

The total response is related to the current produced by a polychromatic flux:

$$s = \frac{I}{\int_{\lambda_1}^{\lambda_2} E_e(\lambda)d\lambda} \quad \textbf{(4.15)}$$

Due to the dependency on the response of the UV meter to the spectrum of the source used for calibration, it is strongly recommended to pick a UV meter that has the closest match to the desired measurement function. In case this is not likely possible, then a correction factor must be calculated for each source to be measured, taking into account the measured absolute spectral responsivity of the UV meter and know the source's relative spectral distribution. Alternately, one can calibrate the meter with a calibration source that is similar in its spectral distribution to the source being measured.

For broadband polychromatic UV sources the spectral mismatch in the intensity measurements is the major uncertainty source, in addition errors can occur due to out of band, non-linear, and non-ideal geometric or spatial response of the photometers.

The typical photometer is composed of a number of simply optical elements, the aperture, the diffuser, the filter and the detector, as shown below in the Figure 4.1. The incident radiation passes through an aperture that limits the active area of the system. A diffuser is often placed after the

aperture and is used to improve the angular response and spatial uniformity of the instrument. An optical filter is then employed to select the spectral region of the incident optical radiation that strikes the detector.

Our application involves the measuring of monochromatic UV source Xenon excimer lamp emitting at 172 nm, in this case a simple broadband UV meter correctly calibrated at that wavelength is generally sufficient.

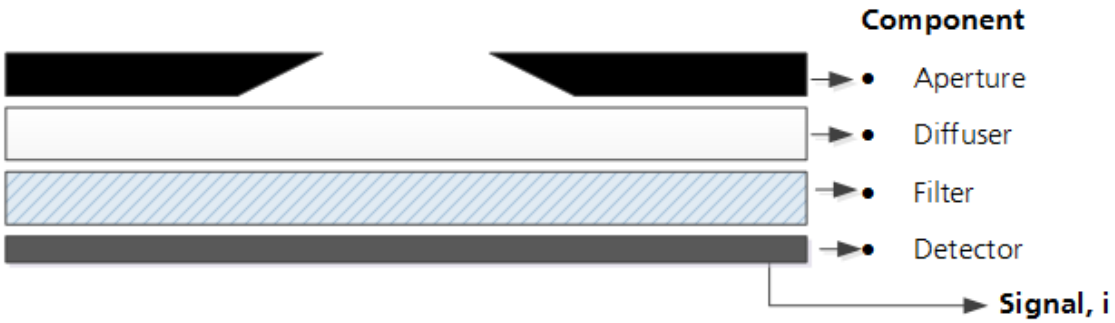

Figure 4.1 Diagram of UV radiometer with optical components [84]

4.3. Materials and methods

4.3.1. Chemical actinometry

The photochemical isomerisation of cis-cyclooctene as an actinometer was proposed first for 185 nm by Srinivasan [85]. This method was generally used to determine the photon flow in VUV and therefore the spectral radian power of low pressure mercury lamps. Thus it is defined to the emission wavelength of these lamps in this domain [86]. This technique was afterwards adapted to measure the radiation of Xe excimer Lamps by Jakob in 1992 during his PhD thesis [18]. The methodology was then repeated and standardized by Heit in 1997 during his PhD thesis and subsequent publications [22, 23, 87]. The Figure 4.2 shows the planar chirality of cis-trans cyclooctene under VUV.

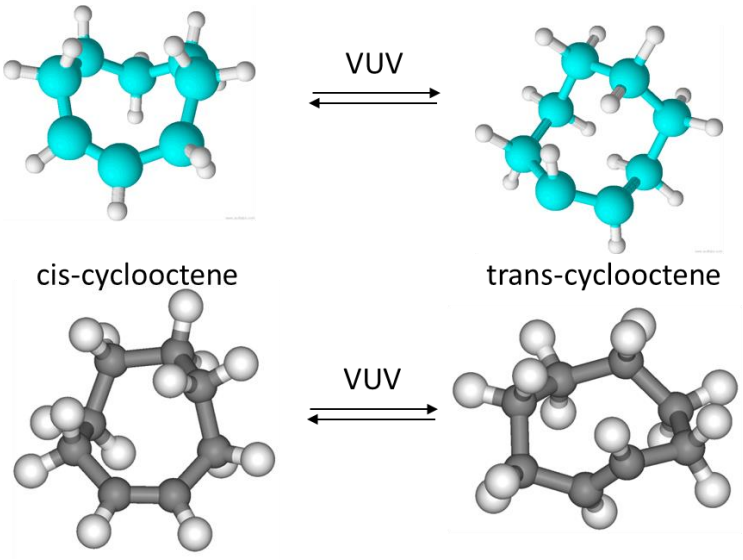

Figure 4.2 Planar chirality cis-trans cyclooctene

Both cyclooctene isomers (cis-trans) absorb in the VUV range, this reaction is reversible. Under continuous irradiation, the concentrations of compounds reach a so called photo-stationary balance. This balance depends on quantum yields of both isomers and their own absorption coefficient. These values were stablish by Jakob at 172 nm and are presented in Table 4.1 [18].

Table 4.1 Molar absorption coefficient and quantum yield of isomerization of cis-trans cyclooctane [18]

	Cis-cyclooctene	Trans-cyclooctene
$\varepsilon_{172\ nm}$ Lmol^{-1}cm^{-1}	6130	7490
$\phi_{iso\ 172\ nm}$	cis→ trans 0,32	trans→ cis 0,44

Cyclooctene is defined as a good actinometer due to its high quantum yield and molar absorption coefficient, as well as, the not presence of significant secondary reactions (<3%) [18].

In practice, the actinometry is realised by the irradiation of cis-cyclooctene. The evolution of the reaction is followed measuring the concentration of the isomers by chromatography analyses in gaseous phase.

At the beginning of the reaction, the flux of photons can be determined by the measure of the decrease of the cis- (respectively, the apparition of trans-) by gas chromatography. Nevertheless, as the trans- absorbs as well and form the cis-, the speed of disappearance of cis- is not directly proportional to the absorbed light intensity anymore. It must be corrected taking into account the reverse reaction

of the trans. Considering both reactions (cis- -› trans- and trans- -› cis-) it is possible to quantitatively describe the rate of disappearance of the cis- [18].

Taking into account the following nomenclature:

$A_c = \varepsilon_c C_c l$ is the absorbance of cis-cyclooctene at time t;

$A_t = \varepsilon_t C_t l$ is the absorbance of trans-cyclooctene at time t;

$A_{tot} = A_c + A_t$ is total absorbance of both isomers at time t;

C_c is the concentration of the substrate cis-cyclooctene in mol L^{-1} at time t;

C_∞ is the concentration of the substrate cis-cyclooctene in mol L^{-1} at photo-stationary state;

C_o is the initial concentration of the substrate cis-cyclooctene in mol L^{-1};

ε_c is the molar decadic absorption coefficient of cis-cyclooctene in $Lmol^{-1}cm^{-1}$;

ε_t is the molar decadic absorption coefficient of trans-cyclooctene in $Lmol^{-1}cm^{-1}$;

$f_c = \frac{A_c}{A_{tot}} = \frac{\varepsilon_c c_c l}{\varepsilon_c c_c l + \varepsilon_t c_t l}$ is the fraction of photons absorbed by cis-cyclooctene at time t;

$f_t = \frac{A_t}{A_{tot}} = \frac{\varepsilon_t c_t l}{\varepsilon_c c_c l + \varepsilon_t c_t l}$ is the fraction of photons absorbed by trans-cyclooctene at time t;

$\phi_{t\to c}$ is the quantum yield of formation of cis-cyclooctene;

$\phi_{c\to t}$ is the quantum yield of formation of trans-cyclooctene;

l is the optical path length or thickness of the solution traversed by the UV radiation;

E_{pc}^{abs} is the number of photons absorbed by cis-cyclooctene in photons s^{-1};

E_{pt}^{abs} is the number of photons absorbed by trans-cyclooctene in photons s^{-1};

E_p^{abs} is the total photons absorbed by both isomers in photons s^{-1};

E_p^o is the incident number of photons to the system in photons s^{-1};

E_λ^0 is the incident spectral radiant power in W;

V is the volume of actinometric solution;

The differential equation describes the kinetics of the cis-cyclooctene isomerisation.

$$-\frac{dC_{cis}}{dt} = \phi_{t\to c}\frac{E_{pt}^{abs}}{V} - \phi_{c\to t}\frac{E_{pc}^{abs}}{V} \qquad \textbf{(4.16)}$$

With $E_{pt}^{abs} = E_p^{abs} f_t$ and $E_{pc}^{abs} = E_p^{abs} f_c$

$$-\frac{dC_{cis}}{dt} = \frac{E_p^{abs}}{V}\left[f_t \phi_{t\to c} - f_c\, \phi_{c\to t}\right] \quad \textbf{(4.17)}$$

$$-\frac{dC_{cis}}{dt} = \frac{E_p^{abs}}{V(\varepsilon_c c_c+\varepsilon_t c_t)}\left[\phi_{t\to c}\varepsilon_t c_t - \phi_{c\to t}\varepsilon_c c_c\right] \quad \textbf{(4.18)}$$

Since there is total absorption, the total photons absorbed by both isomers is equal to the incident photon flow (number of photons) to the system $E_p^{abs} = E_p^o$

$$-\frac{dC_{cis}}{dt} = \frac{E_p^o}{V(\varepsilon_c c_c+\varepsilon_t c_t)}\left[\phi_{t\to c}\varepsilon_t c_t - \phi_{c\to t}\varepsilon_c c_c\right] \quad \textbf{(4.19)}$$

Assuming that neither of the two isomers undergoes any secondary reaction, the sum of their concentrations at any time t would be equal to the final concentration of the irradiated isomer.

$$c_o = c_c + c_t \quad \textbf{(4.20)}$$

using the molar fraction,

$y = \frac{c_c}{c_o}$ is the molar fraction cis-cyclooctene at time t;

$y_\infty = \frac{c_\infty}{c_o}$ is the molar fraction cis-cyclooctene at photo-stationary state;

And expressing the concentration in mole fraction the kinetic of the isomerization is described as,

$$-\frac{dy}{dt} = \frac{E_p^o}{Vc_o[\varepsilon_t+(\varepsilon_c-\varepsilon_t)y]}\left[\phi_{t\to c}\varepsilon_t(1-y) - \phi_{c\to t}\varepsilon_c y\right] \quad \textbf{(4.21)}$$

Reorganizing

$$-\frac{dy}{dt} = \frac{E_p^o(\phi_{t\to c}\varepsilon_t+\phi_{c\to t}\varepsilon_c)}{Vc_o(\varepsilon_c-\varepsilon_t)}\frac{\left(\frac{\phi_{t\to c}\varepsilon_t}{\phi_{t\to c}\varepsilon_t+\phi_{c\to t}\varepsilon_c}+y\right)}{\left(\frac{\varepsilon_t}{\varepsilon_c-\varepsilon_t}+y\right)} \quad \textbf{(4.22)}$$

$$k_1 = \frac{E_p^o(\phi_{t\to c}\varepsilon_t+\phi_{c\to t}\varepsilon_c)}{Vc_o(\varepsilon_c-\varepsilon_t)} = \frac{E_p^o k_3\,\phi_{t\to c}}{Vc_o k_2} \quad \textbf{(4.23)}$$

$$k_2 = \frac{\phi_{t\to c}\varepsilon_t}{\phi_{t\to c}\varepsilon_t+\phi_{c\to t}\varepsilon_c} = -y_\infty \quad \textbf{(4.24)}$$

$$k_3 = \frac{\varepsilon_t}{\varepsilon_c-\varepsilon_t} \quad \textbf{(4.25)}$$

$$\frac{dy}{dt} = k_1\frac{(k_2+y)}{(k_3+y)} \quad \textbf{(4.26)}$$

$$\left[1+\frac{(k_3-k_2)}{(k_2+y)}\right]dy = k_1 dt \quad \textbf{(4.27)}$$

Integrating

$$\int_{y_o}^{y}\left[1+\frac{(k_3-k_2)}{(k_2+y)}\right]dy=-\int_{t_o}^{t}k_1\,dt \tag{4.28}$$

$$(y-y_o)+(k_3-k_2)\ln\left(\frac{y+k_2}{y_o+k_2}\right)=-k_1t \tag{4.29}$$

$$(y-y_o)+(k_3+y_\infty)\ln\left(\frac{y-y_\infty}{y_o-y_\infty}\right)=-\frac{E_p^o k_3\,\phi_{t\to c}}{Vc_o y_\infty}t \tag{4.30}$$

By introducing a function $f(c_c)$ one obtains

$$f(c_c)=\frac{1}{k_3}(c_c-c_o)+\left(c_o+\frac{c_\infty}{k_3}\right)\ln\left(\frac{c_c-c_\infty}{c_o-c_\infty}\right)=-\frac{E_p^o\,\phi_{t\to c}}{Vy_\infty}t \tag{4.31}$$

By plotting $f(c_c)$ over the test duration t, a straight line with slope m results

$$m=-\frac{E_p^o\,\phi_{t\to c}}{Vy_\infty} \tag{4.32}$$

so that the absorbed photon flux, in this case and under the conditions of the experiment the incident number of photons can be calculated

$$E_p^o=-mV\frac{y_\infty}{\phi_{t\to c}} \tag{4.33}$$

4.3.1.1. Reagents

Cis-cyclooctene (Alpha, 95%) and n-pentane (AppliChem,99%) have been used without further purification. Trans-cyclooctane was first prepared on a small scale by irradiating a solution of degassed n-pentane solution of cis-cyclooctene. This experiment was carried out in the same photo-reactor described below. Separation of the cis-trans cyclooctene was examined using different capillary GC columns and different conditions of GC analysis. A good separation of the isomers was achieved on an Agilent column 19091J-413 30m, internal diameter 320µm film thickness 0,25 µm with a temperature program starting at 40°C.

4.3.1.2. Photo-reactor

The flat micro channel reactor apparatus described in chapter 3 was used for the radiation measurements. Minor modifications of the periphery were required to fit the system in a fume hood for safety reasons. It consists of two Xe excimer UV Lamps contained in a metallic housing with UV reflectors (Xeradex System) emitting 172 nm radiation through the window, the system is positioned under the

Flat micro channel reactor (see Figure 3.5). The Flat micro channel reactor is connected to a 0,5 L jacketed reactor glassware as reservoir with, a cooling glass column and a gear pump VerderGear VGS096 (Verder, Germany) which controls the flow. All tubing and periphery are made of materials with highly crack and stress resistance, low permeability, no moisture absorption and low level of chemicals absorption to assure no contamination of the cis-trans cyclooctene. The system was modified to be completely sealed tight and to work in temperatures below 10 degrees Celsius to prevent evaporation of solvents. The complete system is presented in Figure 4.3.

Of special interest is the use of the optimal operational parameters for the avoidance of the generation of depletion zones. Experimental results discussed in Chapter 3, exhibited a marked dependence of the initial reaction rates of oxidation with the volumetric flow rate and channel thickness.

Results showed that a channel thickness below 500 μm and flow rate above 1000 mL/min as the optimal combination of operational parameters in this system; reflected, on higher reaction rates, (i.e. faster MB oxidation). For the purpose of this work, the channel thickness of 250 μm and volumetric flow of 2200 mL/min were used in the experiments.

A. Nitrogen flowmeter
B. Electrical Power supply
C. Manometer
D. Reactor body + Xeradex double lamp system
E. Flowmeter
F. Cooling system
G. Storage tank 0,5L with jacket
H. Pump (gear pump)

Figure 4.3 Front view VUV AOP Laboratory scale reactor system used for the study

Temperature was kept among the range of 7 to 10℃ and it was recorded during the course of each experiment. This temperature range was desired in order to hold evaporation losses to the minimum

extend possible, since solvent has low boiling point. A cooling solution mixture of 30% ethylene glycol EG and water was employed in order to reach this temperature range.

4.3.1.3. Actinometric procedure

Solutions of cis-cyclooctene in n-pentane were irradiated under identical conditions. In each experiment 400 mL of the solution containing 0,11 mol/L of cis-cycooctene were circulated in the photochemical reactor for 60 minutes. Taking into account the absorption coefficient of cyclooctene, the initial concentration used assures that all incident radiation is being absorbed during the experiment. Throughout the experiments samples were taken for GC analysis. Temperature of the system was kept constant the entire radiation time.

4.3.1.4. Analysis

Gas chromatographic analyses were performed on a GC-FID system from Agilent Technologies Model 7890A. The column used was a nonpolar Agilent Technologies HP-5 column (30mx0.32mmx0.25µm). Calibration curves were stablished for cis-cyclooctene and trans-cyclooctene. From two stock solutions with known concentration of the isomer different solutions were prepared at different dilution factors.

4.3.2. Photometry

Currently the field of photometry in the UV region is an important field of research due to the multiple applications and the need of finding higher sensitivity, more quantitatively accurate photometric information as well as more immediate data availability; the advance in semiconductors and their use in photodetectors has as a result semiconductor detectors offering small size, ruggedness, and easiness to use.

One of the most important questions for UV detectors in the UV range is how to block the visible solar radiation for absolute measurements of UV. This question has been answered and the problem overcome by using bulky band filters to block the visible radiation background in Si photo-detectors, and the development of wide bandgap semiconductor specifically the AlGaN which is solar blind. In this study we used both photo detectors.

4.3.2.1. Detectors

4.3.2.1.1. Si-photodiode

Si Photodiode S8551 from Hamamatsu, developed for the detection of ArF excimer lasers (193 nm), which the manufacturer assure is more stable and sensitive to VUV than conventional Si-photodiodes [88]. This sensor has an active area of 5,8 x 5,8 mm. Relative responsivity and the spectrum of a Xenon excimer lamp are shown in the Figure 4.4.

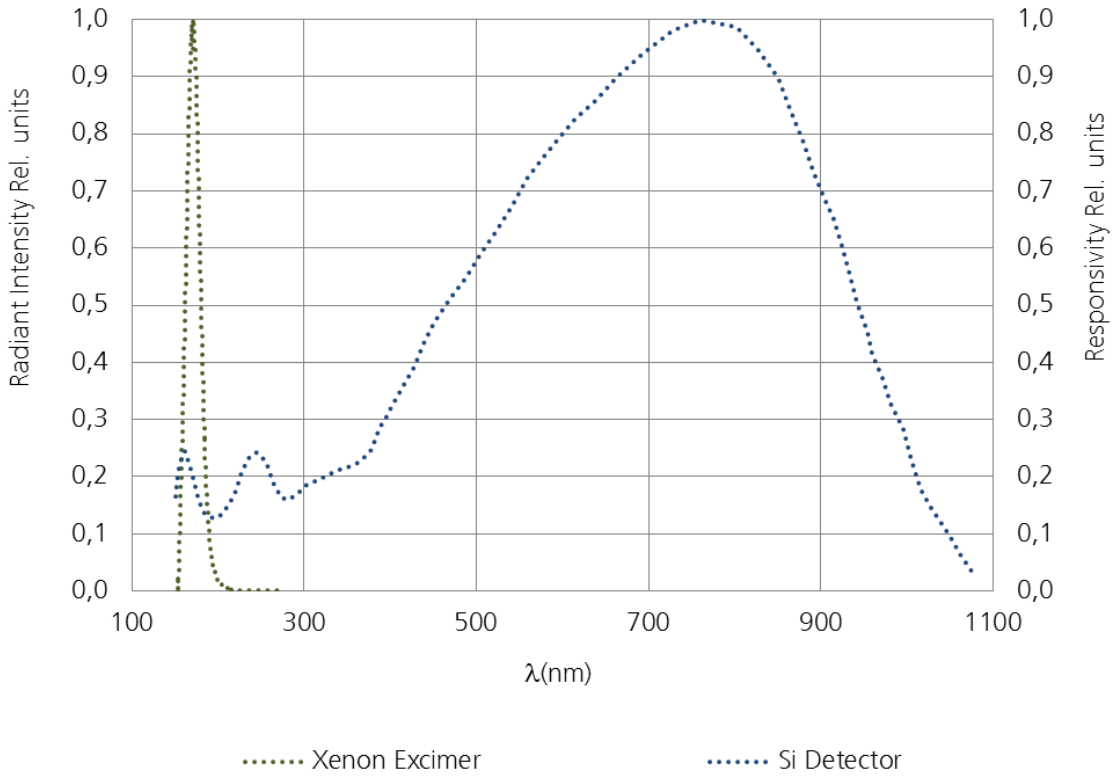

Figure 4.4 Spectrum of an Xe Excimer lamp; and the spectral responsivity of a the Si UV-detector

As mentioned in chapter 2, the xenon excimer emission shows a band in the VUV region ranging from wavelengths of 160 nm to 200 nm. The xenon excimer emission shows a pick at a wavelength of 172 nm with a full width at half maximum (FWHM, half-width) of 14nm. Although nearly no other emission is present (0,07%UVC, 0,22%VIS and 0,78%NIR)[56], the responsivity of the sensor extends to the UVC, VIS and NIR. Absolute responsivity for the detection range, where xenon excimer emission is present, is shown in Figure 4.5.

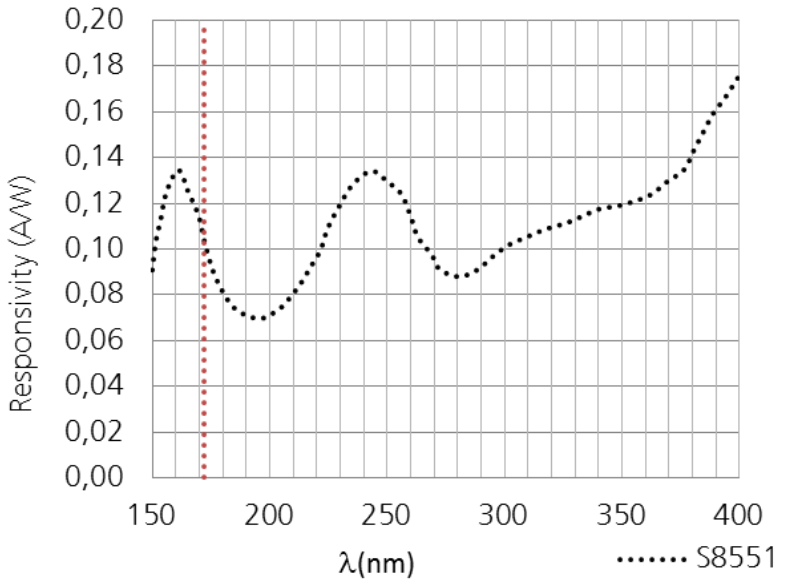

Figure 4.5 Absolut spectrum responsivity of the Si UV detector

It is important to notice, that due to emission of the Xe excimer Lamp outside of the range of interest (VUV < 200 nm) a correction of the measurement has to be performed. The theoretical value to be corrected represents 4,3 % of influence in the absolute response.

4.3.2.1.2. AlGaN detector

Researchers at the Fraunhofer Institute for Applied Solid State Physics (IAF) in Freiburg have developed a new UV detector in collaboration with colleagues at the Fraunhofer Institutes for Manufacturing Technology and Advanced Materials (IFAM), for Optronics, System Technologies and Image Exploitation (IOSB), for Silicon Technology (ISIT) and for Physical Measurement Techniques (IPM).

The detector is based on aluminium gallium nitride (AlGaN) technology and can tolerate continuous exposure to UV light without damage. The sensor is particularly suited to applications involving very high UV intensities, and for tasks that require the monitoring of specific spectral ranges. This is due to the fact that the detector is set to operate under a defined maximum wavelength threshold. In this case the sensor detects all UV light emitted at wavelengths below the set limit.

Relative and absolute responsivity of the Fraunhofer developed detector (AlGaN) is shown in Figure 4.6 and Figure 4.7 respectively.

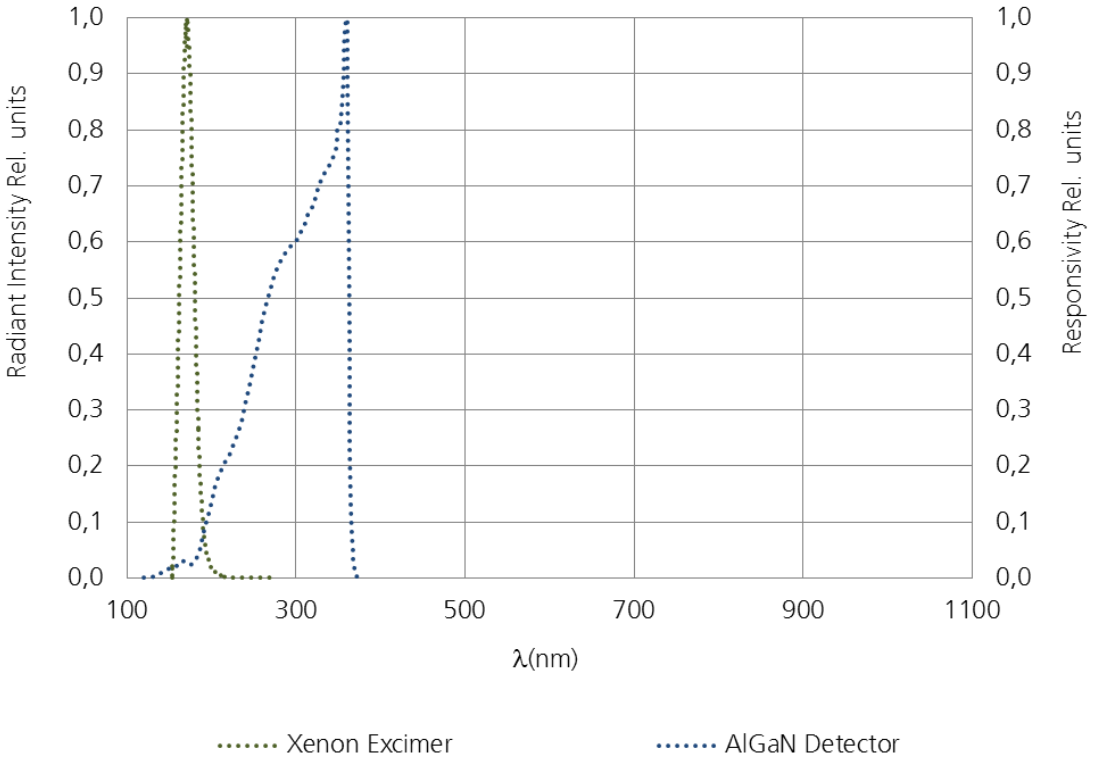

Figure 4.6 Spectrum of an Xe excimer lamp; and the spectral responsivity of a the Fraunhofer AlGaN UV detector 02

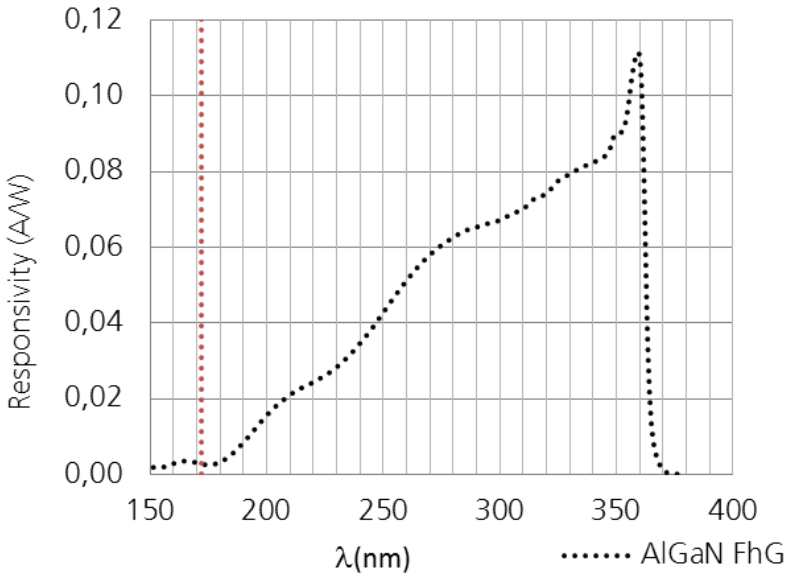

Figure 4.7 Absolut spectrum responsivity of a the Fraunhofer AlGaN UV detector 02

The Fraunhofer AlGaN detector has no responsivity above 380 nm. The responsivity of the sensor does not extend to the VIS and NIR regions. The influence of the 0,07% of UV-C radiation emitted

by the lamp represents a theoretical 1,3 % influence in the absolute response of the AlGaN detector due to radiation outside of the range of interest. Therefore a correction in the absolute measurement is not required.

4.3.2.2. Measurement setup

To determine the radiation intensity reaching the window of the photo-reactor described in section 4.3.1.2., a motor-driven XY table was constructed in conjunction with a detector, so that complete surface can be travelled with the detector. This XY table was built in a gas tight container where a Nitrogen atmosphere can be established for the measurements.

The measurement setup is shown schematically in Figure 4.8. By means of the two stepping motor tables arranged perpendicular to each other, a detector (Si or AlGaN) mounted in the detector holder can be moved over the lamp surface. As a result, the intensity distribution of the photo-reactor in the detection plane can be determined. The figure also shows the coordinate system used in the measurements. The origin of the coordinate system is in each case approx. 3 mm outside the lamella window in the upper left corner of the lamp system.

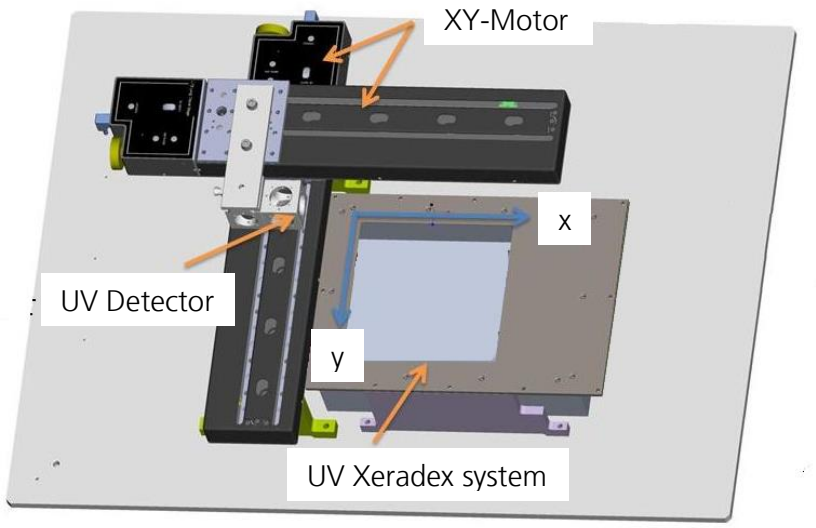

Figure 4.8 Measurement setup (schematic)

For measurements in conjunction with the build platform, additional spacer disks can be inserted, with them the stepper motor table can be elevated via these adapter pieces, so that the measurements at different distances from the photo-reactor surface are possible. The Figure 4.9 shows an image of the test setup with the built-in UV detector and the photo-reactor frame.

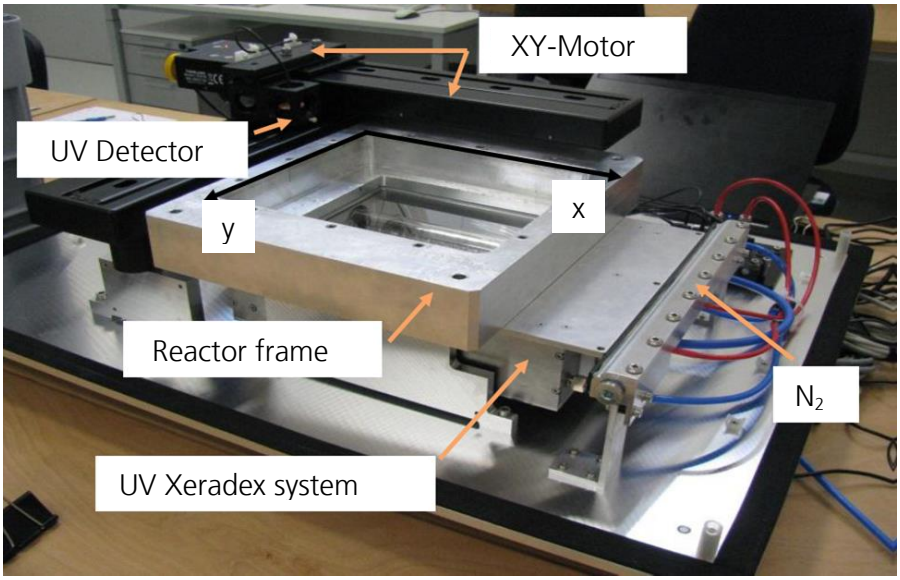

Figure 4.9 Picture of the measuring setup

For the measurements, the detectors are operated in the "short-circuit mode", the photocurrents are measured with a data logger from the company Keithley, type 2410.

4.3.2.3. Radiometric procedure

The measurement setup was purged with Nitrogen until the Oxygen detector showed no oxygen in the system. UV radiation was started and measurements of the intensity using sampling grids of 10 mm x 10 mm were used. The detector was connected to the data logger Keithley, type 2410, the Thorlab motor-driven XY table and data logger were controlled by an in-house developed matlab algorithm for positioning and data acquisition.

4.3.2.4. Analysis

After each measurement data was analyzed and transformed using the responsivity spectrum of each detector to calculate the local Irradiance (flux density) in mW/cm2.

$$E_A = \frac{I_D}{A_d s_\lambda} \quad \textbf{(4.34)}$$

I_D is electrical current generated by the detector in Ampere;

A_d is the active area of the detector cm^2;

s_λ is the response of a radiometer AW^{-1};

With the help of the software Design Expert the measurement points were analyzed and a surface response was generated.

4.4. Results and discussion

4.4.1. Chemical actinometry

The Figure 4.10 represent the experimentally observed variation of the isomers cis-, trans-cyclooctene versus the irradiation time. The decrease of cis-cyclooctene, initial substrate present in the irradiated solution, is proportional to the evolution of trans-cyclooctene. As the experiment progress the concentrations of the isomers lean towards the theoretical photo-stationary conditions.

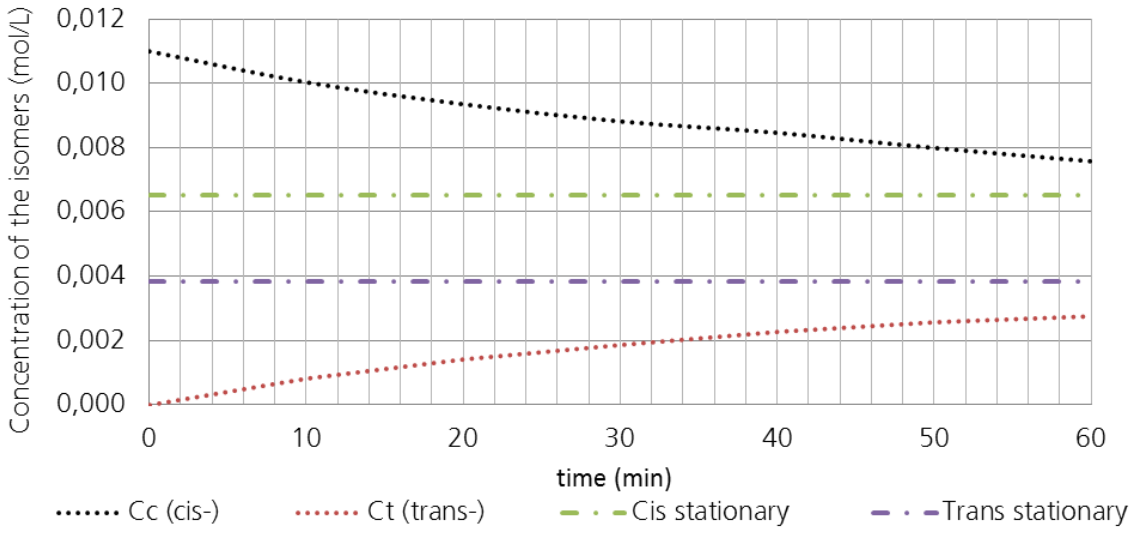

Figure 4.10 Evolution of concentration of the isomers in purified pentane versus the irradiation time. The values at the photo-stationary balance (63% cis, 37% trans) are indicated.

Initially the transformation of the cis-cycloctene to trans-cycloctene occurs rapidly with a constant slope, with an increase of concentration of trans-cyclootene, this starts absorbing radiation and turning as to cis-cycloctene, the formation and disappearance of the two isomers slows down and tend to reach a theoretical photo-stationary equilibrium, this equilibrium was not reached in experiments. The photo-stationary balance follows the relation (65% cis-, 35% trans-) [18].

Following the method described in section 4.3.1, plotting $f(c_c)$ versus irradiation time yields good linear correlation for cis-cyclooctene solutions of purified solvent. The Figure 4.11 shows the plot of $f(c_c)$ versus time.

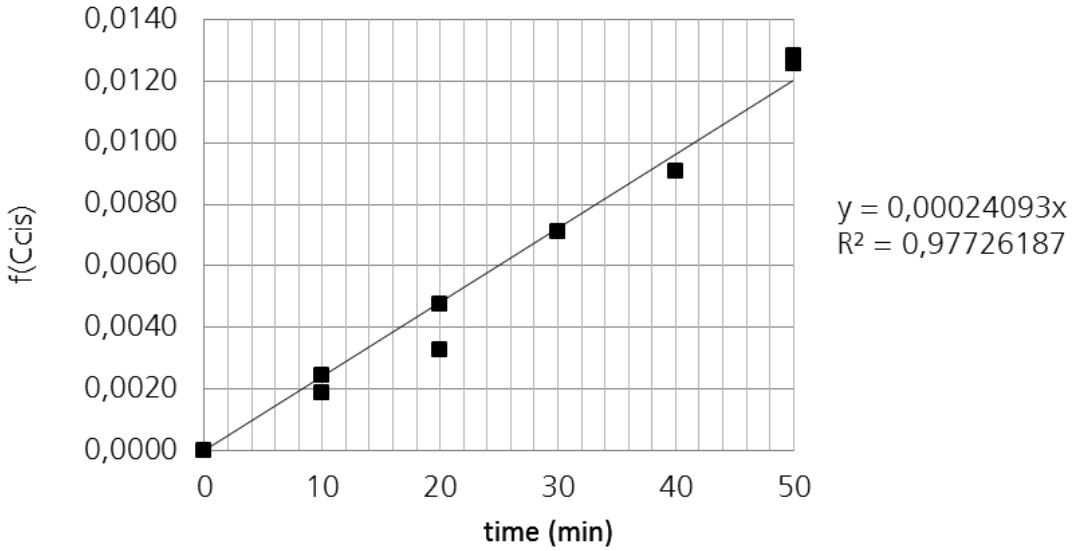

Figure 4.11 Plot of the function $f(C_c)$ versus irradiation time

Using the slope of the linear correlation and introducing the corresponding values into the equation 4.31, one can calculate the incident number of photon (photons/s), the spectral radiant power (W) and the irradiance (w/cm^2). The

Table 4.2 summarizes the results of the actinometric procedure.

Table 4.2 Calculated incident number of photons, spectral radiant power and the irradiance for the used photo-reactor setup chemical actinometry

c_o cis-cyclooctene mol L^{-1}	m from plot ($f(c_c)$vs. t)	E_p^o mol photons s^{-1}	E_λ^0 W	$E_{\lambda A}^0$ mW cm^{-2}
0,011	0,000241	2,30x 10^{-6}	1,59	5,41

The obtained spectral radiant power of the system is therefore 1,59 W at 172 nm, the Irradiance is then the spectral radiant power of the system divided by the effective are (quartz window). The Irradiance of the system was then calculated to be 5,41mW/cm^2.

4.4.2. Radiometry

Responses of the Si-photodiode and AlGaN-sensor were obtained. Using the equation 4.32, one can obtain the punctual Intensity in the specific point. The area of detectors and the responsivity at 172nm are summarized in the Table 4.3.

Table 4.3 Characteristics of the radiometer detectors

Detector	Specific Area of detection	Responsivity at 172 nm
Si-Photodiode Hammamatzu S8551	**33,6 mm2**	**0,100 A/W**
AlGaN L2416-B1-G04 Fraunhofer IPM (Calibrated)	**0,327 mm2**	**663 µA/W**

The response current along the measured area for each detector is shown in the Figure 4.12 for Si photodiode and Figure 4.13 for AlGaN sensor; the surface response was obtained with the software Design Expert.

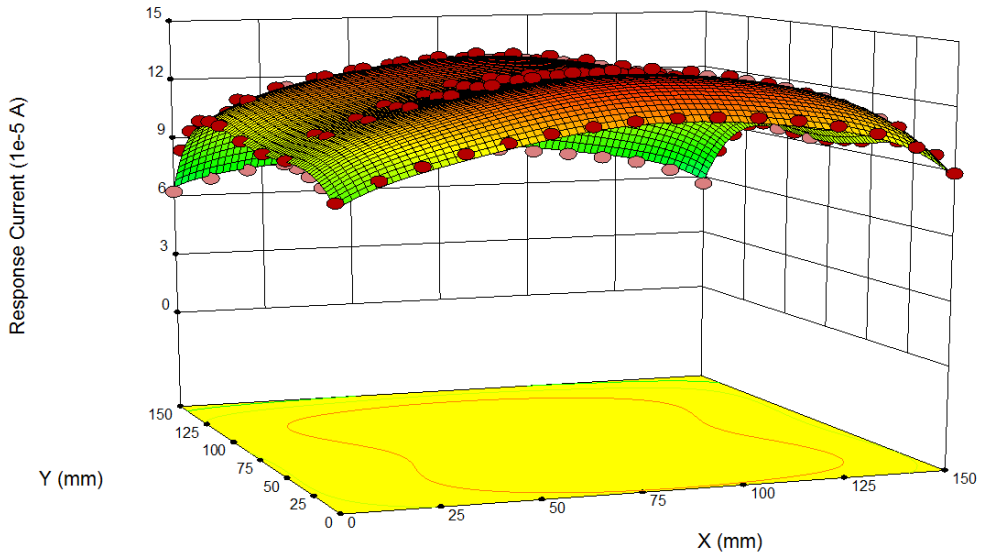

Figure 4.12 Response current Si-Photodiode Hammamatzu S8551, reactor window

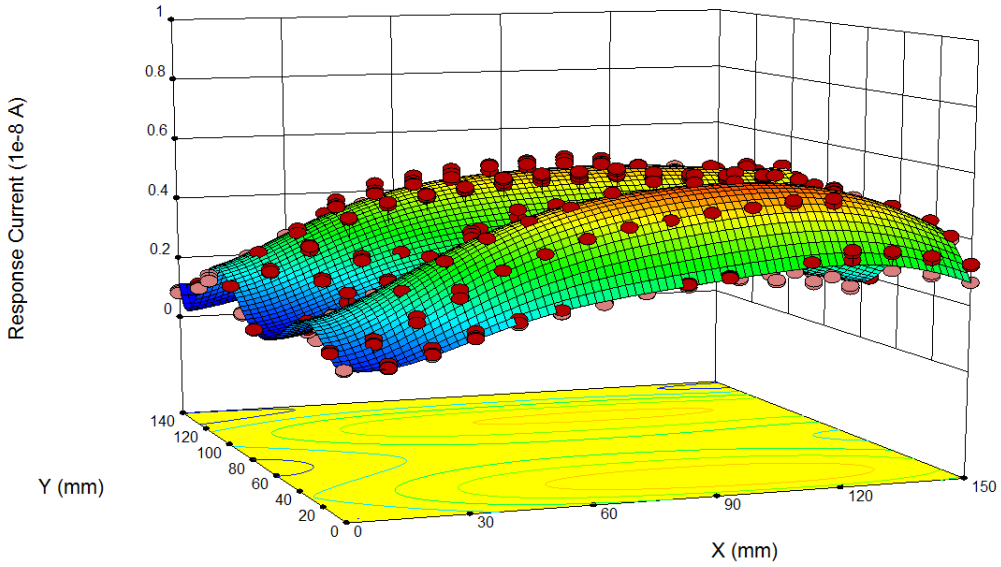

Figure 4.13 Response current AlGaN Fraunhofer L2416-B1-G04, reactor window

Using the response current for each spatial data-point and introducing the corresponding values into the equation 4.32, one can calculate the irradiance (w/cm^2) and the spectral radiant power (W).

The following Figure 4.14 and Figure 4.15 show the calculated irradiance distribution obtained with each sensor.

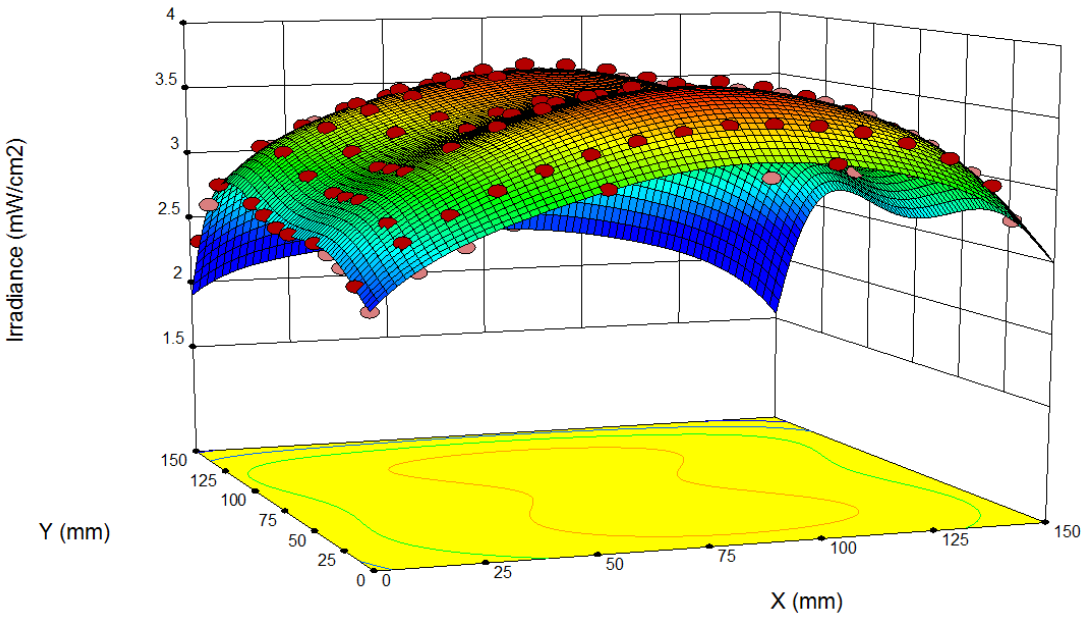

Figure 4.14 Irradiance distribution obtained using the Si-Photodiode Hammamatzu S8551

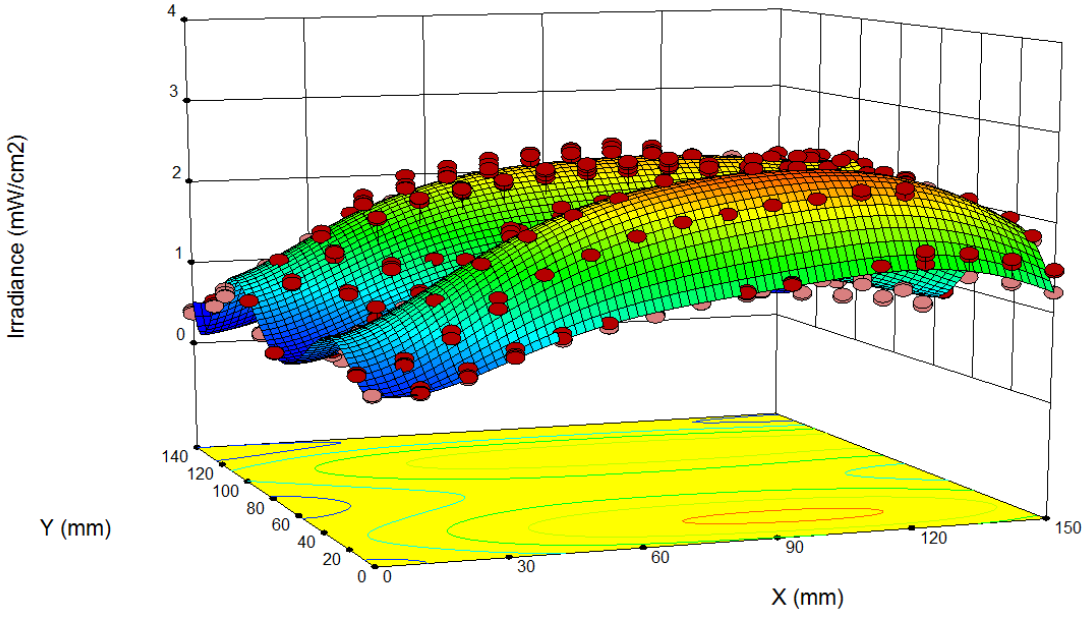

Figure 4.15 Irradiance distribution obtained using the AlGaN Fraunhofer L2416-B1-G04

The irradiance along the area of the photo-reactor is not homogeneous, the point of maximum irradiation are lengthwise parallel to the position of the lamps in the Xeradex System. The calculated spectral radiant power at 172 nm using the Si-photodiode is 1,04 W and using the AlGaN is 0,42 W respectively.

4.4.3. Comparison of methodologies

Irradiance and spectral radiant power calculated from measurements using three different methodologies are summarized in the Table 4.4.

Table 4.4 Characteristics of the radiometer detectors

Method	Irradiance mW/cm^2	Spectral radiant power W at 172 nm
Chemical Actinometry cis-trans cyclooctene	**5,41 mW/cm^2**	**1,59 W**
Si-Photodiode Hammamatzu S8551	**3,52 mW/cm^2**	**1,04 W**
AlGaN L2416-B1-G04 Fraunhofer (Calibrated)	**1,43 mW/cm^2**	**0,42 W**

Strong difference in the irradiance and spectral radiant power measured at 172 nm radiation for the same system using three different methods was found; these differences can be discussed analysing the error sources and assumptions taken into account for each method.

- Chemical actinometry cis-trans cyclooctene:

  Absorption of pentane is not exactly known at 172 nm, the authors of the method developed and standardised for chemical actinometry assumed that the absorption of pentane at 172 is similar to the absorption at 185 nm therefore negligible. Absorption of high energy radiation by pentane may lead to the formation of organic radicals which may affect the isomer system cis-trans cyclooctene by side reactions.

  Quantum yield of cis-cyclooctene and trans-cyclooctene are not exactly known at 172 nm, the authors of the method developed and standardised for chemical actinometry assumed these two values are equal to those first researched at 185 nm. Taking into account the balance equation which describes the kinetics of the cis-cyclooctene, the quantum yield is inversely proportional to the spectral radiant power; a higher quantum yield (which would be expected when compared with 185 nm) will therefore leads to a lower calculated spectral radiant power.

- Si-Photodiode Hammamatzu S8551:

  The response of Si-photodiodes is not only observable in the VUV range; it is also present in the UV, VIS and infrared. The emission of Xenon excimer lamps in the VUV and UV range is well known and described in literature and section 2.3.2 of this study. The setup used for experiments has an additional 10 mm quartz plate window (which is in contact with the fluid to be studied). Giving that, and taking into account the luminescence phenomena of the quartz window in the

  Blue-violet 3,4 eV (365 nm) and violet 3 eV (420 nm) range of spectra [89], it was observed a long-lived, red luminescence colour with an approximately stable intensity in irradiated quartz. This luminescence emitting a broad double-peak at 645 and 725 nm[90] reaches the Si-photodiode; the responsivity of the Si-photodiode for electromagnetic radiation at 365, 420, 645 and 725 nm is high enough to distress/mask the measurement with this sensor.

  In Figure 4.16 it can be observed the red luminescence of the quartz glass part of the reactor frame around the Oxram xenon excimer lamp used for experiments.

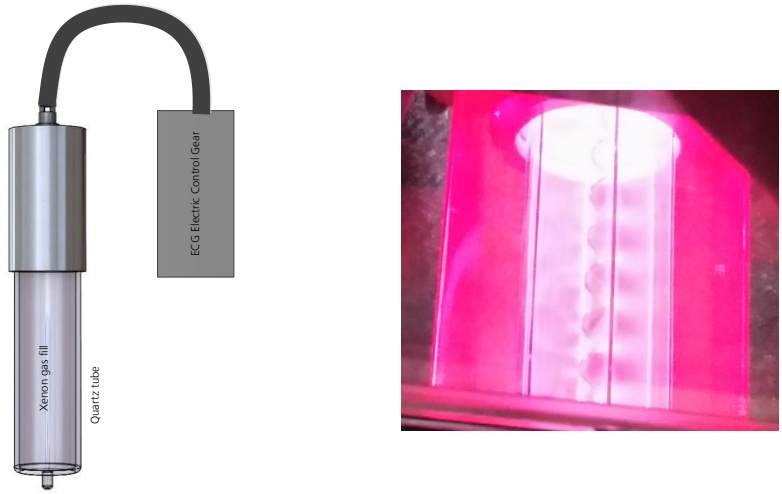

Figure 4.16 Luminescence phenomena of the quartz window in the red range emission of a broad double peak at 645 and 725 nm

In Figure 4.14 the irradiance distribution measured with the Si-photodiode shows a homogeneous irradiation, in terms of VUV, the radiation of interest, this behaviour is unlikely because the system walls (Aluminium) do not reflect this radiation. However this material is good reflector of larger wavelengths for example radiation at 365 and 420 nm (luminescence of the quartz window). Additionally to this phenomenon, the Si-photodiode is also actively responsive to those wavelengths. The results of Si-photodiode measurements have a high probability of being mask by the response of the detector for the radiation of the luminescence of the quartz window.

- AlGaN L2416-B1-G04 Fraunhofer:

  AlGaN-sensor is blind for radiation above 360 nm, it does not have any responsivity in the range of luminescence of the quartz window. The sensor shows no degradation in the time used. The sensor present a lower responsivity when compared with Si-photodiodes, however it is not relevant when measuring high intensity and high energy photons. It is necessary a data logger able to measure current in the range of nano amperes.

The Table 4.5 present a summary of the advantages and disadvantages of the methodologies studied in this chapter.

Table 4.5 Summary advantages and disadvantages of the methodologies

Method	Advantages	Disadvantages
Chemical Actinometry	When it is stablish taking into account all interactions between chemicals and radiation is a reliable method. It is common practice for other wavelengths in close systems without recirculation.	The use of organic solvent with boiling point 37°C, requires strict control of temperature. It cannot be used in systems where Lamps are in direct contact with the medium (contact external high voltage electrodes can produce explosion) Especially in the case of radiation at 172 nm. Not all interactions are known. Some interactions are assumed to be similar to those at 185 nm Absorption of the solvent is neglected but may exist and have an influence in the measurement
Si-Photodiode Hammamatzu S8551	Commercially available, fast development of equipment in this field. It is reliable and useful for low intensity radiation sources and for other applications. Plug and play system Accurate, reliable and stabile for UVC wavelengths	Degradation of the sensor by radiation at 172 nm Sensor response not just to VUV also UV-VIS and NIR Sensor response is larger at UV, VIS and NIR than in the range of interest Filter must be used; therefore the measurement is not a direct measurement is a difference of several measurements. Filters block always the radiation with higher energy (VUV) there are not filter which block low energy radiation and are permeable by high energy radiation in VUV range
AlGaN L2416-B1-G04 Fraunhofer (Calibrated)	Sensor is blind to radiation with a wavelength longer than 360 nm specially calibrated sensor for 172 nm Sensor responses just to high Intensity radiation Minimal degradation by radiation at 172 nm	Responsivity lower than Si photodiode, however no relevant if there is a calibration of the sensor and when it is used for measurement of high Intensity radiators

Taking into account the results, the chemical actinometry and the Si-photodiode methods have a larger sources of uncertainty in the measurement, the irradiance and spectral radiant power which will be consider for this study are those results from the AlGaN sensor from Fraunhofer.

4.5. Conclusions

The lack of a standardize method for irradiation measurements at 172 nm motivated the work of the present chapter of this thesis, the main goal of the work was to study different approaches to measure the radiation intensity of UV systems which use radiation at 172 nm and stablish a method for UV characterisation at this wavelength.

In order to find UV measurement procedures with the lowest uncertainties, it is necessary to deeply analyse the measurement problem, each methodology has its own limitations and uncertainties and an objective measurement of radiation intensity must compare different methodologies.

Three approaches for the radiation intensity measurement of radiation at 172 nm were tested in house. Chemical actinometry and photometry using two different detectors were selected for analysis.

Chemical actinometry methods have to take into account the absorption process, quantum yields and conditions of experiment and analysis of the components generated or consumed; photometric methods must have into account the use of the matching photometer to the application; the matching of the calibration source to the application measurement; and the characterization of the radiometer for its spectral response and any other parameter that may affect the measurement [84].

A measurement setup was conceived, built and tested for two photometric devices the Si photodiode and the AlGaN-detector. The radiation intensity using this setup can be scanned in all the radiation area, moving the detector (two dimensional) using two coupled electro mechanical arms moving along the complete plane of the radiation. Homogeneity of radiation can be expressed. Punctual as well as overall radiation intensity can be measured.

Measured and calculated irradiance values differ strongly from one method to the other. Actinometry and Si photodiode methods were found to have a larger number of uncertainty sources and are not suitable for performing Intensity measurements to the photo-reactor system in this study.

Spectral mismatch between the responsivity of the sensor and the direct and indirect emissions of the system were a major uncertainty source. It is important to pick a UV meter that has the closest match

to the desired measurement function. If that is not possible, then a correction factor must be measured or calculated. It is a must to measure the absolute spectral responsivity of the UV meter and know the source's relative spectral distribution.

Due to the responsivity of the sensor, its blindness to higher wavelengths (avoiding interferences from luminescence), the time efficiency, accuracy, availability and existence of a calibrated sensor the method using AlGaN-detector will be further researched and used for intensity measurements of the next generation radiation sources in this thesis and further studies.

The measurements were performed in close collaboration between Fraunhofer IGB in Stuttgart and Fraunhofer IPM in Freiburg.

A measurement setup was designed, built and used for the measurement of radiation intensity at 172 nm. An operational procedure for measurements of radiation intensity at 172 nm was stablished for future uses in the field.

5. Measurement of absorption coefficient of water around 172 nm

5.1. Introduction

As described in earlier chapters, the absorption phenomena is the base of photo-chemical processes. Therefore there is a need to describe and study in detail this phenomenon during VUV AOPs. The absorption process specifically of radiation at 172 nm in water is the precursor of the generation of the hydroxyl radical needed for oxidation as well as defines the spatial distribution of this and the subsequent reaction.

The intensity of light decreases exponentially with distance, and absorption can be measured from intensity of transmitted light. The absorption process is mathematically described by the Beer-Lambert law explained in chapter 2. Using this mathematical expression, the absorption coefficient which describes the extent to which the radiant flow of a beam is reduced as it passes through a specific material, can be calculated.

In this chapter a concept for the study of absorption process as well as a review of the relevant literature on optical constants specifically the absorption coefficient of water in the range from 100 to 200 nm is presented. Methodologies for the measurement of the absorption coefficient are described and one of them the transmission method is used for absorption coefficient measurements. A measurement setup was designed and built, the absorption coefficient of water under the range of interest was measured. Experimental results and analysis of the collected data are presented.

It was found during this study that the absorption coefficient measured in laboratory is larger than the value used until now in the literature of VUV AOPs. Description of the significance this founding has in the spatial distribution of the photo chemical reactions for oxidation is presented.

5.2. Measurement methods of optical constants

In order to characterize the spatial behavior of the absorption process by measuring the absorption coefficient of water at 172 nm, the following relevant concepts described in chapter 3 are going to be use: reflection, refraction, absorption, absorbance, transmission, radiant power, irradiance, dose, photon, photon flow and absorbed photon. Additionally the following concepts are essential; to study the absorption process it is required to follow the Intensity of the radiation spatially; the intensities of

the incident and the transmitted beam are correlated by a mathematical expression, which quantitatively describes the exponential attenuation of radiation by transmitting into an absorbing medium [20, 28].

- Mathematical expression absorption process: When a parallel monochromatic beam of electromagnetic radiation passes through an absorbing medium (e.g., absorbing substances in a dilute solution or gas), the absorbance of the beam in the medium is proportional to the absorption path length, and to the concentration, or in the gas phase to the pressure of the absorbing species. The law can be expressed as

$$\boldsymbol{A_{10} = \log \frac{E_\lambda^0}{E_\lambda^{trans}} = \log \frac{1}{T} = -\log T = \varepsilon_\lambda cl} \quad \textbf{(5.1)}$$

Or

$$\boldsymbol{E_\lambda = E_\lambda^0 x 10^{-\varepsilon cl}} \quad \textbf{(5.2)}$$

Where,

A_{10} is the decadic absorbance of a beam of collimated monochromatic radiation in a homogeneous isotropic medium;

E_λ^0 is the incident spectral radiant power;

E_λ^{trans} is the transmitted spectral radiant power;

T is the transmittance, which is defined as the ratio of the transmitted spectral radiant power to that incident on the sample;

ε_λ is the molar decadic absorption coefficient in $Lmol^{-1}cm^{-1}$;

c is the concentration of the substrate in mol L^{-1};

l is the thickness of the solution traversed by the UV radiation;

- Molar decadic absorption coefficient ε_λ: it is defined as the absorbance divided by the absorption path-length, l , and the amount of concentration, c :

$$\boldsymbol{\varepsilon_\lambda = \frac{A_{10}}{cl}} \quad \textbf{(5.3)}$$

- Decadic absorption coefficient: it is defined as the absorbance divided by the optical path-length. Since absorbance is a dimensionless quantity, the coherent SI unit for a is m^{-1}; the common unit is cm^{-1}.

$$a = \boldsymbol{\varepsilon_\lambda} c = \frac{\boldsymbol{A_{10}}}{l} \quad \textbf{(5.4)}$$

Several authors have been representing the absorption process also in terms of Naperian logarithm and defined therefore the following concepts.

- Attenuation cross section σ_λ: it is defined as the Naperian absorbance divided by the absorption path-length, l , and the number density of the attenuating species i, $\mathrm{n_i}$:

$$\sigma_\lambda = \frac{A_n}{\mathrm{n_i l}} \tag{5.5}$$

- Naperian absorption coefficient: it is defined as the Naperian absorbance divided by the optical path-length. Since absorbance is a dimensionless quantity, the coherent SI unit for α is m^{-1}; the common unit is cm^{-1}.

$$\alpha = \sigma_\lambda \mathrm{n_i} = \frac{A_n}{\mathrm{l}} \tag{5.6}$$

The Naperian absorption coefficient and the decadic absorption coefficient can be related as follow:

$$\mathrm{a} = \frac{\alpha}{\ln(10)} \tag{5.7}$$

This is valid just under the case of *uniform* attenuation.

Information concerning optical properties of water is of great significance for the photo induced AOPs. Knowledge of optical properties of water is a first step to characterize and understand the spatial distribution of the AOPs using radiation at a wavelength of 172 nm.

The degradation of any organic substance in AOPs is primary initiated with hydroxyl radicals generated by the photolysis of water at 172 nm. The photolysis is the result of absorption process of high intensity radiation by water, this generation occurs just in the photoreaction zone which its reach is defined by the optical properties of water in this range.

To calculate the total penetration of radiation in water, the absorption coefficient of water at 172 nm is needed. This total penetrations defines the photoreaction zone thickness for the generation of hydroxyl radicals in photo induced AOP. The most used value in literature for the calculation of the total penetration is 550 cm^{-1} [20, 57]. Using the mathematical expression of the absorption process and assuming 99% absorption of VUV radiation at 172nm, it is possible to calculate the theoretical penetration of radiation.

$$A_{10} = \log\frac{\mathrm{E}_\lambda^0}{\mathrm{E}_\lambda^{\mathrm{trans}}} = \log\frac{100\%}{1\%} = 2; \quad \mathrm{l} = \frac{A_{10}}{\mathrm{a}} = \frac{2}{550\ \mathrm{cm^{-1}}} = 0{,}00364\ \mathrm{cm}$$

This calculation establishes that 99% of the incident radiation at 172nm is absorbed by pure water in a zone of 36,4 µm thickness. This value represents the theoretical photo-reaction zone of the VUV

oxidation process [20]. Due to the small photo reaction zone, it is really important for the photo-reactor design to have an accurate measurement of the absorption coefficient.

- Depth of penetration: it is defined as the inverse of the decadic or naperian absorption coefficient. If the decadic absorption coefficient, a is used, the depth of penetration $1/a$ is the distance at which the spectral radiant power E_λ decreases to one tenth of its incident value E_λ^0. If the Naperian absorption coefficient α is used, the depth of penetration $1/\alpha$ is the distance at which the spectral radiant power decreases to $1/e$ of its incident value [64].

5.2.1. Measurement of optical constants

Optical properties of water (optical constants) have been studied since the beginning of the spectrometry. Several methods for different ranges in wavelength have been reported. The optical constants can be measured at a given wavelength by direct methods or inferred from photometric or polarimetric measurements. An example of a direct method is the measurement of the index of refraction using a prism. This technique is usually restricted to non-absorbing materials. Indirect methods are also based on the measurement of the refractive index by other means, these methods include ellipsometry, the measurement of transmittance and reflectance at near-normal incidence, and reflectance measurements at oblique incidence.

The absorption coefficient of a material can be calculated from the measurement of the refractive index in a range where the material absorbs the radiation, therefore the concept refractive index and its relation with other properties is described

- Refractive index: the refractive index of a medium N is generally expressed as the ratio of the velocity of light c in vacuum to its velocity v in the medium; N=c/v. In the case of attenuation the refractive index becomes a complex function of the frequency of the light wave. The complex refractive index $N(\lambda) = n(\lambda) + ik(\lambda)$. Where the real part, *n* is related to the velocity, and *k*, the extinction coefficient is related to the decay, or damping of the oscillation amplitude of the incident electromagnetic wave. The optical properties of the material are therefore governed by the interaction between the material and the electric field of the electromagnetic wave.
  The electric field of the electromagnetic wave traveling in a material can be represented as follow: If a plane wave of frequency (*f*) propagates through a solid with velocity (*v*) in a direction defined by (*x*), the electric field (*E*) is described by the following progressive wave equation:

$$E = E_0 e^{i2\pi f\left[t-\left(\frac{x}{v}\right)\right]} \quad \textbf{(5.8)}$$

Where E_0 is the incident electric field vector and $i2\pi f\left[t-\left(\frac{x}{v}\right)\right]$ is the displacement at time t after a disturbance, created by the electric field at a point situated at x along the propagation.
The velocity of propagation in the absorbing medium can therefore be represented using the complex refractive index. Reorganizing the progressive wave equations result as follow:

$$E = E_0 e^{i2\pi ft} e^{-i2\pi nx} e^{-2\pi fkx/c} \quad \textbf{(5.9)}$$

Here we see that κ gives an exponential decay, as expected from the absorption process. Since the radiant power of an incident wave is proportional to the square of the electric field the relation between the Naperian absorption coefficient α and the extinction coefficient k are expressed as:

$$\ln \frac{E_\lambda^0}{E_\lambda^{trans}} = \frac{4\pi fkx}{c} \quad \textbf{(5.10)}$$

Therefore

$$\alpha = \frac{4\pi fk}{c} \quad \textbf{(5.11)}$$

As a summary, in materials where an electromagnetic wave can lose its energy during its propagation, the case of water under VUV, the imaginary part of the complex refractive index, the extinction coefficient, k is commonly used for reporting in literature. This extinction coefficient is related with the Naperian absorption coefficient α and the wavelength or the electromagnetic radiation being absorbed by

$$\alpha = \frac{4\pi k}{\lambda} \quad \textbf{(5.12)}$$

The most relevant methodologies to measure optical constants are briefly described in this section.

5.2.1.1. Reflection at oblique incidence

There exist a number of methods which can be used to determine n and k from reflectance measurements at oblique incidence. In this context, there are two special angles which are taken into account in these methods: the principal angle of incidence which must be determined by polarimetric methods and the Brewster, or pseudo-Brewster (pB), angle.

The principal angle is defined as the angle of incidence at which the phase difference of the reflected light with respect to the incident is $\pi/2$. A linearly polarized wave, different from s or p wave, is reflected as elliptically polarized with the major and minor axes parallel or perpendicular to the plane of incidence when the angle of incidence is the principal angle.

The Brewster angle is defined as the angle of incidence at which the p-polarized reflectivity vanishes, at this angle the incident p-polarized wave is totally refracted into the second medium. Consequently, a wave with arbitrary elliptic polarization, except for the linear p-polarization, is reflected as linearly s-polarized. The same is true for un-polarized or partially polarized light. For absorbing materials the Brewster angle does not appears and the Pseudo-Brewster angle is defined for them; for absorbing materials reflection reach a minimum but never zero, the angle at which this minimum occurs is then the pseudo-Brewster angle, and, if k>0, the pseudo-Brewster angle is greater than the Brewster angle. The Table 5.1 shows the different approaches to obtain the absorption coefficient using reflection at oblique incidence.

Table 5.1 Reflection at oblique incidence approaches

Method	Description
1	reflectance at two angles of incidence using natural or polarized radiation
2	ratio R_p/R_s at two angles of incidence
3	R_s and R_p at one angle of incidence
4	pseudo-Brewster angle and R_s or R_p at that angle
5	pseudo-Brewster angle and R_p/R_s at that angle
6	pseudo-Brewster angle and R_p, R_s or R_p/R_s at any other angle of incidence

In principle only two measurements are required, but, because of possible errors in the measurements, a redundancy of measurements is more useful and gives an indication of the errors involved in determining n and k.

Although these methods can be used at any wavelength, their sensitivities to errors in measurements of reflectance, or of the angles involved, or of the state of polarization are functions of both n and k as well as the angle of incidence, as well as the state of polarization. Thus there may be parts of the n-k plane, angles of incidence, and states of polarization, for which the lack of sensitivity reduces their accuracy to unacceptable values [91].

The accuracy of methods using two media, and their usefulness, in view of tough experimental problems, is uncertain. When light reflects at a water surface, reflectance is determined according to the complex refractive index, composed of refractive index n and extinction coefficient. The problem here is the strong absorption of the water vapor which interfere with measurements. Painter and co-workers calculated the absorption spectra of water from reflectance measurements [92], but poor sensitivity of the reflection measurements has prevented the study of important questions such as how minute levels of dissolved substances affect absorption bands of water [73].

5.2.1.2. Transmittance method

The absorption coefficient can be determined by measuring the transmittance of a known thickness of material and calculating a using Lambert's law after correcting the transmittance measurements for reflection losses at the surfaces.

Although some researchers reported transmittance spectra of water down to 155 nm wavelengths or below with preparing extremely thin water film such as 285 nm thick, these methods were not convenient and suffered from repeatability, here the main problem was dissolution of the window material (magnesium fluoride, calcium fluoride) in water and experimental difficulties like a controlled oxygen free atmosphere [68].

5.2.1.3. Inelastic X-ray scattering

A fundamental property of a material in relation to light is its oscillator strength distribution, i.e., how strongly it absorbs light as a function of wavelength. Using inelastic X-ray scattering the oscillator strength distribution can be measured. This technique is a photon-in photon out x-ray spectroscopy, in which the incident photon resonantly excites a core-hole state, that consequently decays by the emission of a scattered photon. The scattering as a whole is inelastic, which means that the energy of the scattered photon is generally lower than the energy of the incident one. The resulting energy loss is transferred to the system, which is left into an excited state. At this point the energy and momentum change of the scattered photon are measured. Inelastic x-ray scattering spectroscopy is in principle equivalent to optical spectroscopy as long as momentum transfer can be approximated to be zero. In literature, measurements of optical constants of water using this technic were reported by Hayashi [72]. Once the oscillator strength distribution is determined precisely for a wide enough energy range, the optical constants such as absorbance and reflectance as well as a number of other properties of the material, some of which are seemingly unrelated to photo-absorption, can be deduced.

It is necessary the use of a Synchrotron and the absorption results have a strong deviation from the other methods in literature [72].

5.2.1.4. Ellipsometry

In ellipsometry it is measured the change in polarization state of the beam of light after non-normal reflection from the sample. The polarization state is defined by two parameters. For example, the

relative phase and relative amplitude of the orthogonal electric field components of the polarized light wave. On reflection both electric field components are modified in a linear way, so a single ellipsometric measurement provides two independent parameters.

The name ellipsometry derives from the fact that linear polarized light after oblique reflection becomes elliptically polarized due to the different reflection coefficients for the s and p polarized light. By measuring the polarization ellipse, one can determine the complex dielectric function of the sample [93].

The measurement procedure is to locate the minimum transmission through the optical system by alternately rotating polarizer and analyzer. Since it is the polarization state and not the intensity which is being measured, the results are unaffected by source intensity fluctuations.

No data has been found of absorption coefficient of water measured with this technique. However there are some systems in the market that assure it can be used with liquids in the VUV range. Similar to the reflection at oblique incidence, one problem to measure optical constants of water can be the strong absorption of the water vapor which interfere with measurements.

5.2.1.5. Attenuated total reflection method

Attenuated total reflection is a technique for determining the optical constants of liquid and solid substances. It differs from other techniques in that the ATR probes the sample with an evanescent wave rather than a collimated beam of light. Evanescent waves are formed when waves traveling in a medium undergo total internal reflection at its boundary because they strike it at an angle greater than the so-called critical angle. Evanescent waves near an interface decay exponentially over a distance (without absorption) comparable to the wavelength [94].

The Figure 5.1 shows schematically the ATR technique. A beam of light is passed through the internal reflection element IRE in such a way that it reflects at least once off the internal surface in contact with the sample (refractive index of the material larger that refractive index of the sample and incident angle to the interface greater that the critical angle). This reflection forms the evanescent wave which extends into the sample. The penetration depth into the sample is typically between 0.5 and 2 µm. The beam is then collected by a detector as it exits the crystal. Most modern spectrometers can be converted to characterize samples via ATR by mounting the ATR accessory in the spectrometer's sample compartment.

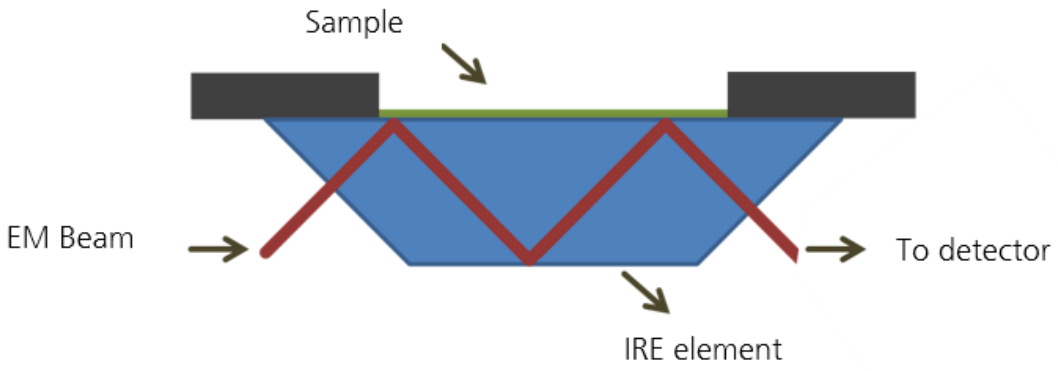

Figure 5.1 Reflection and refraction as a light beam passes from one medium

However due to the complexity of the method, the use of IRE under VUV conditions has to fulfill the following conditions to assure internal reflection and transmittance:

- The refractive index of the IRE must be greater than that of the sample material (aqueous solution).
- The IRE material must have sufficient transmittance in the measured wavelength range VUV.

For the specific case of water, IRE materials such as sapphire with higher refractive index than water have insufficient transmittance, while materials with sufficient transmittance (magnesium fluoride, calcium fluoride, and synthetic quartz) have lower refractive indices than water in the VUV region as well as problems related with solubility in water [73].

5.2.2. Literature review on absorption coefficients of water at 172nm

A list of primary references in the scientific literature on spectral measurements of the optical properties of water and compilations of water's refractive index and extinction coefficient can be easily prepared, however the main data found belongs to the range of long-wavelength where the water is relatively transparent [71]. The Figure 5.2 shows a summary of the most relevant authors and their absorption coefficient values reported as well as the year of the study.

Just a few authors discuss the absorption coefficient of water in the range of vacuum UV. The most relevant study and compilation of data in the range of 100 to 200 nm was performed by Painter [92]. Painter determined the optical and dielectric properties of liquid water in the vacuum UV range.

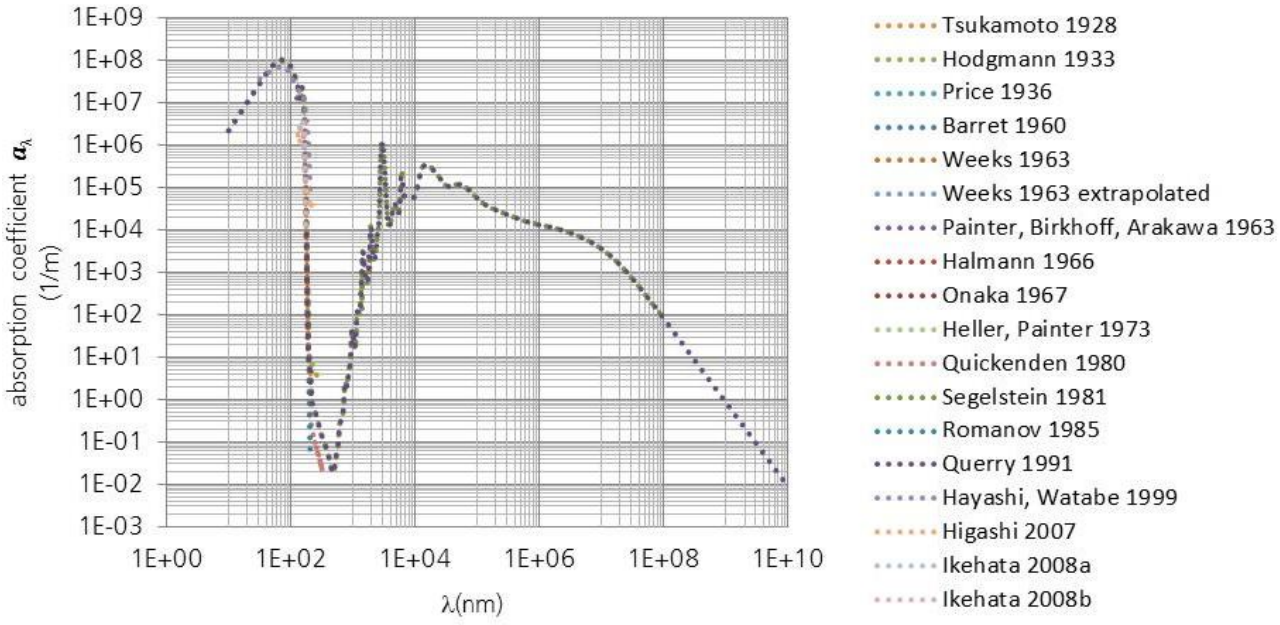

Figure 5.2 Decadic absorption coefficient of liquid water VUV range. Redraw different authors [33, 57, 66-74]

At the same time Painter compared his experimental data with data collected from other authors. Querry and Segelstein have presented the most representative and complete compilation of data for the optical properties of water, and their work is part of the Handbook of Optical Constants of solids second edition [71].

The Table 5.2 contains the most relevant literature sources of optical constants for water in the VUV range. The year of publication, the range of work and the methodologies used are as well summarized.

The Figure 5.3 shows the values reported of absorption coefficient of water under VUV in the range of work of this study.

The literature data and the spectral distribution of radiation of a Xe excimer lamp were plot in the same figure for descriptive purposes. The distribution of radiation is plotted using relative units. The penetration of VUV radiation for total absorption was calculated for the reported optical constants for each Author. The total penetration calculated differs from Author to Author.

Table 5.2 Relevant literature of optical properties of water in VUV

Author	Year	Range (nm)	Type	Method
Tsukamoto [92]	1928	180-220	Measured	Transmittance
Price [92]	1936	180-190	Measured	Transmittance
Barret [95]	1960	185-190	Measured	Transmittance
Weeks [57]	1963	170-190	Measured	Transmittance
Weeks [57]	1963	160-170	Extrapolated	
Halmann Platzner [96]	1966	180-185	Measured	Transmittance
Onaka [68]	1967	150-210	Measured	Transmittance
Painter [92]	1969	125-180	Measured	Reflectance
Heller [97]	1973	48-163	Measured	Reflectance
Quickenden [66]	1980	196-320	Measured	Transmittance
Segelstein [69]	1981	10-1e10	Compilation	
Romanov [70]	1985	186-205	Measured	Transmittance
Querry [71]	1997	10-1e10	Compilation	
Hayashi [72]	1999	25-1800	Measured	Inelastic X-ray scattering
Higashi [73]	2007	130-220	Measured	ATR
Ikehata [74]	2008	140-180	Measured	ATR

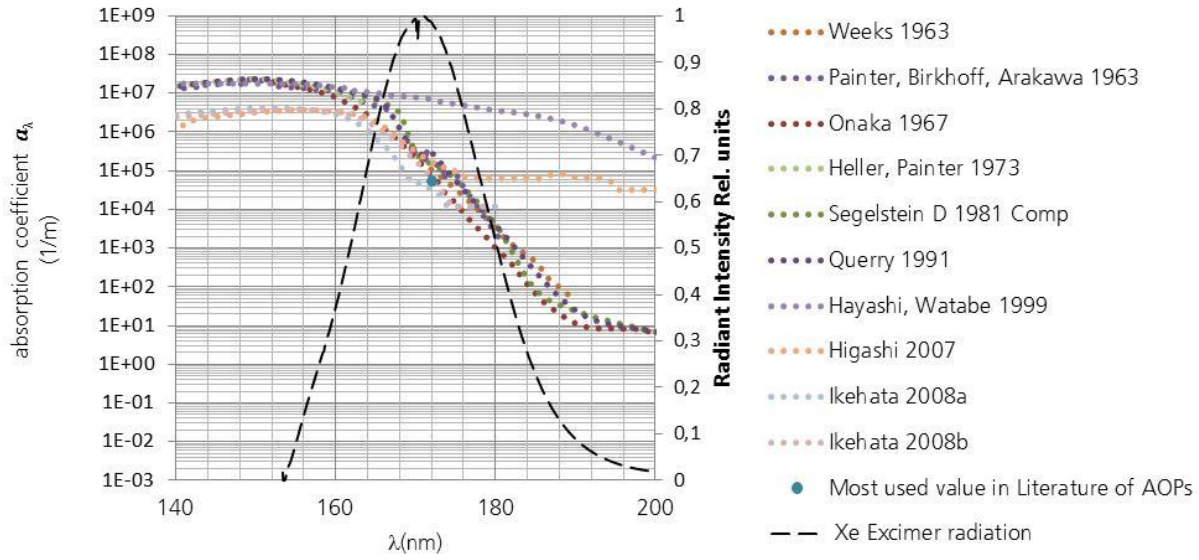

Figure 5.3 Decadic absorption coefficient of liquid water at 172 nm "monochromatic" Xe excimer radiation. Redraw different authors [33, 57, 66-74]

The Figure 5.4 represent the total penetration calculated from the values reported in literature, in other words the theoretical photo reaction zone for photo induced AOP for the relevant literature in the range of work.

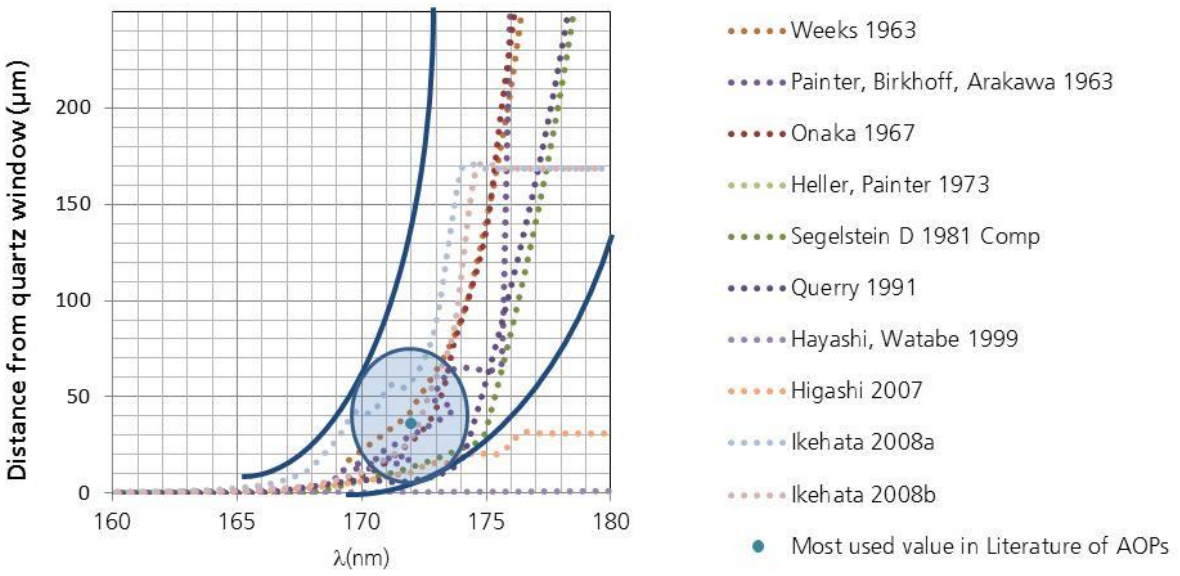

Figure 5.4 Calculation of total absorption penetration of VUV in liquid water using information from different authors.

Analysing the description of the methods, the difficulties and challenges distinctive of each method as well as the measures taken by the authors. It was decided to use the transmittance method for measurements and calculation of the absorption coefficient of water in the range of work, using materials which are not water soluble for the windows (in literature several methods used calcium fluoride windows which have high transmittance in the region but can be damage by water due to its solubility in water) and taking special care controlling the oxygen free atmosphere needed for measurements. The setup, methodology and measures taken are described in the following section.

5.3. Materials and methods

5.3.1. Transmission method

As described before the transmission method measures the relation of the power transmitted to the incident power in a thin film sample of the material to be characterized. In this case it was necessary to build a complete setup. The setup comprises a radiation source, an electro-mechanic arm which moves the sample holder, a sample holder and a detector. The setup installed in a gas tight chamber

where a non-absorbing nitrogen atmosphere was maintained. In this range of VUV radiation, oxygen absorbs strongly, this absorption engages the production of ozone. Even the smaller traces of oxygen were found to have a negative interference in the measurements.

In order to eliminate the effects which reflection has on transmission measurements, the following correction is performed. When a light ray goes from one material to another and these materials have different refraction index, a part of this ray is reflected. The simplest case is described for a smooth and flat interface and causes a specular reflexion (no diffused). The fraction of light reflected depends on the angle between the incident beam and the interface of the two materials. In the case of a ray perpendicular to the surface, general case of spectrophotometry, the fraction f of light reflected of a beam passing from a material 1 with n_1 as refraction index to material 2 with n_2 as refraction index, is given by Fresnel expression:

$$f = \left(\frac{n_1 - n_2}{n_1 + n_2}\right)^2 \quad \textbf{(5.13)}$$

In transmission through a glass plate, two reflecting surfaces are involved. If the fraction reflected at each surface is f, and only a single reflection at each surface is considered, the fraction transmitted is:

$$T = (1 - f)^2 \quad \textbf{(5.14)}$$

Considering next the reflection losses of a bean passing through a glass cell containing a liquid, there are two glass-nitrogen and two glass-liquid surfaces in the system. For each surface the fraction reflected can be denoted f_1 and f_2.

$$T = (1 - f_1)^2 x (1 - f_2)^2 \quad \textbf{(5.15)}$$

Considering now the special case of VUV, where most materials absorb radiation the fraction of the incident radiation transmitted in the whole system is:

$$T = (1 - b) x (1 - b_c)^2 x (1 - f_1)^2 x (1 - f_2)^2 \quad \textbf{(5.16)}$$

Where b and b_c are the fractions absorbed by the solution and the two walls of the cell, respectively. The values of f1, f2 and b_c can be calculated from the refractive index and internal transmission of the Corning material and the refraction index of nitrogen and water.

The term $(1 - b)$ is the transmittance refers just to the absorption phenomena in the water film.

$$T_{abs} = (1 - b) = \frac{E_{\lambda}^{trans}}{E_{\lambda}^{0}} = 10^{-(A_{10})} = 10^{-(al)} \quad \textbf{(5.17)}$$

The experimentally observed transmission must therefore corrected to obtain the transmittance of the absorption process in water as follow:

$$\frac{T}{(1-b_c)^2 x (1-f_1)^2 x (1-f_2)^2} = T_{abs} = (1-b) \quad \textbf{(5.18)}$$

Once the observer transmission is corrected, we use the mathematical expression for absorption process which relates transmittance of the absorption process, thickness of the sample l, and absorption coefficient a to calculate it through the equation 5.17.

5.3.2. Experimental setup

The setup built for determining the absorption coefficient is based on the principle of a one beam spectrophotometer. The light, emitted by a monochromatic radiation source (Xe excimer Lamp), passes through a cell (thin film sample holder) and then arrives to a photo-detector (VUV spectrophotometer Maya Pro Ocean Optics). The value of the absorption coefficient is then calculated from the relation of Transmittance of different sample thickness.

The assembly must respect some conditions. The complete setup has to be under a controlled nitrogen atmosphere without traces of oxygen or water vapor. The spectrophotometer has from manufacture a nitrogen purge inlet. In facts, oxygen and water vapor absorb strongly radiation in this spectral region. Working with closed and tight cells or sample holders with different optical paths has to be possible. As the lamp emits only one peak at 172 nm, we decided to work without neither filter nor mono-chromator. The cell or sample holder must be transparent for the spectral region, different materials where tested, the maximum transmission window in this spectral region was found to be the Corning HPFS® 8655 Fused Silica.

- The radiation source

The OSRAM XERADEX® lamp has outstanding 35 percent conversion efficiency (electrical to UV) at 172 nm. The Figure 5.5 shows a representation of the OSRAM XERADEX lamp. It is operated via a patented pulsed mode, using the corresponding electronic control gear (ECG). The quartz bulb functions as a dielectric barrier within an electrode system, which prevents the formation of an electric arc during the discharge phase. When xenon is excited by pulsed voltage across the electrodes, unstable xenon excimer molecules (Xe2*) are formed from the xenon atoms. These molecules dissociate by emitting VUV radiation at 172 nm. The XERADEX® lamps emit incoherent VUV radiation. No cooling of the lamp is required, as the temperature of the radiator never exceeds 80 °C [52].

Figure 5.5 Radiation source xenon excimer lamp

- Sample holder

Thin uniform films of water are required to perform the measurements due to the strong absorption. The setup was designed to be used with different spacers which regulate the channel thickness of the water film from 5µm to 20 µm. Surfaces of the transparent windows were manufactured and polished by Docter Optics Express Glass Services using the HPFS® 8655 Fused Silica from Corning. The Figure 5.6 shows the schematic of the thin film sample holder using two transparent CORNING HPFS® 8655 fused silica windows.

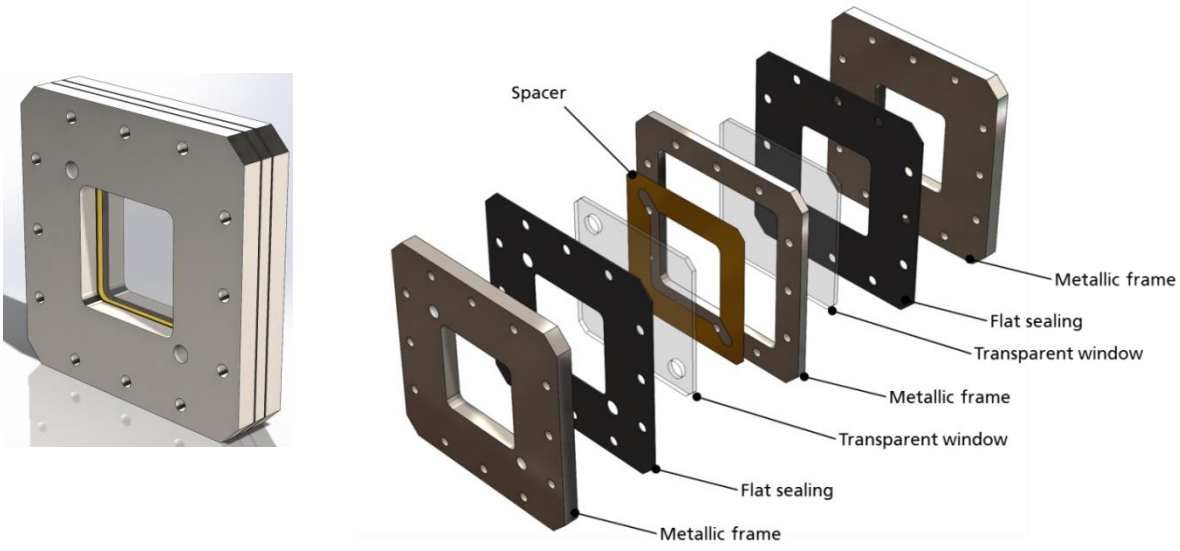

Figure 5.6 Thin film Sample holder transparent windows CORNING HPFS® 8655 fused silica

- Detector

Maya 2000 Pro Spectrometer customized by Ocean optics for the Extra-Deep UV extends spectral measurements to 153 nm. The Figure 5.7 shows the schematic representation of the lamp, sample holder and spectrometer used for the measurements.

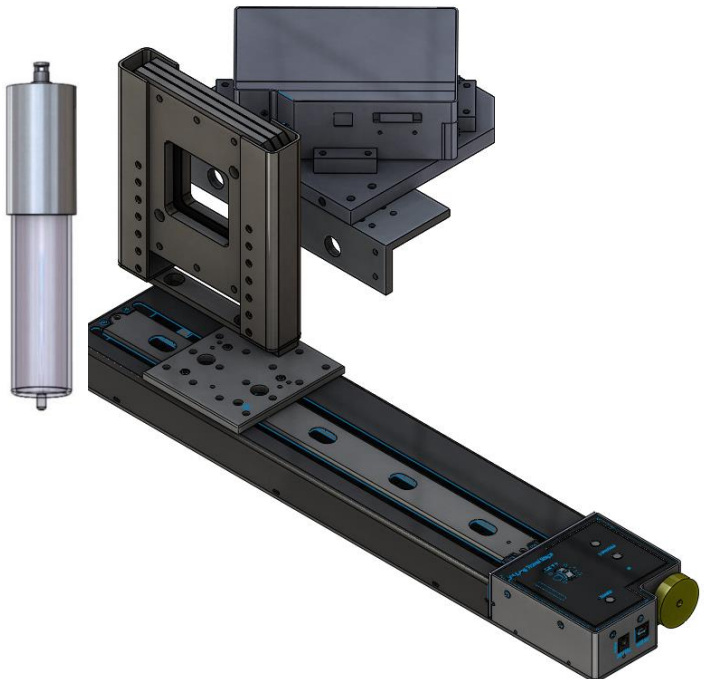

Figure 5.7 Schematic representation experimental setup.

The spectrometer has a spectral response which varies in the range from 153 nm until 300 nm wavelengths. The spectrometer uses the Hamamatsu S10420 Back-thinned 2D FFT-CCD detector.

It has a grating H7 UV-UPGD for the special spectral region and an installed optical bench entrance aperture of 25 µm width. The spectrometer is controlled with the help of the software Oceanview, the spectral data is collected and analysed with the help of such software.

Due to the interaction of radiation at 172 nm and air, the experimental setup was installed inside of a gas tight chamber with an oxygen sensor; the chamber can be purged with nitrogen until oxygen is not more detectable before starting experiments. The Figure 5.8 shows the gas tight chamber were the experimental setup was installed for measurements.

Figure 5.8 Gas tight chamber for the controlled nitrogen atmosphere. Experimental setup

5.4. Results and discussion

Preliminary experiments were performed to allow characterization of the measurement system. First, the spectrometer response was studied. The spectral emission of the Xe excimer Lamp was measured and compared with literature. The Figure 5.9 shows the comparison of the literature spectrum and the measured spectrum.

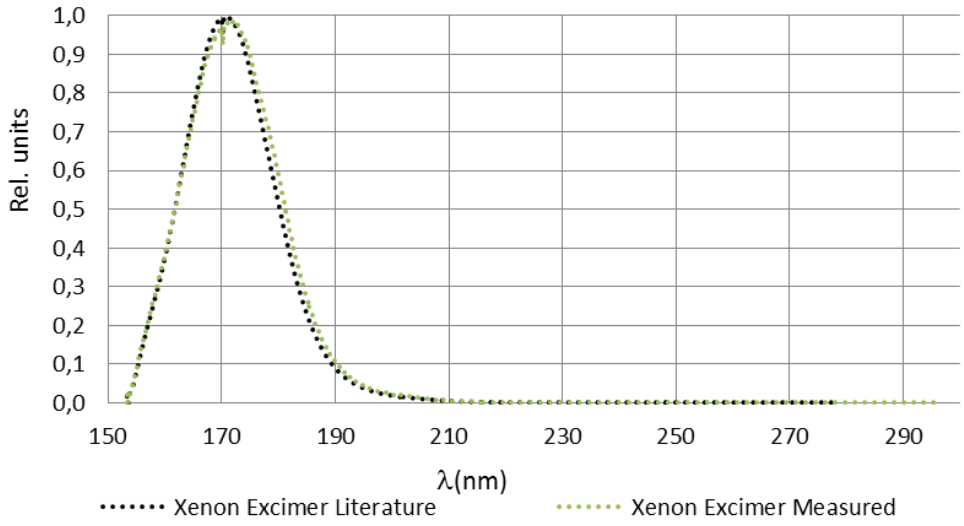

Figure 5.9 Comparison spectral emission of xenon excimer lamp literature and measured data.

The measurement is strongly affected by oxygen presentence in the setup. The Figure 5.10 shows the differences in spectrum when oxygen is present. The spectrum measured under air atmosphere shows a short wide expanded peak displaced with maximum at 185 nm, during purging nitrogen the recorded signal increases steadily and stabilizes when oxygen concentration is below 100 ppm, the peak maximum is located at 172 nm, under this conditions the spectral emission shows a tail toward the highest wavelengths (190 nm). The ratio of the peak area measured in the presence of oxygen (air) and the area of the peak in nitrogen atmosphere is about 8%.

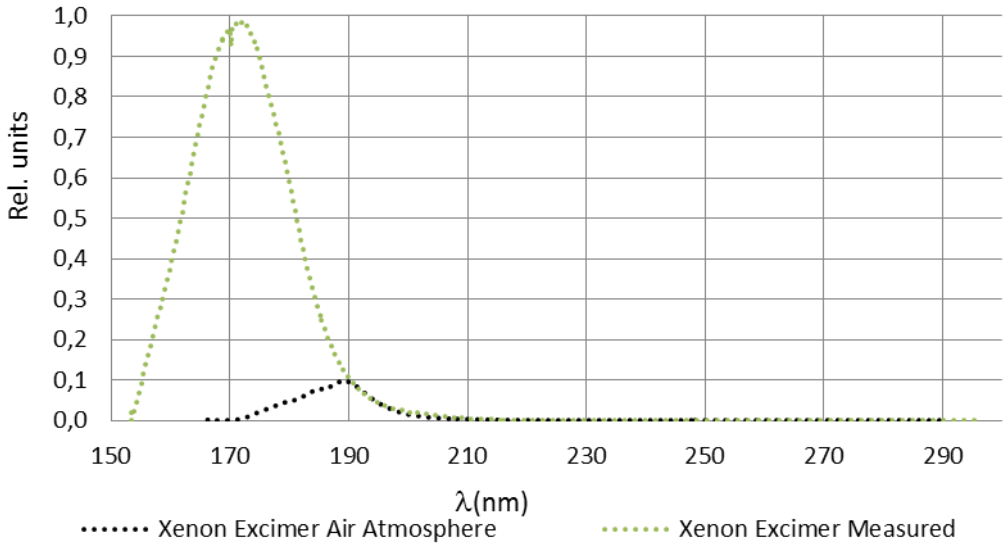

Figure 5.10 Comparison spectral emission of xenon excimer lamp under nitrogen atmosphere and air

5.4.1. Thin film 5µm, 10µm and 20µm water samples

Deionized water was use for the experiments and 300 measurements for each thickness were performed. The direct spectral emission of the lamp was measured with the sample holder system in between and without it alternating using the electronic thorlab arm. Position of the sample holder was adjusted to permit measurements always at the same spot of the window. The Figure 5.11 shows an example of the data acquired in each measurement. The transmittance was then calculated and corrected following the steps of the methodology presented in section 5.3.1. From the corrected data the absorption coefficient of water was then calculated. The Figure 5.12 shows the transmitted spectrum measured and the calculated Transmittance of 10 different measurement campaigns called groups, where each group has 10 repetitions.

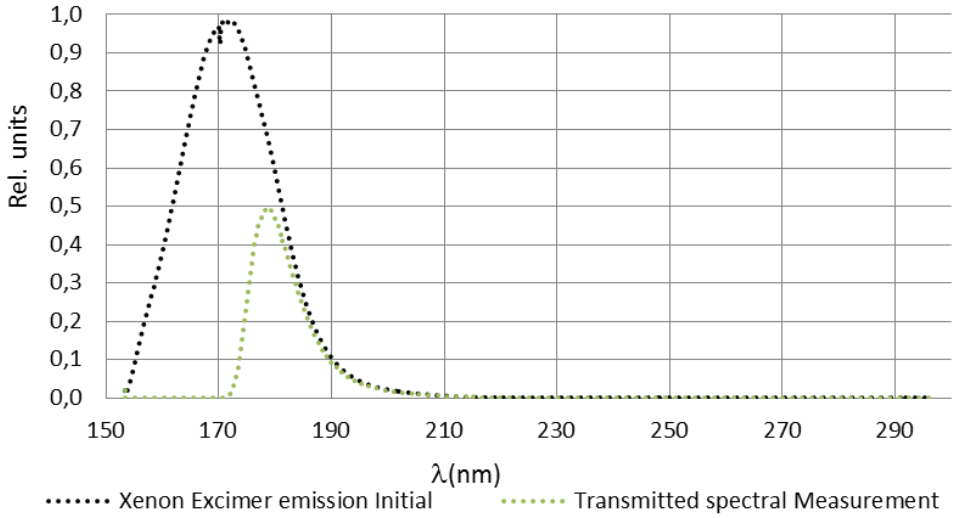

Figure 5.11 Spectral emission of xenon excimer lamp and transmitted spectral measurement for one measurement

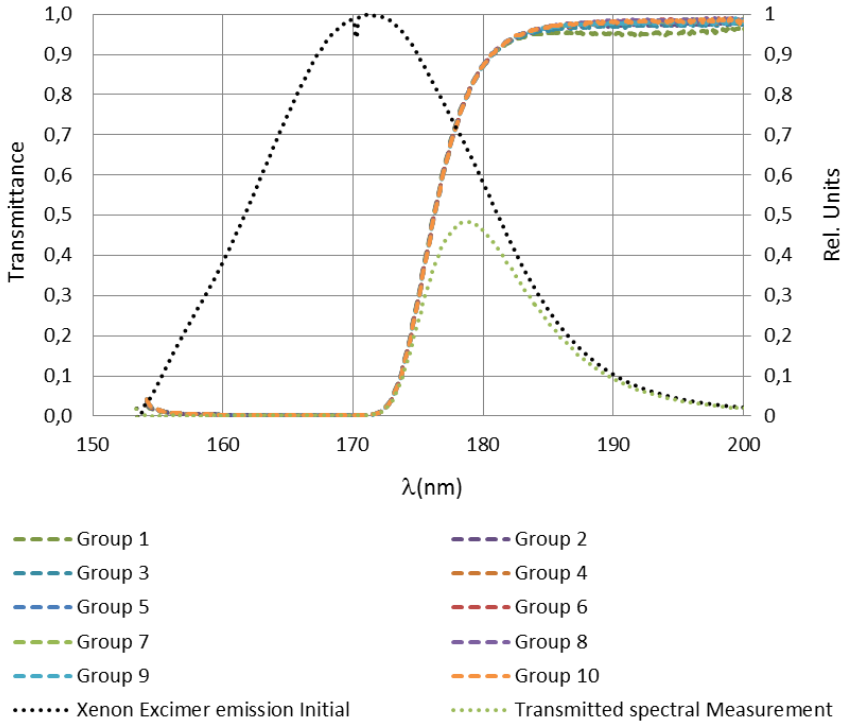

Figure 5.12 Calculated and corrected transmittance for 10 groups of 10 measurements of the same thickness, comparison with spectral data

The absorption coefficient of water was calculated in the range of work from the experimental data acquired; the Figure 5.13 shows the final reported values of the calculated absorption coefficient containing both the average value of absorption coefficient and the uncertainty in the mean values.

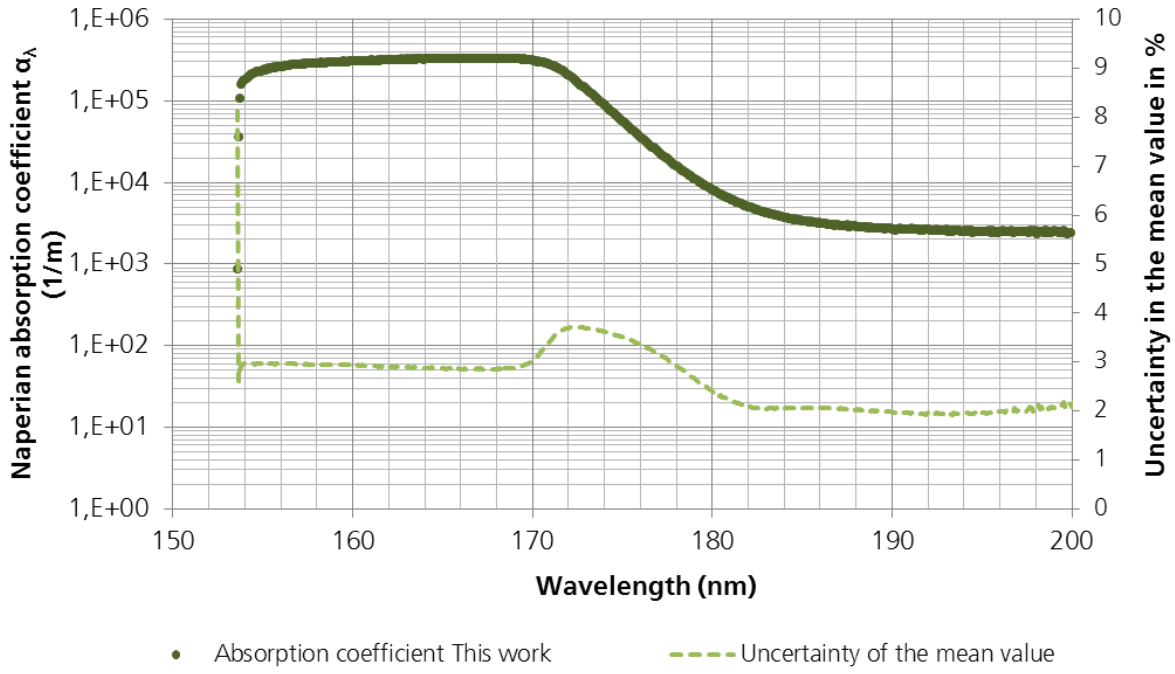

Figure 5.13 Calculated absorption coefficient of water in the range of measurement and the uncertainty of the mean value

A comparison of the results of this study with the literature is presented in the Figure 5.14; the results of this study showed a higher absorption coefficient than the values reported in literature in the range of 170 to 180 nm. The values obtained are 3 times higher than those reported by Painter et al [92], Barrett and Mansell [33] and weeks [57] in the sixties.

Similar values to the literature were found when comparing with Higashi who used the method attenuated total reflection in 2007 [73]. In the other hand, values similar to the literature of the sixties were measured just in the cases where bubbles in the cell were found after the experiment. Radiation is transmitted better through the bubbles therefore a lower absorption coefficient may be observed. The presence of bubbles in the sample holder were due to human error in filling the sample holder. The error was identified and corrected for the subsequent measurements. Below 170 nm the thickness of 5 µm of water film absorbs almost all the radiation this is the lower limit of measurement of the system.

To perform reliable measurement of the absorption coefficient below 170 nm, smaller channel thicknesses must be studied and thicknesses in the range of 0,1 µm to 5 µm should be achieved.

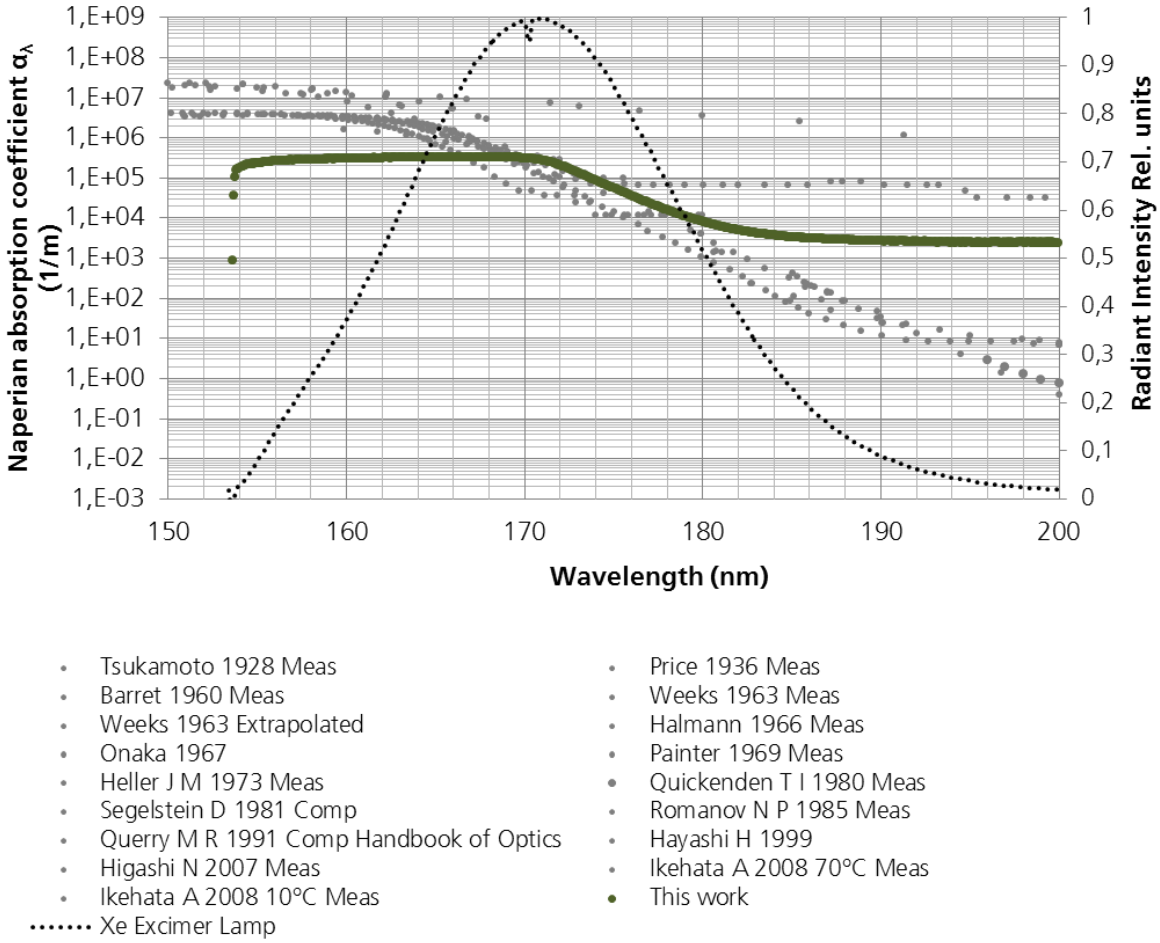

Figure 5.14 Comparison of the calculated absorption coefficient of water in the range of measurement and the values from Literature

The penetration of light assuming total absorption was calculated using the absorption coefficient found in this study and compared with values calculated from literature. The Figure 5.15 shows the results.

The penetration of VUV in these measurements shows to be three times smaller than the most used value in the literature of AOPs. Total absorption of the radiation at 172 nm happens in a layer of water smaller than 36 µm.

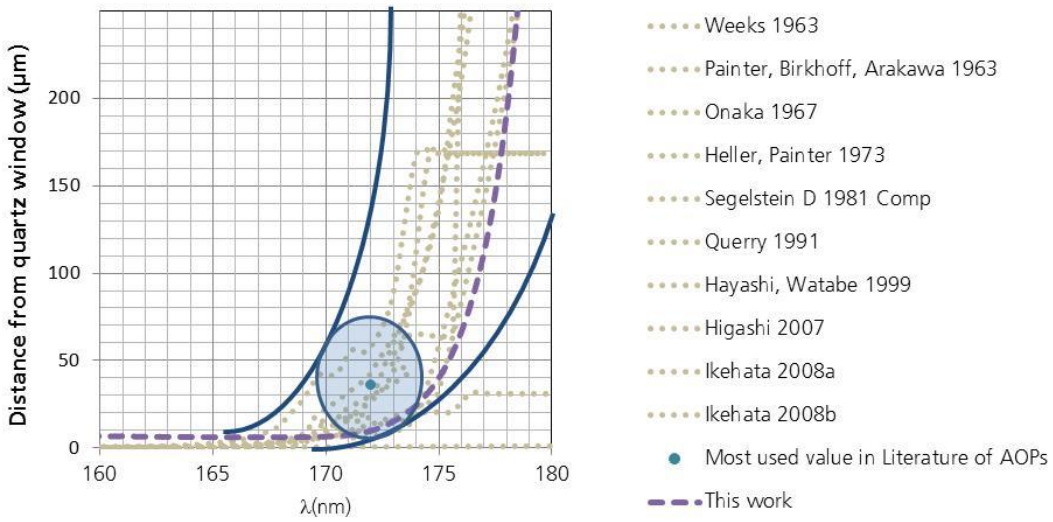

Figure 5.15 Comparison of the total absorption penetration of VUV using the calculated absorption coefficient of water in the range of measurement and comparison with the total absorption penetration of VUV from literature.

5.5. Conclusions

The main goal of the work in this chapter was to study the absorption of radiation at 172 nm in water.

A measurement setup concept for absorption coefficient measurements for short-penetrating wavelength or strong absorbing materials was conceived, built and tested. A methodology for absorption coefficient measurements for short- penetrating wavelength and strong absorbing materials was stablished.

Total penetration of radiation at 172nm in water happens in a layer three times smaller than the value reported in literature in the sixties and most used in the studies of AOPs using xenon excimer lamps. Similar values of absorption coefficient to the literature were found when comparing with Higashi who used the method attenuated total reflection in 2007 [73].

Disagreement with the literature could be attributed to the different radiation source used. In this thesis a monochromatic xenon excimer lamp was used. The use of non-monochromatic hydrogen radiation sources in the studies in the literature requires the use of mono-chromators and filters; the use of additional equipment make the measurement more complex due to the different absorption processes through the materials and a radiation intensity reduction in each sub-system. Therefore strong mathematical corrections take place in those studies. In the short-wavelength the transmission of most mono-chromators is very low and a relative small fraction of unwanted radiation of longer

wavelength for which transmission is high can result in a disproportionately large effective intensity of the long wavelength component due to responsivity of the detectors.

Radiation responsible for the photolysis of water and the generation of the hydroxyl radicals is strongly absorbed in water. Stronger absorption as initially assumed means that the photoreaction zone of photo-induced AOPs is actually smaller. A smaller photo reaction zone and the formation of the boundary layer explained in Chapter 3 implies that a stronger focus must be given to the mixing conditions close to the interface between quartz and water where the radiation is absorbed.

6. Hydroxyl radical formation

6.1. Introduction

After studying the absorption process of VUV radiation in water and pondering the high absorption of VUV radiation in a small layer of water, the principal photo-chemical reaction in this process was studied. The homolysis of water occurs as consequence of the absorption of radiation below 190 nm in water, this reaction produces mainly hydroxyl radicals and hydrogen atoms [33].

The quantification of the generation of hydroxyl radicals using VUV radiation is vital for the dimensioning of photo induced Advanced Oxidation Process without additives. In this chapter a study of the existing literature in the field of water homolysis is presented, the different values of quantum yield of hydroxyl radical generation in the range of VUV are summarized and the measurement of hydroxyl radicals is performed.

The setup used along this PhD study was then adjusted for the measurement of the quantum yield of hydroxyl radical generation, taking into account optimized operational conditions, flow rate and channel thickness of the photo reactor to prevent depletion zones where the hydroxyl radicals are not efficiently used.

The hydroxyl radical production was therefore quantified using the well-known scavenger of hydroxyl radical's methanol. From the degradation rate of methanol and the radiation intensity measured in Chapter 4 of this study, the quantum yield of hydroxyl radical generation under optimized condition was calculated.

6.2. Measurement of hydroxyl radicals

The absorption process was studied and presented in chapter 5; the absorption process refers in general to a reduction of the intensity of any form of radiated energy as a result of energy conversion in a medium. When electromagnetic radiation is absorbed in a medium it causes changes in the electronic state of components in the medium (electronically exited state of the components).

When a molecule or atom absorbs UV radiation its electronic state changes. This excited singlet state can result in one of three effects described below [98].

- Return to the ground state either by emission of a photon (fluorescence) or by converting the excess energy to heat (internal conversion).

- Transform to a 'metastable' long-lived triplet excited state (conversion, called intersystem crossing), which can then emit a photon (phosphorescence) or convert the excess energy to heat.
- Undergo chemical reaction (i.e., photochemistry) with quantum yields (ϕ_λ) from the excited state (either from the initially formed state or from the lowest triplet state). Photochemistry involves breaking or rearrangement of chemical bonds in the molecule.

The absorption process of electromagnetic radiation in the range of study (172 nm) in water results in the last described effect: Chemical reaction, where the water is homolysed and hydroxyl radicals and hydrogen atoms are produced. The Figure 6.1 shows the possible resulting effects after the absorption process takes place.

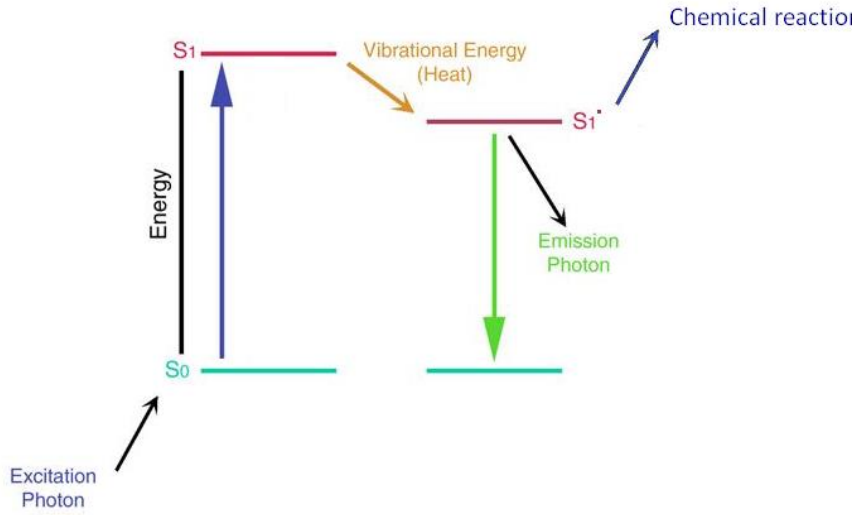

Figure 6.1 Absorption and the resulting effects

In order to study the generation of the hydroxyl radicals the following concepts are used:

- Quantum Yield ϕ_λ : it is defined as a quantitative measure of the overall efficiency of a photo-physical or photo-chemical process [65]. It is a unit-less constant which usually ranges from zero to one; several authors denote it as mol Einstein^{-1} (Einstein = mol photons).
  Quantum yields greater than one indicate photo-induced chain reactions, which may involve radical species or photo-generation of a catalyst. The quantum yield can be expressed in terms of the reactant or the product. It is usually dependent on the wavelength of the absorbed UV radiation, however many photo-chemical systems exist that have a constant quantum yield over a defined

range [20]. If a system or reaction has a constant and well known quantum yield, this one can be used for the measurement of the absorbed photon flow E_p^{abs} ; this systems are called actinometers, and they are used to measure the absorbed photon flow in photo-reactors of specific geometry and for a well-defined spectral range [20].

$$\phi_\lambda = \frac{dn(M)/dt}{E_p^{abs}} \quad \textbf{(6.1)}$$

6.2.1. Water photochemical homolysis by far ultraviolet radiation

As studied before, water strongly absorbs UV radiation at wavelength λ<190nm, this absorption results into a photochemical reaction, Equation (2.4) [33]. This photochemical reaction leads to chemical bond dissociation with formation of $H^\bullet$ and $^\bullet OH$ and hydrated electrons e^-_{aq} as main primary species [33].

The hydroxyl radicals $^\bullet OH$ generated from the homolysis of water, the base of AOPs, is a powerful oxidizing agents and reacts with most organic compounds by different types of reactions:

- Abstraction of a hydrogen atom: usually with aliphatic hydrocarbon groups, Equation (2.11),
- electrophilic addition: usually with unsaturated or aromatic hydrocarbon groups, Equation (2.12),
- electron transfer: usually with inorganic compounds, Equation (2.13) and
- radical-radical reactions, Equation (2.15).

The hydroxyl radical generated by photochemical homolysis disappears rapidly due to its high reactivity with almost every substance. Therefore, its presence is limited to the region where it is generated continuously. The $^\bullet OH$ radical absorbs UV weakly, only a small fraction of UV is actually absorbed, since the steady-state concentration of $^\bullet OH$ radicals is usually below 10^{-9} M [20].

In respect of the photochemical homolysis of liquid water and aqueous solutions using Vacuum Ultraviolet radiation, relatively little work has been done. However it was stablished that liquid water homolysed to $H^\bullet$, $^\bullet OH$ and e^-_{aq} [33] and the quantum yields for these species were determined using various scavengers to trap the hydroxyl radical. A summary of the current literature in the topic is presented in Table 6.1.

Table 6.1 Quantum yield for the generation of hydroxyl radicals with VUV

Author	Year	Range (nm)	Solution	Quantum yield	Method
Barrett und Baxendale[33]	1960	184,9	Aqueous solution of Methanol and ethyl acetate, H_2O_2	ϕ_λ H_2 = 0,6	H_2 evolution H_2O_2Actinometry (H_2O_2 ϕ_λ=1) $_{184,9nm}$
Sokolov[31]	1966	184,9	Pure water Aqueous solutions of methanol	ϕ_λ OH, H=0,45 $\phi_\lambda H_2$=0,02$_{pure\ water}$	H_2 evolution EtOH Actinometry (H_2 ϕ_λ=0,63) $_{184,9nm}$
Sokolov and Stein[30]	1966	147,0	Pure Water Aqueous solutions of oxygen, methanol, ethanol and isopropanol	ϕ_λ OH, H=0,7	H_2 evolution CO_2 Actinometry (CO ϕ_λ=1,1) $_{147,0nm}$
Getoff and Schenck[32, 99]	1968	123,6 147,0 184,9	Aqueous solutions of formate and ethanol	ϕ_λ OH, H=1,03 ϕ_λ OH, H=0,72 ϕ_λ OH, H=0,33 $\phi_\lambda H_2$=0,022$_{pure\ water}$	Oxalate evolution O_2 Actinometry (O_3 ϕ_λ=2)$_{123,6\ and\ 147,0nm}$ EtOH Actinometry (H_2 ϕ_λ=0,50)$_{184,9nm}$ N_2O Actinometry (-N_2O ϕ_λ=1)$_{184,9nm}$
Heit and Braun[75]	1997	172,0	Aqueous solutions of methanol	ϕ_λ OH, H=0,42	Methanol degradation Cis-trans cyclooctene Actinometry (-Cis ϕ_λ=0,32)$_{172nm}$ (-trans ϕ_λ=0,44)$_{172nm}$

The Table 6.2 shows the summary of the quantum yield values found in literature for the generation of hydroxyl radical using VUV.

Table 6.2 Summary Quantum yield for the generation of hydroxyl radicals with VUV [58]

Wavelength	Quantum yield
λ (nm)	ϕ_λ ·OH (mol ·OH/mol of photons)
193,3	0
184,9	0,33
172,0	0,42
147,9	0,7
123,6	1

The Figure 6.2 is presenting the values of quantum yield found in literature; an interpolation of the data previously published for other wavelengths is done, this may represent inaccuracy, given the lack of data.

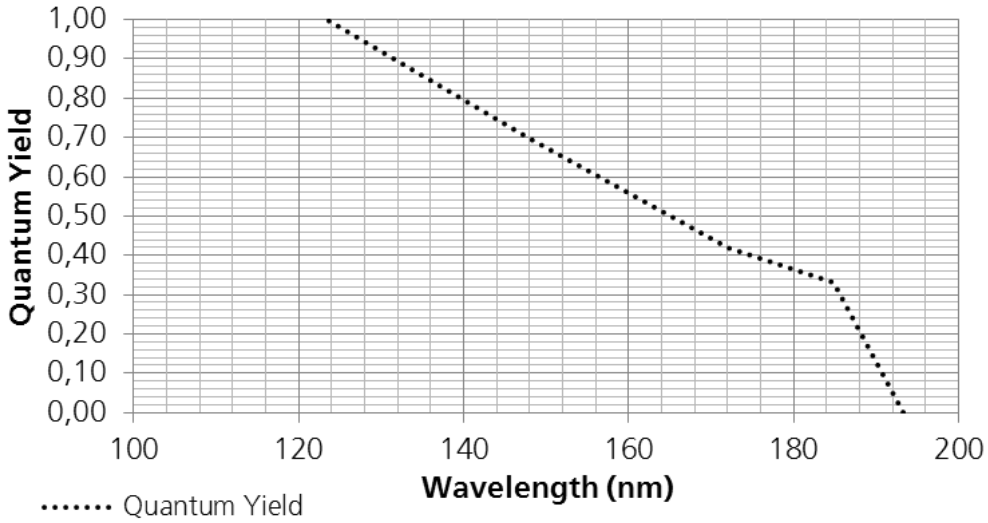

Figure 6.2 Quantum yield of photochemical homolysis of water at different wavelengths [58]

6.2.2. Methanol as indirect quantifier of hydroxyl radical formation

Methanol has been taken as a model compounds for the quantum yield quantification of hydroxyl radical formation in VUV due to the size of the molecule and the well-known reaction path mechanism of the oxidation and its reaction with hydroxyl radicals [30, 31, 33, 75]. For the presented study, the work done by Heit and Braun [75] is of special interest. The authors determined the production rate of hydroxyl radicals under 172 nm irradiation with a Xenon-Excimer lamps through the degradation of the model component methanol in aqueous solutions, taking into account by products formation.

The reaction system of VUV irradiated methanol solutions can be described as [100-105]:

Methanol has a very high absorption in the VUV spectral region and the decadic absorption coefficient at 172 nm of pure methanol falls around the 400000 m^{-1} [103], which is considerably higher than that of water.

Absorption of VUV radiation by methanol results in photochemical reactions with the following quantum yields [103]:

$$CH_3OH + VUV \rightarrow CH_3O^{\bullet} + H^{\bullet} \qquad \phi_\lambda = 0{,}69 \qquad \textbf{(6.2)}$$

$$CH_3OH + VUV \rightarrow HOCH_2^{\bullet} + H^{\bullet} \qquad \phi_\lambda = 0{,}08 \qquad \textbf{(6.3)}$$

$$CH_3OH + VUV \rightarrow CH_2O + H_2 \qquad \phi_\lambda = 0{,}06 \qquad \textbf{(6.4)}$$

$$CH_3OH + VUV \rightarrow CH_3^{\bullet} + {}^{\bullet}OH \qquad \phi_\lambda = 0{,}05 \qquad \textbf{(6.5)}$$

In solutions with water, the fraction of VUV absorbed is directly related with the concentration of methanol. Using the molar absorption coefficient of water and methanol it is possible to calculate the percentage of absorption of radiation in mixtures of water methanol as function of the concentration of methanol. The Figure 6.3 shows the percentage of radiation absorbed by methanol in a solution water-methanol at different concentrations.

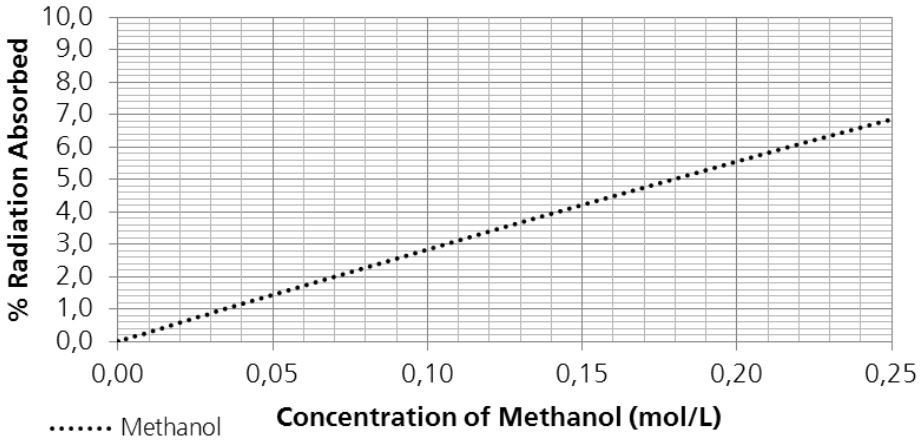

Figure 6.3 172 nm radiation absorbed by methanol in aqueous solutions

At concentrations below 0,1 mol/L one may assume that photons are almost quantitatively absorbed by water molecules, leading to water homolysis. If methanol solutions concentrations exceed this value, the absorption of radiation by methanol and its consequently photochemical reactions must be taken into account.

Additionally, at low concentrations of methanol the degradation occurs by hydrogen abstraction reaction with $^{\bullet}OH$ and $H^{\bullet}$ radicals.

$$CH_3OH + {}^{\bullet}OH \rightarrow HOCH_2{}^{\bullet} + H_2O \qquad k = 9{,}7x10^8\ Lmol^{-1}s^{-1} \qquad \textbf{(6.6)}$$

$$CH_3OH + H^{\bullet} \rightarrow HOCH_2{}^{\bullet} + H_2 \qquad k = 2{,}6x10^6\ Lmol^{-1}s^{-1} \qquad \textbf{(6.7)}$$

If oxygen is present in the solution, the resulting hydroxy-methyl radicals react with it to produce the corresponding peroxyl radicals:

$$HOCH_2{}^{\bullet} + O_2 \rightarrow {}^{\bullet}OOCH_2OH \qquad k = 4{,}9x10^9\ Lmol^{-1}s^{-1} \qquad \textbf{(6.8)}$$

The generated peroxyl radicals lead to formate ions following the equation:

$$2({}^{\bullet}OOCH_2OH) \rightarrow 2HCOO^- + 2H^+ + H_2O_2 \qquad k = 2{,}1x10^9\ Lmol^{-1}s^{-1} \qquad \textbf{(6.9)}$$

Formate ion and formic acid react with hydrogen atoms or hydroxyl radicals to form the protonated or deprotonated formyl radical:

$$HCOOH + {}^{\bullet}OH \rightarrow HCOO{}^{\bullet} + H_2O \qquad k = 1{,}3x10^8\ Lmol^{-1}s^{-1} \qquad \textbf{(6.10)}$$

$$HCOOH + {}^{\bullet}OH \rightarrow {}^{\bullet}COO^- + H_2O \qquad k = 3{,}2x10^9\ Lmol^{-1}s^{-1} \qquad \textbf{(6.11)}$$

$$HCOOH + H^{\bullet} \rightarrow HCOO{}^{\bullet} + H_2 \qquad k = 6{,}1x10^7\ Lmol^{-1}s^{-1} \qquad \textbf{(6.12)}$$

$$HCOOH + H^{\bullet} \rightarrow {}^{\bullet}COO^- + H_2 \qquad k = 2{,}1x10^8\ Lmol^{-1}s^{-1} \qquad \textbf{(6.13)}$$

The reactions of the protonated and the deprotonated formyl radicals with molecular oxygen will finally lead to carbon dioxide:

$$HCOO{}^{\bullet} + O_2 \rightarrow CO_2 + O_2{}^{\bullet -} \qquad k = 2{,}4x10^9\ Lmol^{-1}s^{-1} \qquad \textbf{(6.14)}$$

$${}^{\bullet}COO^- + O_2 \rightarrow CO_2 + HO_2{}^{\bullet} \qquad k = 3{,}0x10^9\ Lmol^{-1}s^{-1} \qquad \textbf{(6.15)}$$

In aqueous solutions of methanol where oxygen is present a complete mineralization can be reached.

On the other hand, in oxygen free solutions, the resulting hydroxy-methyl radicals product of the hydrogen abstraction due to reaction of methanol with hydrogen atoms and hydroxyl radicals, react between each other to generate methanol and formaldehyde as well as ethylene glycol following the reactions:

$$HOCH_2{}^{\bullet} + HOCH_2{}^{\bullet} \rightarrow CH_3OH + CH_2O \qquad k = 2{,}0x10^8\ Lmol^{-1}s^{-1} \qquad \textbf{(6.16)}$$

$$HOCH_2{}^{\bullet} + HOCH_2{}^{\bullet} \rightarrow (CH_2OH)_2 \qquad k = 1{,}0x10^9\ Lmol^{-1}s^{-1} \qquad \textbf{(6.17)}$$

Formaldehyde and ethylene glycol both as well react with hydrogen atoms and hydroxyl radicals by way of Hydrogen abstraction:

$$CH_2O + {}^{\bullet}OH \rightarrow CHO^{\bullet} + H_2O \qquad k = 1{,}9x10^{9}\ Lmol^{-1}s^{-1} \qquad \textbf{(6.18)}$$

$$(CH_2OH)_2 + {}^{\bullet}OH \rightarrow {}^{\bullet}CHOHCH_2OH + H_2O \qquad k = 1{,}8x10^{9}\ Lmol^{-1}s^{-1} \qquad \textbf{(6.19)}$$

$$CH_2O + H^{\bullet} \rightarrow CHO^{\bullet} + H_2 \qquad k = 1{,}0x10^{7}\ Lmol^{-1}s^{-1} \qquad \textbf{(6.20)}$$

$$(CH_2OH)_2 + H\bullet \rightarrow \bullet CHOHCH_2OH + H_2 \qquad k = 1{,}5x10^{7}\ Lmol^{-1}s^{-1} \qquad \textbf{(6.21)}$$

The photo-reactor system used by Heit and Braun consisted of an annular (coaxial) setup with an incoherent excimer VUV source in the centre with outward directed radiation (Figure 6.4 right) [75], coupled with a separate reservoir of 350 mL. The solution entered at the bottom of the reactor, streamed up along the lamp and left the reactor by the outlets at the top towards the reservoir. The entire volume recirculated accounted for 1 L.

The annular channel thickness of the system used by Heit and Braun was 2,5 mm, due to the limited penetration of VUV radiation at 172 nm in the solution the photoreaction zone was in that case 3 orders of magnitude smaller than the channel size without mixing enhancement, and as studied in chapter 3, a depletion zone has a high probability to be present.

A depletion zone may prevent the complete use of the hydroxyl radicals generated and far away from a kinetic controlled regime (instead limited by mass transfer). Flow conditions in the measurements according to the authors, were kept among the range of 700 < Re < 2800, and the authors of the studied argues that there was no influence of mixing on the rate of methanol degradation within the limits of the equipment.

As described in Chapter 3 the probability of formation of boundary layers larger than the photo reaction zone is relevant enough to affirm than even by Reynold numbers between 700 and 2800 no active exchange of substrate is taking place between the bulk flow and the photo-reaction zone, therefore the system is highly probable under limited mass transfer regime. The reaction chemistry of the solution was study in detail. Moreover the rate of methanol degradation was used to calculate the quantum yield of water homolysis at 172 nm [23, 75].

The Figure 6.4 shows the schematic representation of the annular (coaxial) incoherent excimer VUV source with outward directed used in the studies of Heit and Braun.

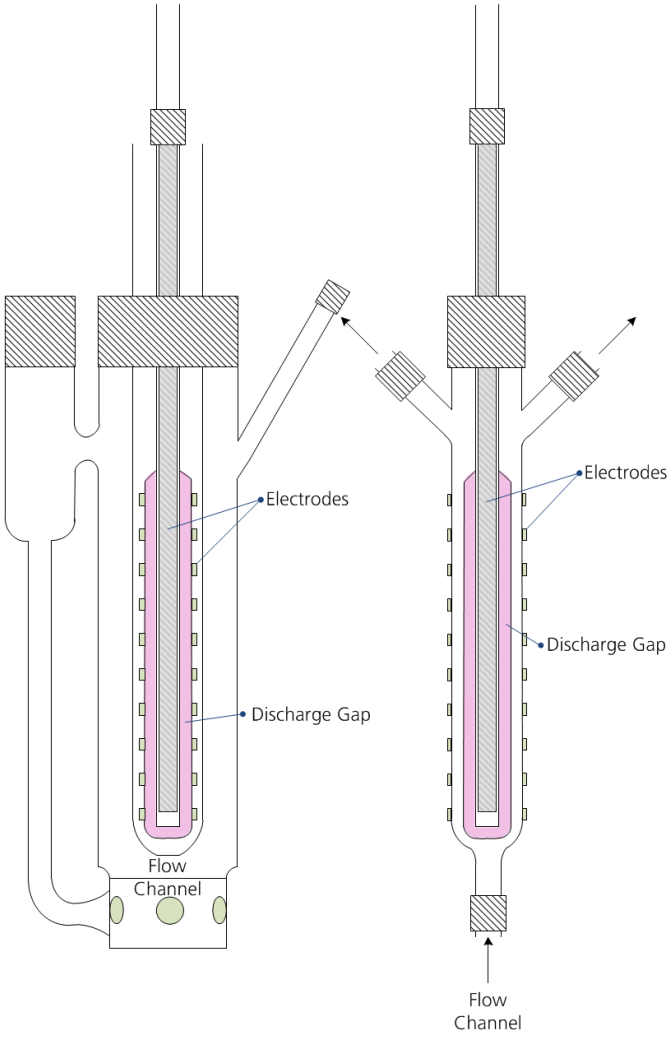

Figure 6.4 Schematic representation of an annular (coaxial) incoherent excimer VUV source with outward directed (redrew from [23, 75])

6.3. Materials and methods

6.3.1. Determination of the hydroxyl radical production rate from methanol degradation

In order to determine the hydroxyl radical production rate in water homolysis, VUV oxidation experiments with aqueous solutions of methanol were performed. Taking into account the reaction system of VUV irradiated methanol solutions the following mass balance can be stablished under the following assumptions and conditions:

Total absorption is taking place in the system and incident photon rate is equal to photons absorbed $E_p^{abs} = E_p^o$. Channel thickness of the photo-reactor should be optimal for complete absorption and good mixing conditions to avoid depletion zones.

Overall kinetics should follow pseudo cero order of reaction for the degradation of methanol[106]. This can be achieved by having a concentration of methanol high enough in the system, to assure that the reaction of methanol with hydroxyl radicals dominates. The interactions which are prevented therefore are the reaction of hydroxy-methyl radicals, formaldehyde or ethylene glycol with hydroxyl radicals. In other words the concentration of methanol should be sufficient to assure there is reaction only with hydroxyl radicals being generated and not that high that it absorbs more than 10 % of the radiation. Experiments are performed between 0,075 mol/L and 0,25 mol/L (2,1 and 6,8% radiation absorbed by methanol respectively) [22, 107].

Degradation of methanol is initiated only by photochemical homolysis reactions 6.8 to 6.11 and hydrogen abstraction by hydroxyl radicals reaction 12 respectively. As stablished and probed by Heit and Braun [75] Hydrogen abstraction by hydrogen atoms equation 6.13 is not taking place in the degradation of methanol solutions system.

The generation of hydroxyl radicals is not directly proportional to the speed of disappearance of methanol. However, by the measurement of the decrease of methanol by Gas Chromatography and including the decrease of methanol in a lower proportion by absorption of VUV radiation, and its parallel generation by the reaction of the hydroxy-methyl radicals (reaction 6.22), the hydroxyl generation can be calculated [75]. Considering all reactions. It is possible to quantitatively describe the rate of disappearance of the methanol as follow:

Taking into account the following nomenclature:

$A_M = \varepsilon_M c_M l$ is the absorbance of methanol at time t;

$A_W = \varepsilon_W c_W l$ is the absorbance of water at time t;

$A_{tot} = A_M + A_W$ is total absorbance of both species at time t;

c_M is the concentration of the substrate methanol in mol L^{-1} at time t;

c_W is the initial concentration of water in mol L^{-1};

ε_M is the molar decadic absorption coefficient of methanol in $Lmol^{-1}cm^{-1}$;

ε_W is the molar decadic absorption coefficient of water in $Lmol^{-1}cm^{-1}$;

$f_M = \frac{A_M}{A_{tot}}$ is the fraction of photons absorbed by methanol at time t;

$f_W = \frac{A_W}{A_{tot}}$ is the fraction of photons absorbed by water at time t;

$\phi_{M\rightarrow P}$ is the sum of quantum yields of reactions 6.8 to 6.11 of degradation of methanol;

ϕ_W is the quantum yield of formation of hydroxyl radical;

l is the optical path length or thickness of the solution traversed by the UV radiation;

E_{pM}^{abs} is the number of photons absorbed by methanol in photons s^{-1};

E_{pW}^{abs} is the number of photons absorbed by water in photons s^{-1};

E_p^{abs} is the total photons absorbed by both species in photons s^{-1};

E_p^o is the incident number of photons to the system in photons s^{-1};

E_λ^0 is the incident spectral radiant power;

V is the volume of experimental solution;

The differential equation describes the kinetics of the methanol degradation.

$$-\frac{dC_M}{dt} = -\frac{dC_M}{dt}\Big|_{OH,VUV} + \frac{dC_M}{dt}\Big|_{22} \qquad \textbf{(6.22)}$$

Where,

$\frac{dC_M}{dt}$ is the total rate of methanol photolysis (reactions 6.8-6.11 and 6.12);

$\frac{dC_M}{dt}\Big|_{OH,VUV}$ is the apparent (measured) rate of methanol degradation;

$\frac{dC_M}{dt}\Big|_{22}$ the rate of methanol production by reaction 6.22;

$$-\frac{dC_M}{dt} = -\phi_{M\rightarrow P}\frac{E_{pM}^{abs}}{V} - \phi_W\frac{E_{pW}^{abs}}{V} + \frac{dC_M}{dt}\Big|_{22} \qquad \textbf{(6.23)}$$

With $E_{pM}^{abs} = E_p^{abs} f_M$ and $E_{pW}^{abs} = E_p^{abs} f_W$

$$-\frac{dC_M}{dt} = -\frac{E_p^{abs}}{V}\left[\phi_{M\rightarrow P} f_M + \phi_W f_W\right] + \frac{dC_M}{dt}\Big|_{22} \qquad \textbf{(6.24)}$$

Since there is total absorption, the total photons absorbed by both species is equal to the incident number of photons to the system $E_p^{abs} = E_p^o$

$$-\frac{dC_M}{dt} = -\frac{E_p^o}{V}\left[\phi_{M\to P} f_M + \phi_W f_W\right] + \frac{dC_M}{dt}\Big|_{22} \quad \textbf{(6.25)}$$

$\frac{dC_M}{dt}\Big|_{22}$ the rate of methanol production by reaction 22 can be evaluated experimentally using the following relation; from reactions 22 and 23 the rate of methanol and ethylene glycol can be expressed as follow:

$$\frac{dC_M}{dt}\Big|_{22} = k_{22}[HOCH_2\bullet]^2 \qquad k_{22} = 2{,}0x10^8\ Lmol^{-1}s^{-1} \quad \textbf{(6.26)}$$

$$\frac{dC_{EG}}{dt} = k_{23}[HOCH_2\bullet]^2 \qquad k_{23} = 1{,}0x10^9\ Lmol^{-1}s^{-1} \quad \textbf{(6.27)}$$

Solving for measurable values

$$\frac{dC_M}{dt}\Big|_{22} = \frac{k_{22}}{k_{23}}\frac{dC_{EG}}{dt} \quad \textbf{(6.28)}$$

$$\frac{dC_M}{dt}\Big|_{22} = 0{,}2\frac{dC_{EG}}{dt} \quad \textbf{(6.29)}$$

The hydroxyl radical generation quantum yield for the production of hydroxyl radicals can be therefore calculated using the following equation

$$\phi_W = \frac{1}{f_W}\left(\frac{V}{E_p^o}\frac{dC_M}{dt} + 0{,}2\frac{dC_{EG}}{dt} - \phi_{M\to P} f_M\right) \quad \textbf{(6.30)}$$

6.3.2. Flat micro channel reactor apparatus

The Flat micro channel reactor apparatus described in chapter 3 with minor modifications of the periphery was used in this chapter. It consist of two Xe excimer UV Lamps contained in a metallic housing with UV reflectors (Xeradex System) emitting 172 nm radiation through the window, the system is positioned under the Flat micro channel reactor.

The channel thickness in the flat micro channel reactor can be modified between 25 and 1500 µm, the radiation reach the reaction channel through a synthetic quartz window 295,8 cm^2 (170 mm x 174 mm). The flow is uniform over the whole synthetic quartz window. The Flat micro channel reactor is connected to a 0,5L jacketed reactor glassware as reservoir with, a cooling glass column and a gear pump VerderGear VGS096 (Verder, Germany) which controls the flow from 100 to 2400 mL/min range. All tubing and periphery are made of materials with highly crack and stress resistance, low permeability, no moisture absorption and low level of chemicals extractables to assure a wide range of experimental fluids and pollutants.

Of special interest is the use of the optimal operational parameters for the avoidance of the generation of depletion zones. Experimental results discussed in Chapter 3, exhibited a marked dependence of the initial reaction rates of oxidation with the volumetric flow rate and channel thickness. Results showed that a channel thickness below 500 μm and flow rate above 1000 mL/min as the optimal combination of operational parameters in this system; reflected, on higher reaction rates, (i.e. faster MB oxidation). Especially in this study where the assumption of degradation of methanol is due to the reaction 1:1 with hydroxyl radical, it is of concern than the experiments are performed under the best conditions for exchange of substrate in the photo reaction zone. For the purpose of this work, the size of 250 μm and volumetric flow of 2200 mL/min were used.

6.3.3. Sampling and experimental design

Methanol analytical grade were purchased from Alfa-Aesar. Double distilled water was employed for the preparation of all the solutions, otherwise stated. During experiments samples were taken for analysis of methanol degradation. Samples were stored in sample vials of 2 ml with cap septa, in order to avoid evaporation losses. After the sampling each one was frozen for further analysis. The Figure 6.5 shows sample vias for storage after experiments.

Figure 6.5 Sample vials for storage of Methanol

According with the reaction system of VUV irradiated methanol solutions presented in section 6.2.1, the following measurements were performed:

Methanol and Ethylene Glycol Analysis. Gas chromatograph employed in all measurements is an Agilent Technologies 7890 A GC System FID detector.

Sampler: Agilent Technologies GC Sampler 120 PAL including an automated Headspace module.

Column: Agilent HP-5, 30m x 0,320mm x 0,25μm.

Stationary: 5% Phenyl / 95% Dimethylpolysiloxane Phase.

In order to measure the quantum yield of hydroxyl radical generation a full factorial design was used. One factor with different number of levels is established. Initial concentration of methanol: Pursuing the aim of quantifying hydroxyl radical production using induced methanol degradation, the initial methanol concentration was varied. The range of concentrations starting at 0,075 mol/L to maximum concentrations of 0,25 mol/L was used. Within this range hydroxyl radical attack will lead mainly to the formation of hydroxymethyl radicals and water. The overall kinetics following pseudo cero order of reaction for the degradation of methanol is to be maintained during the experiment. The Table 6.3 shows the factor, level and ranges used in the experimental design.

Table 6.3 Factors, levels and range definition for experimental design

Factor	Levels	Ranges
Initial Concentration MeOH	6	0,075; 0,100; 0,125; 0,150; 0,175; 0,200; 0,250 mol/L

The software Design Expert® 9 was used to stablish the experimental design. The optimal D-Custom design was selected. In this option, the software allows the inclusion of several levels for one factor of interest. Finally, is worth to mention that it allowed a minimization of the number of runs without losing robustness in the design. A total of 24 runs were proposed, while this model includes a number of additional center points.

6.4. Results and discussions

The degradation of methanol and the generation of Ethylene glycol were monitored during experiments. The Figure 6.6 is an example of the experimental data collected for one experiment.

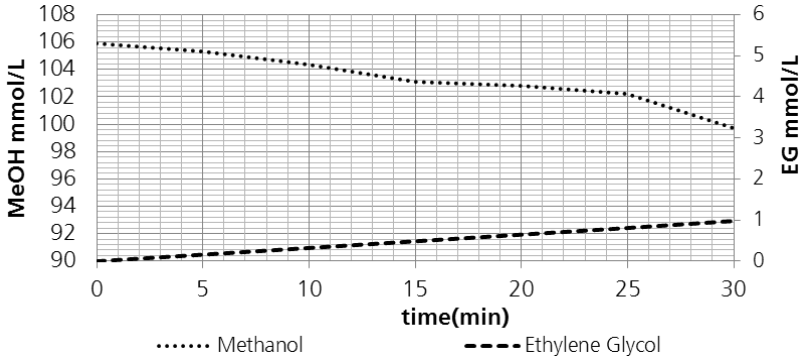

Figure 6.6 Methanol and ethylene glycol concentrations as a function of irradiation time example of one experiment

Results of the experiments for different initial methanol concentration are summarized in Figure 6.7. As expected the degradation curves are best represented by a linear fitting which slope represent the observed zero order rate constant. This kinetic regime behavior was validated in the range of work.

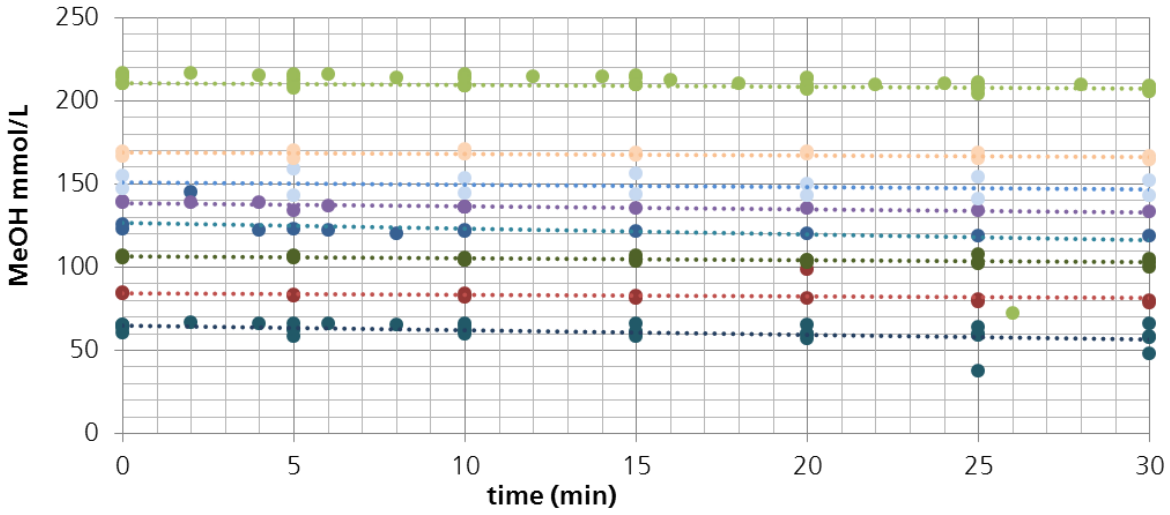

Figure 6.7 Methanol concentrations as a function of irradiation time different initial concentrations

The observed zero order rate constants were calculated for each group of same initial concentration experiments. The Table 6.4 summarizes the results.

Table 6.4 Observed zero order rate constants MeOH

Experiment	Initial concentration MeOH	Observed zero order rate constant
1-5	65 mmol/L	-0,170 ± 0,035 mmol/Lmin
6-7	85 mmol/L	-0,108 ± 0,060 mmol/Lmin
8-10	105 mmol/L	-0,138 ± 0,043 mmol/Lmin
11-12	125 mmol/L	-0,171 ± 0,015 mmol/Lmin
13-14	140 mmol/L	-0,168 ± 0,012 mmol/Lmin
15-16	155 mmol/L	-0,159 ± 0,003 mmol/Lmin
17-18	165 mmol/L	-0,159 ± 0,003 mmol/Lmin
19-24	215 mmol/L	-0,165 ± 0,025 mmol/Lmin
$\bar{x} \pm \Delta\bar{x}$ - 0,155 ± 0,011 mmol/Lmin		

All values of the observed zero order kinetic constants were obtained at methanol conversion of less than 10% to prevent reaction of molecules different of methanol with hydroxyl radicals. The rate of methanol degradation is nearly constant over the concentration range with a value of -0,155 ± 0,011 mmol/Lmin. This effect occurs when methanol degradation occurs just by hydroxyl radicals. At lower concentrations the kinetic regime behavior will be directly dependent on the concentration exhibiting first order kinetic behavior.

At higher concentrations the degradation of methanol by means of VUV absorption and direct photolysis increases and the kinetic regime behavior changes. The kinetic constants will increase until reaching a maximum were total absorptions by methanol occurs as explained by Bolton [106] and experimentally tested by Oppenländer [107].

The observed zero order kinetic constant is of great importance for the calculation of the hydroxyl radical generation rate (quantum yield of hydroxyl radical generation). In this case, and following the model described for calculation the kinetic constant, is equal to $\frac{dC_M}{dt}$.

Results of the experiments for the production of ethylene glycol for different experiments are summarized in Figure 6.8. In this case the production curves are as well represented by a linear fitting. During the experiment ethylene glycol is being accumulated in the system and due to the small concentration does not compete with methanol for the reaction with hydroxyl radicals.

At methanol conversion of less than 10% the change in concentration of ethylene glycol is constant. This kinetic regime behavior and the accumulation of ethylene glycol were validated in the range of work.

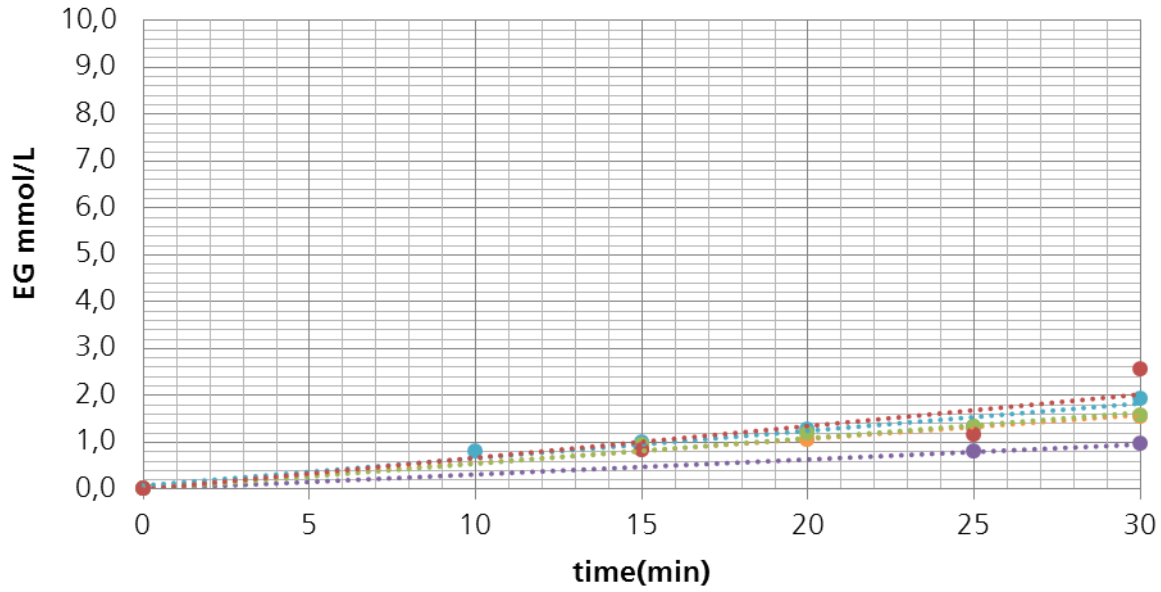

Figure 6.8 Ethylene glycol evolution concentrations as a function of irradiation time and different initial concentrations

The observed rate constants were calculated for each group of same initial concentration of methanol experiments. The Table 6.5 summarize the results.

Table 6.5 Observed rate constants EG

Experiment	Initial concentration MeOH	Observed rate constant
8-10	105 mmol/L	0,046 ± 0,014 mol/Lmin
11-12	125 mmol/L	0,032 ± 0,003 mol/Lmin
15-16	155 mmol/L	0,053 ± 0,002 mol/Lmin
17-18	165 mmol/L	0,055 ± 0,002 mol/Lmin
19-24	215 mmol/L	0,062 ± 0,009 mol/Lmin
	$\bar{x} \pm \Delta\bar{x}$ **0,050 ± 0,003 mol/Lmin**	

The observed kinetic constant of generation of ethylene glycol is as well of great importance and part of the calculation of the hydroxyl radical generation rate (quantum yield of hydroxyl radical generation). In this case, and following the model described for calculation, the kinetic constant is equal to $\frac{dC_{EG}}{dt}$.

The hydroxyl radical generation rate (quantum yield) can be then calculated using equation 6.31. and results of radiation intensity are measured in chapter 4.

For each of the methods used for the radiation intensity measurements the quantum yield of hydroxyl radical generation was calculated. The Table 6.6 below summarized the results.

Table 6.6 Observed quantum yield for the formation of hydroxyl radicals

Method	Radiation intensity	Quantum yield OH radical
Actinometry	5,11 mW/cm^2	0,50 ± 0,02 molOH/mol Photons
Si-photodiode	3,52 mW/cm^2	0,73 ± 0,02 molOH/mol Photons
AlGaN detector	1,43 mW/cm^2	1,82 ± 0,02 molOH/mol Photons
	ϕ_W **1,82 ± 0,02 molOH/mol Photons**	

The quantum yield was calculated following 3 different measurement methods for the Intensity of radiation emitted by a Xe excimer as well as optimized photo-reactor conditions to avoid depletion of substrate and poor use of the hydroxyl radicals formed.

Quantum yield value obtained by using actinometry results is 0,50 ± 0,02 molOH/mol photons. This value is slightly higher than the literature value of 0,42 ± 0,02 molOH/mol photons obtained by the same procedure. However as seen and discussed in chapter 4. The radiation intensity calculated using the results of actinometry may contain uncertainties due to the assumptions of the methodology.

The quantum yield for the generation of hydroxyl radicals obtained in this study by using the measurements of the Si-photodiode detector (affected by fluorescence of quartz)) is 0,73 ± 0,02 molOH/mol photons.

The quantum yield for the generation of hydroxyl radicals obtained in this study by using the Si photodiode detector is 0,73 ± 0,02 molOH/mol photons. (Affected by fluorescence of quartz)

The quantum yield for the generation of hydroxyl radicals obtained in this study by using measurements of the calibrated AlGaN detector is 1,82 ± 0,02 molOH/mol photons. (Blind for radiation higher than 380 nm)

Quantum yields greater than 1 are possible for photo-induced or radiation-induced chain reactions, in which a single photon may trigger a long chain of transformations. This implies that the chemical system may be more complex than the system modeled for calculation.

In order to explore the accuracy of the method further work must be invested in the detailed description of the system to determine the quantum yield for the generation of hydroxyl radicals.

6.5. Conclusions

The main goal of the work in this chapter was to study and test the methodology to calculate the quantum yield for the generation of hydroxyl radicals under 172 nm radiation.

The production of hydroxyl radicals was explored by means of reaction with OH radical scavenger methanol using the flat lamp reactor chamber developed for chapter 3.

An optimized photo-reactor system and experiments under operational parameters which elude the generation of depletion zones are necessary for the efficient measurement of the generated hydroxyl radicals. Despite of the influence of the measured irradiance in the calculated quantum yield the use of optimal operational conditions for the complete use of hydroxyl radicals being generated, reveals a higher value of quantum yield when compared with the literature.

Following the exact methodology used in Literature with the optimized photo-reactor system for better use of the hydroxyl radicals the increase of quantum yield measured is 20% higher than the value reported in Literature for radiation at 172 nm.

The quantum yield for the generation of hydroxyl radicals obtained in this study by using the measurements of the calibrated AlGaN detector (blind for radiation higher than 380 nm) is 1,82 ± 0,02 molOH/mol photons. Quantum yields greater than 1 are possible under the following situations:

- Absorption of radiation in the first step involves production of atoms or free radicals which initiate a serie of chain reactions,

- formation of intermediate products which will act as a catalyst, if reactions are exothermic, the heat evolve may activate other molecules without absorbing the additional quanta of radiation and finally
- the active molecules, produce after absorption of radiation, may collide with other molecules and activate them in turn activate other reacting molecules.

This implies that the chemical system model may be more complex than the system modeled for calculation. For future developments and description of the phenomena the chain reactions which may be present in the photolysis of water should be studied.

The influence of the measured irradiance in the final calculation of quantum yield for the generation of hydroxyl radicals was described. The different methods used bring uncertainties to the final calculation.

The gained accurate value for the quantum yield of hydroxyl radical generation will lead to a better understanding of the potential of xenon excimer lamps for the Advanced Oxidation Processes for water remediation.

The understanding of photo-chemical processes where strong absorption takes place in small layer will open the possibilities of new technologies for chemical synthesis.

In order to explore more accurate methods further work must be invested in the detailed description of the scavenging system to determine the quantum yield for the generation of hydroxyl radicals.

7. VUV Flat lamp-reactor system - Characterization with MB and case study micro-pollutants

7.1. Introduction

In this thesis, different phenomena present in the photo-induced advance oxidation process were studied. The understanding of those phenomena and the recent development of flat xenon excimer lamps by Fraunhofer Institute for Interfacial Engineering and Biotechnology lead to the design and construction along this thesis of a Lamp-reactor system for VUV Advanced Oxidation. Once the system was built a similar characterization to that presented in chapter 3 was performed for this system, in order to find the best operational conditions for oxidation of the model substance Methylene blue.

In order to test the oxidation process using this new system, a screening of literature to identify relevant pollutant and micro-pollutants – in particular such with persistent characteristic - was performed. It was found that B. Kuch and H. Steinmetz 2012 at the Institute for Sanitary Engineering, Water Quality and Solid Waste Management in Stuttgart (ISWA) have proposed a list of individual substances not only classified as a relevant pollutants, also representing the behavior of groups of substances in waters with similar physico-chemical properties. The study of degradation of those substances may work as guiding parameters for the understanding of the pathways of the listed substances into water environments, their behavior and effects in natural and technical environments (Wastewater treatment plants) [108].

Five substances were selected for oxidation studies. Methylene Blue used as a reference model substance as in earlier chapters and the last four belonging to the list proposed by B. Kuch and H. Steinmetz classified as a relevant pollutants:

- Carbamazepine and Sulfaquinoxaline as representative substances of the group pharmaceuticals. These substances are low degradable by municipal wastewater treatment plants WWTP and are classified as recalcitrant and persistent [109-112]
- Bisphenol A representing the behaviour of group of substances coming from the chemical industry and
- Caffeine from the group of food ingredient, commonly present in the inflow and outflow of wastewater treatment plants which are not degradable by even well operated municipal WWTP [113, 114]

The concentration of the mentioned model substances (Carbamazepine, Sulfaquinoxaline, Bisphenol A and Caffeine), the total organic carbon and the toxicity were followed during irradiation in the new developed flat lamp-reactor system. Toxicity refers to the degree to which a substance or particular mixture of substances can damage an organism such as an animal, bacterium or plant, as well as the effects on a substructure of the organism like a cell (cytotoxicity) or an organism, in this study we focused to cytotoxicity against COS and VERO cells, cell lines isolated from an African green monkey kidney.

The experimental setup has been installed for this experimental campaign at the Center for Process and Environmental Engineering CEPIMA belonging to the department of Chemical Engineering of the Universitat Politècnica de Catalunya Barcelona Tech. The four months visiting research activity was part of the European PhD School on Advanced Oxidation Processes program.

The degradation of the pollutants follow pseudo-first order degradation kinetics, the pseudo first order kinetic constants and the VUV dose for the degradation of the selected pollutants are reported. As analogy with disinfection processes, irradiance of photo-chemical reactors, UV dose of degradation of specific pollutants are useful parameters for future scale-up and industrialization of VUV Advanced Oxidation Processes.

The safe application of the photo-induced AOP under study for the removal of the selected substances was investigated. Toxicity in particular, the cytotoxicity tests based on cell lines culture were carried out using samples at different times in the experimentation. Particularly, VERO and COS cells were selected and tested against the samples. Both cell lines were isolated from an African green monkey kidney [113].

The assessment of toxicity in photo-induced AOP is of importance due to the possibilities of integration of this treatment into existing waste water treatment plants, especially where the AOP process is used to initially break down recalcitrant molecules leaving the less complex molecules to be degraded by biological steps.

Effluent from the photo-induced AOP requires to be no toxic for other sub processes in the system, especially biological treatments. The coupling of AOPs and biological processes for the complete degradation of recalcitrant and persistent pollutants is a promising cost optimization measure for the smooth introduction of these technologies in existing wastewater treatment plants [115].

7.2. Literature review

7.2.1. Contaminants of Emerging Concern

A large number of studies have shown that the aquatic environment is increasingly burdened with anthropogenic trace pollutants [1-6]. The spectrum of substances ranges from active ingredients of pharmaceutical, natural and synthetic hormones, constituents of personal care products (synthetic fragrances and disinfectants) to plasticizers, stabilizers, flame retardants and other industrial chemicals. Members of the above mentioned group of substances are commonly present in surface water and wastewater all over the world at varying concentrations [5, 7-12].

Some of those substances have been detected and reported in literature to be present in influent wastewater, effluent wastewater and water bodies in the ranges of 0,01 µg/L to 100 µg/L, the work of Rivera-Jaimes 2018 summarizes different studies in the field [5].

According to their application and their environmental behavior, the substances can be transported via different paths. Into the municipal wastewater, organic trace substances are discharged via industrial and commercial wastewater discharges, domestic wastewater as well as precipitation water discharges from sealed areas.

The discharge of organic trace substances of the municipal waste water into the environment can take place via sewage treatment plant effluents, precipitation and mixed water discharges as well as through the agricultural sewage sludge utilization. The Figure 7.1 shows the possible source and pathways for the occurrence of pharmaceutical residues in water.

Estimations in literature [6, 13] show that organic trace substances from centralized sewage treatment plants play a primary role in the pollution of the aquatic environments in Europe. Therefore and in order to perform a selective treatment and prevent discharges of organic traces in the environment alternatives to central wastewater disposal as separate collection and treatment of heavily polluted wastewater streams has been in several publications openly suggested [13]. Examples are in situ treatment of industrial wastewater or pharmaceutical hospital wastewater by different combination of technologies.

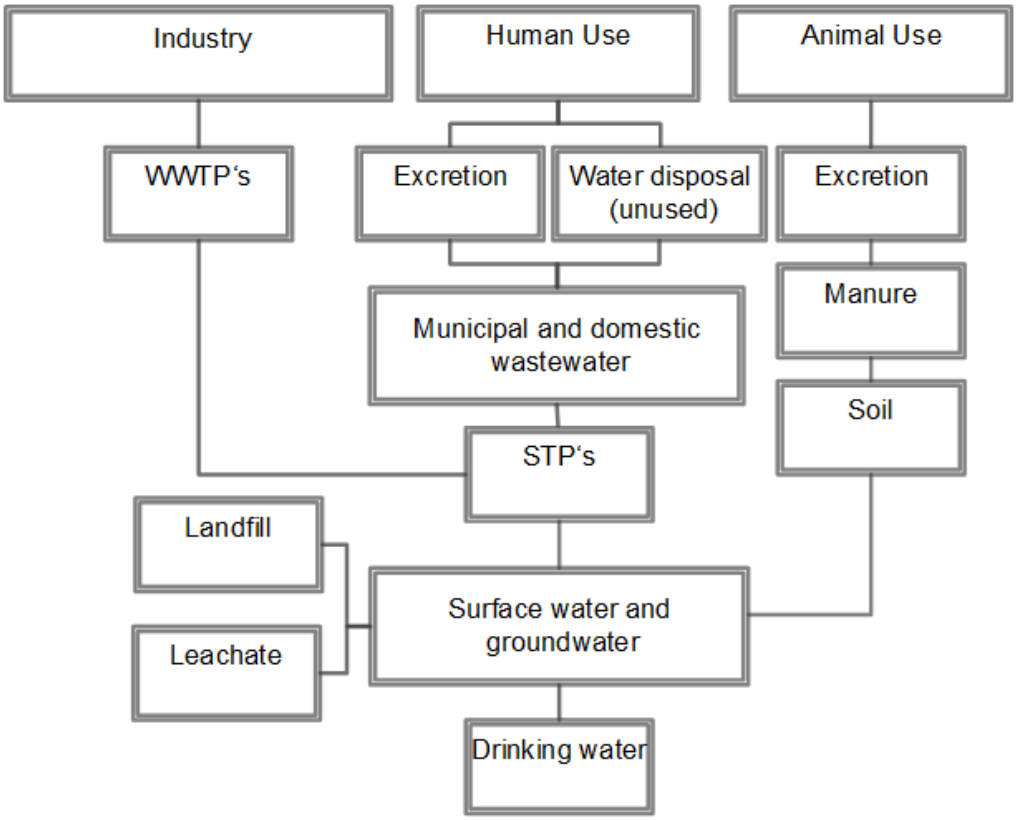

Figure 7.1 Possible sources, pathways for the occurrence of pharmaceutical residues in the aquatic environment [1, 2, 14, 15]

Many organic pollutant extend via domestic wastewater into municipal sewer systems. The separation associated with other highly contaminated household wastewater streams such urine is not meaningful in industrialized countries with existing wastewater infrastructure. Therefore, the use of technical measures to reduce the discharge of organic trace substances focuses primarily on the central sewage and sludge treatment. Of particular importance is the development of technical solutions for the upgrading or expansion of conventional wastewater treatment, in this regard Advanced Oxidation Processes.

No targeted elimination of hazardous organic substances has been implemented in the planning and operation of municipal centralized wastewater treatment plants to this point. However and due to the requirements of the European Commission Water Framework Directive (EC WFD) (Directive 2000/60/EC) on the state of European surface waters, this could change in the near future. The EC WFD marked the beginning of a new era for European water management based on a holistic approach focusing on understanding and integrating all the different aspects related to the water environment to be effective and sustainable [16].

Several amendments have been introduced to the EC WFD. As a first step the Directive 2455/2001/EC, established a list of priority substances (PS), including the priority hazardous substances (PHS) that became the Annex X of WFD. Especially priority hazardous substances PHS are the PS that "are persistent, toxic and liable to bio accumulate, or that give rise to an equivalent level of concern".

This Directive 2455/2001/EC amends Directive 2000/60/EC that specifies that specific measures must be adopted to reduce or even, in the case of for priority hazardous substances, to cease the discharges, emissions and losses into the aquatic environment, within 20 years after their adoption at Community level. The final purpose is achieving concentrations approaching background values for naturally occurring substances and close to zero for man-made synthetic substances. As a result, additional measures would be necessary in many cases in the wastewater sector to reduce the discharge of organic hazardous trace substances. The ideal way to minimize the discharge of such substances would be a production ban of such substances, as this is not possible in many cases the elimination of hazardous substances from wastewater hast to be further studied [17].

Due to the different types of inputs and the unmistakable variety of substances, the total pollution of a body of water can by no means be comprehensively represented. Despite extensive investigations, the knowledge about the pathways of the substances into the aquatic environment, their behavior and their effects in natural and technical systems as well as the interactions in complex substance mixtures is insufficient. The reasons for the lack of knowledge are, in particular, the large variety of materials subject to constant change and due to the very different physico-chemical properties an extremely different behavior of individual substances.

B. Kuch and H. Steinmetz 2012 at the Institute for Sanitary Engineering, Water Quality and Solid Waste Management in Stuttgart (ISWA) have proposed a list of individual substances that represent the behavior of groups of substances in waters with similar chemical-physical properties as guiding substances for the understanding of the pathways of those into water environments, their behavior and effects in natural and technical environments (WWTP) [108]. The Table 7.1 shows the substances proposed by B. Kuch and H. Steinmetz as reference for the assessment of organic hazardous trace substances. Since it is not possible to know and investigate all relevant substances at a given time, and it is not the goal of this study to do so, a number of components not yet studied in photo-induced AOPs were chosen from the above mentioned list. Carbamazepine and Sulfaquinoxaline as representative substances of the group pharmaceuticals. Bisphenol A representing the behavior of group of substances coming from the chemical industry and Caffeine from the group of food ingredient.

Table 7.1 Reference substances for the assessment of the behaviour of organic trace substances in sewage treatment plants and surface waters ISWA [108]

Number	Substance
	Chemicals from Industry
1	Bisphenol A (BPA), 4-nonylphenol (NP). 4-tert-octylphenol (OP)
2	EDTA, NTA
3	Phosphorорg. links
4	Benzothiazole
	Urban Pesticides
5	Mecoprop (MCPP), 2-methyl-4-chlorophenoxyacetic acid (MCPA)
6	Terbutryn
7	Triclosan
	Food ingredient
8	Caffeine
9	Synthetic sweeteners
10	Cholesterol and the like
	Others
11	Polycyclic aromatic hydrocarbons (PAH)
12	Polychlorinated biphenyl (PCB)
13	Polybrominated diphenyl ethers (PBDE)
	Pharmaceuticals
14	Ibuprofen
15	Diclofenac
16	Naproxen
17	Carbamazepine
18	Sulfamethoxazole
19	X-ray contrast media
20	Natural and Synth. hormones
	Personal care
21	Synthetic perfumes 6-acetyl-1,1,2,4,4,7-hexamethyltetraline (AHTN), 1,3,4,6,7,8-hexahydro-4,6,6,7,8,8-hexamethylcyclopenta-γ-2-benzopyran (HHCB),
22	N, N-diethyltoluamide (DEET), insect repellent
23	Triclosan

Carbamazepine has been detected worldwide in the range of concentrations from 0,5 µg/L to 3,5 µg/L in different wastewater treatment plants effluents, but also in concentrations from 0,02 µg/L to 0,5 µg/L in water bodies [5, 109]. Sulfaquinoxaline has been detected in the range of concentrations from 0,005 µg/L to 0,040 µg/L in surface waters [116] and groundwater 0,001 to 0,112 µg/L [117]. Bisphenol A has become a constant in the environment as a result of its high production, consumption, and subsequent environmental introduction.

It has been found in concentrations from 0,0005 µg/L to 0,41 µg/L in surface water, in sewage effluents from 0,018 µg/L to 0,702 µg/L, in sediments from 0,01 to 0,19 mg/kg and in sewage sludge from 0,004 to 1,363 mg/kg dry weight [118-120]. Caffeine has been detected in the influent and effluent of wastewater treatment plans in the range of 0,016 µg/L to 102 µg/L and 0,007µg/L to 51 µg⁄L respectively [9, 121].

It is also important to mention that studies in different kinds of wastewater treatment plants, for example livestock WWTP, hospital WWTP and pharmaceutical manufacturer WWTP, present a higher concentration of pharmaceuticals and organic hazardous organic pollutants than municipal wastewater treatment plants, and are therefore a strong player in the impact of accumulation of those substances in water bodies as well as in living organisms in water [122, 123].

The constant presence of these substances in the environment and their capability of bioaccumulation are issues of great importance for ecosystems and human health, therefore this thesis studies the performance of the photo-induced oxidation in the degradation of the above mentioned pollutants.

7.2.2. Photo-induced VUV Advanced Oxidation Processes

As presented in previous chapters, water strongly absorbs UV radiation at wavelength λ<190nm, this absorption results into a photochemical reaction Equation (2.4). This photochemical reaction is known as a homolysis of water and it leads to chemical bond dissociation with formation of $H^{\bullet}$ and $^{\bullet}OH$ and hydrated electrons e^{-}_{aq} as main primary species [33].

The hydroxyl radicals $^{\bullet}OH$ generated from the homolysis of water, the base of Advanced Oxidation Processes, is one of the most powerful oxidizing agents known and reacts with most organic compounds. This radical can oxidize organic and inorganic substrates (M, R-H…) by different types of reactions: abstraction, electrophilic addition, electron transfer and radical-radical reaction. Due to its reactivity, the hydroxyl radical is rapidly consumed and its reactions are limited to the region where it is generated.

In respect of the photo-induced advanced oxidation of organic pollutants, a number of examples from the literature reveal the huge potential of the photo induced VUV AOP for oxidizing and mineralizing organic hazardous and persistent contaminants, the Table 7.2 summaries the most relevant reported studies performed in this field.

Table 7.2 Summary of relevant studies of mineralization under VUV using excimer lamps [20].

Substrate	P_{el} [W]	Irradiated Volume [L]	$[c_0]$ in mg/L	$[c_f]$ in mg/L	Mineralization	Group of substances	References
1,1,1-Trichloroethane	150	2,95	24,9	0 (90 min)	TOC<0,5ppm 120 min	Industry	[124]
1,1,2-Trichloroethane (ground water sample)	142	3,00	1	3 (70 min)	---	Industry	[125]
1,2-Dichloroethane	100	3,00	n.s.			Industry	[126]
1,2-Dichloroethene (ground water sample)	142	3,00	20,0	0	---	Industry	[124]
1,2-Ethanediol	155	1,00	-	-	---	Other	[127]
2,4-Dichlorophenol	155	1,00	100	0 (40 min)	TOC < 1 (180 min)	Industry	[127]
2,4-Dichlorophenol	105	1,00	100	0 (40 min)	TOC < 1 (180 min)	Industry	[61, 128]
2-Chlorodibenzo-p-dioxin	hv	3-4 mL	-	-	-	Industry	[129]
3-Amino-5-methylisoxazole	150	0,75	49	0 (40 min)	TOC < 1 (200 min)	Industry	[62]
4-Chlorophenol	155	1,00	92	---	TOC < 3,0 (180 min)	Industry Pesticides	[19, 127]
4-Chlorophenol	150	0,75	64			Industry Pesticides	[62]
4-Chlorophenol	150	3,00	64,3			Industry Pesticides	[130]
4-Chlorophenol	100	n.s.	30			Industry Pesticides	[126]
Acetic acid	155	1,00	122		TOC < 3,8 (180 min)	Industry Food ingredient	[127]
Alcohols (C_1 - C_8)	155	1,00	-	-	---	Industry Other	[127]
Atrazine	150	0,22	21,56		TOC (90%reduction 180 min)	Pesticide	[131]
Azo dyes	150	0,80	-			Industry	[124]
Dissolved molecular oxygen	200	1,00	---		---	Other	[75]
FE^{III}-EDTA	105	5,00	75	---	---	Other	[61]
Formaldehyde	150	0,80	30	---	---	Industry Other	[124]
Formic Acid	155	1,00	186		TOC < 1 (180 min)	Industry Other	[127]
Hexacyanoferrate(II)	hv	0,17	5 mmol/L	---	---	Other	[132]
Hexacyanoferrate(III)	hv	0,17	5 mmol/L	---	---	Other	[132]

Substrate	P_{el} [W]	Irradiated Volume [L]	$[c_0]$ in mg/L	$[c_f]$ in mg/L	Mineralization	Group of substances	References
Humic acid	150	0,350	500	---	---	Other	[133]
Landfill leachate	300	4,00	15 TOC	10 TOC (350 min)	---	Other	[134]
Methanol	200	1,00	~ 8000	~ 6400	---	Other	[22]
Methanol	200	1,00	117	---	TOC < 1 (180 min)	Other	[127]
Methanol (+ NO^-_3)	150	0,22	135	---	TOC < 1 (140 min)	Other	[135]
Oxygen	hv	n.s.	n.s.	---	---	Other	[136]
Phenol	155	1,00	60		TOC (50%reduction 180 min)	Industry	[127]
Phenol (+ NO^-_3)	150	0,22	71		TOC < 1 (120 min)	Industry	[137]
Potassium cyanide (KCN): CN^-	150	0,22	33			Industry Other	[62]
Potassium nitrate (KNO_3): NO^-_3	150	0,22	20			Other	[62]
Propanone (acetone)	155	1,00	37,7		TOC (50%reduction 180 min)	Industry Other	[127]
Rhodamine B	150	4,00	11		TOC (20%reduction 180 min)	Other	[134]
Sodium nitrite ($NANO_2$): NO^-_2	150	0,22	17			Other	[62]
Tetrachlormethane	hv	n.s.	23	0 (70 min)	---	Industry	[138]
Trichloroacetic acid	100	3,00	n.s.			Industry	[126]
Trichloroethene	150	2,95	21	0 (20 min)	--	Industry	[124]
Trichloroethene (ground water sample)	150	3,00	103	0 (90 min)	---	Industry	[125]
Trichloromethane	150	2,95	26,1			Industry	[124]
Methylene Blue	20	10	10	0 (200 min)	TOC (60% reduction 240 min)	Other	[21]

As presented in previous chapters, studies obtained from the literature review are based on, or were performed using, setups with a mismatch between reactor channel and light penetration (the photo-reaction zone in micrometers is 3 orders of magnitude smaller than the channel size in millimeters); as explained in chapter 3 and 6 this mismatch increases the probability of appearance of depletion zones in the photo-reactor, this prevent the complete use of the hydroxyl radicals being generated

and the chemical regime is far away from a kinetic controlled regime (instead limited by mass transfer and diffusion).

Furthermore the constant presence of priority substances in the environment is an issue of great importance for ecosystems and human health, therefore this thesis studies the performance of the photo-induced oxidation in the degradation of them and demonstrate the potential of this technology as a solution for this issue.

7.3. Materials and methods

7.3.1. Flat lamp-reactor system

The flat lamp-reactor system consist of 4 flat Xenon excimer Lamps emitting 172 nm radiation, each lamp is coupled with a reactor system where lamp surface is in direct contact with the flowing solution, schematic of the Fraunhofer lamp is shown in Figure 7.2.

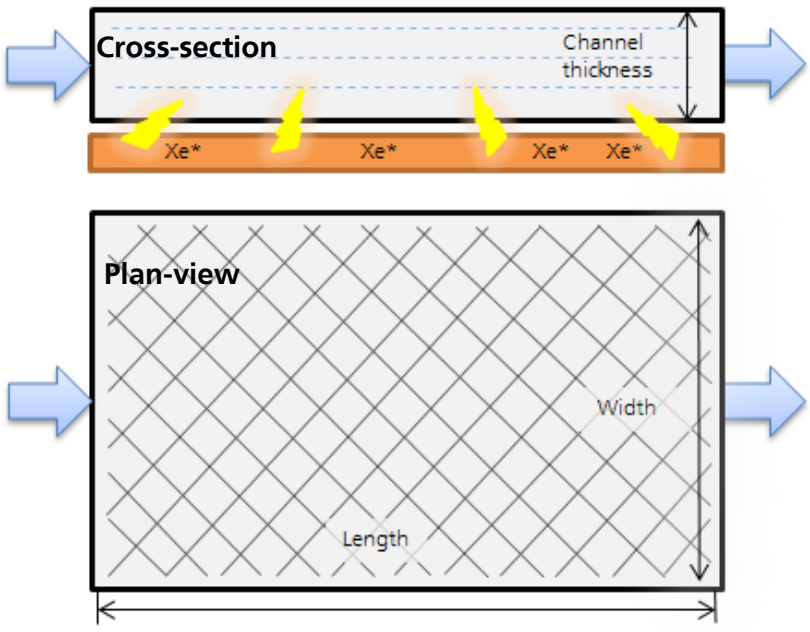

Figure 7.2 Laboratory Setup photo-reactor, Fraunhofer Lamps

The system was designed to have a variable channel thickness between 250 and 1250 µm. Each reactor has an active irradiation area of 310,5 cm^2. The inlet and outlet of the reactor were designed in a way it is obtained a uniform flow over the active irradiation area.

The flat lamp-reactor system is connected to a 2 L jacketed reactor glassware as reservoir with, a magnetically coupled centrifugal pump Sondermann BGR 1.5 (Sondermann, Germany), flow can be controlled and varies from 50 to 250 L/h range.

All tubing and periphery are made of materials with highly crack and stress resistance, low permeability, no moisture absorption and low level of chemicals extractable to assure a wide range of experimental fluids and pollutants.

A net-like turbulence promoter is installed in the chamber meeting two functions, electrode for the xenon excimer flat lamp and mixing enhancement [139, 140].

Of special interest is the use of the optimal operational parameters for the avoidance of the generation of depletion zones, having a maximum use of the hydroxyl radicals generated. A series of experiments were performed using the model substance MB to characterize the system.

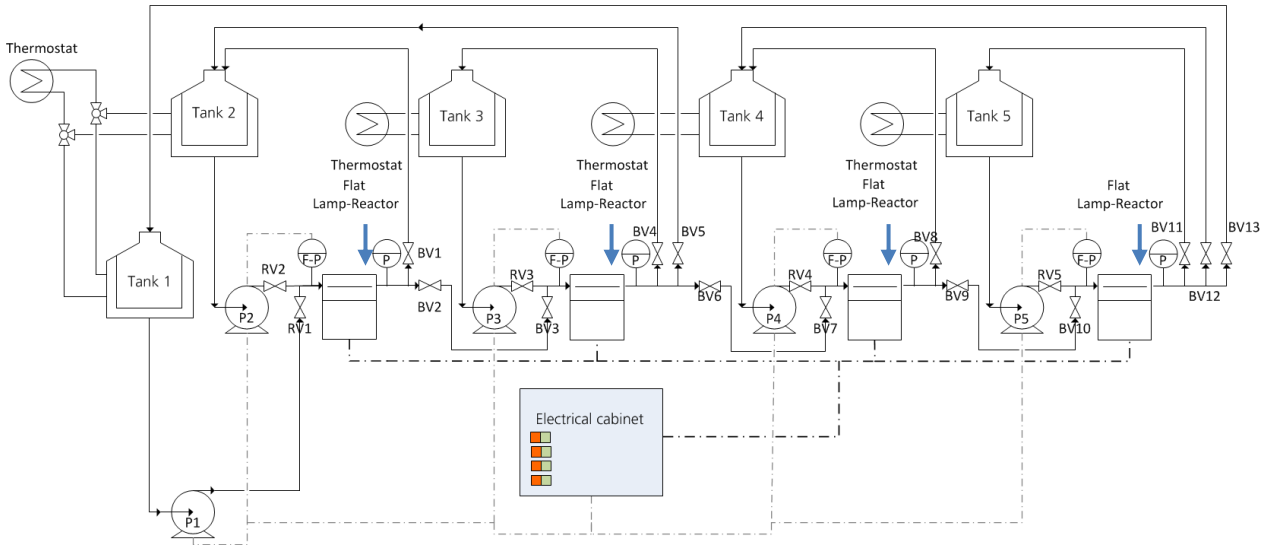

Figure 7.3 Schematic representation of the flow loop used for the study

The whole plant consists of four flat lamp-reactor systems, five jacketed reactors (glassware) as reservoirs, 5 pumps, piping valves and control system schematically represented in Figure 7.3. The system was designed to be flexible in operation and give the opportunity to perform a long term investigation in the degradation of pollutants in Fraunhofer institute IGB. The plant can be operated in these three situations:

- One loop four reactors in series: one tank is connected in series to all four flat lamp-reactors.

- Two parallel loops of two reactors in series: two separate circles of one tank connected to two flat lamp-reactors.
- Four loops of four reactors in parallel: four separate circles of one tank connected to the respective flat lamp-reactor in parallel circuit.

This study is focused on the 4 circuits/reactors in parallel due to characterization purposes, each reactor was investigated separately. Each circuit consists of a reactor, a pump, a tank as well as a flowmeter and a pressure measurement system for the flat lamp-reactor system. The systems are built taking special care than air does not get in contact with the VUV radiation, as a safety measurement due to the formation of ozone when VUV is in contact with air; one ozone sensor is installed nearby the lamp-reactor systems. The complete setup is shown in Figure 7.4.

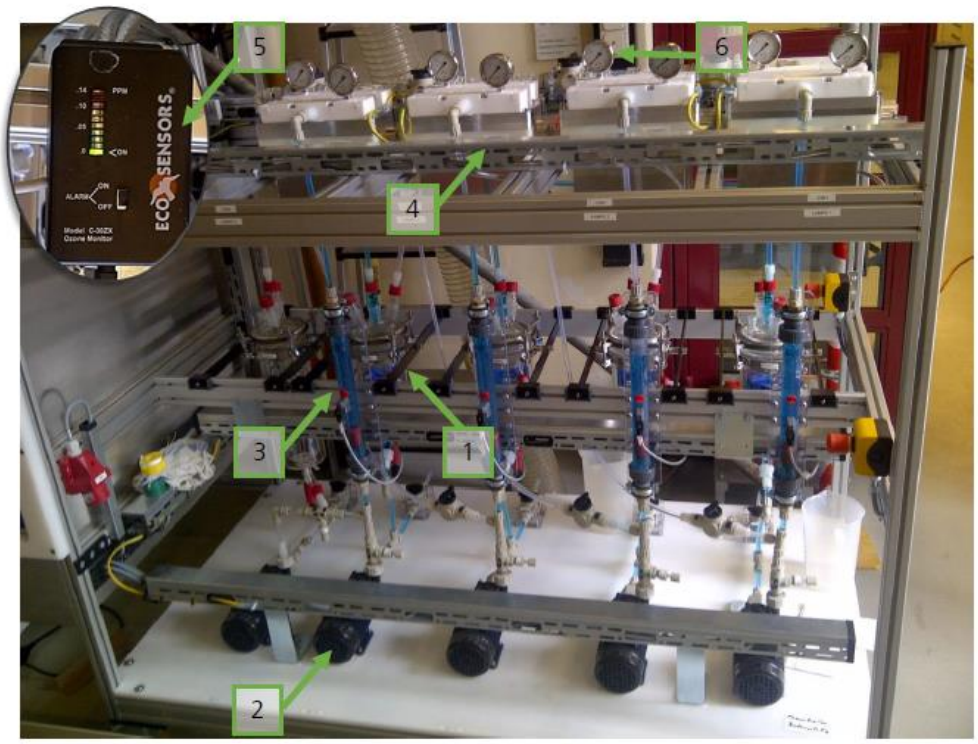

1. Tank
2. Pump
3. Flowmeter
4. Reactor body Flat lamp
5. Ozon sensor
6. Manometer

Figure 7.4 Front view VUV AOP laboratory scale 4 reactors system used for the study

Each reactor has a control point where it is possible to see the emitting radiation of the luminescence of quartz after absorption of VUV. The Figure 7.5 shows the control point during operation.

These control point are just a small piece of quartz connected to the lamp which comes out of the reactor and due to the fluorescence of the quarts it can be optically controlled if the lamps ignited during the operation.

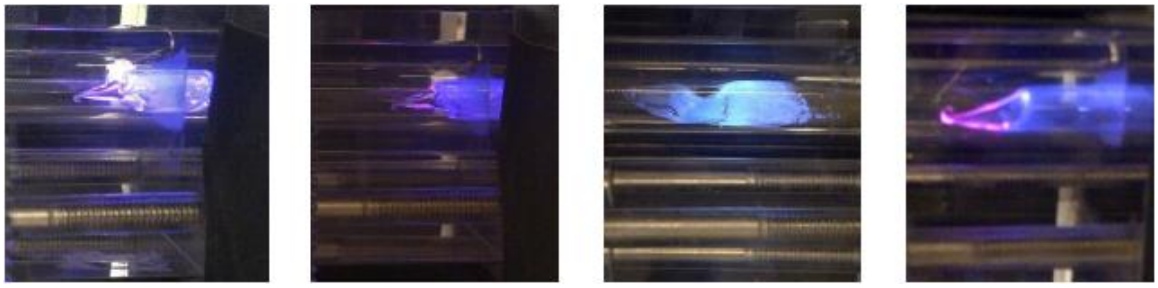

Figure 7.5 Control point during operation of each reactor

7.3.2. Irradiance measurements

A specially setup to hold the recent developed xenon excimer lamps from Fraunhofer IGB was built to measure the irradiance of the lamps. Each lamp was installed and tested separately and the irradiance was measured at the surface of the lamp using the AlGaN calibrated sensor described in chapter 4. Measurements were performed at the face which will be exposed to the fluid. The sensor was installed in a 2 arms thorlab X-Y table with the ability of scan the whole flat window, the sensor was kept parallel to the window at a constant distance. The Figure 7.6 shows the Setup built for the measurements of Irradiance of flat lamps.

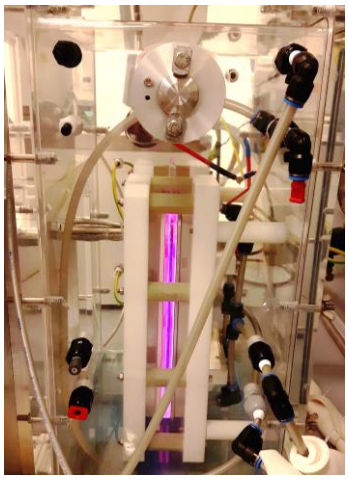

Figure 7.6 Irradiance measurement set up

Measurements were performed in hermetic chamber under a nitrogen atmosphere to prevent absorption of radiation by Oxygen from air. Irradiance measurement results are summarized in Table 7.3, all the lamps were filled with Xenon and sealed by hand, this is a complex process that at this stage was not standardized, therefore the differences in irradiance values between the lamps.

Table 7.3 Irradiance measured for each reactor

Lamp Reactor	Irradiance
1	1,52 mW/cm^2
2	1,36 mW/cm^2
3	0,98 mW/cm^2
4	1,26 mW/cm^2

7.3.3. Model chemicals for oxidation experiments

Five substances were selected from the literature to test the system. The selected substances part of this study are Methylene Blue, Carbamazepine, Sulfaquinoxaline, Bisphenol A and Caffeine.

MB was used as a model substance for the characterization of the lamp-reactor systems, its properties are described in numeral 3.3.2.

Carbamazepine and Sulfaquinoxaline, pharmaceuticals which are low degradable by municipal WWTP, therefore classified as recalcitrant and persistent. Their properties are presented in Table 7.4 [109, 110, 141].

Bisphenol A and Caffeine, chemical from the industry and food ingredient respectively, commonly present in the inflow of wastewater treatment plants, they are biodegradable in well operated municipal WWTP, but its appearance in water surfaces may classified them to analyse the performance of water treatment technologies, their properties are presented in Table 7.5 [142, 143].

Carbamazepine (CBZ) is an antiepileptic drug used to control seizures, it is used for the treatment of seizure disorders, for relief of neuralgia, and for a wide variety of mental disorders; The global consumption of CBZ was reported in literature to be 1014 tons per year [109]. Approximately 72% of orally administered carbamazepine is absorbed, while 28% is unchanged and subsequently discharged through the faeces. It is one of the most frequent detected pharmaceutical residues in water bodies so far. Carbamazepine has been proposed as an anthropogenic marker in water bodies [144].

Sulfaquinoxaline sodium (SQX) is an antibiotic used to prevent coccidiosis in poultry, swine, and sheep by inhibiting the synthesis of nucleic acids and proteins in microorganisms. The quinoxaline group

within SQX exhibits mutagenic and carcinogenic properties, it was reported that low levels of SQX in the environment have been shown to encourage the formation of strains of antibiotic-resistant bacteria [111, 145].

Table 7.4 Reference substances selected for this study (Pharmaceuticals)

Properties	
Carbamazepine	
Structure	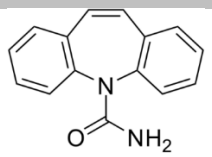
CAS No.	298-46-4
Molecular weight	236,3 g/mol
Water solubility	205,0 mg/L
Uses	It is a medication used primarily in the treatment of epilepsy and neuropathic pain
Initial concentration	20,0 mg/L
Initial TOC theoretical	15,2 mg/L
Sulfaquinoxaline	
Structure	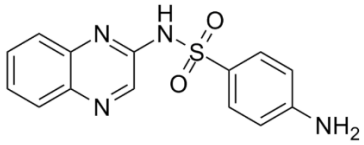
CAS No.	59-40-5
Molecular weight	300,4 g/mol
Water solubility	45,1 mg/L
Uses	It is a veterinary medicine which can be given to cattle and sheep to treat coccidiosis.
Initial concentration	25,0 mg/L
Initial TOC theoretical	13,7 mg/L

Bisphenol A (BPA) is an intermediate in the production of polycarbonate and epoxy resins, flame retardants, and other specialty packaging products. It is consider an emerging contaminant being released in the environment in the manufacture process and during the life-time of plastic bottles and packaging as well as from landfill leachates. Worldwide production of BPA is reported in literature and it was estimated to be 1.620 tons per year [142]. It is xenobiotic, it can be absorbed and accumulate in living beings. This compound disturbs the behaviour of aquatic life by Endocrine Disruptive Effects (EDE) at low level concentrations.

To some extent, BPA can be eliminated through traditional physical, chemical, or biological treatments. Nevertheless, because of its estrogenic action, and the fact that chlorination disinfection processes can lead to products with higher EDE and/or toxicity, BPA should be completely removed from wastewater and water sources [146].

Table 7.5 Reference substances selected for this study (Industry and food ingredient)

Properties	
	Bisphenol A
Structure	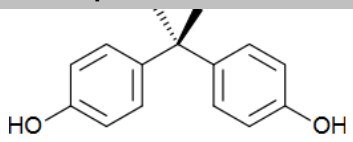
CAS No.	80-05-7
Molecular weight	228,3 g/mol
Water solubility	300,0 mg/L
Uses	BPA is employed to make certain plastics and epoxy resins. BPA-based plastic is clear and tough, and is made into a variety of common consumer goods, such as water bottles, sports equipment, CDs, and DVDs
Initial concentration	30,0 mg/L
Initial TOC theoretical	23,0 mg/L
	Caffeine
Structure	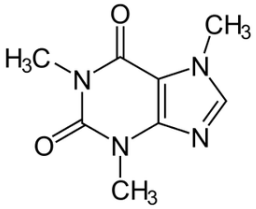
CAS No.	58-08-2
Molecular weight	194,19 g/mol
Water solubility	20,0 g/L
Uses	It is a central nervous system (CNS) stimulant of the methylxanthine class
Initial concentration	30,0 mg/L
Initial TOC theoretical	14,7 mg/L

Caffeine is by far the most universally used legal drug, being present in foods, beverages or combined with analgesics in order to enhance their effects. Caffeine is widely found in influent and effluent of sewage treatment plants, soil and surface water. It is one of the compounds present in higher concentration in influent of wastewater treatment plants, therefore it has been suggested to be used as a tracer of recent fecal contamination marker [147].

The oxidation of Carbamazepine, Sulfaquinoxaline, Bisphenol A and Caffeine have been topic of research at the Centre for Process and Environmental Engineering CEPIMA, the group of Dr. Montserrat Perez-Moya group in Barcelona has investigated the fate of these pollutants using different Advanced Oxidation Processes like ozonation, Fenton and photo Fenton [112-114, 148-150]. It has been proved that the hydroxyl radical produced by those AOPs is able to oxidize the four substances selected. This thesis studies the performance of the photo-induced oxidation in the degradation of Carbamazepine, Sulfaquinoxaline, Bisphenol A and Caffeine.

Variation of the concentration of the mentioned model substances, the total organic carbon and the toxicity were follow during irradiation. Total organic carbon (TOC) is a sum parameter containing not only the carbon in the contaminant but also the carbon contained in by-products, it is a non-specific indicator of water quality which lets know the degree of degradation/mineralization of the overall contamination. Additionally toxicity along the experiments is an indication of the biodegradability of the by products resulting from the oxidation of the model substances.

7.3.4. Analytics

7.3.4.1. Determination of total organic carbon (TOC)

The amount of carbon bound in organic compounds is commonly used as an indirect measurement of the organic substances in a sample and as a non-specific indicator for water and wastewater quality. As it is practically unmanageable to identify and follow the generation and decay of all the intermediates formed during the oxidation process, the evolution of TOC is understood as a global parameter which concerns all organic compounds in the sample. A Shimadzu TOC-VCSH/CSN analyzer is used in this work for measuring total carbon (TC). In this equipment, the sample is carried through an oxidation catalyst-filled combustion tube heated to 680 °C by means of a carrier gas (purified air) at a controlled flow rate; the sample is completely oxidized to CO_2, which is dehumidified and later detected by a non-dispersive infrared detector (NDIR).

Parallel an acidified sample is bubbled with the carrier gas perturbing the inorganic carbon IC equilibrium and taking the CO_2 (carbonate and bicarbonate in acid solutions turn to CO_2); the mixture is dehumidified and detected by a non-dispersive infrared detector (NDIR). TOC is then determined by subtracting IC from TC. For TC quantification, four linear calibration curves, ranging from 0-10, 0-20, 0-100 and 0-200 mg/L were available, while two calibration curves were established for IC quantification, ranging from 0-10 and 0-20 mg/L.

7.3.4.2. Determination of contaminant concentration

The concentration measurements of each specific pollutant were performed by photometry for Methylene Blue as described in chapter 3 and by high performance liquid chromatography (HPLC). The last is a quantification technique that involves the separation of the components of a sample when they are forced to flow at high pressure through a packed column (stationary phase) driven by a liquid mixture (mobile phase). Components in the sample are separated one from another by the column than involves various chemical and/or physical interactions between their molecules and the packing particles. These separated components are detected at the exit of the column by an infra-red detector that measures their amount. The quantification is based in calibration curves constructed from solutions with known composition and allows measuring the concentration of the pattern contaminant and therefore its evolution along processing time.

The AgilentR 1200 series HPLC used in this study consists in a modular system equipped with a manual injector, a mobile phase degasser, a quaternary pump, a heating oven and a diode array detector. When the sample is manually injected, it is mixed with the mobile phase and carried out by the quaternary pump throughout the stationary phase for the components to be separated and then they are sent to the detector. The time taken by the compound to travel from the column to the detector is known as retention time and it depends on the pressure, the nature of the stationary phase, the composition of the solvent and the temperature of the column. The Table 7.6 shows the chromatographic conditions used for the contaminants studied in this study.

Table 7.6 Chromatographic conditions used for this study

Substance	Mobile phase	Stationary phase	Temp (°C)	λ (nm)	Flow (mL/min)	Retention time (min)
Carbamazepine	70 % Water 30 % Acetonitrile	Akady 5 µm C-18 150x4.6 mm	25	210	1,5	1,1
Sulfaquinoxaline	55 % Methanol 45 % water 0,1 % Formic acid	Akady 5 µm C-18 150x4.6 mm	20	254	1	2
Bisphenol A	70 % Methanol 30 % water	Akady 5 µm C-18 150x4.6 mm	20	224	1	3,9
Caffeine	70 % Water 30 % Acetonitrile	Agilent Zorbax Eclipse XDB-C18 5µm 4,6x150 mm	25	274	1,5	1,1

The HPLC is connected to a ChemStationR software, using it the different methods for different substances can be programmed and data acquisition and processing is performed. HPLC grade reagents and filtered milliQ water were used as mobile phases. Calibration curves where plotted to stablish the

instrumental response to the analytical signal, 6 points calibration curves were plotted and linear regression results in R^2 higher than 0,998.

7.3.4.3. In-vitro toxicity using cell cultures

COS cells and VERO cells are a lineage of cells used in cell culture. The Vero cell lineage was isolated from kidney epithelial cell extracted from an African green monkey, they are a continuous lineage meaning that it has an abnormal number of chromosomes and can be replicated through many cycles of division and not become senescent (biological aging). The COS cells corresponds to fibroblast-like cells derived from monkey kidney tissue. COS cells are obtained by immortalizing CV-1 cells with a version of the SV40 virus that can produce large T antigen but has a defect in genomic replication (promoting wild replication). Both cell lines are used for screaning for the toxin Escherichia coli and used as well as host cells for growing viruses to measure replication in the presence or absence of a pharmaceutical. In water treatment they are used for the toxicity measurement of water contaminants. COS and VERO cells were cultured in Dulbecco's Modified Eagle Medium (DMEM) supplemented with 10% fetal bovine serum, 1% penicillin/streptomycin, and 2 mM L-glutamine at 37°C in a humidified atmosphere with 5% CO_2 and 95% air.

The culture medium was changed every 2 days and, for subculture, cell monolayers were rinsed with PBS and detached by incubation with trypsin-EDTA (0.25%) at 37°C for 2-5 min. Cell concentration was determined by counting with a Neubauer chamber and employing 4% trypan-blue as dye vital. Detached cells with viability >95% were used for toxicity assays. Aliquots of 200 µL containing 104 cells were seeded in each well of a culture plate of 96 well and culture during 24 h to allow cell attachment to the plate.

After, the media were aspired and the samples in half-dilution prepared with culture medium were evaluated for cellular toxicity by exposing cells to direct contact with the samples prepared. Then, the plates were incubated for another 24 h. Finally, cell viability was determined by the MTT assay, and then, the mortality was calculated for each sample as the difference between the viability of the control (medium without substance) and the sample.

The samples were evaluated using five replicates and the results were average and graphically represented. To determine the cytotoxic concentration (LC50) of the substances in study, the viability or cell death is determined by different concentrations of the substances prepared by dilution in culture medium.

7.4. Results and discussions

7.4.1. Methylene Blue oxidation preliminary screening experiments

In this section, solutions of methylene blue MB (initial concentration 25 mg/L and theoretical TOC of 15 mg/L) were oxidized. Different operational parameters (combination of flow and channel thickness of the reactor) were tested. Five different channel thickness 250, 500, 750, 1000 and 1250 µm as well as five different recirculation flows 50, 100, 150, 200 and 250 L/h were used.

An example of the degradation of Methylene Blue for five experiments all of them performed in reactor 4 with channel thickness of 250 µm at different flows is presented in the Figure 7.7.

The initial reaction rate of the degradation of Methylene Blue, the time for reduction of concentration of MB in one order of magnitude were determined and compared. Tables 7.6 and 7.7 report the initial reaction rate, the time for MB to be reduced 90% (one order of magnitude) for each Reactor; experiments were performed for 20 minutes of irradiation.

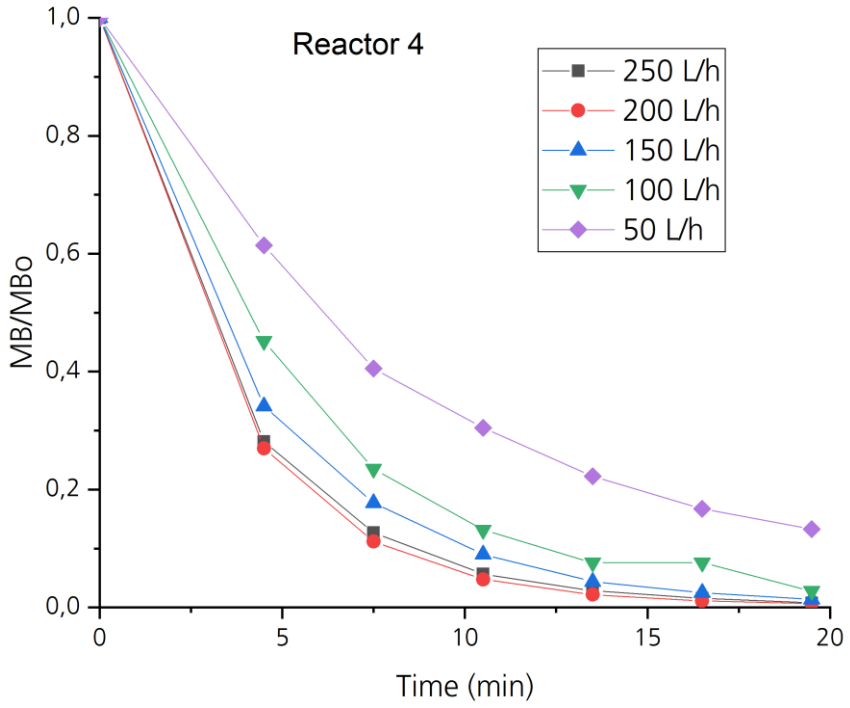

Figure 7.7 Evolution of normalized concentration MB in time at different flows, channel thickness 250µm R4

An increase in the initial reaction rate with the increase or recirculation flow is one of the trends we evidence in chapter 3, results of experimentation with MB in the second setup corroborate that the increase in flow velocity and the use of net-like mixing promoter reduces the probability of generation of depletion zones where hydroxyl radical is not being use.

From the results the initial reaction rate also reaches a plateau and the best results were found to be combining operational parameters maximum flow and channel thickness above 750 µm.

Table 7.7 Experimental result, Ri initial reaction rate, time MB to be reduced 50% (half-life) for reactor 1 and 2

		Reactor 1		Reactor 2	
Thickness (µm)	**Flow (L/h)**	**Ri (mg/Lmin)**	**Time MB to be reduced 90%(min)**	**Ri (mg/Lmin)**	**Time MB to be reduced 90%(min)**
250	50	3,7	11,3	2,5	17,0
	100	4,6	8,6	3,1	13,8
	150	5,3	6,6	4,2	8,8
	200	6,1	5,5	4,7	7,4
	250	5,5	6,1	4,6	7,3
500	50	3,5	10,7	3,2	11,7
	100	5,0	7,9	4,7	8,8
	150	5,4	6,3	4,7	7,7
	200	5,8	6,9	5,2	8,8
	250	5,8	5,8	5,3	7,2
750	50	2,4	15,7	2,7	16,2
	100	3,6	10,0	3,5	10,9
	150	4,5	8,1	4,2	9,2
	200	5,2	6,6	4,4	8,3
	250	5,1	6,5	4,7	7,8
1000	50	4,1	8,6	4,2	9,5
	100	5,5	6,5	5,0	7,6
	150	5,7	5,7	5,1	6,5
	200	6,2	4,4	5,6	5,6
	250	6,5	4,5	5,9	5,4
1250	50	3,6	8,3	3,8	8,8
	100	4,4	4,8	4,7	5,7
	150	6,7	5,0	6,0	5,9
	200	6,1	5,1	6,1	5,6
	250	6,5	5,0	6,4	5,7

Results from reactor 3 and 4 show the same pattern. From the results the initial reaction rate also reaches a plateau and the best results were found to be combining operational parameters maximum flow and channel thickness above 750 µm.

The initial reaction rate was plotted for each combination of operational parameters, the results were analyzed and represented as a surface response in Figure 7.8.

In the surface response it is shown that a plateau of maximum initial reaction rate is reached for flow velocities above 150 L/h in all channel thicknesses.

Table 7.8 Experimental result, Ri initial reaction rate, time MB to be reduced 50% (half-life) for reactor 3 and 4

		Reactor 3		Reactor 4	
Thickness (µm)	**Flow (L/h)**	**Ri (mg/Lmin)**	**Time MB to be reduced 90%(min)**	**Ri (mg/Lmin)**	**Time MB to be reduced 90%(min)**
250	50	3,0	13,9	2,4	>20,0
	100	4,4	9,9	3,6	12,2
	150	5,3	6,9	4,2	9,4
	200	6,0	5,7	4,8	7,4
	250	5,2	6,6	4,6	7,7
500	50	3,1	12,2	2,6	15,6
	100	4,2	9,2	4,0	11,1
	150	5,5	7,1	4,1	9,8
	200	6,4	6,4	4,7	9,4
	250	5,8	6,8	5,1	8,0
750	50	3,3	13,4	2,3	>20,0
	100	4,4	8,7	3,6	11,1
	150	5,3	7,0	4,4	8,6
	200	5,4	5,2	4,9	7,1
	250	5,6	6,5	5,4	6,3
1000	50	4,5	8,5	4,0	9,9
	100	5,9	5,9	5,2	7,4
	150	6,1	5,5	5,7	6,4
	200	6,7	4,5	5,8	5,1
	250	6,7	4,5	6,3	5,0
1250	50	5,2	7,5	4,2	8,7
	100	7,0	5,1	6,2	6,4
	150	7,0	4,9	6,1	5,9
	200	6,9	4,6	6,6	5,2
	250	7,5	4,5	8,1	4,5

In this region of flows above 15 L/h, the Net like mixing promoter successfully generate secondary flows in the cross-section, generating a mixing of the laminar layers overcoming the lack of substrate exchange, bringing substrate to the photo-reaction zone and showing a comparable effect in the initial reaction rates. The plateau of initial reaction rate is observable along the whole range of channel thicknesses with flows larger than 150 L/h.

Taking into account the results of these screening experiments the best region for conducting experiments for photo-induced advanced oxidation of pollutants is the range of channel thicknesses between 750 µm and 1250 µm and operational flow between 150 and 250 L/min.

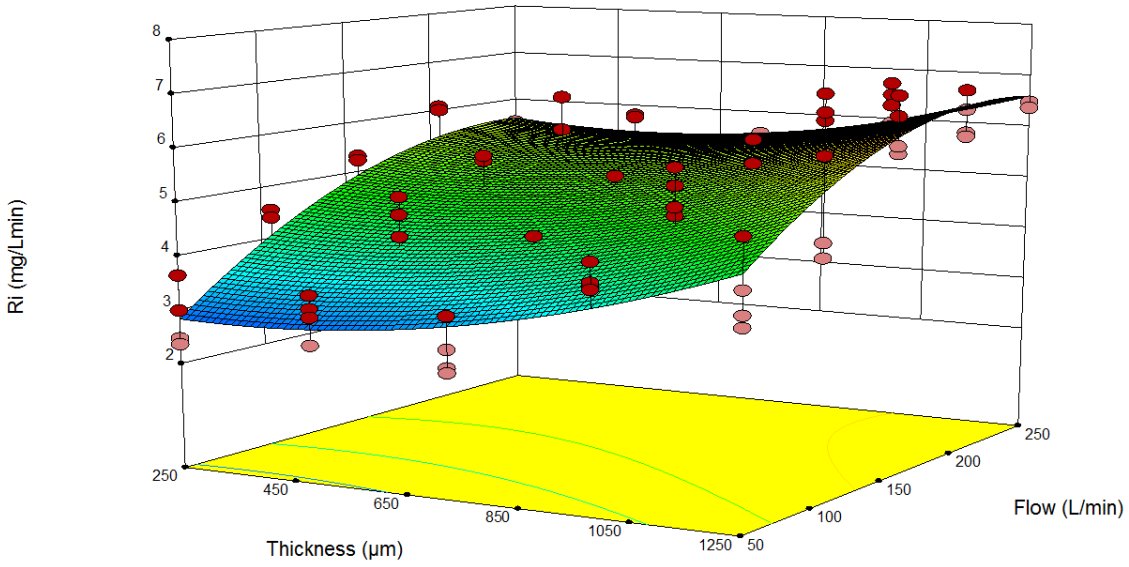

Figure 7.8 Generated surface of the relation Initial reaction rate, channel thickness and flow during all experiments all four flat lamp-reactor system in the plant

These results are in well agreement with results of chapter 3 where it was evidenced that the net-like promoters prevent the effect of boundary layer development and help to avoid the depletion of substrate in the photo-reaction zone.

7.4.2. Sulfaquinoxaline degradation

7.4.2.1. Preliminary experiments

In order to confirm the results obtained with Methylene Blue a number of oxidation experiments with Sulfaquinoxaline were performed. As described before the initial reaction rate of destruction of MB

in the system reaches a maximum at flows higher than 150 L/h and this maximum seems to be independent of the channel thickness from 750 to 1250 µm; for the oxidation experiments, Sulfaquinoxaline solutions with concentrations between 6 to 25 mg/L (TOC values between 2,5 and 13 mg/L) were tested despite being much higher than that found in wastewaters and groundwater (between 0,001 to 0,040 µg/L) [6, 112, 116].

These high concentrations allow following the evolution of the contaminant and take into account the detection limit of the available measurement equipment 500 µg/L. Operational parameters were restrained to the region between 750 and 1250 µm using maximum Flow 250L/h. Two experiments were performed at 250 µm channel thickness for comparison. In total 16 experiments were performed for different SQX concentrations at natural pH.

As example of the evolution of SQX and TOC during experiments, the results of one experiment (Pre 16) is show in the Figure 7.9.

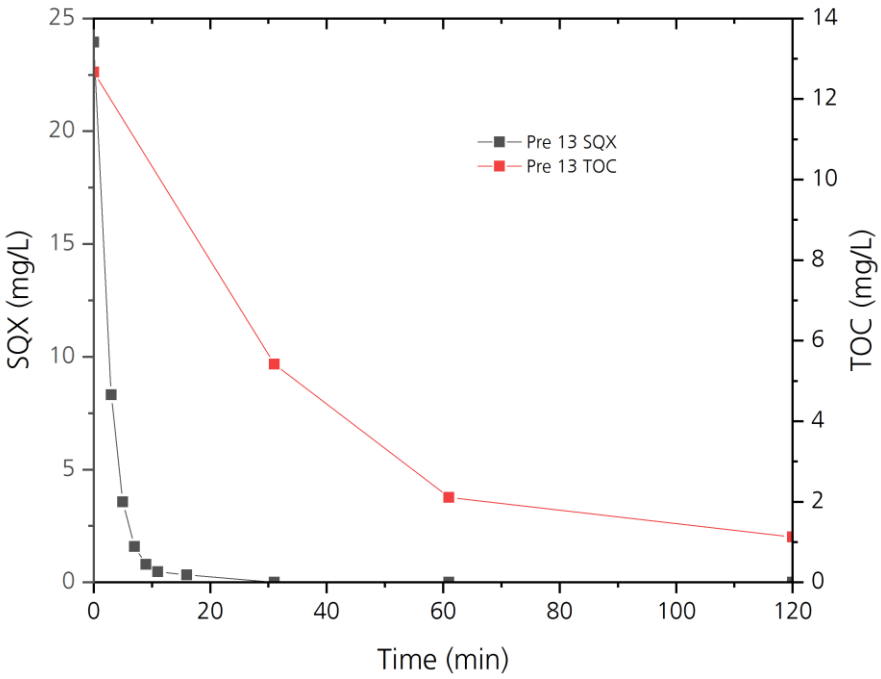

Figure 7.9 Evolution of concentration of SQX and TOC of one preliminary experiment initial SQX concentration 24 mg/L, channel thickness 1250 µm, flow 250 L/min performed in reactor R2

The SQX molecule is no longer detectable after 20 minutes of irradiation, TOC decreases progressively reaching TOC reduction higher than 80% of the initial value. This behaviour was observed in all preliminary experiments. Sulfaquinoxaline degradation by photo-induced advanced oxidation presents a pseudo-first order degradation rate following the equations 7.1, 7.2 and 7.3.

$$\frac{dy}{dt} = ky \quad \textbf{(7.1)}$$

$$y = y_0 e^{kt} \quad \textbf{(7.2)}$$

$$\frac{y}{y_0} = e^{kt} \quad \textbf{(7.3)}$$

Sulfaquinoxaline being a complex molecule and not biodegradable was completely oxidize by the photo-induced AOP to the limit of detection. Mineralization was reached TOC was reduce almost completely. The results confirmed that the technique can be used successfully for oxidation of pharmaceuticals and results are in concordance and follow a pseudo first order degradation as the degradation of Methylene Blue.

In the Table 7.9 the initial reaction rate at 2 minutes, the time for SQX to be reduced 90% (one order of magnitude) and the pseudo-first order degradation rate constant of the preliminary experiments at different initial concentrations are reported. Preliminary experiments were performed under 120 minutes of constant irradiation and continues recirculation. In all cases SQX was successfully oxidized and not detectable after maximum 40 minutes of irradiation.

Table 7.9 Experimental result, Ri initial reaction rate, time SQX to be reduced 90% (one order of magnitude) for different concentrations and different channel thicknesses

Experiment Number	Thickness (μm)	Initial SQX (mg/L)	Ri (mg/Lmin)	Time SQX to be reduced 90%(min)	Pseudo-first order k (min^{-1})
Pre 1	250	15,5	3,0	9,5	-0,25
Pre 2	250	20,5	3,6	10,6	-0,22
Pre 3	750	9,5	3,1	4,6	-0,57
Pre 4	750	11,3	3,3	5,9	-0,45
Pre 5	750	22,7	6,5	5,8	-0,44
Pre 6	1250	6,0	1,1	26,7	-0,24
Pre 7	1250	6,7	1,4	14,4	-0,29
Pre 8	1250	6,8	1,3	2,8	-0,30
Pre 9	1250	7,8	1,8	10,2	-0,36
Pre 10	1250	9,7	2,9	5,7	-0,48
Pre 11	1250	10,0	2,2	9,7	-0,31
Pre 12	1250	10,2	1,6	15,4	-0,20
Pre 13	1250	11,4	2,4	9,7	-0,30
Pre 14	1250	15,3	4,5	5,8	-0,46
Pre 15	1250	17,3	3,6	8,8	-0,28
Pre 16	1250	24,0	6,2	6,3	-0,37

The surface response used to analyze the trend of changes in the initial reaction rate for the experiments under different operational parameters is shown in Figure 7.10. It does not reveal significant effects on the initial reaction rate with different channel thickness at the same initial SQX concentration. However the initial reaction rate changes progressively when different initial SQX concentration is used.

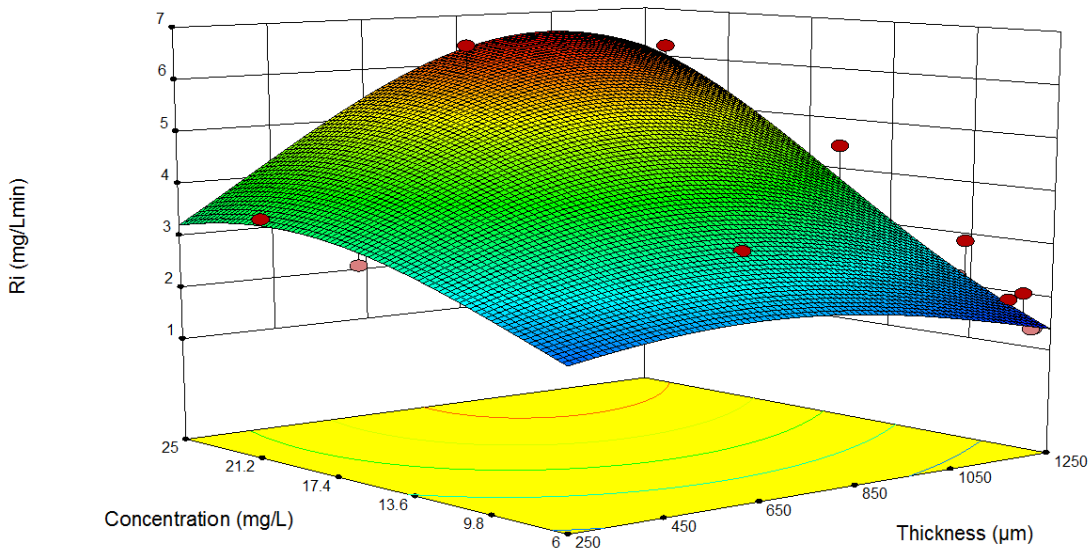

Figure 7.10 Generated surface of the relation Initial reaction rate, channel thickness and initial concentration of SQX experiments flat lamp-reactor system

The results from the preliminary experiments regarding the effects on initial reaction rate at different initial concentrations are coherent and can be explained by the different initial availability of substrate in the photo reaction zone at different initial concentrations of SQX. Lower the initial concentration, lower the availability of substrate in the photoreaction zone.

7.4.2.2. Constant initial concentration at different pH values

Subsequent for the later experiments with Sulfaquinoxaline it was decided to perform experiments using fixed operational parameters. Channel thickness 1250 µm, maximum flow 250 L/h. Initial concentration of SQX was from this moment constant at 30 mg/L, experiments were performed under 120 minutes of constant irradiation and continues recirculation.

Unlike other AOPs where the hydroxyl radical production is not constant and depends on addition and concentration of auxiliary substances as hydrogen peroxide, ozone or iron ion, photo-induced advanced oxidation using VUV produces a constant amount of hydroxyl radicals, and its constant production is function just of the irradiance. In AOPs using auxiliary substances the pH strongly affect the generation of hydroxyl radicals. For example in ozonation two main oxidants may be acting in the oxidation process (molecular O_3 and OH radical). Lower pH (pH < 4) favors the oxidation via molecular ozone. Increase of pH favors O_3 decomposition into hydroxyl radicals. In pH > 10, O_3 is instantaneously decomposed into hydroxyl radicals. In pH 7 both oxidants act [112]. In Fenton and photo Fenton processes the most suitable pH has been reported to be slightly below 3.0 due to the chemical equilibrium of ferrous-ferric species in water. A range between 2.5 and 4.0 is frequently reported as optimal for Fenton processes [14].

Degradation of Sulfaquinoxaline at different initial pH values was carried out to compare oxidation in different conditions, results are show in Figure 7.11. Different experiments using 2 of the flat-reactor systems were performed using 1,8 Liters of solution of Sulfaquinoxaline in distilled water at initial concentration of 30 mg/L. The experiments were performed by duplicate for each pH conditions.

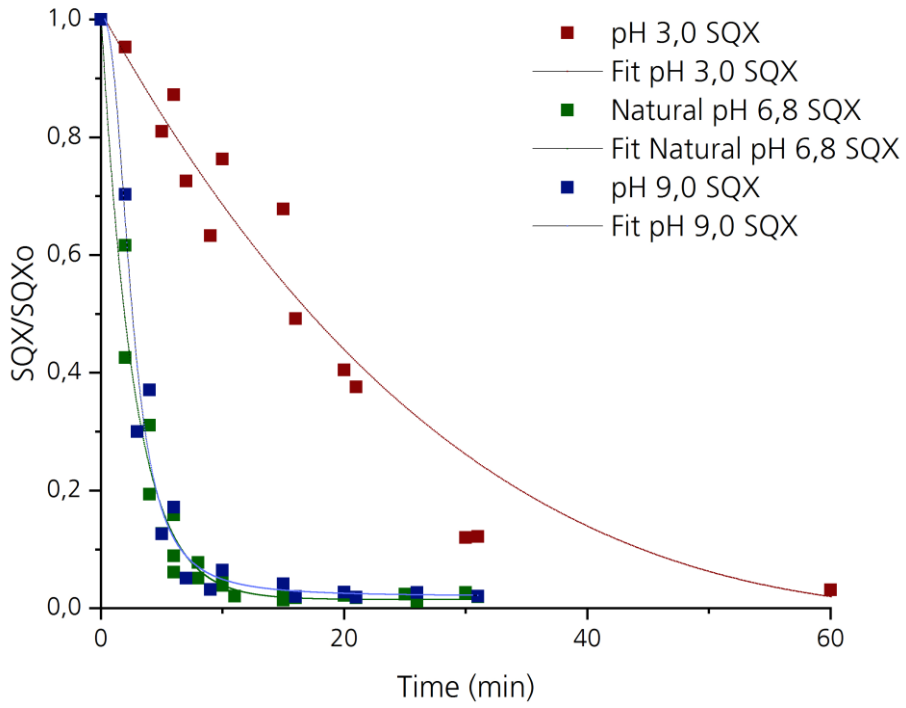

Figure 7.11 Evolution of normalized concentration SQX in time at different pHs

As it is appreciated in the Figure 7.11 during experiments at natural pH and basic solutions at pH 9, the degradation of Sulfaquinoxaline by means of photo-induced advanced oxidation is not affected. Under acidic conditions pH 3, the degradation of SQX is appreciable affected and its degradation slows down, reduction of SQX concentration in one order of magnitude takes 40 minutes more than under basic and natural pH conditions where the reduction in concentration of one order of magnitude takes place around the first 15 minutes of experiment. As mentioned in the preliminary studies Sulfaquinoxaline degradation by photo-induced advanced oxidation presents a pseudo first order degradation rate, the reaction constant k for the unaffected by pH experiments is k=-0,38±0,03 min^{-1} and for the affected experiments under acidic conditions is k=-0,05±0,01 min^{-1}.

Total organic carbon was measured every 30 minutes along the experiments. Total organic carbon reduction after 120 minutes of experimentation for each group of experiments was analyzed, results of the delta TOC under different pH conditions is shown in Figure 7.11. The average initial TOC was 12,55±0,80 mg/L. As well as in the evolution of the concentration of SQX, TOC evolution is affected by acidic pH values. An interesting result is that by using TOC a slight difference in the oxidation process can be seen between experiments at natural pH and basic pH.

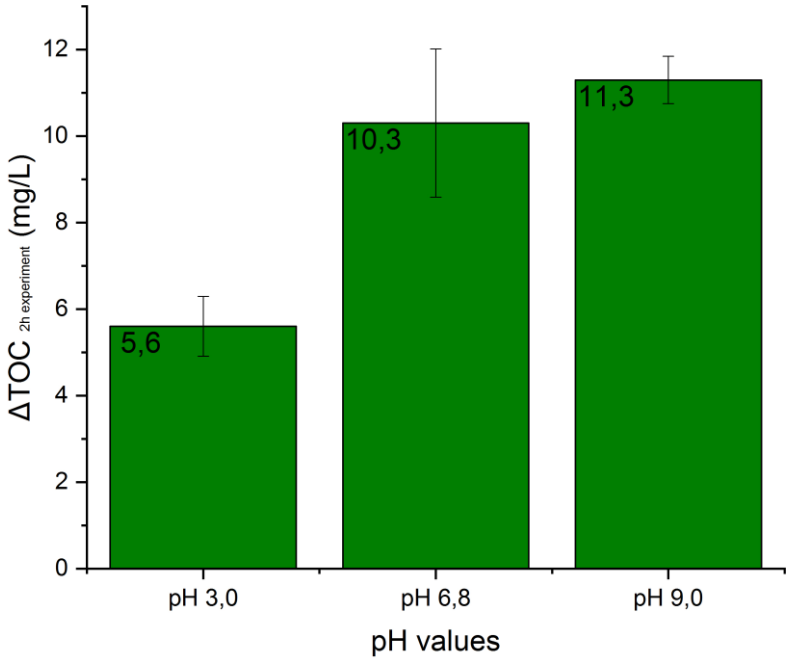

Figure 7.12 Delta TOC in mg/L for experiments at different pH (initial TOC 12,55±0,8 mg/L)

The changes denote a difference of 2,5 mg/L comparing the natural pH to acidic conditions and 1,0 mg/L comparing to basic conditions. When the complete mineralization is the focus, an initial pH

adjustment to basic conditions of the systems may increase in 10% the efficiency of the oxidation in the range of concentration used for experiments.

The reduction on TOC values represent a degradation of 60, 82 and 90% of the total TOC for experiments under acidic, natural and basic pH conditions during the 120 minutes of radiation. If the complete mineralization is the focus, an initial basification of the systems may increase in 10% the efficiency of the mineralization in the range of concentration used for experiments.

These results can be interpreted as follow: The reactivity of sulfonamides in photo-induced oxidation may relate strongly to their pKa values (about 5,8); in acidic conditions, protonated species of sulfonamides are predominant what may increase the number of extraction reactions needed to oxidize the molecule using hydroxyl radicals. Studies using ozone for the oxidation of Sulfaquinoxaline reported than ozonation in acidic conditions shows a favorable effect in the oxidation process [112, 151]. Taking into account the need of pH adjustment necessary for other AOPs, the photo-induced AOP presents an advantage due to the fact that the oxidation process can be applied without adjusting pH which represent handling of chemicals and cost in initial and final pH adjustment.

7.4.3. Carbamazepine degradation

Carbamazepine solutions of 20 mg/L concentration were irradiated (this is the only substance which could not be tested in higher concentrations due to the limits in solubility), despite the concentration of the experiments being much higher than that found in wastewaters and groundwater (between 0,5 to 3,5 µg/L) [5, 6, 109, 110, 143] Results are show in Figure 7.13.

These high concentrations allow following the evolution of the contaminant and take into account the detection limit of the available measurement equipment. Operational parameters were restrained to the region 1250 µm using maximum flow 250L/h, at different pHs. The experiments were performed by duplicate for each pH conditions.

As it is appreciated in the Figure 7.13 during experiments at natural pH, basic solutions at pH 9 and acid solutions at pH 3, the degradation of Carbamazepine by means of photo-induced advanced oxidation is not affected. Reduction of CBZ one order of magnitude takes in all cases less than 10 minutes. Carbamazepine degradation by photo-induced advanced oxidation presents a pseudo first order degradation rate, the reaction constant k for the unaffected by pH experiments is k=-0,41±0,03 min^{-1}.

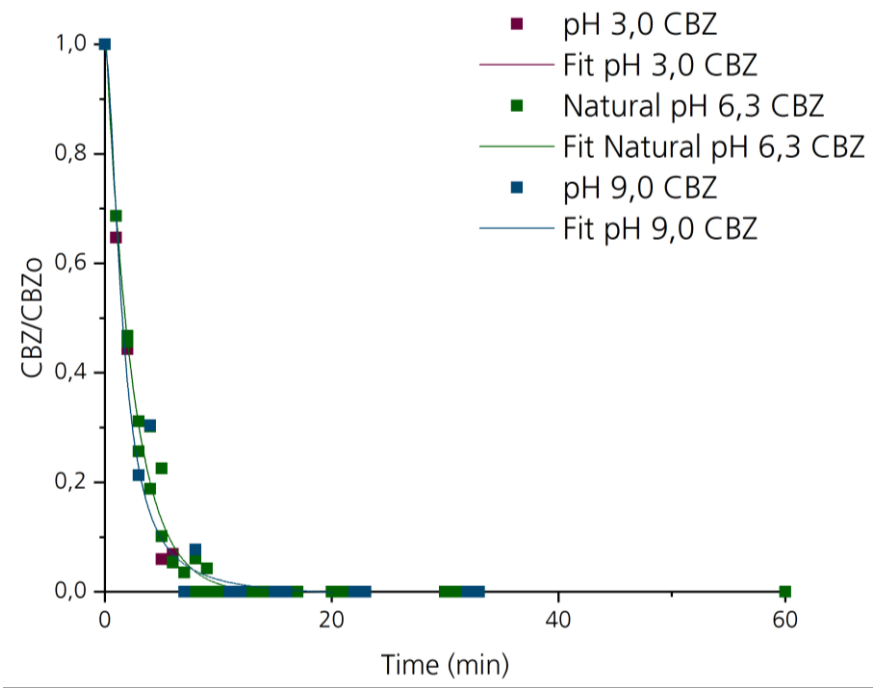

Figure 7.13 Evolution of normalized concentration CBZ in time at different pHs

Total organic carbon was measured every 30 minutes along the experiments. Total organic carbon reduction after 120 minutes of experimentation for each group of experiments was analyzed, results of the delta TOC under different pH conditions is shown in Figure 7.14. The average initial TOC was 15,22±0,60 mg/L.

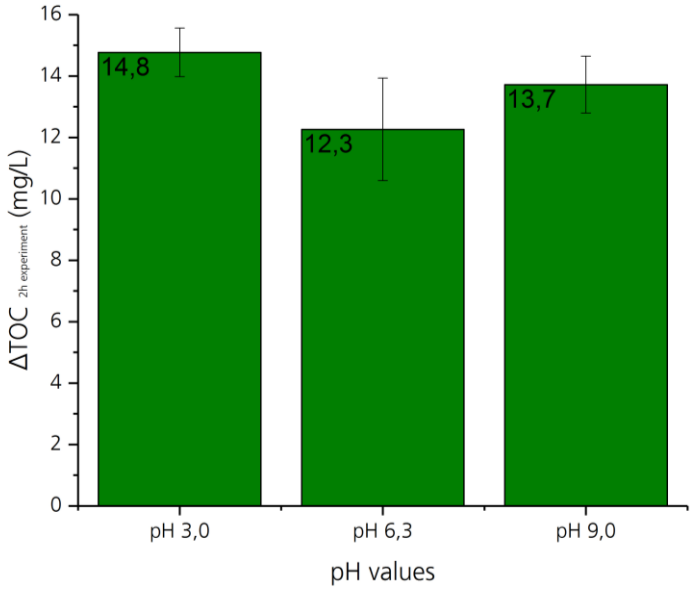

Figure 7.14 Delta TOC in mg/L for experiments at different pH

The changes represent a difference of 2,5 mg/L comparing the natural pH to acidic conditions and 1,4 mg/L comparing to basic conditions. The reduction on TOC values represent a degradation of 95, 80 and 90% of the total TOC for experiments under acidic, natural and basic pH conditions during the 120 minutes of radiation.

The degradation of Carbamazepine by photo-induced advanced oxidation does not have a visible effect by changes in the pH, however if the complete mineralization is the focus, an initial acidification or basification of the systems may increase between 10 to 15% the efficiency of the mineralization in the range of concentration used for experiments.

7.4.4. Bisphenol A degradation

Bisphenol A solutions of 30 mg/L concentration were tested, despite being much higher than that found in wastewaters and groundwater (between 0,018 to 3,44 µg/L) [6, 108, 118-120]. These high concentrations allow following the evolution of the contaminant and take into account the detection limit of the available measurement equipment. Operational parameters were restrained to the region 1250 µm using maximum flow 250L/h, experiment were performed at different pH to investigate the effects on oxidation, results are show in Figure 7.15. The experiments were performed by duplicate for each pH conditions.

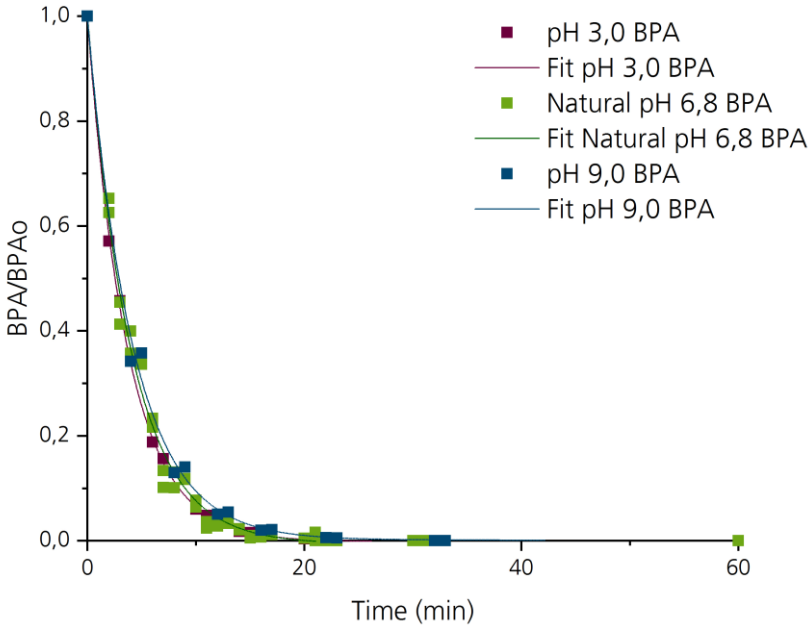

Figure 7.15 Evolution of normalized concentration BPA in time at different pHs

As it is appreciated in the Figure 7.15 during experiments at natural pH, basic solutions at pH 9 and acid solutions at pH 3 the degradation of Bisphenol A by means of photo-induced advanced oxidation is not affected. Reduction of BPA one order of magnitude takes in all cases less than 12 minutes. BPA degradation by photo-induced advanced oxidation presents a pseudo first order degradation rate, the reaction constant k for the unaffected by pH experiments is k=-0,25±0,01 min^{-1}.

Total organic carbon was measured every 30 minutes along the experiments. Total organic carbon reduction after 120 minutes of experimentation for each group of experiments was analyzed, results of the delta TOC under different pH conditions is shown in Figure 7.16. The average initial TOC using BPA solution was 23,70±0,50 mg/L. Differently from the evolution of the concentration of BPA, TOC evolution is slightly affected by changes of pH conditions.

The changes on pH have an influence in the TOC reduction and represent only a slight negative difference of 1,2 mg/L comparing the natural pH to acidic conditions and 1,5 mg/L comparing to basic conditions. The reduction on TOC values represent a degradation of 75, 80 and 73% of the total TOC for experiments under acidic, natural and basic pH conditions during the 120 minutes of radiation.

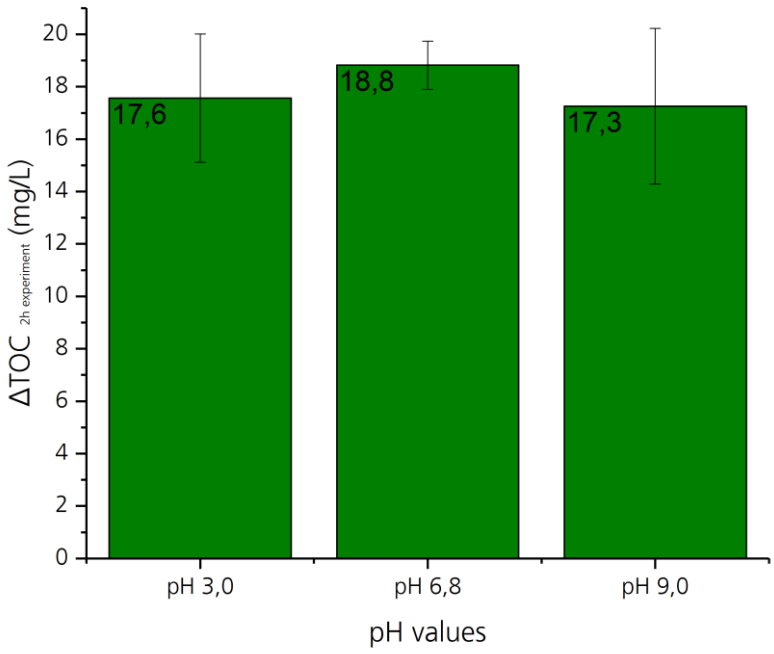

Figure 7.16 Delta TOC in mg/L for experiments at different pH

The degradation of Bisphenol A by photo-induced advanced oxidation does not have a visible effect by changes in the pH, however if the complete mineralization is the focus, an initial change of pH in the systems may decrease in 6-8% the efficiency of the mineralization in the range of concentration used for experiments. This decrease is negligible.

7.4.5. Caffeine degradation

Caffeine solutions of 30 mg/L concentration were tested, despite being much higher than that found in wastewaters and groundwater (between 0,016 to 102 µg/L) [6, 9, 108, 121]. These high concentrations allow following the evolution of the contaminant and take into account the detection limit of the available measurement equipment. Operational parameters were restrained to the region 1250 µm using maximum Flow 250L/h, experiment were performed at different pH to investigate the effects on oxidation, results are show in Figure 7.17. The experiments were performed by duplicate for each pH conditions.

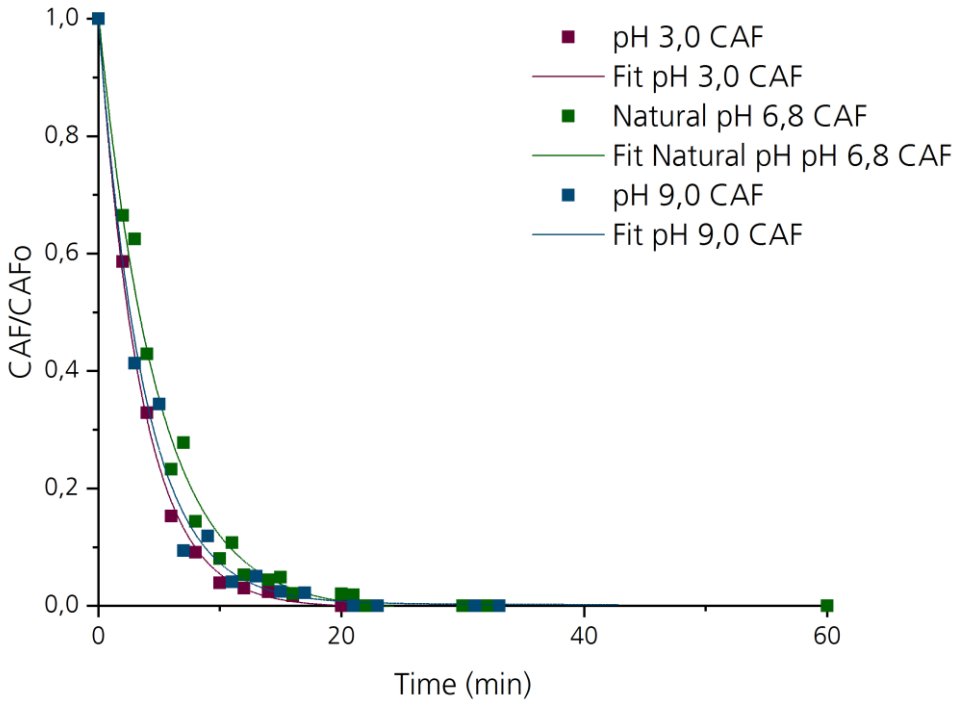

Figure 7.17 Evolution of normalized concentration CAF in time at different pH

As it is appreciated in the Figure 7.17 during experiments at natural pH, basic solutions at pH 9 and acid solutions at pH 3 the degradation of Caffeine by means of photo-induced advanced oxidation is apparently not affected. Reduction of CAF one order of magnitude takes place in all cases in less than

18 minutes. CAF degradation by photo-induced advanced oxidation presents a pseudo first order degradation rate, the reaction constant k for the unaffected by pH experiments is $k=-0,23\pm0,01 min^{-1}$.

The average initial TOC for experiments using CAF was 16,57±0,40 mg/L. Total organic carbon reduction after 120 minutes of experimentation for each group of experiments was analyzed, results of the delta TOC under different pH conditions is shown in Figure 7.18.

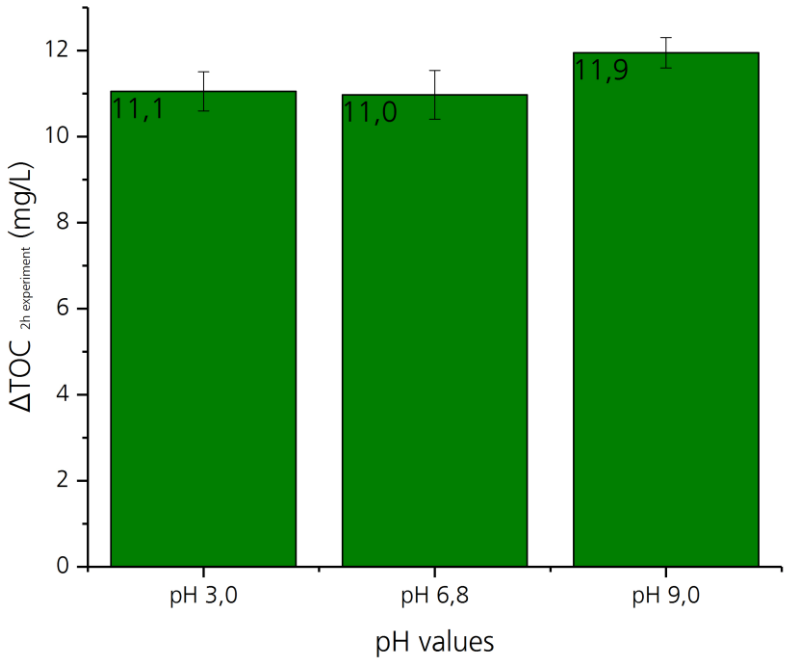

Figure 7.18 Delta TOC in mg/L for experiments at different pH

As presented for the evolution of the concentration of CAF, TOC evolution is not affected by changes of pH conditions. The reduction on TOC values represent a degradation of 75, 75 and 80% of the total TOC for experiments under acidic, natural and basic pH conditions during the 120 minutes of radiation.

7.4.6. Comparison of experiments single substances

The results of degradation by means of photo induced oxidation showed a complete reduction of the substances selected. 100% elimination of the target component was achieved before 20 minutes of experiment. Carbamazepine shows the fastest degradation followed by Sulfaquinoxaline, Bisphenol A and Caffeine. The experimental results for neutral pH were adjusted to a pseudo first order kinetic

with pseudo first order constant of -0,41±0,03, -0,38±0,03, -0,25±0,01 and -0,23±0,01 min^{-1} respectively. The Figure 7.19 shows the evolution of normalized concentration of SQX, CBZ, BPA and CAF calculated by using the pseudo first order kinetic constants found from the experimentation.

The oxidation profile of the different substances show two different degradation velocities, SQX and CBZ show a faster degradation than BPA an CAF, this behavior may be attributed to the differences in molecular structure, since SQX and CBZ have a slyly higher hydrogen density in the structure than BPA and CAF.

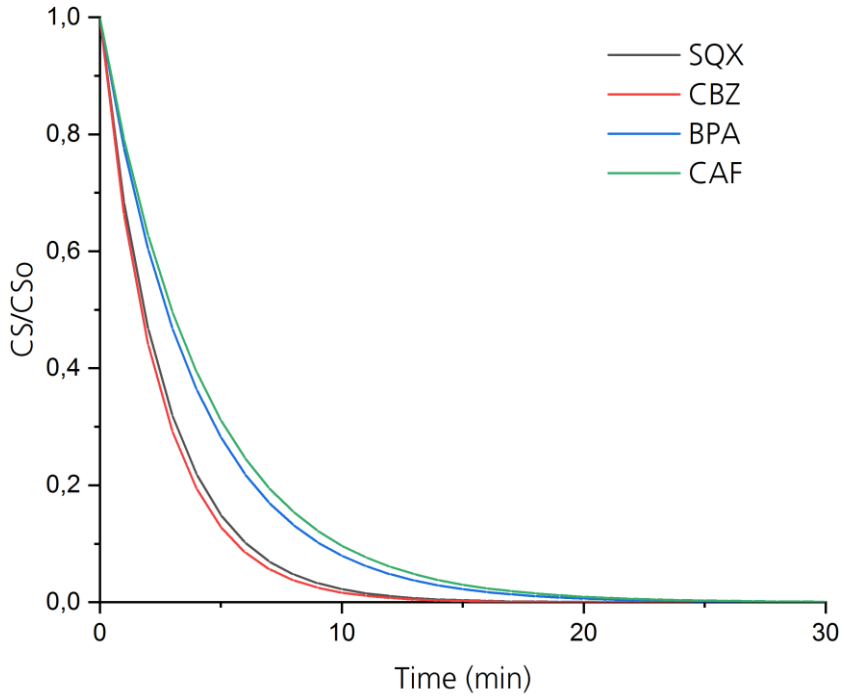

Figure 7.19 Evolution of normalized concentration of the substances using the pseudo first order constant from the experimental oxidation results

Therefore there is a higher probability of hydrogen abstraction reaction with hydroxyl radicals with SQX and CBZ than with BPA and CAF. Other structural difference which could play a role in the difference of oxidation velocity is the that, SQX and CBZ, they both contain in the structure primary amino groups which are more susceptible to hydrogen abstraction reaction caused by the attach of hydroxyl radicals than other functional groups, therefore the SQX and CBZ molecules may break easily on these point. They are highly susceptible to hydroxyl radical attack. On the other hand CAF containing more stable tertiary amino groups resists longer the attack of hydroxyl radicals. In the case of

BPA, which does not contain amino groups, the slower oxidation velocity may be attributed mainly to the lower hydrogen density in the molecule.

7.4.7. UV Dose required for degradation of the model substances

In order to compare UV related technologies the concept of UV dose can be used. The UV dose concept is useful to directly relate the energy consumption of an oxidation process using UV radiation for the oxidation. The Figure 7.20 shows the UV Dose necessary to oxidize the studied substances by means of photo induced oxidation.

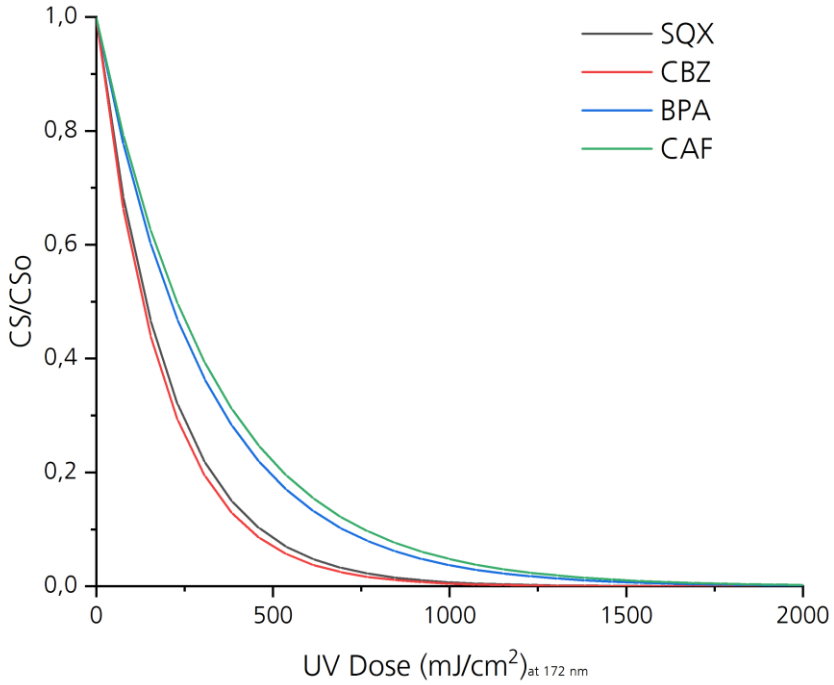

Figure 7.20 UV dose necessary to eliminate SQX, CBZ, BPA and CAF calculated from experiments

In order to reduce the concentration of SQX and CBZ one order of magnitude (initial concentration of Substances SQX 30 mg/L and CBZ 20 mg/L), it is needed in the photo-induced oxidation system use in this thesis a dose minimum of 500 mJ/cm^2. In the case of BPA and CAF (initial concentration of substances BPA and CAF 30 mg/L), it is needed a dose minimum of 750 mJ/cm^2. A study reports the minimum dose to reduce the concentration of similar molecules Sulfamethoxazole, Sulfamethazine, Sulfadiazine, Trimethoprim and Bisphenol A one order of magnitude using UV and hydrogen peroxide

as an oxidation process. Initial concentration of 1µM (0,90 to 1,12 mg/L) of the substances and addition of hydrogen peroxide were reported for the experiments. The required UV dose for the oxidation of sulfamethoxazole (one order of magnitude reduction) was 860 mJ/cm^2 and for the other components including Bisphenol A UV doses higher than 900 mJ/cm^2 were required [152]. A recent study reports the minimum dose to reduce the concentration of similar molecules Sulfamethoxazole, Diclofenac, Iopromide, Ventafaxine, Metoprolol and Carbamazepine one order of magnitude using UV and hydrogen peroxide as an oxidation process.

Initial concentrations of 1,5 µg/L, 3,6 µg/L, 2,8 µg/L, 1,2 µg/L, 1,7 µg/L and 0,9 µg/L respectively and 0,6 mM addition of hydrogen peroxide were reported for the experiments. The required UV dose for the oxidation of Sulfamethoxazole, Diclofenac, Iopromide and Ventafaxine (one order of magnitude reduction) was 1200 mJ/cm^2 and for Metoprolol and Carbamazepine less than 40 % reduction was achieved [153].

Comparing the reported results of other UV driven AOPs with the result of this thesis, a lower UV dose and no use of additives for the oxidation of the studied substances in a higher range of concentrations can be recognized. Even though a direct comparison cannot be performed, there is still high potential for the use and further development of this technology.

The production of a database containing data of UV dose requirements for different initial concentrations and degrees of oxidation may support the further design and scale up of oxidation processes using the VUV photo-induced oxidation technology.

7.4.8. Energy consumption required for the degradation of the model substances

Using the theoretical 60% efficiency of Xenon excimer lamps producing radiation at 172 nm and assuming all the radiation is being use for the oxidation process, the theoretical energy consumption for VUV generation can be calculated; the Figure 7.21 shows the results of the calculation.

The low theoretical energy consumption for the reduction in concentration of the studied substances reflects the high potential of this technology.

However further developments, scale up and onsite validation is necessary to have an effective comparison of the energy consumption with other AOP technologies.

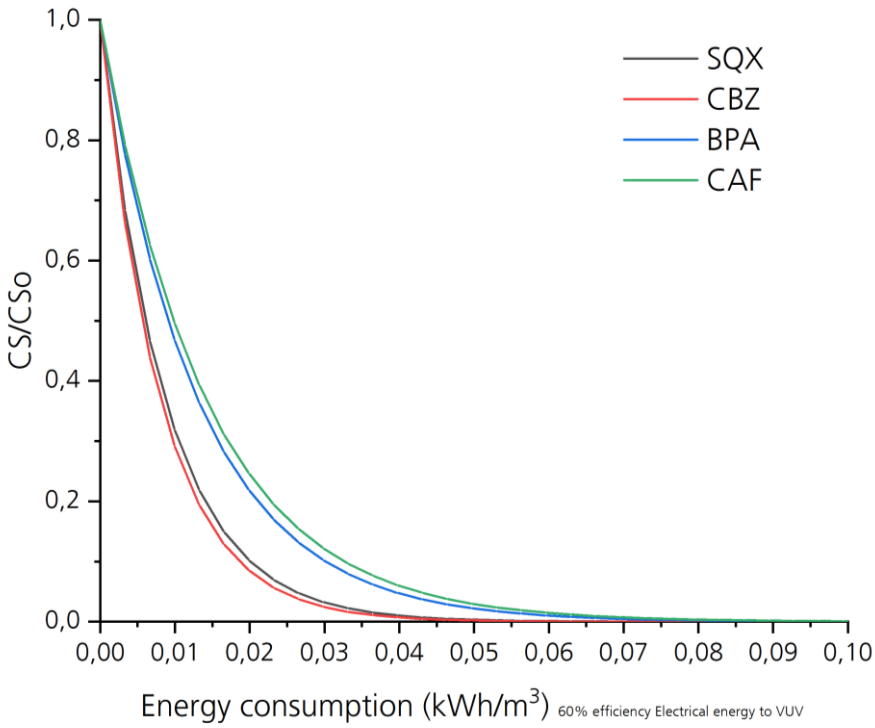

Figure 7.21 Energy consumption of a system with 60% efficiency electrical energy to UV necessary to eliminate SQX, CBZ, BPA and CAF calculated from experiments

7.4.9. Toxicity evolution during experiments

Once the elimination of the target components and the mineralization process were analyzed, Toxicity studies were performed during all reaction span. Toxicity refers to the degree to which a substance or particular mixture of substances can damage an organism such as an animal, bacterium or plant, as well as the effects on a substructure of the organism such a cell (cytotoxicity) or an organism (hepatotoxicity). An important idea behind toxicity is that effects are dose dependent. Toxicity is measured by its effects on a target organism, tissue or cell. Because individuals typically have different levels of response to the same dose of a toxic substance, a population level measure of toxicity is related to the probability of an outcome for a given number of individuals in a population.

For many aromatic compounds, the initial oxidation steps usually lead to the formation of aldehydes as intermediates with higher cyto-toxicity. For example oxidation of 1,4-dioxane by UV/AOPs is reported to generate glycolaldehyde and formaldehyde as intermediates which induce toxicological responses 100 times higher than 1,4-dioxane itself [154]. Glycolaldehyde was reported to be highly cytotoxic to HK-2 cells and caused depletion of adenosine triphosphate (ATP), release of lactate de-

hydrogenase (LDH), and degradation of enzymes as well as selected phospholipids [155]. Glycolaldehyde was reported to also induced growth inhibition and oxidative stress in human breast cancer cells [156]. Increase in toxicity due to generation of aldehydes as intermediates byproducts is a big concern in the field of advanced oxidation processes. The toxicity of the initial substances and the oxidation by products was followed. The Figure 7.22 show the mortality of the COS cell as function of time for each substance for different experiments at natural, acid or basic pH.

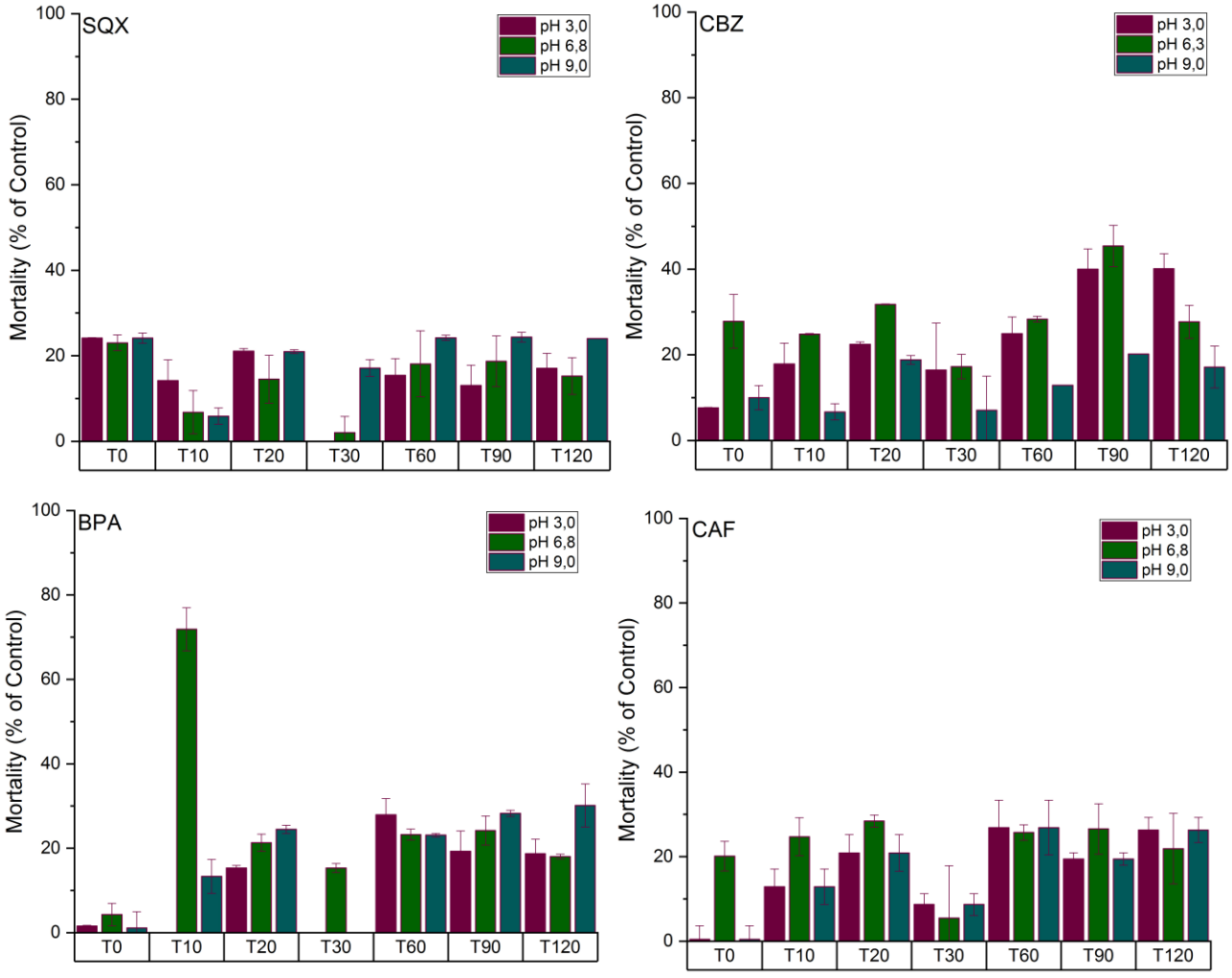

Figure 7.22 Evolution mortality of COS cells in time for different experiments at different pH

The toxicity was then followed using a two cell lines (VERO and COS cells) to determine the toxicity of the studied substances as well as their oxidation byproducts. The VERO and COS cells are cell lines derived from African green monkey kidney epithelial cell but their morphology is different [113]. The

morphology of VERO cells corresponds to epithelial-like cells while the morphology of COS cells corresponds to fibroblast-like cells (ATCC®, Manassas, VA, USA).

Increase in mortality is present just in the case of BPA experiments in natural pH during the first minutes, byproducts present in this stage of the oxidation are therefore more toxic for the COS cells, however after 20 minutes when the BPA is not anymore traceable the mortality decreased what it is then translated in a decrease in toxicity of byproducts.

No increase of toxicity was found with this method for the oxidation of SQX and CAF using photo-induced oxidation. There is a small increase of mortality of COS cells for CBZ experiments at low and neutral pH at 90 minutes of irradiation, and it decrease at the end of the experiments.

The toxicity was follow with a second line cell the VERO. The Figure 7.23 show the mortality of the VERO cell as function of time for each substance for different experiments at natural, acid or basic pH.

There is no significant change in the mortality of VERO cells with any of the substances; there is no evolution of toxicity higher than the initial toxicity of the substance by byproducts of the oxidation process using VERO cells.

Not only degradation of the trace substances was reached, also mineralization was evident. Toxicity measurements show no increase along the process for SQX, CBZ and CAF. A slightly reduction pattern can be seen in the toxicity for SQX. Worth to mention BPA toxicity decreases during oxidation under natural pH of the substance, however experiments at low and high pH show a slightly increase on toxicity.

All the cytotoxicity assays using both VERO and COS cells confirm the safe application of this treatment for the removal of SQX, CBZ, BPA and CAF. For both cell types, Figure 7.22 and Figure 7.23, show a percentage of mortality in the same order of magnitude than the original substance.

Moreover, cytotoxicity assays revealed the feasibility of the VUV photo-induced treatment for the removal of the substances in the study as well as the possibility to stop this process at any convenient time.

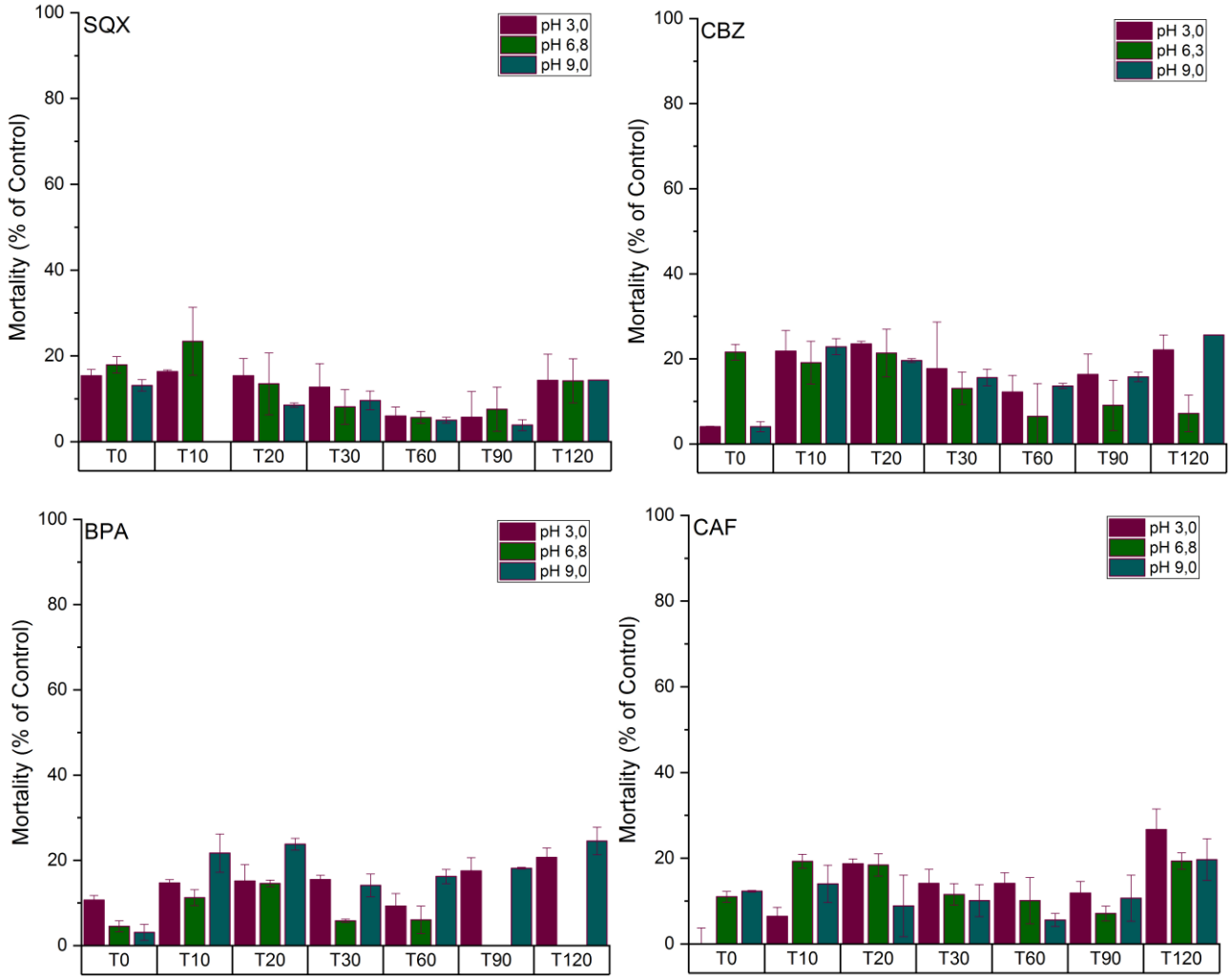

Figure 7.23 Evolution mortality of VERO cells in time for different experiments at different pH

7.4.10. Degradation of a mixed solution containing SQX, CBZ, BPA and CAF

In order to investigate interferences in the degradation process of each component in presence of other organic material, the degradation of a mixture solution was studied. Four experiments of degradation by means of photo-induced oxidation were performed, one experiment in each reactor in parallel. Operational parameters were restrained to the region 1250 µm using maximum Flow 250L/h. A solution containing SQX, CBZ, BPA and CAF at concentrations of 30, 20, 30 and 30 mg/L of the respective components was used. The concentration of individual substance and TOC were followed during the experiment. Concentration reduction along time is presented in the Figure 7.24.

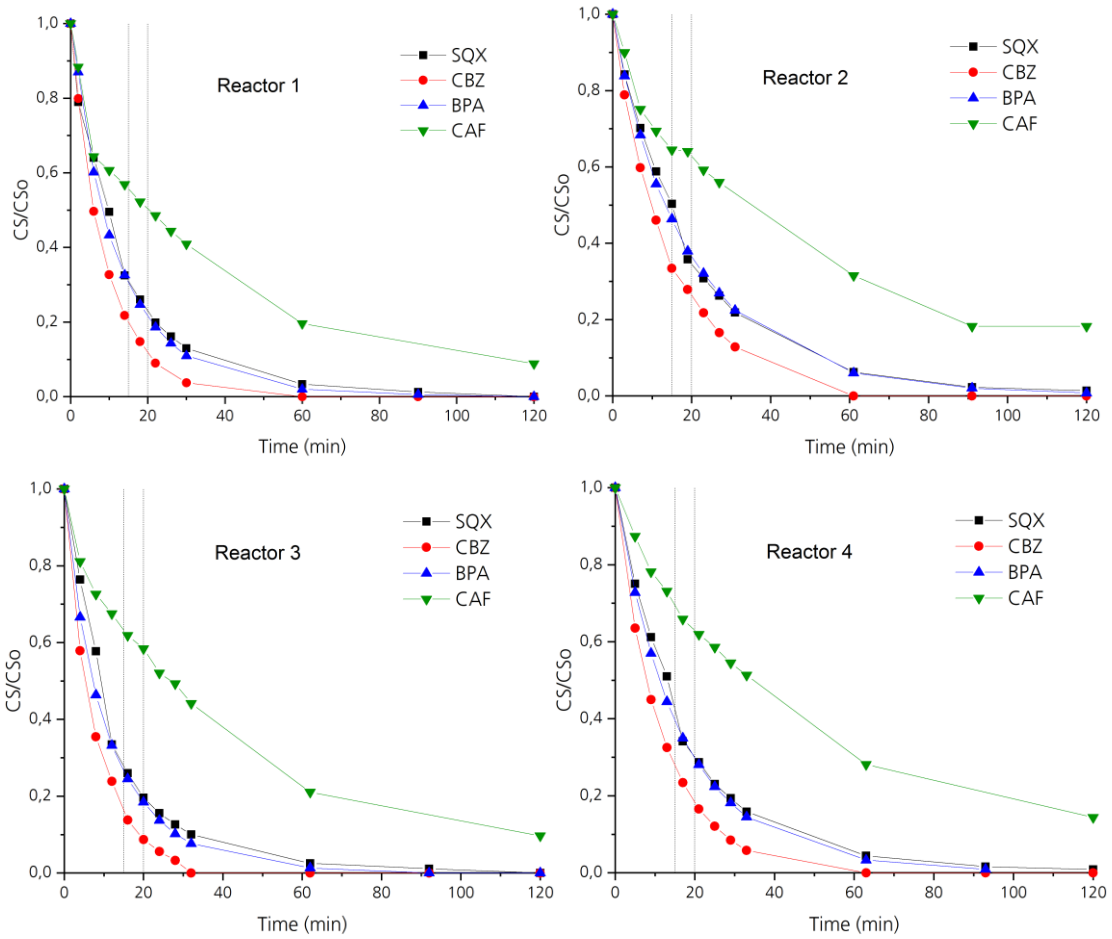

Figure 7.24 Evolution of normalized concentration of SQX, CBZ, BPA and CAF in time for each reactor

The water matrix components, in this case the chemical substances in the mixture, all react with hydroxyl radicals, lowering the efficiency of the process when focusing the efficiency in one specific substrate. The vertical lines in the figures at time 15 and 20 are the times at the substances SQX,CBZ and BPA, CAF are not anymore detected for individual experiments.

In experiments using a mixture of components the separately trend of individual experiments is well observable. Carbamazepine shows the fastest degradation followed by Sulfaquinoxaline and Bisphenol A, these two substances degrade almost at the same rate, and caffeine degradation is significantly slower than the other substances with pseudo first constant of -0,10±0,01, -0,07±0,01, -0,07±0,01 and -0,03±0,01 min^{-1} respectively. The pseudo first constants are lower in the mixture experiments in comparison to individual experiments in 75, 81, 72 and 86% respectively.

For SQX, CBZ and BPA destruction of the pollutants was achieved, complete CAF degradation was not reached the molecule seems to be more stable to oxidation as the pharmaceuticals SQX and CBZ

or the hormone like chemical BPA when they are combined and higher load of organic material is present in the solution.

The oxidation profile of the different substances show two different degradation velocities, SQX, BPA and CBZ show a faster degradation than CAF, this behavior may be attributed to the differences in molecular structure and to the interaction of the oxidation byproducts and the targeted substances. At this stage is difficult to conclude which interaction is affecting the velocity of degradation.

One structural difference which could still play a role in the difference of oxidation velocity is the that, SQX and CBZ, they both contain in the structure primary amino groups which are more susceptible to hydrogen abstraction reaction caused by the attach of hydroxyl radicals than other functional groups, therefore the SQX and CBZ molecules may break easily on these point. They are highly susceptible to hydroxyl radical attack.

The evolution of TOC during the experiments was recorded; the Figure 7.25 shows the results for the experiments. Total delta TOC for the oxidation of mixed solution containing SQX, CBZ, BPA and CAF is higher than those deltas of TOC in experiments with individual substance, results are presented in Figure 7.26.

The photo-induced AOP shows the mineralization power for single substances as well as for mixtures of substances where the organic load is higher and complex. The higher TOC reduction in the experiments with the mixture can be attributed to the complete use of the hydroxyl radicals oxidizing substrate and due to higher availability of substrate in the photoreaction zone.

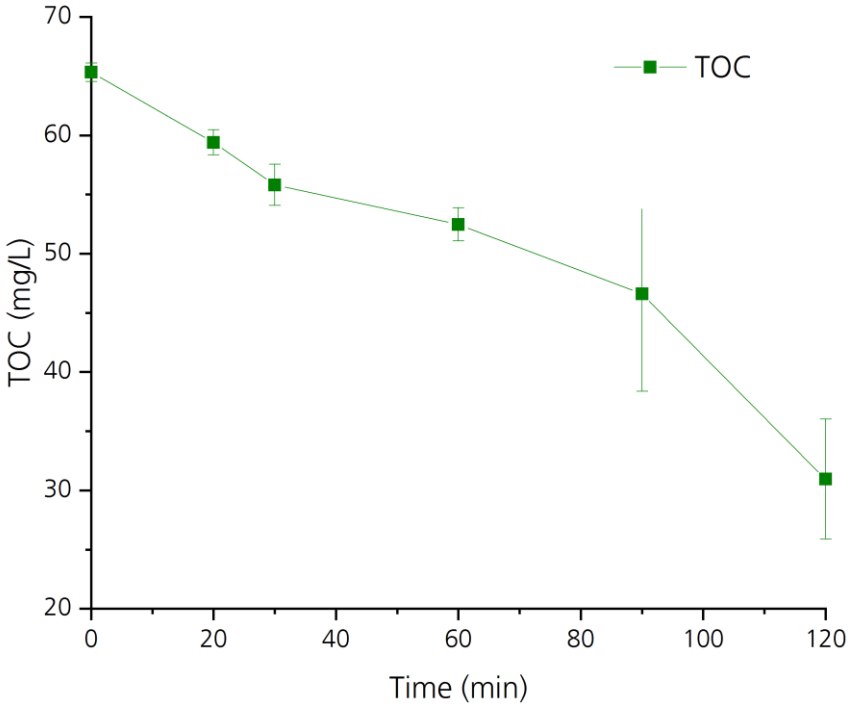

Figure 7.25 Evolution of TOC concentration in time oxidation of mixed solution containing SQX, CBZ, BPA and CAF

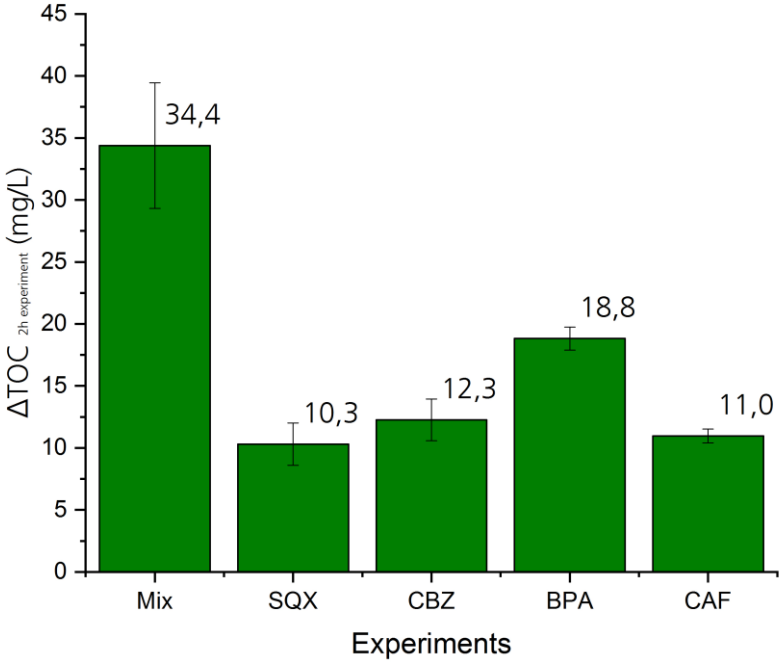

Figure 7.26 Delta TOC in mg/L comparison mixed solution experiment and individual substance experiments

7.4.10.1. UV dose calculation and energy consumption oxidation mixed solution containing SQX, CBZ, BPA and CAF

The UV Dose and the energy consumption by means of UV production were calculated for experiments using the mixture solution. The pseudo first order constant found for the degradation of the substances was use for the calculation. The Figure 7.27 shows the UV Dose necessary to destroy the studied substances by means of photo induced oxidation when mixed.

In order to reduce the concentration of the substances one order of magnitude from the initial concentration, (initial concentration of Substances SQX, BPA and CAF 30 mg/L and CBZ 20 mg/L), it is needed in the photo-induced oxidation a dose minimum of 2000 mJ/cm^2 for CBZ, a dose of 3000 mJ/cm^2 for SQX and BPA. A higher dose is required to oxidize CAF, minimum 6000 mJ/cm^2 are required with this substance is present in mixture solution.

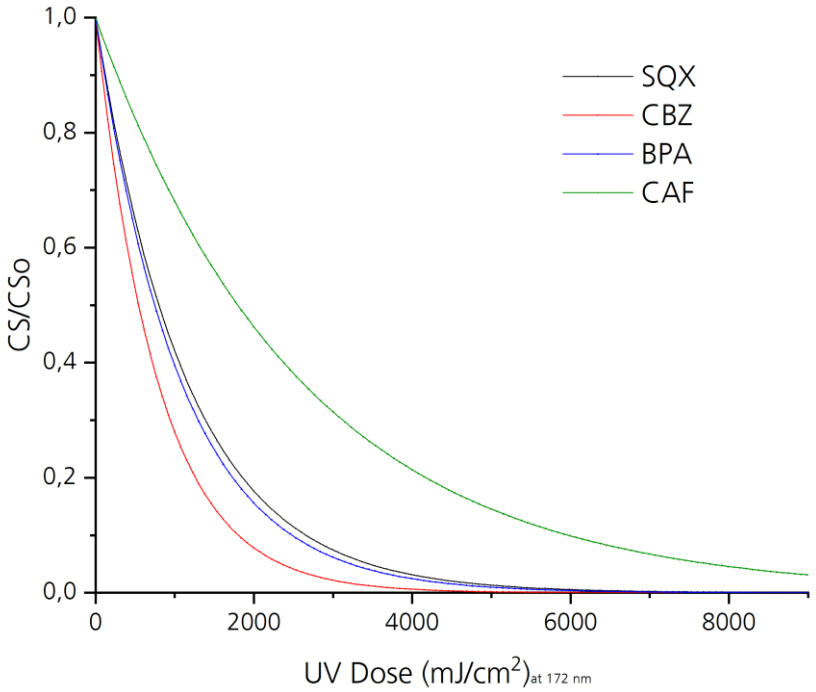

Figure 7.27 UV dose necessary to eliminate SQX, CBZ, BPA and CAF calculated from experiments using a mixture solution

Additionally, using the theoretical 60% efficiency of Xenon excimer lamps producing radiation at 172 nm and assuming all the radiation is being use for the oxidation process, the theoretical energy consumption for VUV generation can be calculated; the Figure 7.28 shows the results of the calculation.

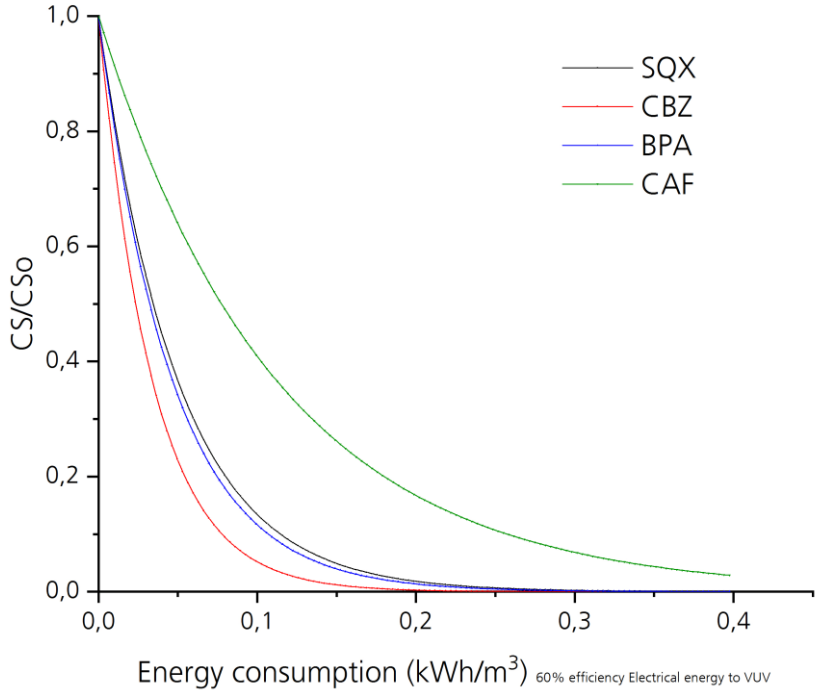

Figure 7.28 Energy consumption of a system with 60% efficiency electrical energy to UV necessary to eliminate SQX, CBZ, BPA and CAF calculated from experiments using a mixture solution

UV dose and energy consumption to provide this dose are important parameters to assess and compare the possible use of this technology for the abatements of recalcitrant components. Further development of lamp-reactor systems, which allow complete use of the UV generated and electrically efficient (reach the theoretical 60% of efficiency electrical energy to UV) are needed, before this technology can reach the market.

In any case is important to mention the photo-induced oxidation using Xenon excimer Lamps present a robust and reliable performance in terms of oxidation of hard degradable substances. Important to mention is the fact that oxidation and mineralization of solutions containing so different substances under VUV photo-induced advanced oxidation using excimer lamps shows a lower selectivity for oxidation and mineralization than other AOPs.

7.5. Conclusions

A Flat lamp-reactor system concept with 4 UV reactors was conceived, built and tested. Lamp design, electronics definition and characterization of operational parameters for the better ignition of the plasma and maximum output of radiation were tested. 2 patents were proposed and accepted describing the oxidation process using the system.

The VUV photo-induced oxidation resulted to be a very promising treatment. It allows the efficient removal of the five model compound MB, SQX, CBZ, BPA and CAF (which were no longer detected after 20.0 min of experiment for individual experiments) and it could allow the total organic matter mineralization by increasing the reaction time span to 120 min. Moreover, cytotoxicity assays revealed the feasibility of the VUV photo-induced treatment for removal of the four model compound SQX, CBZ, BPA and CAF as well as the possibility to stop this process at any convenient time due not evident increase of toxicity.

The holdup of the photo-induced oxidation is the kinetics of the process, which is expected due to the reactor size, illuminated volume (VIRR = 1.1 x 10^{-3} L) employed. Scale up of the system using larger irradiation areas would translate directly to a proportional increase of the process kinetics.

The VUV photo-induced Advance Oxidation process using Xenon Excimer Lamps show advantages in comparison with other oxidation technologies. Some of these advantages are:

- the steady and local production of strong oxidizer hydroxyl radical by water photolysis without the addition of supplementary oxidation agents or additives,
- not strong selectivity of the process.
- the efficient oxidation and mineralization of the substances (hazardous organic water pollutants) using VUV light
- the byproducts along the experiment were not source of increase in toxicity for COS and VERO cells
- the values of Dose for oxidation purposes of specific substances and mineralization will in future lead to a better design and scale up of the technology for specific and continues processes
- the calculated energy consumption of 0,1 kWh/m^3 to eliminate trace substances which initial concentration is by far larger than those found in water bodies is one of the attractiveness of this technology for future developments.

8. Overall results and discussion

In this chapter the main results of this thesis are presented and discussed. Additionally the basis for the conclusions and the recommendations for future works are described.

As discussed along the thesis, VUV photo induced Advanced Oxidation Process and its autonomy in the production of hydroxyl radicals for the oxidation process without additives presents a huge potential to be a solution for the oxidation of hardly degradable persistent pollutants in water. However, due to the special singularities of the process, it was identified that photo-reactors in the photo-induced AOP, by today, work below energy-efficient operations due to a non-ideal use of the VUV radiation. The strong absorption of radiation by water, which translates into a short photon penetration into the media and a small photo reaction zone, makes the quantification of fundamental parameters such as photo-chemical rate constants (quantum yield of generation of hydroxyl radicals), to become a challenging task. For example a lack of mixing generates substrate depletion zones where hydroxyl radicals are generated but cannot be efficiently used for oxidation therefore not quantified. These constrains lead to important challenges in the construction of efficient photo reactors.

In order to address this challenge, activities were concentrated in three clusters (Figure 8.1): the radiation interactions, the reactor design and the oxidation process. The three clusters interact between each other and every advance in one of them affects the advances of the others. The radiation interaction cluster focuses on the absorption process, the radical generation, the photo reaction zone definition and radiation detection and Intensity of radiation. The cluster reactor design focuses on the material for maximum transmission, lamp flow-chamber coupling, the effects of flow-chamber dimensions, hydrodynamics, boundary layers and mixing enhancement strategies. The cluster oxidation process focuses on the radical generation and its quantification by oxidation of methanol, validating hydrodynamic strategies and effects of flow-chamber dimensions on the efficient oxidation of Methylene Blue. Additionally the validation of the oxidation and mineralization of selected relevant pollutants and effects of toxicity along the treatment, as well as the calculation of the effective energy consumption for the oxidation of the pollutants are part of this cluster. The Figure 8.1 shows the continuous interaction loop of the three clusters for the definition of an efficient VUV photo-induced AOP.

Figure 8.1 Continuous interaction loop for the definition of an efficient UV photo-induced AOP

A number of iterations following the interaction of the above mentioned clusters were performed during this thesis. Initially the state of the science and technology was assessed through literature search and its analysis. An initial definition and parametrization of simplified numeric models gave the first overview of the interactions of the three clusters and helped to identify the points where this study subsequent deepened. A first version of a micro-channel reactor chamber was designed and built. It was afterwards coupled with a commercial excimer lamp system for the introductory process characterization.

During the first try of process characterization (chapter 3) a second iteration between clusters specially oxidation process and reactor design was analyzed; it was experimentally demonstrated that the channel thickness and the flow velocity play an important role in the overall efficiency of the oxidation process and it was observed that, at every channel thickness and low flow rate, a very slow oxidation takes place. With increases of the flow rate the oxidation velocity increases as well until a maximum, where, independently of the flow rate, the velocity of oxidation remains constant. However when channel thicknesses above 500 µm were used in the photo-reactor the oxidation efficiency reached a pseudo maximum value lower than that reached when channel thicknesses below 500 µm were used. In other words, for channel thicknesses larger than 500 µm a diffusion limited scenario for the oxidation process was present, where no all hydroxyl radicals are used for oxidation. This phenomena was evident in all channel thicknesses above 500 µm. In the contrary for channel thicknesses below 500 µm a higher value of efficiency was observed. In this case the flow conditions in the small channel were having a higher effect on the oxidation process and the system operates under reaction controlled scenario instead of diffusion limited. Calculation of the theoretical boundary layer formation in flat channels under different Reynolds number and at different distances from the inlet shows that after a few centimeter from the inlet the boundary layer has a high probability to be larger than the photo reaction zone (calculation for a smooth flat plate). This phenomena is present even in Reynolds number deeply in the turbulent regime. Photo reactors, having large channel thicknesses above 500 µm, will present boundary layers (where laminar flow and diffusion controlled transport of substances takes place) larger than the photo reaction zone (where the hydroxyl radicals are formed), therefore the oxidation process will occur under diffusion controlled regime. In order to increase the efficiency of the oxidation process, secondary flows have to be considered in the photo reactor system. Strong secondary flows will perturb the stability of the boundary layer. In steady state flow, boundary layers are stable. They just become unstable when the local Reynolds number within the boundary layer exceeds a value of 600. Therefore laminar flow will occur everywhere in the boundary layer on a flat plate when the overall Reynolds is less than $1{,}2 \times 10^5$ [83]. Laminar flow within the boundary layer - when this one is larger than the Photo-reaction zone in the photo induced AOP - leads to diffusion controlled scenarios were the generated hydroxyl radicals are not used efficiently. Avoiding laminar flow within the boundary layer is achieved only by controlling the dimensions of the channel thickness to be smaller than 500 µm in the case of the Photo-induced AOP or by the introduction of secondary flows to perturbing the laminar flow within the layer.

Two different methods for the introduction of secondary flows were investigated, the herringbone grooves structures in one of the surfaces of the reaction chamber and the net-like turbulence promoters inside of the chamber.

The introduction of alternating packages of herringbone grooves in micro-channels where laminar flow regime is taking place and viscous forces dominate, generates transverse flows in the channel, resulting in two counter rotating vortices along the channel length. The alternation of the packages of grooves disturbs the relative untouched elliptic points in each of the vortices, this reorientation of the circulating flow produces chaotic mixing [80].

Experimentally, the herringbone grooves showed an increase of the efficiency of oxidation just for channel thicknesses smaller than 500 µm and experiments where the flow was low from 100 to 1000 mL/min. These results are promising for solving the problem of large scale setup build for high throughput where pressure drop inside the systems should be kept at the minimum.

The second method investigated was the netlike turbulence promoter. A woven net placed in the flow channel induces secondary flows promoting the exchange of substrate between the bulk flow and the photo reaction zone. Experimentally, the introduction of netlike turbulence promoter had an effect in the efficiency of the oxidation just for channel thicknesses larger than 500 µm and experiments where the flow was larger than 1000 mL/min. These results are promising for solving the problem of cost-efficient manufacture of setups where channel thickness cannot be accurate maintain in the micrometer range due to limitations by materials and tooling processes. However, the solution of inducing secondary flows by means of netlike turbulence promoters does have as well its limited reach, channels larger than 1500 µm with netlike turbulence promoters won't have an effect on the mixing of the bulk flow with the photoreaction zone.

Subsequently and once the first try of process characterization was performed having as a results a better understanding of the channel thickness interaction with the photo reaction zone and the operational parameters, the radiation intensity of the system was investigated as part of the cluster radiation interaction. Two different approaches for the radiation intensity measurements were taken: the relative method of *chemical actinometry* and the absolute method of *photometry*. (Chapter 4)

Chemical actinometry was used, applying the photochemical isomerization of cis-, trans-cyclooctene. This method was first proposed for 185 nm by Srinivana [85]. It was generally used to determine the photon flow and radiation intensity below 200 nm for low pressure mercury lamps with a peak of

radiation at 185 nm. This technique was afterwards adapted to measure the radiation of Xe excimer Lamps by Jakob in 1992 during his PhD thesis [18].

Quantum yields of cis-, trans- cyclooctene isomerization are not exactly known at 172 nm. The authors of the method for the chemical actinometry assumed the quantum yield of isomerization being similar to those first measured at 185 nm.

The values of irradiance measured in this thesis using the methodology of Jakob gave as a result an irradiance of 5,41 mW/cm^2 for the photo-reactor system.

However, it is worth to mention that, taking into account the mass balance equations which describes the kinetic of the system cis-, trans- cyclooctene, the quantum yield is inversely proportional to the spectral radiant power. Therefore, the use of a higher quantum yield (which would be expected at 172 nm when compared with 185nm) would lead to a lower calculated radiant power.

Due to the inconsistences identified in the chemical actinometry, photometry was investigated as method to measure radiation intensity. Initially a Si-photodiode - the S8551 from the company Hammamatzu - was used to detect and quantify the radiation intensity. Unfortunately, the response of the Si-photodiode is not only observable in the VUV range; it is also present in the UV, VIS and infrared range of the spectrum with a higher responsivity in the last ranges of the spectrum. Responses of the sensor contain not only the absorbed VUV radiations but also the response to other ranges of the spectrum. The emission peaks of the Xenon excimer lamp in the VUV and UV range is well defined. However, the complete setup used for the photo induced AOP has an additional 10 mm quartz plate window. Due to luminescence phenomena of the quartz window in the blue violet (365 nm), violet (420 nm) and red (645 nm), the Si-photodiode detection - which is active as well to those wavelengths - was interfered. A Si-photodiode is actively responsive to a broad range of wavelengths and extremely fragile to radiation in the VUV. Strong degradation of the Si-photodiode was encounter and replicability of measurements could not be ensured. The values of irradiance measured in this thesis using the photometry method with the Si photodiode was 3,52 mW/cm^2 for the photo-reactor system.

A second detector - the AlGaN L2416-B1-G04, developed by Fraunhofer IAF and IPM in Freiburg Germany - was used. The AlGaN detector has a special feature. It is blind for radiation above 360 nm. Its responsivity in the range of UV and luminescence of quartz is neglectable. The sensor was calibrated for radiation below 200 nm. The sensor does not show degradation in the time window of experiments and reproducibility of measurements could be achieved. The values of irradiance measured in this thesis using this method was 1,43 mW/cm^2 for the photo-reactor system. Using this

method, it can be ensured that the measured irradiance correspond only to the VUV emission of the system.

Being able to filter and measure the actual radiation intensity of the system which induce chemical reaction, leads to a better quantification of fundamental parameters in the photo-induced Advance Oxidation Process.

Once the characterization of the radiation intensity was finished, the focus was to deepen the understanding of the cluster radiation interaction. Therefore the following step was to investigate the radiation penetration in water and to measure the absorption coefficient of radiation in water in the range of work (Chapter 5). The methodology chosen to measure the absorption process was the transmission method. In this method, it was measured the relation of the resulting spectrum transmitted through a thin film sample of water to the incident spectrum. A complete tailor made setup was conceptually designed and build. The setup comprises a radiation source Osram Xeradex, an electro-mechanic arm Thorlab which moves the sample holder, a sample holder manufactured in house using special quartz plates CORNING HPFS 8655 polished to ensure smooth surfaces and a detector - the Maya Pro Spectrophotometer customized by Ocean optics for extra Deep UV extended spectral measurements starting at 153 nm. The whole system installed in a gas tight chamber where a non-absorbing atmosphere was maintained. In order to eliminate the effects, which reflection has on transmission measurements, correction of the observed transmission was performed.

From experiments, total penetration of radiation at 172 nm in water happens in a layer three times smaller than the value reported in literature in the sixties. This is an important outcome as those values are the most used in the studies of photo induces AOP to the moment. Results of this thesis in terms of absorption coefficient are similar to those reported by Higashi in 2007. Higashi used a different methodology, the attenuated total reflection and his results could be confirmed [73].

Radiation responsible for the photolysis of water and the generation of hydroxyl radicals is strongly absorbed in water. Stronger absorption than that reported in literature for the photo induced AOP was found in this thesis experimentally, absorption coefficient at 172 nm is 180 000 m^{-1}. This result translates directly into changes in the dimensions of the photo reaction zone. A grater absorption means a smaller photo reaction zone than initially assumed and the generation of hydroxyl radicals occurs in the first 11 µm from the lamp. This result has a strong correlation with the importance of mixing conditions and prevention of formation of boundary layers in photo induced AOP reactors. Strong mixing measures has to be taken to efficiently use the hydroxyl radicals being generated.

Channel thicknesses in Photo reactors using Xenon excimer cannot exceed the dimensions found previously (Chapter 3).

As a following step, efforts were redirected to the cluster oxidation process where the characterization of the radical generation was the goal. In this step the main objective was the measurement of hydroxyl radical formation. Methanol was used as a model compound due to the size of the molecule and the known reaction path mechanism of the oxidation with hydroxyl radicals. The work done in this specific problem by Heit and Braun [75] was essential and is of special interest in this part (Chapter 6).

The quantum yield for the generation of hydroxyl radicals is directly influenced by the measurement of radiation intensity. Taking this into consideration, the quantum yield for the generation of hydroxyl radicals was calculated and evaluated using the different measurements of radiation intensity from chapter 4. First the quantum yield using the radiation intensity from the cis-, trans- cyclooctene was calculated as 0,50 ± 0,02 molOH/mol photons. This value is slightly higher than the literature value of 0,42 ± 0,02 molOH/mol photons obtained by the same procedure. However as seen and discussed in chapter 4. The radiation intensity calculated using the results of actinometry may contain uncertainties due to the assumptions of the methodology.

Next, the quantum yield for the generation of hydroxyl radicals obtained in this study by using the measurements of the Si-photodiode detector (affected by fluorescence of quartz)) was calculated as 0,73 ± 0,02 molOH/mol photons.

Finally, the quantum yield for the generation of hydroxyl radicals obtained in this study by using the measurements of the calibrated AlGaN detector (blind for radiation higher than 380 nm) is 1,82 ± 0,02 molOH/mol photons. Quantum yields greater than 1 are possible for photo-induced or radiation-induced chain reactions, in which a single photon may trigger a long chain of transformations. This implies that the chemical system may be more complex than the system modeled for calculation.

The gained accurate value for the quantum yield of hydroxyl radical generation will lead to a better understanding of the potential of xenon excimer lamps for the Advanced Oxidation Processes for water remediation. As well as further quantification of fundamental parameters such photo-chemical rate constants. In order to explore the accuracy of the method, further work must be invested in the detailed description of the system to determine the quantum yield for the generation of hydroxyl radicals.

Using the result obtained until this point regarding the three clusters for UV photo induced oxidation process, a new concept combining Lamp-reactor in one system using Flat lamps developed by Fraunhofer IGB was designed and built. The lessons learned were applied to the design where channel thicknesses mixing promoters and needed flow rates were taken into account for the overall setup. During this process, two Patents were proposed and accepted describing the oxidation process and the photo-reactor setup. The lab scale system built contains 4 Lamp-reactors. Each Lamp-reactor is connected to a 2 L jacketed glassware tank. The Lamp-reactor and the reservoir tank are coupled with a magnetic centrifugal pump from the company Sonderman BGR. For oxidation experiments the solution containing the substances to be oxidized is flowing inside the loop reservoir Lamp-reactor in a batch process. The volumetric flow and the channel thickness in the Lamp-reactor system can be varied.

The focus from now on was put in the cluster oxidation process. In order to validate the system and investigate the performance of the photo induced oxidation process, five substances were selected. Methylene Blue MB (indicator of the oxidation process in several studies in the field of AOP), Carbamazepine CBZ (antiepileptic drug used to control seizures, it is one of the most frequent detected pharmaceutical residues in water bodies so far and proposed as an anthropogenic marker in water bodies [144]), Sulfaquinoxaline SQX (antibiotic used to prevent coccidiosis in animals, the quinoxaline group exhibits mutagenic and carcinogenic properties, it was reported that levels of SQX in the environment encourage the formation of antibiotic-resistant bacteria [111, 145]), Bisphenol A BPA (intermediate in the production of polycarbonate and epoxy resins, flame retardants and other special packaging products, it is biologically active due to its endocrine disruptive estrogenic action in aquatic life) and Caffeine CAF (by far the most universal used legal drug, it is one of the compounds present in higher concentrations in influents and effluents of sewage treatment plants [147]).

Concentration of the selected substances, the global parameter TOC and the toxicity (cytotoxicity against COS and VERO cells, cell lines isolated from an African green monkey kidney) during experiments were followed.

The photo induced oxidation allows the efficient removal of the five model compounds, which were no longer detected after a dose of 1500 mJ/cm^2. The total organic matter mineralization was achieved after a dose of 9000 mJ/cm^2 . Moreover, cytotoxicity assays revealed the feasibility of the photo induced AOP treatment for removal of the model components SQX, CBZ, BPA and CAF as well as the possibility to stop this process at any convenient time. No increase in toxicity during the oxidation process gives the impression that the byproducts in the photo induced AOP are not similar to the well

know aldehydes by products, for example glycol aldehyde and formaldehyde as intermediates of oxidation by other means which induce toxicological responses 100 times higher than the original substance, for example 1,4-dioxane itself [154].

The photo-induced Advance Oxidation process using Xenon Excimer Lamps shows advantages in comparison with other oxidation technologies. Some of these advantages are:

- the steady and local production of strong oxidizer hydroxyl radical by water photolysis without the addition of supplementary oxidation agents or additives,
- not strong selectivity of the process, pH independency
- the efficient oxidation and mineralization of organic substances (organic water pollutants) using VUV light,
- the by-products along the experiments for the substances studied were not source of increase in toxicity for COS and VERO cells, which is an evidence of the possibility of coupling this AOP with biological processes.

Additionally the values of dose for oxidation purposes of specific substances and mineralization will in future lead to a better design and scale up of the technology for specific and continues processes. The calculated energy consumption of 0,1 kWh/m^3 to eliminate trace substances which initial concentration is by far larger than those found in water bodies is one of the attractiveness of this technology for future developments.

9. Summary and outlook

9.1. Summary

Photo induced advanced oxidation by means of xenon excimer lamps have been confirmed to be efficient for the degradation and mineralization of persistent substances such as pharmaceuticals (Sulfaquinoxaline SQX and Carbamazepine CBZ), chemicals coming from the industry (bisphenol A BPA) and food ingredients (caffeine CAF); all of them, substances that are present and have a serious impact in natural water bodies.

A rigorous experimental campaign was used to investigate the degradation of a model component (MB) under different operational parameters, as well as degradation and mineralization performance of the different substances SQX, CBZ, BPA and CAF. The experiments were performed with the aim of identifying the influence of operational parameters, pH conditions, and absence and presence of organic load in the oxidation and mineralization process. Cytotoxicity assays were performed to follow the by products toxicity along the experiments.

In general the oxidation of hardly degradable substances was achieved, the oxidation by means of UV photo-induced AOP showed low dependency to pH conditions, no strong selectivity and the capacity of mineralization. The cytotoxicity of the by products does not overpass the initial toxicity of the tested substances along experiments, giving the possibility to stop the process at any convenient time.

It was found, that special attention has to be taken to operational conditions and efficient mixing along the lamp surface, where the hydroxyl radicals (the oxidation agent) are being formed. The calculation of boundary layer thickness at different Reynolds and distances inflow distances and the results from experimental validation makes evident the difficulty to reach exchange between bulk flow and photo reaction zone even a large Reynold numbers, leaving as an alternative just the changes in dimensions of the photo reactors. Photo induced oxidation process is fluid dynamic dependent, the right combination of geometry and mixing conditions is necessary to reach maximum oxidation performance.

Furthermore, characterization of Excimer lamps was approached by 2 different methods, chemical actinometry and photometry detection base on electrical response of a reacting to light system. It was identified the uncertainties sources coming from each method. These uncertainties sources are a strong cause of error. For the development of photo induced advanced oxidation processes with excimer lamps is necessary to have certainty in the irradiance of lamps and the effective measurement

of the radiation responsible for the photolysis of water. It was identified the strong degradation of commercial detectors when exposed to VUV. A newly developed AlGaN detector was identified as a novel solution for the measurement of irradiation below 200 nm radiation due to the special blindness in the range of fluorescence of quartz.

Additionally, absorption of radiation at the wavelength emitted by Xenon excimer lamps was found to be stronger as reported in literature; therefore the photo reaction zone in oxidation processes using Xenon excimer lamps is smaller than assumed and calculated in literature. Boundary layers around the radiation source are definitely larger than the photo reaction zone, what intensifies the importance of generating a strong mixing close to the reaction layer in order to have an efficient use of the radicals.

With regard to the generation of hydroxyl radicals, the measurement of production rate and quantum yield depends strongly on operational conditions and accurate measurement of the irradiance of the radiation source. Comparing with Literature, a higher quantum yield of generation of hydroxyl radicals was calculated from the experimental approach due to the special care on the operational conditions and the use of channel thicknesses and mixing conditions to avoid the generation of depletion zones where hydroxyl radical are not captured with the scavenger chosen.

The quantum yield for the generation of hydroxyl radicals obtained in this study by using the measurements of the calibrated AlGaN detector (blind for radiation higher than 380 nm) is 1,82 ± 0,02 molOH/mol photons. Quantum yields greater than 1 are only possible for photo-induced or radiation-induced chain reactions, in which a single photon may trigger a long chain of transformations. This implies that the chemical system model used may be more complex than the system modeled for calculation. In order to explore more accurate methods further work must be invested in the detailed description of the scavenging system to determine the quantum yield for the generation of hydroxyl radicals.

The different experimental setups developed for this thesis, between the photoreaction reactors, Irradiance measurement setups, absorption of radiation in thin films of fluid and the gained results in knowledge enabled as an outcome the filing of 2 patents the participation in publications and research projects, as well as generation of basis for the design of a demo-plant based on a flat-lamp-reactor-system for the further studies of UV photo-induced oxidation of contaminants in water.

9.2. Outlook

The following investigative effort must be taken toward the generation of a library of information regarding oxidation of different substances, in terms of total mineralization, toxicity and interferences with different scavengers of hydroxyl radicals and other substances which may affect the oxidation process.

Another important approach to be started after this thesis is the modelling of the oxidation process in terms of specific substance as well as sum parameter TOC for the future application of the advanced oxidation field using Xenon excimer Lamps. Photo induced advanced oxidation can be applied before or after conventional water treatment according to the final objective of the treatment. It can be applied also for the drinking water sector when the focus is the destruction of trace pollutants which may reach households, or directly in the manufacture processes where ultrapure water is needed and low TOC is required.

10. References

1. Heberer, T., *Occurrence, fate, and removal of pharmaceutical residues in the aquatic environment: a review of recent research data.* Toxicology Letters, 2002. 131(1-2): p. 5-17.

2. Petrovic, M., *Analysis and removal of emerging contaminants in wastewater and drinking water.* TrAC Trends in Analytical Chemistry, 2003. 22(10): p. 685-696.

3. Belgiorno, V. and L. Rizzo, *Emerging contaminants into the environment: Contamination pathways and control*. 2012, University of Salerno. ASTER 164.

4. Ivashechkin, P.V. and M. Dohmann, *Elimination organischer Spurenstoffe aus kommunalem Abwasser*. 2006, Publikationsserver der RWTH Aachen University. Aachen. p. 246.

5. Rivera-Jaimes, J.A., C. Postigo, R.M. Melgoza-Alemán, J. Aceña, D. Barceló, and M. López de Alda, *Study of pharmaceuticals in surface and wastewater from Cuernavaca, Morelos, Mexico: Occurrence and environmental risk assessment.* Science of The Total Environment, 2018. 613-614: p. 1263-1274.

6. Götz, C.W., J. Hollender and R. Kase, *Mikroverunreinigungen - Beurteilungskonzept für organische Spurenstoffe aus kommunalem Abwasser*. Studie im Auftrag des Bundesamtes für Umwelt (BAFU). 2011, Dübendorf, Switzerland. Eawag.

7. Paíga, P., L.H.M.L.M. Santos, S. Ramos, S. Jorge, J.G. Silva, and C. Delerue-Matos, *Presence of pharmaceuticals in the Lis river (Portugal): Sources, fate and seasonal variation.* Science of The Total Environment, 2016. 573: p. 164-177.

8. Quadra, G.R., H. Oliveira de Souza, R.S. Costa and M.A.S. Fernandez, *Do pharmaceuticals reach and affect the aquatic ecosystems in Brazil? A critical review of current studies in a developing country.* Environmental Science and Pollution Research, 2017. 24(2): p. 1200-1218.

9. Balakrishna, K., A. Rath, Y. Praveenkumarreddy, K.S. Guruge, and B. Subedi, *A review of the occurrence of pharmaceuticals and personal care products in Indian water bodies.* Ecotoxicology and Environmental Safety, 2017. 137: p. 113-120.

10. Verlicchi, P., M. Al Aukidy and E. Zambello, *Occurrence of pharmaceutical compounds in urban wastewater: Removal, mass load and environmental risk after a secondary treatment—A review.* Science of The Total Environment, 2012. 429: p. 123-155.

11. Luo, Y., W. Guo, H.H. Ngo, L.D. Nghiem, F.I. Hai, J. Zhang, S. Liang, and X.C. Wang, *A review on the occurrence of micropollutants in the aquatic environment and their fate and removal during wastewater treatment.* Science of The Total Environment, 2014. 473-474: p. 619-641.

12. Li, W.C., *Occurrence, sources, and fate of pharmaceuticals in aquatic environment and soil.* Environmental Pollution, 2014. 187: p. 193-201.

13. Welker, A., *Occurrence and fate of organic pollutants in combined sewer systems and possible impacts on receiving waters.* Water Science and Technology, 2007. 56(10): p. 141-148.

14. Yamal Turbay, E., *Efficient Operation of photo-Fenton Process for the Treatment of Emerging Contaminants in Water Solutions*. 2013, UPC. Barcelona.

15. Esplugas, S., D. Bila, L. Gustavo T Krause and M. Dezotti, *The Ozonation and Advanced Oxidation Technologies to Remove Endocrine Disrupting Chemicals (EDCs) and Pharmaceuticals and Personal Care Products (PPCPs) in Water Effluents.* 2007. 149.

16. Teodosiu, C., G. Barjoveanu and D. Teleman, *SUSTAINABLE WATER RESOURCES MANAGEMENT 1. RIVER BASIN MANAGEMENT AND THE EC WATER FRAMEWORK DIRECTIVE.* Environmental Engineering & Management Journal (EEMJ), 2003. 2(4).

17. Parliament, E., *Directive 2000/60/EC of the European Parliament and of the Council of 23 October 2000 establishing a framework for Community action in the field of water policy*, in *327*. 2000.

18. Jakob, L., *Traitement des eaux par photocatalyse et photolyse V-UV: Degradation oxidative de polluants organiques*. 1992, Ph. D. EPFL, Lausanne.

19. Jakob, L., T.M. Hashem, S. Bürki, N.M. Guindy, and A.M. Braun, *Vacuum-ultraviolet (VUV) photolysis of water: oxidative degradation of 4-chlorophenol.* Journal of Photochemistry and Photobiology A: Chemistry, 1993. 75(2): p. 97-103.

20. Oppenlaender, T., *Photochemical Purification of Water and Air*. 2003, Weinheim. WILEY-VCH.

21. Toro Santamaria, J.M., *Development of a reactor design for Vaccum UV irradiation of wastewater (Master Thesis)*. 2011, University of Stuttgart. Stuttgart. p. 150.

22. Heit, G., A. Neuner, P.-Y. Saugy and A.M. Braun, *Vacuum-UV (172 nm) Actinometry. The Quantum Yield of the Photolysis of Water.* J. Phys. Chem. A, 1998. 102(28): p. 5551-5561.

23. Heit, G., *Entwicklung und Anwendung neuer Verfahren zur photochemischen Prozeßanalyse. Optische In-Situ-Sauerstoffmessung, VUV-Aktinometrie und numerische Simulation*. 1997.

24. Crapulli, F., *Disinfection and advanced oxidation of highly absorbing fluids by UV/VUV light: process modeling and validation*. 2015 Electronic Thesis and Dissertation Repository. 2753.

25. Poyatos, J.M., M.M. Muñio, M.C. Almecija, J.C. Torres, E. Hontoria, and F. Osorio, *Advanced Oxidation Processes for Wastewater Treatment: State of the Art.* Water, Air, and Soil Pollution, 2009. 205(1-4): p. 187-204.

26. Glaze, W.H., J.W. Kang and D.H. Chapin, *The Chemistry of Water-Treatment Processes Involving Ozone, Hydrogen-Peroxide and Ultraviolet-Radiation.* Ozone-Science & Engineering, 1987. 9(4): p. 335-352.

27. Wöhrle, D., M.W. Tausch and W.-D. Stohrer, *Photochemie: Konzepte, Methoden, Experimente*. 1998, Weinheim. WILEY-VCH.

28. Bolton, J.R., *Ultraviolet Applications Handbook*. Third Edition ed. 2010, Edmonton, Canada. ICC Lifelong Learn Inc.

29. Hind, A., *Spectrophotometry - Takes measure of deep-UV lithography.* Photonics Spectra, 2001. 35(12): p. 82.

30. Sokolov, U. and G. Stein, *Photolysis of Liquid Water at 1470 Å.* The Journal of Chemical Physics, 1966. 44(5).

31. Sokolov, U., *Photolysis of Liquid Water at 1849 Å.* The Journal of Chemical Physics, 1966. 44(9).

32. Getoff, N. and G.O. Schenck, *Primary Products of Liquid Water Photolysis at 1236, 1470 and 1849 Å.* Photochemistry and Photobiology, 1968. 8(3): p. 167-178.

33. Barrett, J. and J.H. Baxendale, *The photolysis of liquid water.* Transactions of the Faraday Society, 1960. 56(0): p. 37-43.

34. Legrini, E. Oliveros and A.M. Braun, *Photochemical Processes for Water Treatment.* Chem. Rev. , 1993. 93: p. 671-698.

35. Malcolm Pirnie, I. and Dr. James P. Malley, Jr., *ULTRAVIOLET DISINFECTION GUIDANCE MANUAL FOR THE FINAL LONG TERM 2 ENHANCED SURFACE WATER TREATMENT RULE.* 2006.

36. Halmann, M.M., *Photodegradation of Water Pollutants*, ed. C. Press. 1995, Boca Raton.

37. Braun, A.M., L. Jakob, E. Oliveros and C.A.O.d. Nascimento, *Up-scaling photochemical reactions.* Advances in photochemistry, 1993. 18: p. 235-314.

38. Miklos, D.B., C. Remy, M. Jekel, K.G. Linden, J.E. Drewes, and U. Hübner, *Evaluation of advanced oxidation processes for water and wastewater treatment – A critical review.* Water Research, 2018. 139: p. 118-131.

39. Conrads, H. and M. Schmidt, *Plasma generation and plasma sources.* Plasma Sources Science and Technology, 2000. 9.

40. Masschelein, W.J., *Ultraviolet Light in Water and Wastewater Sanitation*. 2002, Boca Raton. Lewis Publishers CRC Press.

41. Koutchma, T.N., L.J. Forney and C.I. Moraru, *Ultraviolet light in food technology : principles and applications*. Contemporary food engineering series ; 8. 2009, Boca Raton, Fla [u.a.]. CRC Press.

42. Ultraviolet, P., *Über UV - Spektralvertreilungen - Spektralverteilungen*. Peschl Ultraviolet GmbH. www.peschl-ultraviolet.com.

43. Birks, J.B., *Excimers.* Reports on Progress in Physics, 1975. 38(8).

44. Tanaka, Y., A.S. Jursa and F.J. Leblanc, *Continuous Emission Spectra of Rare Gases in the Vacuum Ultraviolet Region. II. Neon and Helium.* Journal of the Optical Society of America, 1958. 48(5): p. 304-307.

45. Kogelschatz, U., B. Eliasson and W. Egli, *Dielectric-Barrier Discharges. Principle and Applications.* Le Journal de Physique IV, 1997. 07(C4): p. C4-47-C4-66.

46. Meisser, M., M. Paraxial, W. Heering and R. Kling. *Resonance behaviour of a pulsed electronic control gear for dielectric barrier discharges*. 2010. IET.

47. El-Deib, A.A., *Modeling of and driver design for a dielectric barrier discharge lamp*. 2010, University of Toronto.

48. Kogelschatz, U. and J. Salge, *High-pressure plasmas: Dielectric-barrier and corona discharges.* Properties and Technical Applications, Low Temperature Plasma Physics, 2001: p. 331.

49. Vollkommer, F. and L. Hitzschke, *Method to operate an incoherently emitting radiation source having at least*. 1997, Patent-Treuhand-Gesellschaft fur elektrische Gluhlampen mbH.

50. Kogelschatz, U., *Dielectric-barrier discharges: Their history, discharge physics, and industrial applications.* Plasma chemistry and plasma processing, 2003. 23(1): p. 1-46.

51. F. Vollkommer, L.H., *Process for operating an incoherently emitting Radiation Source.* p. W094/23442

52. Rainer Kling, M.P., Markus Roth, *High Efficiency Ozone Production with Excimer Lamps*. Karlsruhe Institute of Technology (KIT), Light Technology Institute, OSRAM GmbH.

53. Sosnin, E.A., T. Oppenländer and V.F. Tarasenko, *Applications of capacitive and barrier discharge excilamps in photoscience.* Journal of Photochemistry and Photobiology C: Photochemistry Reviews, 2006. 7(4): p. 145-163.

54. Gellert, B. and U. Kogelschatz, *Generation of excimer emission in dielectric barrier discharges.* Applied Physics B Photophysics and Laser Chemistry, 1991. 52(1): p. 14-21.

55. Eliasson, B. and U. Kogelschatz, *UV excimer radiation from dielectric-barrier discharges.* Applied Physics B: Lasers and Optics, 1988. 46(4): p. 299-303.

56. Trampert, K.E., M. Paravia, R. Daub and W. Heering. *Total spectral radiant flux measurements on Xe excimer lamps from 115 nm to 1000 nm*. in *Optical Measurement Systems for Industrial Inspection V*. 2007. Munich. SPIE. Optical metrology.

57. Weeks, J.L., G.M. Meaburn and S. Gordon, *Absorption coefficients of liquid water and aqueous solutions in the far ultraviolet.* Radiat Res, 1963. 19: p. 559-67.

58. Gonzalez, M.G., E. Oliveros, M. Wörner and A.M. Braun, *Vacuum-ultraviolet photolysis of aqueous reaction systems.* Journal of Photochemistry and Photobiology C: Photochemistry Reviews, 2004. 5(3): p. 225-246.

59. Zvereva, G.N., *Investigation of water decomposition by vacuum ultraviolet radiation.* Optics and Spectroscopy, 2010. 108(6): p. 915-922.

60. Atkinson, R., D.L. Baulch, R.A. Cox, J.N. Crowley, R.F. Hampson, R.G. Hynes, M.E. Jenkin, M.J. Rossi, and J. Troe, *Atmos.* Chem. Phys., 2004. 4: p. 1461-1738.

61. Oppenländer, T., *Photochemische Methoden der Wasserbehandlung mit Excimer-Durchflußphotoreaktoren und Vakuum-UV-Oxidation eines Eisen-EDTA-Komplexes.* Chemie Ingenieur Technik, 1997. 69(12): p. 1782-1786.

62. Gonzalez, M. and A. Braun, *VUV photolysis of aqueous solutions of nitrate and nitrite.* Research on Chemical Intermediates, 1995. 21(8): p. 837-859.

63. Oppenländer, T., G. Baum, F. Streiff, P. Mathys, and G. Schneider, *Einsatz von Statischen Mischern in Excimer-Durchflußphotoreaktoren zur Abwasserbehandlung durch Vakuum-UV-Oxidation.* Chemie Ingenieur Technik, 1996. 68(1-2): p. 155-158.

64. Verhoeven, J.W., *Glossary of terms used in photochemistry (IUPAC Recommendations 1996).* Pure and Applied Chemistry, 1996. 68(12): p. 2223-2286.

65. Braun, A.M., M.-T.r.s. Maurette and E. Oliveros, *Photochemical technology*. 1991, Chichester. Wiley.

66. Quickenden, T.I. and J.A. Irvin, *The ultraviolet absorption spectrum of liquid water.* The Journal of Chemical Physics, 1980. 72(8): p. 4416.

67. Painter, L.R., *Optical Measurements of Liquid Water in the Vacuum Ultraviolet.* The Journal of Chemical Physics, 1969. 51(1): p. 243.

68. Onaka, R. and T. Takahashi, *Vacuum UV Absorption Spectra of Liquid Water and Ice.* Journal of the Physical Society of Japan, 1968. 24(3): p. 548-550.

69. Segelstein, D.J., *The complex refractive index of water*. 1981, University of Missouri--Kansas City.

70. Romanov, N.P. and V.S. Shuklin, *Transparency of Water over the Range 186–500 nm.* Journal of Applied Spectroscopy, 1984. 41(4): p. 1189-1193.

71. Querry, M.R., D.M. Wieliczka and D.J. Segelstein, *Water (H2O)*, in *Handbook of Optical Constants of Solids*, D.P. Edward, Editor. 1997, Academic Press: Burlington. p. 1059-1077.

72. Hayashi, H., N. Watanabe, Y. Udagawa and C. Kao, *The complete optical spectrum of liquid water measured by inelastic x-ray scattering.* Proc Natl Acad Sci U S A, 2000. 97(12): p. 6264.

73. Higashi, N., A. Ikehata and Y. Ozaki, *An attenuated total reflectance far-UV spectrometer.* Rev Sci Instrum, 2007. 78(10): p. 103107.

74. Ikehata, A., N. Higashi and Y. Ozaki, *Direct observation of the absorption bands of the first electronic transition in liquid H2O and D2O by attenuated total reflectance far-UV spectroscopy.* J Chem Phys, 2008. 129(23): p. 234510.

75. Heit, G. and A. M. Braun, *VUV-photolysis of aqueous systems: Spatial differentiation between volumes of primary and secondary reactions.* Water Science and Technology, 1997. 35(4): p. 25-30.

76. Da Costa, A.R., A.G. Fane, C.J.D. Fell and A.C.M. Franken, *Optimal channel spacer design for ultrafiltration.* Journal of Membrane Science, 1991. 62(3): p. 275-291.

77. Stroock, A.D., S.K.W. Dertinger, A. Ajdari, I. Mezić, H.A. Stone, and G.M. Whitesides, *Chaotic mixer for microchannels.* Science, 2002. 295(5555): p. 647-651.

78. Kirtland, J.D., G.J. McGraw and A.D. Stroock, *Mass transfer to reactive boundaries from steady three-dimensional flows in microchannels.* Physics of Fluids, 2006. 18(7): p. 073602-073602-13.

79. Schuster, H.G., *Transport and Mixing in Laminar Flows: From Microfluidics to Oceanic Currents (Annual Reviews of Nonlinear Dynamics and Complexity*. 1 ed, ed. R. Grigoriev. 2011. Wiley-VCH. 190.

80. Williams, M.S., K.J. Longmuir and P. Yager, *A practical guide to the staggered herringbone mixer.* Lab on a Chip, 2008. 8(7).

81. Ottino, J.M., *Mixing, chaotic advection, and turbulence.* Annual Review of Fluid Mechanics, 1990. 22(1): p. 207-254.

82. Hoigné, J. and H. Bader, *Rate constants of reactions of ozone with organic and inorganic compounds in water--I: Non-dissociating organic compounds.* Water Research, 1983. 17(2): p. 173-183.

83. Batchelor, G.K., *An Introduction to Fluid Dynamics by G. K. Batchelor.* Cambridge Core, 2000.

84. Larason, T.C. and C.L. Cromer, *Sources of Error in UV Radiation Measurements.* Journal of Research of the National Institute of Standards and Technology, 2001. 106(4): p. 649-656.

85. Srinivasan, R. and J.A. Ors, *Organic photochemistry with 6.7-eV photons: bicyclo [n. 1.0] alkanes and tricyclo [3.2. 1.02, 4] octane.* Journal of the American Chemical Society, 1978. 100(22): p. 7089-7091.

86. Abdelkader, T.M.H., *The use of VUV and UV-C light sources for advanced oxidation processes*. 1998, Karlsruhe. Karlsruhe.

87. Kuhn, H.J., S.E. Braslavsky and R. Schmidt, *Chemical actinometry (IUPAC Technical Report).* Pure and Applied Chemistry, 2009. 76(12): p. 2105.

88. Hamamatsu Photonics Solid State, S., *Si Photodiode*. 2011.

89. Anatoly Trukhin, K.T., *Luminescence of alpha-quartz.* 2012.

90. Ramseyer, K., J. Baumann, A. Matter and J. Mullis, *Cathodoluminescence colours of a-quartz.* p. 9.

91. Hunter, W.R., *Measurement of optical properties of materials in the vacuum ultraviolet spectral region.* Applied Optics, 1982. 21(12): p. 2103-2114.

92. Painter, L.R., R.D. Birkhoff and E.T. Arakawa, *Optical Measurements of Liquid Water in the Vacuum Ultraviolet.* The Journal of Chemical Physics, 1969. 51(1): p. 243-251.

93. Barth, J., R.L. Johnson and M. Cardona, *Chapter 10 - Spectroscopic Ellipsometry in the 6–35 eV Region*, in *Handbook of Optical Constants of Solids*, D.P. Edward, Editor. 1997, Academic Press: Burlington. p. 213-246.

94. Sprokel, G.J. and J.D. Swalen, *Chapter 4 - The Attenuated Total Reflection Method*, in *Handbook of Optical Constants of Solids*, D.P. Edward, Editor. 1997, Academic Press: Burlington. p. 75-95.

95. Barrett, J. and A.L. Mansell, *Ultra-Violet Absorption Spectra of the Molecules H2O, HDO and D2O.* Nature, 1960. 187(4732): p. 138-138.

96. Halmann, M. and I. Platzner, *Temperature dependence of absorption of liquid water in the far-ultraviolet region.* The Journal of Physical Chemistry, 1966. 70(2): p. 580-581.

97. Heller, J.M., *Collective oscillation in liquid water.* The Journal of Chemical Physics, 1974. 60(9): p. 3483.

98. Yoon, M.S., B.J. Kim and H.J. Sung, *Pumping and mixing in a microchannel using AC asymmetric electrode arrays.* International Journal of Heat and Fluid Flow, 2008. 29(1): p. 269-280.

99. Getoff, N., *Primärprodukte der Wasserphotolyse bei 1849 \AA.* Monatshefte für Chemie/Chemical Monthly, 1968. 99(1): p. 136-147.

100. Ross, F. and A.B. Ross, *Selected specific rates of reactions of transients from water in aqueous solution. III. hydroxyl radical and perhydroxyl radical and their radical ions*. National Bureau of Standards. 130.

101. Ross, F. and A.B. Ross, *Selected specific rates of reactions of transients from water in aqueous solution. Hydrated Electron, Supplemental Data*. National Bureau of Standards. 130.

102. Ross, F. and A.B. Ross, *Selected specific rates of reactions of transients from water in aqueous solution. II. Hydrogen Atom*. National Bureau of Standards. 130.

103. Von Sonntag, C. and H.-P. Schuchmann, *Photolysis of Saturated Alcohols, Ethers, and Amines*, in *Advances in Photochemistry*, J.N.P. Jr, G.S. Hammond, and K. Gollnick, Editors. 2007, John Wiley & Sons, Inc. p. 59-145.

104. Buxton, G.V., C.L. Greenstock, W.P. Helman and A.B. Ross, *Critical Review of rate constants for reactions of hydrated electrons, hydrogen atoms and hydroxyl radicals (·OH/·O– in Aqueous Solution.* Journal of Physical and Chemical Reference Data, 1988. 17(2): p. 513-886.

105. J. W. T. Spinks. R. J. Woods, A., *An Introduction to Radiation Chemistry, Third Edition, John-Wiley and Sons, Inc., New York, Toronto 1990. ISBN 0-471-61403-3. 574 Seiten, Preis: DM 91, 45.* Berichte der Bunsengesellschaft für physikalische Chemie, 1991. 95(3): p. 451-451.

106. Bolton, J., K. G. Bircher, W. Tumas and C. A Tolman, *Figures of Merit for the Technical Development and Application of Advanced Oxidation Process.* Journal of Advanced Oxidation Technologies 1996. 1(1): p. 13–17.

107. Oppenländer, T. and R. Schwarzwälder, *Vacuum-UV Oxidation (H2O-VUV) with a Xenon Excimer Flow-Trough Lamp at 172 nm: Use of Methanol as Actinometer for VUV Intensity Measurement and as Reference Compound for OH-Radical Competition Kinetics in Aqueous Systems.* Journal of Advanced Oxidation Technologies, 2002. 5(2): p. 155-163.

108. Kuch, B.S., H., *Methodik zur Ableitung von Referenzparameter zur Bewertung des Verhaltens von organischen Spurenstoffen in Abwasseranlagen und Oberflächengewässern*. "Mikroschadstoffe und Nährstoffrückgewinnung - Praxiserfahrungen und Umsetzungspotenzial in der Abwasserreinigung", ed. S.B.z. Siedlungswasserwirtschaft. Vol. Stuttgarter Berichte zur Siedlungswasserwirtschaft Band 211. 2012, Stuttgart. Vulkan-Verlag GmbH 49-64.

109. Zhang, Y., S.-U. Geissen and C. Gal, *Carbamazepine and diclofenac: removal in wastewater treatment plants and occurrence in water bodies.* Chemosphere, 2008. 73(8): p. 1151-1161.

110. Dai, C.-M., X.-F. Zhou, Y.-L. Zhang, Y.-P. Duan, Z.-M. Qiang, and T.C. Zhang, *Comparative study of the degradation of carbamazepine in water by advanced oxidation processes.* Environmental Technology, 2012. 33(10-12): p. 1101-1109.

111. Liao, Q.-N., F. Ji, J.-C. Li, X. Zhan, and Z.-H. Hu, *Decomposition and mineralization of sulfaquinoxaline sodium during UV/H2O2 oxidation processes.* Chemical Engineering Journal, 2016. 284: p. 494-502.

112. Urbano, V., M.G. Maniero, M. Pérez Moya and J.R. Guimarães. *Influence of pH and ozone on Sulfaquinoxaline ozonation*. in *EAAOP 2015: 4th European Conference on Environmental Applications of Advanced Oxidation Processes: Athens, Greece: October 21-24, 2015: proceedings book*. 2015.

113. Pérez-Moya, M., T. Kaisto, M. Navarro and L.J. del Valle, *Study of the degradation performance (TOC, BOD, and toxicity) of bisphenol A by the photo-Fenton process.* Environmental Science and Pollution Research, 2017. 24(7): p. 6241-6251.

114. Yamal-Turbay, E., M. Graells and M. Pérez-Moya, *Systematic Assessment of the Influence of Hydrogen Peroxide Dosage on Caffeine Degradation by the Photo-Fenton Process.* Industrial & Engineering Chemistry Research, 2012. 51(13): p. 4770-4778.

115. Mandal, T., S. Maity, D. Dasgupta and S. Datta, *Advanced oxidation process and biotreatment: Their roles in combined industrial wastewater treatment.* Desalination, 2010. 250(1): p. 87-94.

116. García-Galán, M.J., M.S. Díaz-Cruz and D. Barceló, *Occurrence of sulfonamide residues along the Ebro river basin: Removal in wastewater treatment plants and environmental impact assessment.* Environment International, 2011. 37(2): p. 462-473.

117. García-Galán, M.J., T. Garrido, J. Fraile, A. Ginebreda, M.S. Díaz-Cruz, and D. Barceló, *Simultaneous occurrence of nitrates and sulfonamide antibiotics in two ground water bodies of Catalonia (Spain).* Journal of Hydrology, 2010. 383(1): p. 93-101.

118. Fromme, H., T. Küchler, T. Otto, K. Pilz, J. Müller, and A. Wenzel, *Occurrence of phthalates and bisphenol A and F in the environment.* Water Research, 2002. 36(6): p. 1429-1438.

119. Leusch, F.D.L., H.F. Chapman, M.R. van den Heuvel, B.L.L. Tan, S.R. Gooneratne, and L.A. Tremblay, *Bioassay-derived androgenic and estrogenic activity in municipal sewage in Australia and New Zealand.* Ecotoxicology and Environmental Safety, 2006. 65(3): p. 403-411.

120. Musolff, A., S. Leschik, F. Reinstorf, G. Strauch, and M. Schirmer, *Micropollutant Loads in the Urban Water Cycle.* Environmental Science & Technology, 2010. 44(13): p. 4877-4883.

121. Guo, Y.C. and S.W. Krasner, *Occurrence of Primidone, Carbamazepine, Caffeine, and Precursors for N-Nitrosodimethylamine in Drinking Water Sources Impacted by Wastewater1*. JAWRA Journal of the American Water Resources Association, 2009. 45(1): p. 58-67.

122. Sim, W.-J., J.-W. Lee, E.-S. Lee, S.-K. Shin, S.-R. Hwang, and J.-E. Oh, *Occurrence and distribution of pharmaceuticals in wastewater from households, livestock farms, hospitals and pharmaceutical manufactures.* Chemosphere, 2011. 82(2): p. 179-186.

123. Larsson, D.G.J., C. de Pedro and N. Paxeus, *Effluent from drug manufactures contains extremely high levels of pharmaceuticals.* Journal of hazardous materials, 2007. 148(3): p. 751-755.

124. Oppenländer, T. and G. Baum, *CKW-Eliminierung aus Wasser durch Vakuum-UV- und UV-Photolyse in Excimer-Durchflußphotoreaktoren.* 1995.

125. Baum, G. and T. Oppenländer, *Vacuum - UV - oxidation of chloroorganic compounds in an excimer flow through photoreactor.* Chemosphere, 1995. 30(9): p. 1781-1790.

126. Wörner, M., Braun and A. M., *Dehalogenation of halogenated organic compounds in aqueous solutions by different photochemical methods*. 1998, Amsterdam, PAYS-BAS. Gordon and Breach Science. 6.

127. Oppenländer, T. and S. Gliese, *Mineralization of organic micropollutants (homologous alcohols and phenols) in water by vacuum-UV-oxidation (H2O-VUV) with an incoherent xenon-excimer lamp at 172 nm.* Chemosphere, 2000. 40(1): p. 15-21.

128. Oppenländer, T., G. Baum, W. Egle and T. Hennig, *Novel vacuum-UV-(VUV) and UV-excimer flow-through photoreactors for waste water treatment and for wavelength-selective photochemistry.* Journal of Chemical Sciences, 1995. 107(6): p. 621-636.

129. Nohr, R.S., *Application of excimer incoherent-UV sources as a new tool in photochemistry: photodegradation of chlorinated dibenzodioxins in solution and adsorbed on aqueous pulp sludge.* Journal of Photochemistry and Photobiology A: Chemistry. 79(1-2): p. 141-149.

130. Hashem, T.M., M. Zirlewagen and A.M. Braun, *Simultaneous photochemical generation of ozone in the gas phase and photolysis of aqueous reaction systems using one VUV light source.* Water Science and Technology, 1997. 35(4): p. 41-48.

131. Gonzalez, M.C., A.M. Braun, A.B. Prevot and E. Pelizzetti, *Vacuum-ultraviolet (VUV) photolysis of water: Mineralization of atrazine.* Chemosphere, 1994. 28(12): p. 2121-2127.

132. László, Z. and A. Dombi, *Oxidation of [Fe(CN)6]4- and reduction of [Fe(CN)6]3- in VUV-irradiated aqueous solutions.* Chemosphere, 2002. 46(4): p. 491-494.

133. M. V. Grichetschkina, N.K.Z., *Vuv-Photolysis. oxidative degradation of organics inhibiting the inverse-Voltammetric determination of heavy metals. 1. Humic substances.* Toxicological & Environmental Chemistry, 1996. 53: p. 143-151.

134. Oppenländer, T. and G. Baum, *Ein modularer Excimer-Durchflußreaktor zur Reinigung belasteter Abwässer durch Vakuum-UV/UV-Doppelbestrahlung ohne Oxidationsmittelzusatz.* 1994.

135. Gonzalez, M.C. and A. Braun, *Vacuum UV photolysis of aqueous solutions of nitrate. Effect of organic matter II. Methanol.* Journal of Photochemistry and Photobiology A: Chemistry, 1996. 95(1): p. 67-72.

136. László, Z., I. Ilisz, G. Peintler and A. Dombi, *VUV Intensity Measurement of a 172 nm Xe Excimer Lamp by means of Oxygen Actinometry.* Ozone: Science & Engineering, 1998. 20(5): p. 421-432.

137. Gonzalez, M.C. and A.M. Braun, *Vacuum-UV photolysis of aqueous solutions of nitrate: effect of organic matter I. Phenol.* Journal of Photochemistry and Photobiology A: Chemistry, 1996. 93(1): p. 7-19.

138. Loraine, G.A., *Short Wavelength Ultraviolet Photolysis of Aqueous Carbon Tetrachloride.* Hazardous Waste and Hazardous Materials, 1993. 10(2): p. 185-194.

139. Egner, S., B. Elkin and J.M. Toro Santamaria, *Vorrichtung zur photochemischen Behandlung oder Reinigung eines flüssigen Mediums*. 2015.

140. Egner, S., B. Elkin and J.M. Toro Santamaria, *Vorrichtung zur photochemischen Behandlung von verunreinigtem Wasser*. 2015.

141. Kümmerer, K., *Pharmaceuticals in the Environment: Sources, Fate, Effects and Risks*. 2013, Germany. Springer Science & Business Media. 568.

142. Cousins, I.T., C.A. Staples, G.M. Klečka and D. Mackay, *A Multimedia Assessment of the Environmental Fate of Bisphenol A.* Human and Ecological Risk Assessment: An International Journal, 2002. 8(5): p. 1107-1135.

143. Sui, Q., J. Huang, S. Deng, G. Yu, and Q. Fan, *Occurrence and removal of pharmaceuticals, caffeine and DEET in wastewater treatment plants of Beijing, China.* Water Research, 2010. 44(2): p. 417-426.

144. Clara, M., B. Strenn and N. Kreuzinger, *Carbamazepine as a possible anthropogenic marker in the aquatic environment: investigations on the behaviour of Carbamazepine in wastewater treatment and during groundwater infiltration.* Water Research, 2004. 38(4): p. 947-954.

145. Campbell, W.C., *History of the discovery of sulfaquinoxaline as a coccidiostat.* The Journal of Parasitology, 2008. 94(4): p. 934-945.

146. Neamţu, M. and F.H. Frimmel, *Degradation of endocrine disrupting bisphenol A by 254nm irradiation in different water matrices and effect on yeast cells.* Water Research, 2006. 40(20): p. 3745-3750.

147. Siqueira, F., Amaral, L., *Degradation of Caffeine by Advanced Oxidative Processes: O3 and O3/UV: Ozone: Science & Engineering: Vol 37, No 4.*

148. Pérez Moya, M., M. Navarro Jordà, H.D. Mansilla and M. Graells Sobré. *Bisphenol A degradation and mineralization by the Fenton and the Photo-Fenton process*. in *8th European Meeting on Solar Chemistry and Photocatalysis: Environmental Applications: SPEA 8: Thessaloniki, Greece 25-28 June 2014*. 2014.

149. Navarro Jordà, M., M. Graells Sobré and M. Pérez Moya. *Degradation and mineralization of Bisphenol A by the photo fenton process*. in *13th Mediterranean Congress of Chemical Engineering: book of abstracts*. 2014.

150. Pérez Moya, M., T. Kaisto, V. Mendoza and L.J. Del. *Study of the degradation performance (TOC, BOD and Toxicity) of Bisphenol A by the photo-Fenton process*. in *EPOA 2015: 8th Aplicaçoes Ambientais Dos Processos Oxidativos Avançados: Belo Horizonte, Brazil: November 3-6, 2015: proceedings book*. 2015.

151. Lin, A.Y.-C., C.-F. Lin, J.-M. Chiou and P.K.A. Hong, *O3 and O3/H2O2 treatment of sulfonamide and macrolide antibiotics in wastewater.* Journal of Hazardous Materials, 2009. 171(1): p. 452-458.

152. Baeza, C. and D.R.U. Knappe, *Transformation kinetics of biochemically active compounds in low-pressure UV Photolysis and UV/H2O2 advanced oxidation processes.* Water Research, 2011. 45(15): p. 4531-4543.

153. Nihemaiti, M., D.B. Miklos, U. Hübner, K.G. Linden, J.E. Drewes, and J.-P. Croué, *Removal of trace organic chemicals in wastewater effluent by UV/H2O2 and UV/PDS.* Water Research, 2018. 145: p. 487-497.

154. Li, W., E. Xu, D. Schlenk and H. Liu, *Cyto- and geno-toxicity of 1,4-dioxane and its transformation products during ultraviolet-driven advanced oxidation processes.* Environmental Science: Water Research & Technology, 2018. 4(9): p. 1213-1218.

155. Poldelski, V., A. Johnson, S. Wright, V. Dela Rosa, and R.A. Zager, *Ethylene glycol(EG)mediated tubular injury: Identification of critical metabolites and injury pathways.* American Journal of Kidney Diseases, 2001. 38(2): p. 339-348.

156. Al-Enezi, K.S., M. Alkhalaf and L.T. Benov, *Glycolaldehyde induces growth inhibition and oxidative stress in human breast cancer cells**. Free Radical Biology and Medicine, 2006. 40(7): p. 1144-1151.